AD-A204 243   UNITED STATES AIR FORCE GRADUATE STUDENT RESEARCH   1/6
PROGRAM PROGRAM TECHNIC..(U) UNIVERSAL ENERGY SYSTEMS
INC DAYTON OH R C DARRAH ET AL. DEC 88
UNCLASSIFIED   AFOSR-TR-89-0041 F49620-85-C-0013   F/G 5/1   NL

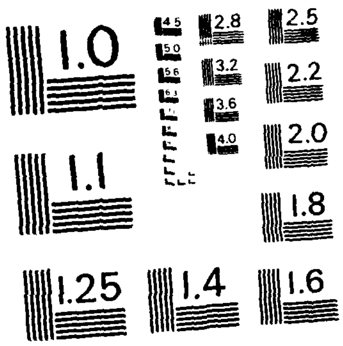
1.0
1.1
1.25
1.4
1.6
1.8
2.0
2.2
2.5
2.8
3.2
3.6
4.0

ECURITY CLASSIFICATION OF THIS PAGE

REPORT DOCUMENTATION PAGE

1a. REPORT SECURITY CLASSIFICATION
UNCLASSIFIED

1b. RESTRICTIVE MARKINGS

2a. SECURITY CLASSIFICATION AUTHORITY

2b. DECLASSIFICATION/DOWNGRADING SCHEDULE

3. DISTRIBUTION/AVAILABILITY OF REPORT
APPROVED FOR PUBLIC RELEASE;
Distribution Unlimited

4. PERFORMING ORGANIZATION REPORT NUMBER(S)

5. MONITORING ORGANIZATION REPORT NUMBER(S)
AFOSR-TR. 8

6a. NAME OF PERFORMING ORGANIZATION
Universal Energy Systems Inc.

6b. OFFICE SYMBOL (If applicable)

7a. NAME OF MONITORING ORGANIZATION
AFOSR/XOT

6c. ADDRESS (City, State and ZIP Code)
4401 Dayton-Xenia Road
Dayton, OH 45432

7b. ADDRESS (City, State and ZIP Code)
Building 410
Bolling AFB, DC 20332-6448

8a. NAME OF FUNDING/SPONSORING ORGANIZATION
Same as #7

8b. OFFICE SYMBOL (If applicable)

9. PROCUREMENT INSTRUMENT IDENTIFICATION NUMBER
F49620-85-C-0013

8c. ADDRESS (City, State and ZIP Code)
same as 7b

10. SOURCE OF FUNDING NOS.

PROGRAM ELEMENT NO.	PROJECT NO.	TASK NO.	WORK UNIT NO.
61102F	3396	D5	

11. TITLE (Include Security Classification)
USAF Graduate Student Summer Support Program - Program Management Report-1988
Vol 1 of 3

12. PERSONAL AUTHOR(S)
dney C. Darrah, Susan K. Espy

13a. TYPE OF REPORT
Annual

13b. TIME COVERED
FROM ______ TO ______

14. DATE OF REPORT (Yr., Mo., Day)
December 1988

15. PAGE COUNT

16. SUPPLEMENTARY NOTATION

17. COSATI CODES		
FIELD	GROUP	SUB. GR.

18. SUBJECT TERMS (Continue on reverse if necessary and identify by block number)

19. ABSTRACT (Continue on reverse if necessary and identify by block number)

See Attached

20. DISTRIBUTION/AVAILABILITY OF ABSTRACT
ASSIFIED/UNLIMITED ☒ SAME AS RPT. ☐ DTIC USERS ☐

21. ABSTRACT SECURITY CLASSIFICATION
IMC:ASSOFOED

22a. NAME OF RESPONSIBLE INDIVIDUAL
Lt Col Claude Cavender

22b. TELEPHONE NUMBER (Include Area Code)
202-767-4970

22c. OFFICE SYMBOL
XOT

DD FORM 1473, 83 APR   EDITION OF 1 JAN 73 IS OBSOLETE.

AFOSR-TR- 89-004

PREFACE

The United States Air Force Graduate Student Research Program (USAF-GSRP) is conducted under the United States Air Force Summer Faculty Research Program. The program provides funds for selected graduate students to work at an appropriate Air Force Facility with a supervising professor who holds a concurrent Summer Faculty Research Program appointment or with a supervising Air Force Engineer/Scientist. This is accomplished by the students being selected on a nationally advertised competitive basis for a ten-week assignment during the summer intersession period to perform research at Air Force laboratories/centers. Each assignment is in a subject area and at an Air Force facility mutually agreed upon by the students and the Air Force. In addition to compensation, travel and cost of living allowances are also paid. The USAF-GSRP is sponsored by the Air Force Office of Scientific Research, Air Force Systems Command, United States Air Force, and is conducted by Universal Energy Systems, Inc.

The specific objectives of the 1988 USAF-GSRP are:

(1) To provide a productive means for the graduate students to participate in research at the Air Force Laboratories/Centers;

(2) To stimulate continuing professional association among the Graduate Students and their professional peers in the Air Force;

(3) To further the research objectives of the United States Air Force;

(4) To enhance the research productivity and capabilities of the graduate students especially as these relate to Air Force technical interests. Keywords: Air Force research, Air Force [illegible], Air Force personnel, research management. (SDW)

During the summer of 1988, 107 graduate students participated. These researchers were assigned to 23 USAF laboratories/centers across the country. This three volume document is a compilation of the final reports written by the assigned students members about their summer research efforts.

AFOSR-TR- 89 0041

Approved for public release;
distribution unlimited.

AIR FORCE OFFICE OF SCIENTIFIC RESEARCH (AFSC)
NOTICE OF TRANSMITTAL TO DTIC
This technical report has been reviewed and is
approved for public release IAW AFR 190-12.
Distribution is unlimited.
MATTHEW J. KERPER
Chief, Technical Information Division

89 2 8 053

UNITED STATES AIR FORCE

GRADUATE STUDENT RESEARCH PROGRAM

1988

PROGRAM TECHNICAL REPORT

UNIVERSAL ENERGY SYSTEMS, INC.

VOLUME I OF III

Program Director, UES
Rodney C. Darrah

Program Manager, AFOSR
Lt. Col. Claude Cavender

Program Administrator, UES
Susan K. Espy

Submitted to

Air Force Office of Scientific Research

Bolling Air Force Base

Washington, DC

December 1988

TABLE OF CONTENTS

PREFACE

The United States Air Force Graduate Student Research Program (USAF-GSRP) is conducted under the United States Air Force Summer Faculty Research Program. The program provides funds for selected graduate students to work at an appropriate Air Force Facility with a supervising professor who holds a concurrent Summer Faculty Research Program appointment or with a supervising Air Force Engineer/Scientist. This is accomplished by the students being selected on a nationally advertised competitive basis for a ten-week assignment during the summer intersession period to perform research at Air Force laboratories/centers. Each assignment is in a subject area and at an Air Force facility mutually agreed upon by the students and the Air Force. In addition to compensation, travel and cost of living allowances are also paid. The USAF-GSRP is sponsored by the Air Force Office of Scientific Research, Air Force Systems Command, United States Air Force, and is conducted by Universal Energy Systems, Inc.

The specific objectives of the 1988 USAF-GSRP are:

(1) To provide a productive means for the graduate students to participate in research at the Air Force Laboratories/Centers;

(2) To stimulate continuing professional association among the Graduate Students and their professional peers in the Air Force;

(3) To further the research objectives of the United States Air Force;

(4) To enhance the research productivity and capabilities of the graduate students especially as these relate to Air Force technical interests.

During the summer of 1988, 107 graduate students participated. These researchers were assigned to 23 USAF laboratories/centers across the country. This three volume document is a compilation of the final reports written by the assigned students members about their summer research efforts.

LIST OF 1988 PARTICIPANTS

NAME/ADDRESS	DEGREE, SPECIALTY, LABORATORY ASSIGNED
Ben A. Abbott Electrical Engineering Dept. Vanderbilt University Nashville, TN 37240 (615) 332-2723	Degree: B.S., Computer Science, 1983 Specialty: Electrical Engineering Assigned: Arnold Engineering Development Center
Antoinne C. Able Meharry Medical College 1005 D.B. Todd Blvd. P O Box 882 Nashville, TN 37208 (615) 361-5303	Degree: M.S., Biology, 1982 Specialty: Biology Assigned: Wilford Hall Medical Center
Stanley D. Adams College of Medicine Meharry Medical College 1005 D.B. Todd Blvd. Nashville, TN 37208 (615) 327-6204	Degree: B.S., Cellular & Molecular Biology, 1987 Specialty: Physiology Assigned: Wilford Hall Medical Center
John D. Allison Dept. of Psychology Univ. of Texas at Austin Mezes Hall 330 Austin, TX 78712 (512) 471-5857	Degree: M.A., Psychology, 1987 Specialty: Comparative Neurobiology Assigned: Human Resources Laboratory: Manpower and Personnel Div.
James E. Angelo Dept. of Physics Univ. of Minnesota - Duluth Duluth, MN 55812 (218) 726-7124	Degree: B.S., Math/Physics, 1986 Specialty: Applied Physics Assigned: Materials Laboratory
John E. Bambery Dept. of Physics University of Pennsylvania Indiana, PA 15701 (412) 357-2611	Degree: B.S. Physics, 1987 Specialty: Computer Analysis Assigned: Avionics Laboratory

Daniel W. Barineau Dept. of Engineering Science Virginia Tech. 1300-B Terrace View Apts. Blacksburg, VA 24060 (703) 552-7867	Degree: Specialty: Assigned:	B.S., Chemical Eng., 1987 Engineering Mechanics Harry G. Armstrong Aerospace Medical Research Laboratory
John W.J. Barnaby Dept. of Electrical Engineering University of Alabama Box 6169, 317 Houser Hall Tuscaloosa, AL 35487-6169 (205) 348-6351	Degree: Specialty: Assigned:	B.S., Electrical Eng., 1987 Electrical Engineering School of Aerospace Medicine
Kathleen M. Bennett Dept. of Engineering Mgmt. University of Dayton 300 College Park Dayton, OH 45469 (513) 229-2699	Degree: Specialty: Assigned:	B.S., Mechanical Eng., 1984 Engineering Management Flight Dynamics Laboratory
Mark N. Beorkrem Dept. of Psychology Washington University One Brookings Drive Campus Box 1125 St. Louis, MO 63130 (314) 889-6536	Degree: Specialty: Assigned:	B.S., Psychology, 1987 Organizational Behavior Human Resources Laboratory: Operations Training Div.
Joel L. Berg Dept. of Eng. Science & Mech. Virginia Polytechnic Inst.&S.U. Blacksburg, VA 24061 (703) 961-6326	Degree: Specialty: Assigned:	M.S., Engr. Mechanics, 1984 Structural Vibrations Astronautics Laboratory
Darwin L. Boyd Dept. of Physics Kent State University Smith Laboratory of Physics Kent, OH 44242 (216) 672-2880	Degree: Specialty: Assigned:	B.S. Physics, 1982 Condensed Matter Physics Materials Laboratory
George C. Boynton Dept. of Physics University of Miami P O Box 248046 Coral Gables, FL 33124 (305) 284-2323	Degree: Specialty: Assigned:	M.S., Physics, 1983 Physics Armament Laboratory

Mark L. Brusseau
Dept. of Soil Science
University of Florida
2169 McCarty Hall
Gainesville, FL 32611-0151
(904) 392-1951

Degree: M.S., Geology, 1984
Specialty: Contaminant Hydrology
Assigned: Engineering & Services Center

Bruce W. Bullard
Dept. of Electrical Eng.
University of Colorado
1420 Austin Bluffs Pkwy.
P O Box 7150
Colorado Springs, CO 80933-7150
(719) 593-3351

Degree: B.S., Electrical Eng., 1988
Specialty: Electrical Engineering
Assigned: Frank. J. Seiler Research Lab.

Franklin A. Bynum
Dept. of Physics
Miami University
Culler Hall
Oxford, OH 45056
(513) 529-5657

Degree: M.S., Physics, 1988
Specialty: Physics
Assigned: Weapons Laboratory

Kevin L. Carmichael
Dept. of Physics
Wright State University
Dayton, OH 45435
(513) 873-2954

Degree: B.S., Physics, 1987
Specialty: Solid State Physics
Assigned: Avionics Laboratory

Lance H. Carter
Dept. of Aerospace Eng.
Virginia Polytechnic Inst.&S.U.
817 Claytor Square
Blacksburg, VA 24060
(703) 953-2289

Degree: B.S., Aerospace Eng., 1987
Specialty: Engineering Mechanics
Assigned: Astronautics Laboratory

David B. Chenault
Dept. of Physics
University of Alabama
Center for Applied Optics
Huntsville, AL 35899
(205) 895-6102

Degree: B.S. Physics, 1986
Specialty: Physics
Assigned: Armament Laboratory

Daniel B. Cook
Dept. of Electro-Optics
University of Dayton
300 College Park
Dayton, OH 45469
(513) 228-4111

Degree: B.S., Physics, 1987
Specialty: Image Processing
Assigned: Avionics Laboratory

Patricia P. Cooper Dept. of Applied Psychology Francis Marion College Florence, SC 29501 (803) 661-1378	Degree: Specialty: Assigned:	M.A., Information Sci., 1974 Psychology Human Resources Laboratory: Operations Training Div.
Otis Cosby, Jr. School of Medicine Meharry Medical College 1005 D.B. Todd Blvd. Nashville, TN 37208 (615) 327-6223	Degree: Specialty: Assigned:	B.S., Natural Science, 1983 Natural Science School of Aerospace Medicine
Richard E. Courtney Dept. of Computing Info. & Sci. Kansas State University 234 Nichols Hall Manhattan, KS 66506 (913) 532-6350	Degree: Specialty: Assigned:	M.S., Computer Science, 1986 Computer Science Rome Air Development Center
Jerry W. Dillon School of Dentistry Meharry Medical College 1005 D.B. Todd Blvd. Nashville, TN 37208 (615) 327-6207	Degree: Specialty: Assigned:	M.S., Microbiology, 1988 Microbiology School of Aerospace Medicine
Charles C. Drake Dept. of Computer Science Jackson State University 1400 Lynch StreetTraining Systems Jackson, MS 39203 (601) 968-2105	Degree: Specialty: Assigned:	B.S., Computer Science, 1987 Computer Science Human Resources Laboratory:
Susan M. Dumbacher Dept. of Aerospace Eng. University of Cincinnati Cincinnati, OH 45225 (513) 475-6185	Degree: Specialty: Assigned:	B.S., Aerospace Eng., 1986 Controls Flight Dynamics Laboratory
Michael K. Ellis Dept. of Computer Science/Eng. University of Arkansas 1900 N. Garland Fayetteville, AR 72703 (501) 575-0722	Degree: Specialty: Assigned:	B.S., Computer Sci., 1988 Neural Network Harry G. Armstrong Aerospace Medical Research Laboratory

Bryan C. Foos Dept. of Civil Engineering Ohio State University 2070 Neil Avenue Columbus, OH 43210 (614) 292-2771	<u>Degree:</u> <u>Specialty:</u> <u>Assigned:</u>	B.S., Civil Engineering, 1988 Geotechnical and Materials Flight Dynamics Laboratory
Ernest J. Freeman Dept. of Biological Sciences Kent State University Kent, OH 44240 (216) 672-2363	<u>Degree:</u> <u>Specialty:</u> <u>Assigned:</u>	B.S., Zoology, 1985 Neurochemistry School of Aerospace Medicine
Peter Gaddis, Jr. Dept. of Sociology Jackson State University 1400 J.R. Lynch Street Jackson, MS 39217 (601) 968-2350	<u>Degree:</u> <u>Specialty:</u> <u>Assigned:</u>	M.A., Sociology, 1988 Alcohol and Drug Studies Human Resources Laboratory: Manpower and Personnel Div.
Douglas P. Gagne Dept. of Mechanical Eng. University of New Hampshire Durham, NH 03824 (603) 868-6160	<u>Degree:</u> <u>Specialty:</u> <u>Assigned:</u>	B.S., Mechanical Eng., 1988 Systems Modeling & Dynamics Materials Laboratory
William L. Geisler College of Polymer Science University of Akron Akron, OH 44325 (216) 375-7500	<u>Degree:</u> <u>Specialty:</u> <u>Assigned:</u>	B.S., Chemical Eng., 1988 Polymeric Materials Astronautics Laboratory
Robert L. Goetz Dept. of Mechanical Eng. Ohio University Athens, OH 45701 (614) 594-3499	<u>Degree:</u> <u>Specialty:</u> <u>Assigned:</u>	B.S., Mechanical Eng., 1987 Mechanical Design Materials Laboratory
David L. Graham Dept. of Mechanical Eng. Northwestern University Tech. 2524 Evanston, IL 60208 (312) 491-3589	<u>Degree:</u> <u>Specialty:</u> <u>Assigned:</u>	B.S., Mechanical Eng., 1988 Mechanical Engineering Astronautics Laboratory

Gary E. Griesheim
Dept. of Civil Engineering
Southern Illinois University
Carbondale, IL 62901
(618) 536-2368

Degree: B.S., Eng. Mechanics, 1987
Specialty: Composite Materials Design
Assigned: Astronautics Laboratory

Edward A. Grissom
Dept. of Electrical Eng.
Tennessee Tech. University
1217 Springdale
Cookeville, TN 38501
(615) 526-1036

Degree: B.S., Electrical Eng., 1983
Specialty: Digital Signal Processing
Assigned: Avionics Laboratory

Virginia A. Gunther
Dept. of Psychology
State Univ. of New York
at Binghamton
Binghamton, NY 13901
(607) 777-4610

Degree: M.A., Exp. Psychology, 1978
Specialty: Cognitive Psychology
Assigned: Harry G. Armstrong Aerospace Medical Research Laboratory

Douglas R. Hansen
Dept. of Civil Engineering
Colorado State University
Room B302
Ft. Collins, CO 80523
(303) 491-8353

Degree: B.S., Wildlife Biology, 1981
Specialty: Environmental Engineering
Assigned: Engineering & Service Center

Thomas K. Harkins
Dept. of Mechanical Eng.
Louisiana State University
1636 Applewood Road
Baton Rouge, LA 70808
(504) 766-3671

Degree: B.S., Mechanical Eng., 1986
Specialty: Flight Dynamics
Assigned: Armament Laboratory

Gary A. Hellenga
Dept. of Mathematical Sciences
Montana State University
1116 South Hedges
Bozeman, MT 59715
(406) 994-5360

Degree: B.S., Mathematics, 1983
Specialty: Applied Mathematics
Assigned: Rome Air Development Center

Andrew Hensley
Dept. of Mechanical Eng.
University of Detroit
Detroit, MI 48603
(313) 927-1242

Degree: B.S., Mechanical Eng., 1988
Specialty: Process Modeling
Assigned: Materials Laboratory

Norman C. Holmes Dept. of Mechanical Engineering University of New Hampshire Durham, NH 03824-3541 (617) 662-6386	Degree: Specialty: Assigned:	B.S., Mechanical Eng., 1984 Mechanical Engineering Flight Dynamics Laboratory
Stephen R. Jenei Dept. of Biology University of Dayton 300 College Park Drive Dayton, OH 45469-0001 (513) 229-2135	Degree: Specialty: Assigned:	B.S., Biology, 1986 Endocrine Physiology Harry G. Armstrong Aerospace Medical Research Laboratory
Alan C. Jewell Dept. of Civil Engineering Colorado State University Fort Collins, CO 80521 (303) 491-5048	Degree: Specialty: Assigned:	B.S., Geophysical Eng., 1984 Geophysical Engineering Weapons Laboratory
Jennifer A. Joyce Dept. of Chemistry Texas A&M University College Station, TX 77843-3255 (409) 845-5345	Degree: Specialty: Assigned:	B.S., Chemistry, 1988 Inorganic Chemistry Frank. J. Seiler Research Lab.
Steven P. Kahn Dept. of Eng. Science & Mech. Virginia Tech. University Blacksburg, VA 24060 (703) 953-1966	Degree: Specialty: Assigned:	B.S., Eng. Science and Mechanics, 1988 Engineering Mechanics Astronautics Laboratory
Elizabeth J. Kavran Dept. of Biology University of Dayton 300 College Park Road Dayton, OH 45429 (513) 229-7660	Degree: Specialty: Assigned:	B.A., Biology, 1987 Biology Harry G. Armstrong Aerospace Medical Research Laboratory
Phyllis Y. Keys Dept. of General Engineering University of Illinois 909 S. Fifth Street Champaign, IL 61820 (217) 332-5010	Degree: Specialty: Assigned:	B.E., General Eng., 1987 Human Factors Occupational and Environment Health Laboratory

Thomas E. Kimble Center for Space Sciences Physics Program Univ. of Texas at Dallas 2601 North Floyd Road P O Box 830688, M.S. FO-22 Richardson, TX 75083-0688 (214) 690-2884	Degree: Specialty: Assigned:	B.A., Economics, 1981 Space Sciences Air Force Geophysics Lab.
Charles L. King Dept. of Industrial Eng. University of Arkansas 4207 Bell Engineering Ctr. Fayetteville, AR 72701 (501) 575-3156	Degree: Specialty: Assigned:	B.S., Industrial Eng., 1988 Management Human Resources Laboratory: Logistics & Human Factors Div.
Scharine Kirchoff Geophysical Institute Univ. of Alaska - Fairbanks P O Box 83328 Fairbanks, AK 99708 (907) 479-5866	Degree: Specialty: Assigned:	M.A., Geology, 1986 Geophysics Air Force Geophysics Lab.
Christopher G. Kocher Dept. of Civil Engineering Southern Illinois University Carbondale, IL 62901 (618) 536-2368	Degree: Specialty: Assigned:	B.S., Eng. Mechanics, 1986 Engineering Mechanics Astronautics Laboratory
Michael J. Koharchik Dept. of Engineering Mechanics The Pennsylvania State Univ. State College, PA 16802 (814) 237-6527	Degree: Specialty: Assigned:	B.S., Aerospace Eng., 1987 Aerospace Structures Astronautics Laboratory
Keith A. Krapels Dept. of Electrical Eng. Memphis State University Memphis, TN 38152 (901) 454-3312	Degree: Specialty: Assigned:	M.S., Electrical Eng., 1986 Electrical Engineering Arnold Engineering Development Center
Richard J. Kunze Dept. of Psychology University of Missouri-Columbia 210 McAlester Hall UMC Campus Columbia, MO 65211 (314) 882-4351	Degree: Specialty: Assigned:	B.A., Psychology, 1986 Experimental Psychology Harry G. Armstrong Aerospace Medical Research Laboratory

Thomas E. Lane
Dept. of Chemistry
Ball State University
Muncie, IN 47306
(317) 285-8078

Degree: B.S., Biology, 1988
Specialty: Immunology & Microbiology
Assigned: School of Aerospace Medicine

Bobby L. Larry
Dental School
Meharry Medical College
1005 D.B. Todd Blvd.
Nashville, TN 37208
(615) 322-9819

Degree: B.S., Biology, 1978
Specialty: Dentistry
Assigned: Wilford Hall Medical Center

Aleshia C. Lewis
Dept. of Biology
Meharry Medical College
1005 D.B. Todd Blvd.
Nashville, TN 37208
(615) 327-6111

Degree: B.S., Microbiology, 1986
Specialty: Microbiology
Assigned: Wilford Hall Medical Center

Yuhong Y. Li
Dept. of Computer Science
University of Nebraska
Lincoln, NE 68588
(402) 472-7211

Degree: M.S., Chemical Eng., 1977
Specialty: Chemical Engineering
Assigned: Avionics Laboratory

Yolanda A. Malone
Dept. of Pharmacology
Meharry Medical College
1005 D.B. Todd Blvd.
Nashville, TN 37208
(615) 327-6111

Degree: M.S., Medicine, 1988
Specialty: Medicine
Assigned: School of Aerospace Medicine

Randal L. Mandock
School of Geophysical Science
Georgia Inst. of Technology
Atlanta, GA 30332
(404) 894-3890

Degree: M.S., Atmospheric Sci., 1986
Specialty: Atmospheric Science
Assigned: Avionics Laboratory

David L. Mayfield
Dept. of Ind./Org Psychology
University of Geor ia
Athens, GA 30602
(404) 542-3053

Degree: B.S., Psychology, 1987
Specialty: Industrial/Organ. Psychology
Assigned: Human Resources Laboratory: Manpower and Personnel Div.

John E. McCord Dept. of Chemistry Murray State University Murray, KY 42071 (502) 762-4490	Degree: Specialty: Assigned:	B.S., Chemistry, 1987 Physical Chemistry Weapons Laboratory
David B. McKenzie Dept. of Civil Engineering Michigan Technological Univ. Houghton, MI 49931 (906) 482-4882	Degree: Specialty: Assigned:	B.S., Civil Eng., 1988 Environmental Engineering Engineering & Services Center
Salvatore P. Miceli Dept. of Aerospace Eng. Sciences Univ. of Colorado - Boulder Campus Box 429 Boulder, CO 80309-0429 (303) 492-6417	Degree: Specialty: Assigned:	B.S., Aerospace Eng., 1988 Unsteady Aerodynamics Frank. J. Seiler Research Lab.
Hisook L. Min Division of Basic Studies Jarvis Christian College Hawkins, TX 75765 (214) 769-2174	Degree: Specialty: Assigned:	M.S., Computer Science, 1987 Applied Physics Armament Laboratory
Deborah J. Mitchell Dept. of Chemistry Prairie View A&M University Drawer C Prairie View, TX 77446 (409) 857-3910	Degree: Specialty: Assigned:	B.S., Chemistry, 1986 Biochemistry Harry G. Armstrong Aerospace Medical Research Laboratory
William A. Moran Dept. of Chemistry Calif. State Univ. -Northridge 18111 Nordhoff Street Northridge, CA 91330 (818) 885-3381	Degree: Specialty: Assigned:	B.S., Chemistry, 1986 Chemistry Astronautics Laboratory
William D. Morse Dept. of Electrical Eng. Ohio State University 205 Dresser Laboratory 2015 Neil Avenue Columbus, OH 43210-1272 (614) 292-2572	Degree: Specialty: Assigned:	B.S., Electrical Eng., 1987 Electrical Engineering Flight Dynamics Laboratory

Lisa F. Weinstein Dept. of Psychology Univ. of Illinois at Urbana-Champaign Aviation Research Lab., Q5 #1 Airport Road Savoy, IL 61874 (217) 244-8728	Degree: M.A., Experimental Psy., 1987 Specialty: Engineering Psychology Assigned: Harry G. Armstrong Aerospace Medical Research Laboratory
Michael A. Zmuda Dept. of Computer Science Wright State University Dayton, OH 45324 (513) 873-2491	Degree: B.S., Compt. Sci. & Math, 1987 Specialty: Pattern Recognition Assigned: Avionics Laboratory

Robert G. Petroit
Dept. of Elect. & Compt. Eng.
Illinois Institute of Tech.
3300 So. Federal
Chicago, IL 60616
(312) 567-3400

Degree: B.S., Electrical Eng., 1987
Specialty: Communications Systems
Assigned: Rome Air Development Center

Peter E. Pidcoe
Dept. of Bioengineering
University of Illinois
Box 4348
Chicago, IL 60680
(312) 996-2331

Degree: B.S., Environ. Mgmt., 1988
Specialty: Signal Processing
Assigned: Human Resources Laboratory: Operations Training Div.

Steven J. Pierce
Dept. of Civil Engineering
Geotechnical Program
Colorado State University
Fort Collins, CO 80523
(303) 491-5048

Degree: B.S., Geology, 1985
Specialty: Geotechnical Engineering
Assigned: Engineering & Services Center

Julia Rennenkampff
Dept. of Mathematics
New York University
251 Mercer Street
New York, NY 10012
(212) 998-3140

Degree: M.S., Mathematics, 1987
Specialty: Waves in Random Media
Assigned: School of Aerospace Medicine

Robert J. Riley
Dept. of Mech. & Aero. Eng.
Cornell University
105 Upson Hall
Ithaca, NY 14853
(607) 255-3623

Degree: B.S., Mechanical Eng., 1987
Specialty: Combustion, Fluid Dynamics
Assigned: Aero Propulsion Laboratory

Mary C. Ritter
Dept. of Biology
Trinity University
715 Stadium Dr.
Box 937
San Antonio, TX 78284
(512) 737-4782

Degree: B.A., Biology, 1988
Specialty: Biological Oceanography
Assigned: School of Aerospace Medicine

Jacqueline Roberts
Dept. of Chemistry
Wright State University
229 Oelman Hall
Dayton, OH 45435
(513) 873-2855

Degree: B.S., Chemistry, 1986
Specialty: Toxicology
Assigned: Harry G. Armstrong Aerospace Medical Research Laboratory

James D. Roberts
Dept. of Engineering
Univ. of Texas-San Antonio
San Antonio, TX 78285
(512) 691-4490

Degree: B.S., Electrical Eng., 1988
Specialty: Order Statistic Filters
Assigned: School of Aerospace Medicine

Matthew S. Rubin
Dept. of Elect. & Compt. Eng.
Ohio University
West Green Drive
Stocker Center 329
Athens, OH 45701-2979
(614) 593-1568

Degree: B.S., Electrical Eng., 1987
Specialty: Microwave Network Theory
Assigned: Rome Air Development Center

John Y. Salinas
Dept. of Medicine
Meharry Medical College
1005 D.B. Todd Blvd.
Nashville, TN 37208
(615) 327-4537

Degree: M.S., Biochemistry, 1984
Specialty: Medicine
Assigned: Wilford Hall Medical Center

Eric O. Schmidt
Dept. of Geophysical Science
Georgia Inst. of Technology
Atlanta, GA 30332
(404) 894-3897

Degree: M.S., Physics, 1983
Specialty: Atmospheric Science
Assigned: Avionics Laboratory

Gregory A. Schoeppner
Dept. of Civil Engineering
Ohio State University
470 Hitchcock
2070 Neil Avenue
Columbus, OH 43210
(614) 292-7304

Degree: M.S., Civil Eng., 1987
Specialty: Civil Engineering
Assigned: Flight Dynamics Laboratory

Douglas J. Sego
Dept. of Organ./Behavior Mgmt.
Michigan State University
232 Eppley East
Lansing, MI 48824
(517) 353-5414

Degree: B.A., Business Info., 1987
Specialty: Organization/Behavior
Assigned: Human Resources Laboratory: Training Systems

Anne L. Siegman
Dept. of Mathematics
University of Miami
1107N 1239 Dickinson Dr.
Coral Gables, FL 33146
(305) 284-2925

Degree: B.A., Mathematics, 1986
Specialty: Mathematics
Assigned: Armament Laboratory

Jeff P. Simmons
Dept. of Engineering
Carnegie Mellon University
Pittsburgh, PA 15213
(412) 268-2684

Degree: M.S., Engineering, 1985
Specialty: Materials Science
Assigned: Materials Laboratory

Kimberly F. Smith
Dept. of Medicine
Meharry Medical College
P O Box 935
1005 D.B. Todd Blvd.
Nashville, TN 37208
(615) 327-6308

Degree: B.S., Microbiology, 1986
Specialty: Epidemiology
Assigned: Wilford Hall Medical Center

Brian K. Spielbusch
Dept. of Electrical Eng.
Univ. of Missouri-Columbia
Truman Campus
600 W. Mechanic
Independence, MO 64050
(816) 276-1250

Degree: B.S., Electrical Eng., 1985
Specialty: Electro Optics
Assigned: Weapons Laboratory

Daryl W. Sprehn
Dept. of Elect. Eng. Tech.
Oregon Inst. of Technology
3201 Campus Drive
Klamath Falls, OR 97601-8801
(503) 882-6890

Degree: B.S., Electrical Eng., 1988
Specialty: Electromagnetic Propagation
Assigned: Rome Air Development Center

Christopher Sullivan
Dept. of Psychology
Colorado State University
Fort Collins, CO 80523
(303) 491-7184

Degree: M.S., Psychology, 1986
Specialty: Experimental Psychology
Assigned: Harry G. Armstrong Aerospace Medical Research Laboratory

David A. Swick
Dept. of Mechanical Eng.
Ohio University
723 Carriage Hill
Athens, OH 45701
(614) 594-4818

Degree: B.S., Mechanical Eng., 1987
Specialty: Mechanical Design
Assigned: Materials Laboratory

Richard A. Swift
Dept. of Aero. & Mech. Eng.
University of Notre Dame
Notre Dame, IN 46556
(219) 239-5430

Degree: B.S., Aeronautical Eng., 1987
Specialty: Structural Mechanics
Assigned: Flight Dynamics Laboratory

Paul R. Tanner Dept. of Physiology Meharry Medical College Nashville, TN 37212 (615) 269-0873	Degree: Specialty: Assigned:	B.A., Psychology, 1986 Sensory Neurophysiology Wilford Hall Medical Center
David F. Thompson School of Mechanical Eng. Purdue University West Lafayette, IN 47906 (317) 494-4903	Degree: Specialty: Assigned:	M.S., Engineering, 1985 Computer Information Flight Dynamics Laboratory
Ronald C. Tomlinson Dept. of Chemistry Wright State University Dayton, OH 45435 (513) 873-2855	Degree: Specialty: Assigned:	B.S., Chemistry, 1987 Polymer Synthesis Materials Laboratory
Robert W. Tramel Dept. of Mathematics Univ. of Tennessee Space Inst. Tullahoma, TN 37388-8897 (615) 455-0631	Degree: Specialty: Assigned:	B.S., Physics, 1986 Computational Fluid Mechanics Arnold Engineering Development Center
Tien N. Tran Dept. of Elect. & Comp. Eng. University of Cincinnati Cincinnati, OH 45221 (513) 475-4247	Degree: Specialty: Assigned:	M.S., Electrical Eng., 1988 Image Coding Avionics Laboratory
John P. VanTassel Dept. of Computer Science Wright State University Dayton, OH 45435 (513) 873-2491	Degree: Specialty: Assigned:	B.A., Computer Studies, 1987 Formal Specifications Avionics Laboratory
Deborah L. Vezie Dept. of Chemical, Bio., and Materials Engineering Arizona State University COB B210 Tempe, AZ 85287 (602) 965-3313	Degree: Specialty: Assigned:	B.S., Biomedical Eng., 1987 Materials Science & Eng. Materials Laboratory
Oden L. Warren Dept. of Chemistry Iowa State University Ames, IA 50011 (515) 294-6342	Degree: Specialty: Assigned:	B.S., Chemistry, 1988 Physical Chemistry Materials Laboratory

Lisa F. Weinstein
Dept. of Psychology
Univ. of Illinois
at Urbana-Champaign
Aviation Research Lab., Q5
#1 Airport Road
Savoy, IL 61874
(217) 244-8728

Degree: M.A., Experimental Psy., 1987
Specialty: Engineering Psychology
Assigned: Harry G. Armstrong Aerospace Medical Research Laboratory

Michael A. Zmuda
Dept. of Computer Science
Wright State University
Dayton, OH 45324
(513) 873-2491

Degree: B.S., Compt. Sci. & Math, 1987
Specialty: Pattern Recognition
Assigned: Avionics Laboratory

PARTICIPANT LABORATORY ASSIGNMENT

C. PARTICIPANT LABORATORY ASSIGNMENT (Page 1)

1988 USAF/UES GRADUATE STUDENT RESEARCH PROGRAM

AERO PROPULSION LABORATORY (AFWAL/APL)
(Wright-Patterson Air Force Base)

1. Robert Riley

ARMAMENT LABORATORY (AD)
(Eglin Air Force Base)

1. George Boynton
2. David Chenault
3. Thomas Harkins
4. Hisook Min
5. Thomas Olsen
6. Anne Siegman

HARRY G. ARMSTRONG AEROSPACE MEDICAL RESEARCH LABORATORY (AAMRL)
(Wright-Patterson Air Force Base)

1. Daniel Barineau
2. Michael Ellis
3. Virginia Gunther
4. Stephen Jenei
5. Elizabeth Kavran
6. Richard Kunze
7. Deborah Mitchell
8. Jacqueline Roberts
9. Christopher Sullivan
10. Lisa Weinstein

ARNOLD ENGINEERING DEVELOPMENT CENTER (AEDC)
(Arnold Air Force Base)

1. Ben Abbott
2. Keith Krapels
3. Robert Tramel

ASTRONAUTICS LABORATORY (AL)
(Edwards Air Force Base)

1. Joel Berg
2. Lance Carter
3. William Geisler
4. David Graham
5. Gray Griesheim
6. Steven Kahn
7. Christopher Kocher
8. Michael Koharchik
9. William Moran

AVIONICS LABORATORY (AFWAL/AL)
(Wright-Patterson Air Force Base)

1. John Bambery
2. Kevin Carmichael
3. Daniel Cook
4. Edward Grissom
5. Yuhong Li
6. Randal Mandock
7. Phillip Pace
8. Eric Schmidt
9. Tien Tran
10. John VanTassel
11. Michael Zmuda

ENGINEERING AND SERVICES CENTER (ESC)
(Tyndall Air Force Base)

1. Mark Brusseau
2. Douglas Hansen
3. David McKenzie
4. James Normann
5. Steven Pierce

C. PARTICIPANT LABORATORY ASSIGNMENT (Page 2)

FLIGHT DYNAMICS LABORATORY (FDL)
(Wright-Patterson Air Force Base)

1. Kathleen Bennett
2. Susan Dumbacher
3. Bryan Foos
4. Norman Holmes
5. William Morse
6. Gregory Schoeppner
7. Richard Swift
8. David Thompson

FRANK J. SEILER RESEARCH LABORATORY (FJSRL)
(USAF Academy)

1. Bruce Bullard
2. Jennifer Joyce
3. Salvatore Miceli

GEOPHYSICS LABORATORY (AFGL)
(Hansom Air Force Base)

1. Thomas Kimble
2. Scharine Kirchoff
3. Thomas Pentecost

HUMAN RESOURCES LABORATORY
(Brooks, Williams and Wright-Patterson Air Force Bases)

1. John Allison
2. Mark Beorkrem
3. Patricia Cooper
4. Charles Drake
5. Peter Gaddis
6. Charles King
7. David Mayfield
8. Jerome Nadel
9. Peter Pidcoe
10. Douglas Sego

MATERIALS LABORATORY (ML)
(Wright-Patterson Air Force Base)

1. James Angelo
2. Darwin Boyd
3. Douglas Gagne
4. Robert Goetz
5. Andrew Hensley
6. Jeff Simmons
7. David Swick
8. Ronald Tomlinson
9. Deborah Vezie
10. Oden Warren

OCCUPATIONAL AND ENVIRONMENT HEALTH LABORATORY (OEHL)
(Brooks Air Force Base)

1. Phyllis Keys

C. PARTICIPANT LABORATORY ASSIGNMENT (Page 3)

ROME AIR DEVELOPMENT CENTER (RADC)
(Griffiss Air Force Base)

1. Richard Courtney
2. Gary Hellenga
3. Robert Petroit
4. Matthew Rubin
5. Daryl Sprehn

SCHOOL OF AEROSPACE MEDICINE (SAM)
(Brooks Air Force Base)

1. John Barnaby
2. Otis Cosby
3. Jerry Dillon
4. Ernest Freeman
5. Thomas Lane
6. Yolanda Malone
7. Conrad Murray
8. Christine Nelson
9. Julia Rennenkampff
10. Mary Ritter
11. James Roberts

WEAPONS LABORATORY (WL)
(Kirtland Air Force Base)

1. Franklin Bynum
2. Alan Jewell
3. John McCord
4. Brian Spielbusch

WILFORD HALL MEDICAL CENTER (WHMC)
(Lackland Air Force Base)

1. Antoinne Able
2. Stanley Adams
3. Bobby Larry
4. Aleshia Lewis
5. John Salinas
6. Kimberly Smith
7. Paul Tanner

RESEARCH REPORTS

RESEARCH REPORTS

1988 GRADUATE STUDENT RESEARCH PROGRAM

Technical Report Number	Title	Graduate Researcher
Volume I		
Armament Laboratory		
1	Two Dimensional Simulation of Railgun Plasma Armatures	George C. Boynton
2	Mueller Matrix Infrared Polarimetry	David Chenault
3	Determining the Aerodynamic Coefficients of High L/D Projectiles Using a Body-Fixed Coordinate System	Thomas Harkins
4	Filter Design and Signal Processing in the Development of Target-Aerosol Discrimination Techniques for Active Optical Proximity Sensors	Hisook Min
5	Viscous Grid Generation About a Two-Store Mutual Interference Problem	Thomas Olsen
6	Arima Modeling of Residuals in AD/KR TDOP Models *** Same Report as Dr. Shamma***	Anne Siegman
Arnold Engineering Development Center		
7	MULTIGRAPH Kernel for Transputer Based Systems .	Ben Abbott
8	Performance Analyses of an IR Laser Scanner System Utilizing Bragg Cell Deflectors and Modulator for Writing Directly on FPAs Under Test	Keith Krapels
9	Test of a Locally Implicit Method for the Euler Equations and an Artificial Dissipation Scheme	Robert Tramel
Astronautics Laboratory		
10	Ground-Based Experimental Control Techniques for Space-Based Structures	Joel Berg
11	An Observer Design for the AFAL Grid	Lance Carter
12	Rheometrics Stress Rheometer Applications	William Geisler

13	Stability of Jets Under the Supercritical State	David Graham
14	In-Plane Fracture in 2-D Carbon-Carbon	Gary Griesheim
15	Experimental Verification of Identification Spillover for Distributed Structures	Steven Kahn
16	The Effects of Elevated Temperature Exposure on the Strength and Microstructure of 2-D Carbon-Carbon	Christopher Kocher
17	Composite-Embedded Fiber-Optic Strain Sensors *** Same Report as Dr. David Jensen ***	Michael Koharchik
18	The Photochemistry of $\mu3$-(η-Diethylacetylene)-Decacarbonyltriosmium in Solid Argon *** Same Report as Dr. Susan Collins ***	William Moran
Engineering and Services Center		
19	Investigation of Sorption Kinetics	Mark Brusseau
20	Estimation of Jet Fuel Contamination in Soils *** Same Report as Prof. Durnford ***	Douglas Hansen
21	Soil Vapor Extraction of Volatile Organic Chemicals *** Same Report as Prof. Hutzler ***	David McKenzie
22	Evaluation of the Computer Program 'Structural Analysis for Severe Dynamic Environments'	James Normann
23	High Intensity Stress Wave Propagation in Partially Saturated Sand *** Same Report as Prof. Wayne Charlie ***	Steven Pierce
Frank J. Seiler Research Laboratory		
24	Super Conducting Thin Films by Laser Evaporation of Bulk Material	Bruce Bullard
25	The Effects of Sodium Chloride on Room Temperature Molten Salts	Jennifer Joyce
26	Unsteady Multiple Body Studies for Two-Dimensional and Three-Dimensional Experiments	Salvatore Miceli

82	An Intelligent Tutor for the IBM System/360 Assembly Language: BIGBLUE *** Same Report as Dr. Sunita Rana ***	Charles Drake
83	Underlying Distributions of the New PACE Variables	Peter Gaddis
84	Development of a General Reliability Simulation Model	Charles King
85	Development of a Candidate Task Taxonomy for Air Force Enlisted Specialties	David Mayfield
86	Form Distortions in Computer Generated Moving Objects: An Assessment of Display Parameters	Jerome Nadel
87	Oculomotor Response to Sinusoidal Stimuli	Peter Pidcoe
88	Air Force Training Evaluation System: A Case Study	Douglas Sego
Occupational and Environmental Health Laboratory		
89	Evaluation of T-9 Noise Suppressor System at McConnell AFB, Kansas	Phyllis Keys
School of Aerospace Medicine		
90	No Report Submitted at this Time	John Barnaby
91	No Report Submitted at this Time	Otis Cosby
92	Standardization of DAIM Precipitate	Jerry Dillon
93	Membrane Alterations Involved in Evoked Release of L-Glutamic Acid from Mossy Fiber Synaptosomes	Ernest Freeman
94	Development of Improved Assays for Cholesterol and Major Lipoprotein Fractions *** Same Report as Dr. Eric Johnson ***	Thomas Lane
95	Glaucoma in U.S. Air Force Aviators - USAF School of Aerospace Medicine Study Group	Yolanda Malone
96	The Separation of HDL2 and HDL3 Using the Technique of Ultracentrifugation *** Same Report as Prof. Joe Ross ***	Conrad Murray
97	Light Beam Interaction Induced by a Transition Metal Complexed to a Tridentate Ligand	Christine Nelson

98	Electromagnetic Wave Propagation in a One-Dimensional Random Medium	Julia Rennenkampff
99	Synchronization of the Chlamydomonas reinhardtii cell cycle through light-dark cycling for subsequent testing with infra-red laser light in experiments concerning human night vision	Mary Ritter
100	Application of Nonlinear Filters to VEP Data *** Same Report as Prof. H. Longbotham ***	James Roberts
Wilford Hall Medical Center		
101	Three Selected Areas of Research in Endocrinology and Metabolism	Antoinne Able
102	Utility of Sensitive Immunoradiometric Assay (IRMA) to Predict Results of Thyroliberin Stimulation Test	Stanley Adams
103	Dental Materials	Bobby Larry
104	In Vitro Culture of Human Keratinocytes with Subsequent Induction of Stratification	Aleshia Lewis
105	Autologous Bone Marrow Transplant for Poor Prognosis Lymphomas - A Pilot Dose Escalation Study of a BACE Regimen and Follow-Up	John Salinas
106	Abdominal Abscess Formation in the Mouse Model	Kimberly Smith
107	I. Impact of Diabetes Mellitus on Overall Health and Functional Status: A Comparison of Two Instruments of Measurement. II. A Comparison of the Effects of Alprazolam, Amitriptyline, and Placebo on Reaction Time in Patients with Chronic Low Back Pain	Paul Tanner

1892s

1988 USAF - UES GRADUATE STUDENT RESEARCH PROGRAM

Sponsored by the

AIR FORCE OFFICE OF SCIENTIFIC RESEARCH

Conducted by the

Universal Energy Systems, Inc.

FINAL REPORT

Prepared by:	G. Christopher Boynton
Academic Rank:	Graduate Student
Department and :	Physics Department
University:	University of Miami
Research Location:	AFATL/SAH
	Eglin AFB, FL 32542-5000
USAF Researcher:	Mr. Kenneth K. Cobb

Date:	26 Aug 1988
Contract No:	F49620-87-R-0004

Two Dimensional Simulation of Railgun Plasma Armatures

by

Manuel A. Huerta

ABSTRACT

We report on our development of a two dimensional MHD code to simulate the internal dynamics of a railgun plasma armature. We use the equations of resistive MHD. with Ohmic heating, and radiation heat transport. We use an explicit Flux Corrected Transport code to advance all quantities in time. Preliminary runs show the growth and shedding of plasma structures in response to a small perturbation upon an initial equilibrium. We completed a run of an isothermal plasma armature that reached the end of a 1 m barrel. We have done many debugging runs of a full radiation heat transport model. At this point we are completing the revised code for this model. We expect to run it in a Cray-2 in the near future.

Acknowledgements

I would like to thank the Air Force Systems Command and the Air Force Office of Scientific Research for sponsorship of this research. I would also like to thank Universal Energy Systems for the efficient way in which they administered the USAF - UES Summer Faculty and Graduate Student Research Program.

I spent the summer at AFATL together with my graduate advisor Dr. M. A. Huerta. Our experience was productive and enjoyable thanks to the cooperation we received from many people at AFATL. First we would like to thank Dr. Sam Lambert for making it possible for us to use the excellent computer resources at AFATL as well as the Cray-2 at the AFWL, Kirtland AFB. Next we would like to thank Mr. Kenneth K. Cobb who helped us so many times in actually getting access to the resources that we needed. We also thank him for interesting discussions of work in rail guns, specially his own B dot coil analysis. We thank Capt. E. Cottle for setting us up with abundant disk space and other resources on the VAX 8650 at site A15. and Mr. Andy Marino for his system assistance on that machine. We also thank the staff of the RSPL at AFATL, specially Mr. Mike Wallace, Capt. Mike Mets, and Mr. Phil Destin, for setting us up on their VAX 785, and for their assistance in getting postscript output from the Printserver 40. We also used the Vax 8650 at the IPL at AFATL and we thank the staff, specially Mr. Lee Prestwood, Mr. Larry Neal, and Matt Shannon. These two machines were valuable in themselves for debugging purposes, but they were essential to let us connect to the UV2 machine at AFATL through which we networked via TELNET to the Cray at AFWL. Last, but not least, we thank Mr. Ron Hunt of AFATL for his help in setting up our accounts at the AFWL and other assistance.

I. INTRODUCTION

My advisor has had contacts with the AFATL/SAH branch since the beginning of their heavy involvement with research on electromagnetic railguns with a plasma armature. An impressive railgun facility has been built on Okaloosa Island at site A15 and there is quite a bit of experimental activity on diagnostics of the arc plasma armature. There are also people there working on developing one dimensional computer simulations of the plasma armature.

I have been working on my doctoral dissertation with Dr. Huerta under a recently expired AFOSR grant on a two dimensional simulation of armature plasmas but we still have not completed the work. One of our principal needs was access to a supercomputer to run our programs. We also could profit from abundant access to a VAX 8650 such as is available at the site A15 railgun facility for debugging purposes. These common interests made it appear that spending a summer of intensive research work would be valuable.

II. OBJECTIVES OF THE RESEARCH EFFORT

Our work centers on continuing the development of a two dimensional time dependent simulation of plasma armatures. We model the plasma with the equations of resistive MHD and we use a two dimensional fully explicit FCT code to advance all quantities in time. The physical effects that we include in our model are the same as in the steady, one dimensional model of Powell and Batteh[1]. Therefore we leave out viscosity, and other effects that can be important in a boundary layer. A good deal of effort has also been expended on developing graphical methods that allow convenient display of the results.

We have done several runs in the University of Miami's VAX 8650, which does about 1,000 steps per hour of CPU time for a plasma with an adiabatic energy equation

and a calculational grid with 20 by 240 cells. Dr. Huerta and I presented a paper[2] with the equations and some of the results of this work for the adiabatic case. We continued the calculation after that paper and in Figure 1 we show the pressure plotted vertically over the rectangular grid that covers the 2-dimensional plasma. Here the pressure distribution is shown after 200,000 time steps that represent an elapsed time of 89.87 μsec. By this point the VAX 8650 has accumulated about 200 hours of CPU time and we have to keep reducing the time step size to avoid numerical instabilities.

Clearly this problem is one that requires a supercomputer. Our objective during the summer of 1988 was to run isothermal and fully heat conducting models at the VAX 8650 available at site A15. We also intended to submit runs at the Cray located at the Air Force Super Computer Center (AFSCC) at the Air Force Weapons Laboratory (AFWL) at Kirtland AFB.

III. COMPUTER FACILITIES UTILIZED IN THE WORK

From the start we enjoyed excellent cooperation from everyone we were connected with. Mr. Kenneth K. Cobb always got us in touch with the right person to get what we needed. We were soon running and debugging in the site A15 VAX 8650 thanks to the assistance of Capt. E. Cottle and Mr. Andy Marino. The early work was delayed because the brand new VAX 8650 would crash often. Another problem was the need to bring down the 8650 because it is not protected against lightning. This was specially bothersome because thunderstorms are common here in the summer. These problems will be remedied when the 8650 is moved to the new building being constructed at site A15 where it will have the proper lightning protection and power conditioning equipment.

We invested some time in learning to use the Cyber 176 at the Math Lab at Eglin

AFB. We gave this up, however, because it was clear that this machine would not be much faster than the 8650 at site A15 because of the many competing users. In order to network to the Cyber, and later on to the Cray, we had to go to the main base, which is about 20 miles away from site A15 because the site is not yet in the network. That is another thing that will be improved when the new building is completed.

We did our networking and computing at the main base using two computer facilities. First the Radar Signal Processing Laboratory (RSPL) where there is a VAX 785. Here we were assisted by Mr. Mike Wallace, and others. We also used the Image Processing Laboratory (IPL) where there is a VAX 8650. From either of these labs we connected to the Math Lab's VAX 8650, called node UV2. From this node we could connect to the Cyber, or via TELNET, later on, to the Cray at the AFSCC. Clearly there were a lot of machines involved and it took time to get accounts in all of them. We encountered crashing problems at these labs too. The IPL's 8650 was brand new and crashed often for its own reasons. A faulty air conditioning system also brought both machines down several times.

We obtained our account numbers in the CRAY-2 at the AFSCC around the beginning of our 7th week. Up until that moment we had been spending most of our time working with the VAX 8650 at site A15. From that moment on we spent most of our time at the main base networking to the Cray and debugging at the IPL computer.

IV. WORK ACCOMPLISHED

We did many runs of a fully heat conducting model, although with fixed ionization fractions. Even with that simplification we found many bugs in the program. The bugs sometimes took time to show themselves and for us to understand what was

happening. Sometimes we thought we were getting a numerical instability and we started to develop an implicit code to advance the temperature in time. Then it turned out that we simply had a programming error. Even now, at the end of the summer research period, we have not had a completely successful run of the fully heat conducting program. We believe that we are close to that goal, however, and that the explicit FCT method will run successfully with a time step size that is not unreasonably small.

We have developed a successful program to calculate the ionization fractions from the Saha equations and include them in our main program. To save CPU time, however, we have developed a lookup table of true temperature and ionization fractions in terms of pressure and density. The main program will interpolate in the table instead of using the Saha equations at each grid point, at each time step.

Rather than continue running the full program we decided it would be wise to use the last few weeks learning to use the Cray and running an isothermal model. We have also been learning the use of the DISSPLA graphics system that is available in the Cray. This seems very powerful but is different from the NCAR system that we have been using.

V. ISOTHERMAL PLASMA

We show some of the results obtained for the isothermal run at the site A15 VAX 8650. Figure 2 shows the progress of the run. It was first submitted on 11 August, 1988 at 10:51. By 11:41 it had done 1000 time steps. By 12:24 it was up to 2000 time steps, and so on. However, it can be seen than in other days it might not run at all, depending on the weather, and whether the system manager could restart it when we were physically not there but working at the main base. The table shows that it would run at a rate of about 1500 time steps per hour of CPU time in the

8650. The run ends when the armature has advanced one meter. We know that this takes about 120000 time steps. Even as this report is being written it has done some 62000 time steps. We will take it down on the last day and finish it at the University of Miami's VX 8650. It is fortunate for us that we have been working with fully compatible machines.

We use a computational grid that has 20 cells in the short direction from rail to rail. The long direction of the grid begins at the rear of the projectile at cell 1 and extends toward the breech for a length of 200 cells. The conducting plasma ends at cell 100. Beyond that there are 100 cells of low density, nonconducting plasma that extends to the end of the computational region. The boundary condition at the 200th cell is very passive so as to have no effect. Essentially any plasma that gets to the end of the computational region with nonzero velocity simply leaves. The nonconducting region is made large so that as the conducting plasma expands toward the rear it will not reach the end of the computational region by the time the run ends. This way we can follow the phenomena that may occur back there.

Figure 3 shows the density profile over the entire grid of 20 by 200 cells after 37.000 time steps. The highest density shown is some 15 kg/m^3. The lowest density is at the rear, with a value of about 0.1 kg/m^3, but plotted with zero height. Figure 4 shows the pressure profile magnified near the region where the plasma density is very low and the the plasma is taken to be nonconducting. Here the equilibrium is showing some strong disturbances building up. Figure 5 shows the vector field for the current density vector J. It shows a deformation of the boundary between the conducting and the nonconducting plasmas, and a buildup of current density right at the interface.

From the above figures it can be seen that at least in the isothermal case, where

the initial equilibrium is 1 dimensional, the plasma seems pretty sturdy. The deformations at the rear boundary grow but do not seem to have a terribly disruptive effect upon the plasma.

VI. RECOMMENDATIONS

We believe it is not self serving to recommend that this work be continued. We have spent about two years working on this difficult problem and we are close to the point where we will have a successful code. This sort of two dimensional simulation will do a lot to obtain further insights into the behavior of plasma armatures. The principal insights so far have been provided by the one dimensional models. Most of the 1 dimensional models have been steady, along the lines of Ref. 1. Recently Batteh and Rolader[3] have reported on a time dependent 1 dimensional simulation.

Our work encompasses all that 1 dimensional work and extends it to 2 dimensions where there are profound differences. For example, not only would the ussal one dimensional equilibrium develop instabilities of various sorts, but a 2 dimensional equilibrium does not even exist. We are hopeful to continue this work and develop impressive displays of the armature simulation. We are excited that the AFSCC provides output to 16mm film. It would really be nice to have movies of the armature simulation in a variety of conditions.

We expect that our accounts at the A15 and the UV2 Vaxes 8650, and at the AFSCC Cray will continue for a while longer so we can conclude this stage of our work.

REFERENCES

1. Powell, J. D., and Batteh, J. H., "Plasma Dynamics of an Arc-Driven Electromagnetic Projectile Accelerator," J. Appl. Phys., **52**, 2717 (1981)

2. Huerta, M. A., and Boynton, G. C.,"Two Dimensional Time Dependent MHD Simulation of Plasma Armatures", Proceedings of the 4th Symposium on Electromagnetic Launch Tecchnology", Austin, Texas, April 1988.

3. Batteh, J. H., and Rolader, G. E., "Modeling of Transient Effects in Railgun Plasma Armatures," U. S. Army Ballistic Research Laboratory, Contract Report No. BRL-CR-567, March 1987.

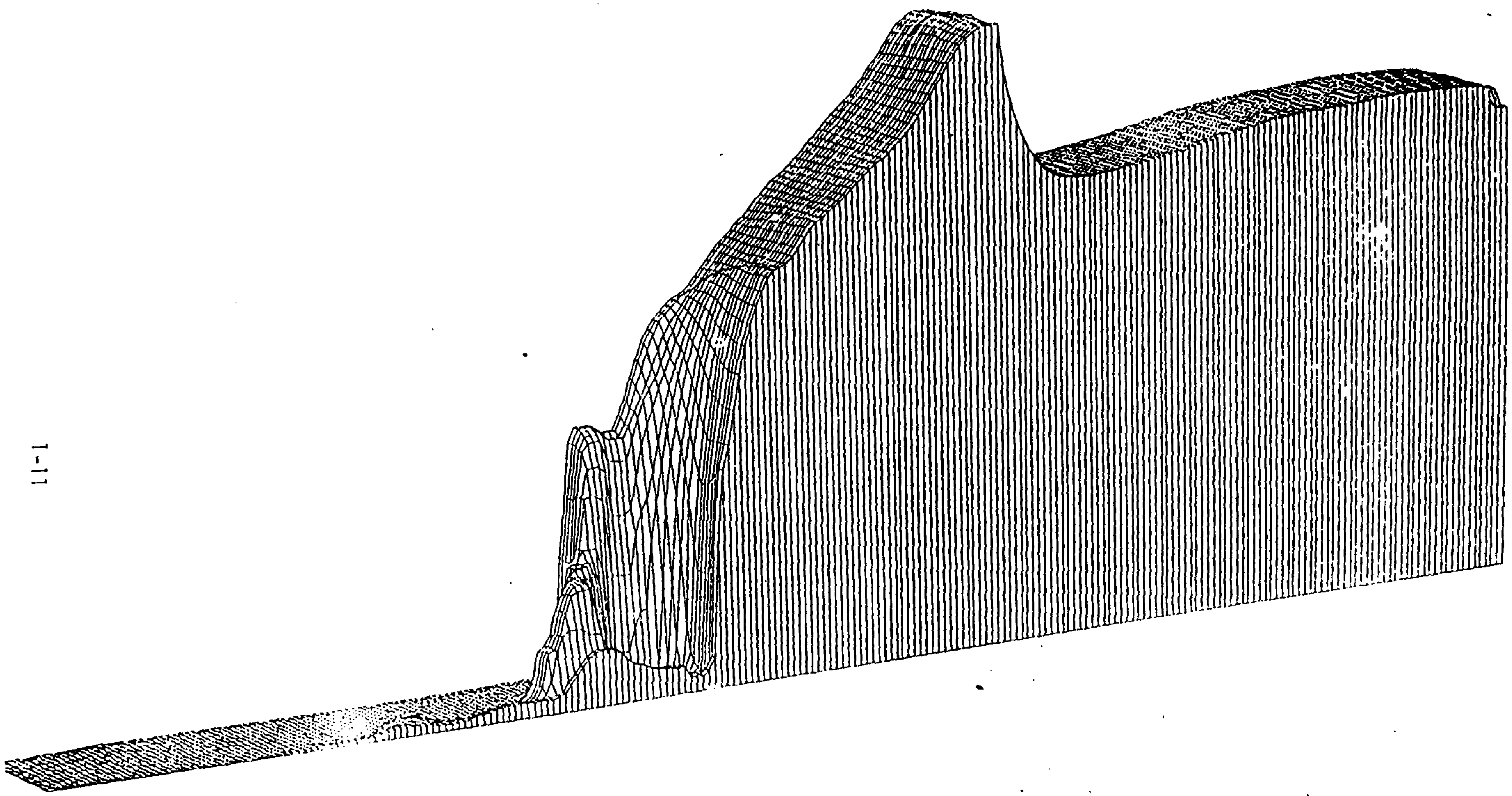

Figure 1

Time 8.9873E-05 s, SFRM = 4.9E-02 m, VFRM = 1.1E+03 m/s, AFRM = 1.22E+07 m/s^2
Projectile toward right
1_240_rho_200000.psc

```
Directory DJA2:[CHRISTPF.ISO_BIG]

M_JX_000000.OUT;2     11-AUG-1988 10:51
M_JX_000000.OUT;1     11-AUG-1988 10:48
M_JX_001000.OUT;1     11-AUG-1988 11:41
M_JX_002000.OUT;1     11-AUG-1988 12:24
M_JX_003000.OUT;1     11-AUG-1988 13:08
M_JX_004000.OUT;1     11-AUG-1988 13:56
M_JX_005000.OUT;1     17-AUG-1988 14:22
M_JX_006000.OUT;1     17-AUG-1988 15:04
M_JX_007000.OUT;1     17-AUG-1988 15:47
M_JX_008000.OUT;1     17-AUG-1988 16:29
M_JX_009000.OUT;1     17-AUG-1988 17:12
M_JX_010000.OUT;1     17-AUG-1988 17:56
M_JX_011000.OUT;1     18-AUG-1988 07:04
M_JX_012000.OUT;1     18-AUG-1988 07:47
M_JX_013000.OUT;1     18-AUG-1988 08:30
M_JX_014000.OUT;1     18-AUG-1988 09:13
M_JX_015000.OUT;1     18-AUG-1988 10:01
M_JX_016000.OUT;1     18-AUG-1988 10:47
M_JX_017000.OUT;1     18-AUG-1988 11:29
M_JX_018000.OUT;1     18-AUG-1988 12:11
M_JX_019000.OUT;1     18-AUG-1988 13:15
M_JX_020000.OUT;1     18-AUG-1988 14:03
M_JX_021000.OUT;1     18-AUG-1988 14:50
M_JX_022000.OUT;1     18-AUG-1988 15:51
M_JX_023000.OUT;1     19-AUG-1988 08:28
M_JX_024000.OUT;1     19-AUG-1988 09:10
M_JX_025000.OUT;1     19-AUG-1988 09:53
M_JX_026000.OUT;1     19-AUG-1988 10:35
M_JX_027000.OUT;1     19-AUG-1988 11:18
M_JX_028000.OUT;1     19-AUG-1988 12:00
M_JX_029000.OUT;1     19-AUG-1988 12:42
M_JX_030000.OUT;1     19-AUG-1988 13:25
M_JX_031000.OUT;1     19-AUG-1988 14:07
M_JX_032000.OUT;1     19-AUG-1988 14:49
M_JX_033000.OUT;1     19-AUG-1988 17:16
M_JX_034000.OUT;1     23-AUG-1988 14:37
M_JX_035000.OUT;1     23-AUG-1988 15:20
M_JX_036000.OUT;1     23-AUG-1988 16:06
M_JX_037000.OUT;1     23-AUG-1988 16:49
M_JX_038000.OUT;1     23-AUG-1988 18:20

Total of 40 files.
```

Figure 2. The file M_JX_001000.out;1 was produced on 11-August-1988, at 11:41. The figure shows the progress of the calculation up to 38,000 time steps.

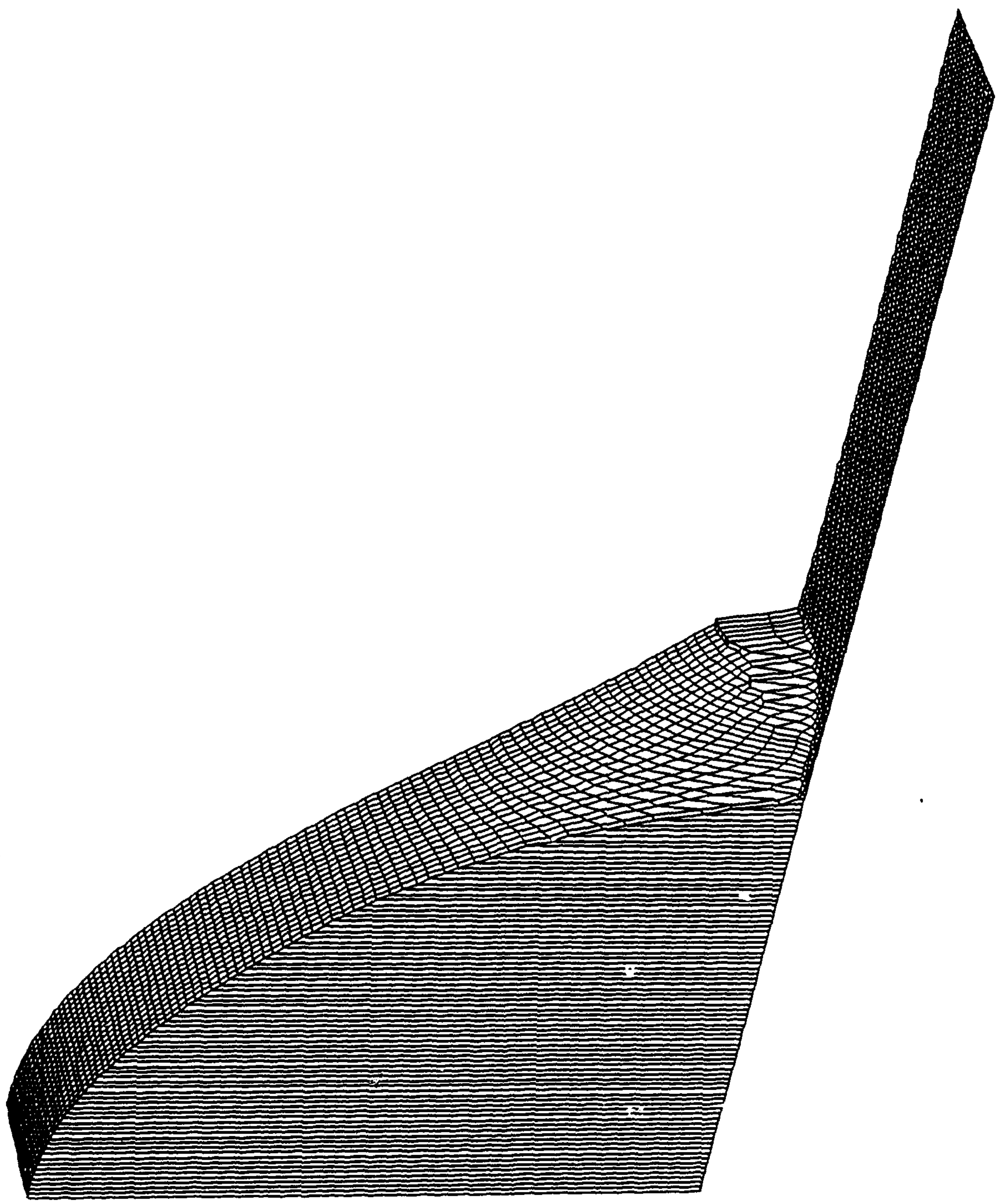

Figure 3. Plasma density profile after 37,000 time steps. The time step **size** is about **3.7** nanoseconds, and the elapsed time is 1.38E-4 sec.in this as well as in all the figures that follow.

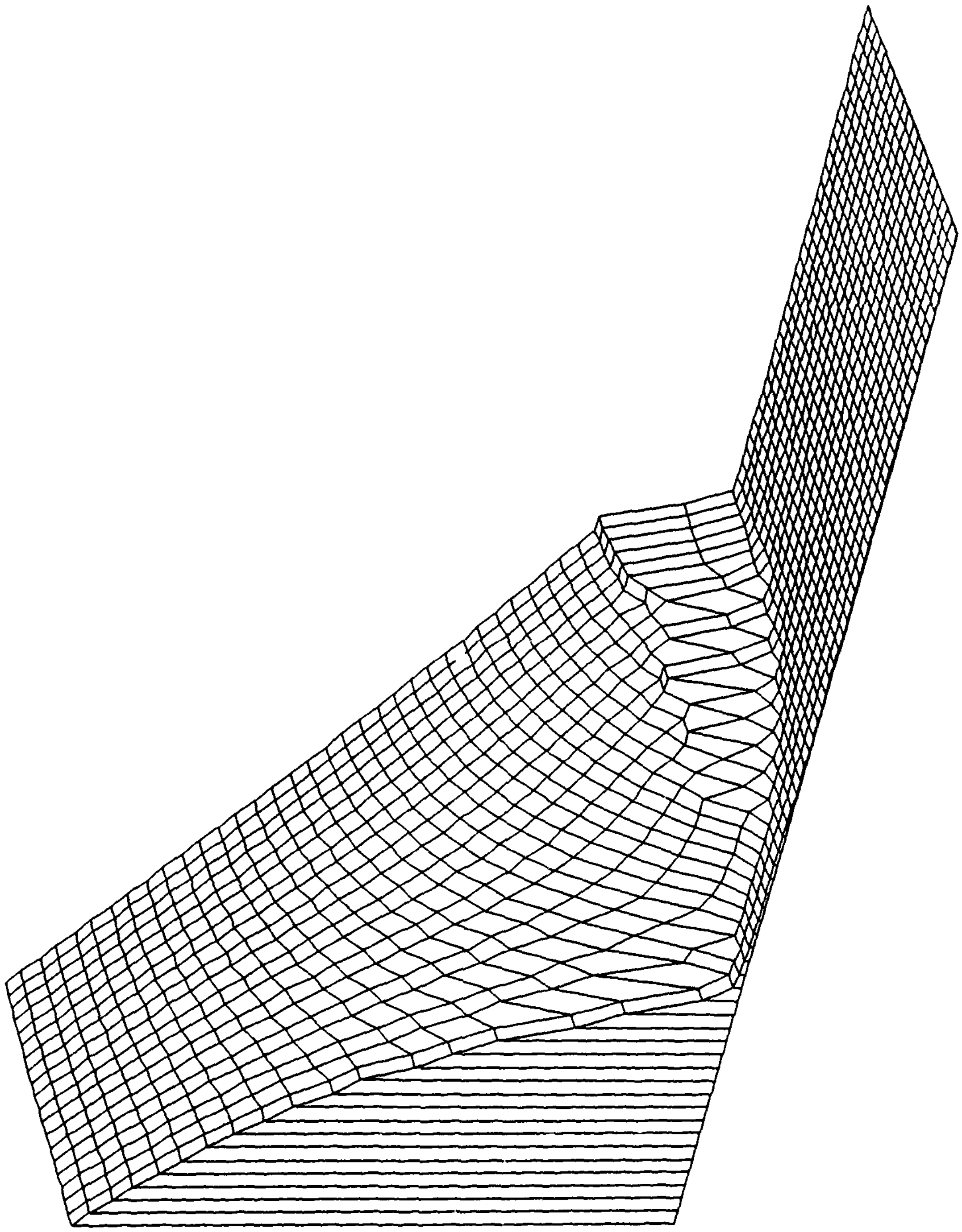

Figure 4. Magnified view of the density profile near the end of the conducting plasma region.

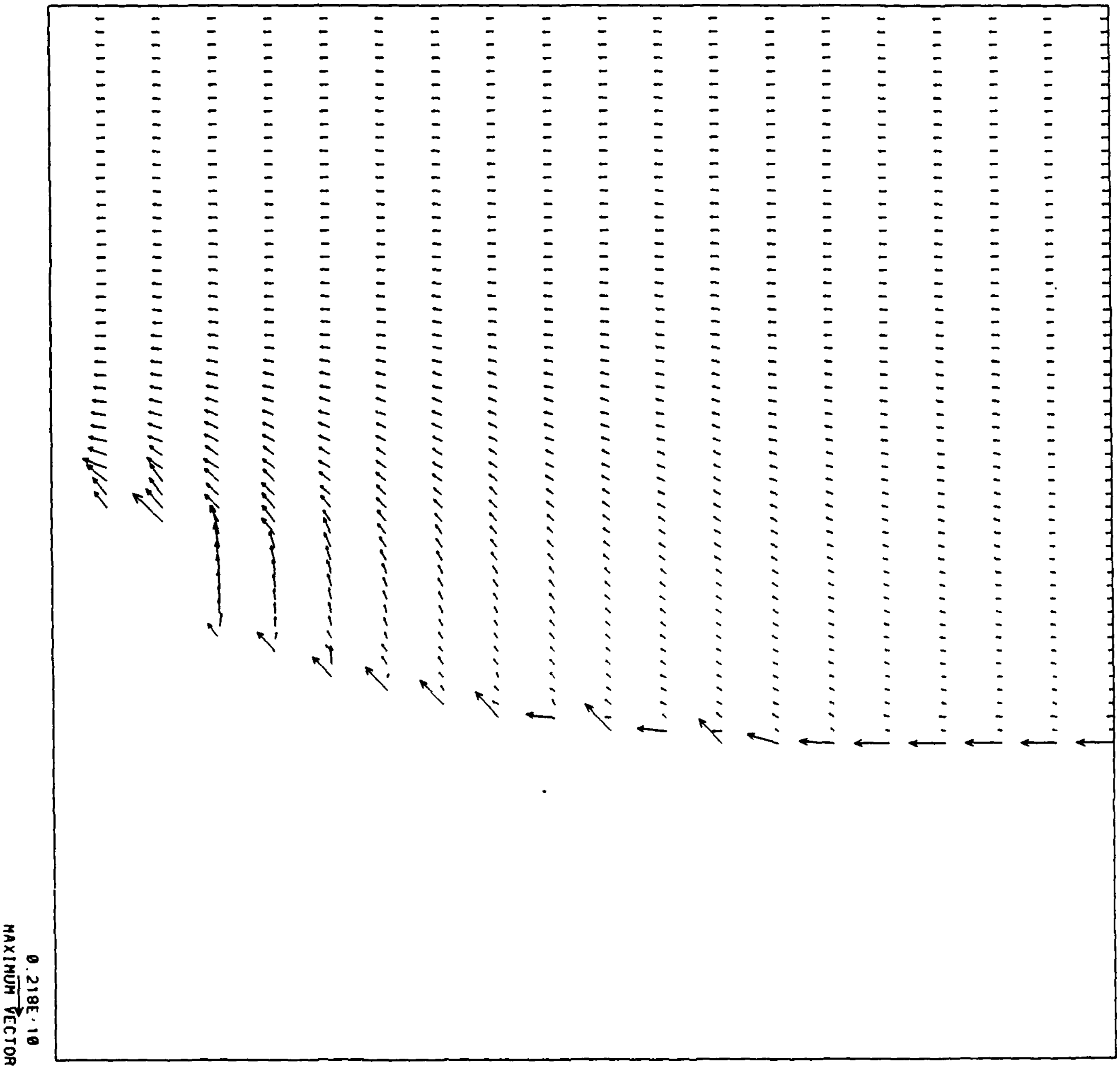

Figure 5. The current density vector field J. It shows a concentration at the end of the conducting region.

1988 USAF-UES SUMMER FACULTY RESEARCH PROGRAM/

GRADUATE STUDENT RESEARCH PROGRAM

Sponsored by the

AIR FORCE OFFICE OF SCIENTIFIC RESEARCH

Conducted by the

Universal Energy Systems, Inc.

FINAL REPORT

MUELLER MATRIX INFRARED POLARIMETRY

Prepared by:	David B. Chenault
Academic Rank:	Graduate Student
Department and University:	Physics Department University of Alabama in Huntsville
Research Location:	USAF AFATL/AGA Eglin AFB, FL 32542
USAF Researcher:	Dennis Goldstein

Date:	22 Aug 88
Contract No:	F49620-88-C-0053

Mueller Matrix Infrared Polarimetry

by

David B. Chenault

ABSTRACT

A polarimeter which operates in the infrared is described. The instrument is capable of measuring the Mueller matrix of crystalline or liquid samples throughout the 3 to 14 μm wavelength region using various infrared lasers or filtered blackbodies as sources. Mueller matrix processing is done immediately following data acquisition. The computer system which advances the rotating elements, acquires and processes the data is described. A system simulation was accomplished and an error analysis is presented. Results using a CO_2 laser source and several known samples are given. Issues for further research are discussed.

ACKNOWLEDGEMENTS

I wish to acknowledge the Office of Scientific Research for their sponsorship of this program. Universal Energy Systems must also be mentioned for their administrative efforts and for making a potentially nightmarish problem in paperwork virtually painless.

I wish to extend my heartfelt gratitude to Mr. Dennis Goldstein as my Effort Focal Point and co-worker. He has directed without dictating and given all my thoughts and concerns consideration equal to his own. His support and consideration were instrumental in making this experience truly rewarding. Lisa Collins must also be mentioned. She carried out many hours of valuable work in running simulations of the system and exhaustive literature searches. I would also like to thank the technicians of the Special Projects Laboratory, Michael Vantassel, Howard McCormick, and Voncile Houston, who had a solution to almost every problem I came across. The people of the AGA branch must also be mentioned for their friendship and congeniality.

I. Introduction

During my tenure as a graduate student, I have become involved with infrared polarimetry, the study of polarization in the infrared region of the spectrum. My work at the University of Alabama in Huntsville (UAH) includes the study of polarization over a broad wavelength range, or spectropolarimetry. The work conducted at Eglin Air Force Base as part of the Graduate Student Research Program is directly related to this work in that the same data reduction algorithm and experimental techniques are used. The laser polarimetry project is indeed somewhat simpler since only one wavelength is investigated at a time. It has thus become a proving ground for experimental methods that will be used in the spectropolarimetry project at UAH as well as being a valuable experiment in its own right.

The air-to-air guidance section (AGA) located at the Air Force Armament Laboratory (AFATL) at Eglin Air Force Base has long been concerned with the development of electrooptical materials for the infrared. Spatial light modulators and programmable masks will become essential in the near future for Air Force tactical applications. The construction of the laser polarimeter at Eglin is essential to characterize the basic material properties of the materials of interest. This data base will provide information upon which further research into the devices themselves will depend.

I have co-authored several papers with Dr. Russell Chipman, professor of physics at UAH, and Mr. Dennis Goldstein, researcher at AFATL/AGA, Eglin AFB, and had several papers presented at professional meetings. The work conducted at Eglin will become part of my dissertation in conjunction with the ongoing work at UAH.

II. Objectives

There is currently a shortage of data in the infrared on

electrooptical materials. This information will become increasingly important as emphasis on the infrared for seekers and other tactical devices increases. One technique to alleviate this shortage is through Mueller matrix infrared polarimetry. If the Mueller matrix of a material is known, the polarization properties are also known. Ideally, the Mueller matrix should be known for a large region of the infrared spectrum, but data at even single laser wavelengths is scarce.

My assignment as a participant of the 1988 Graduate Student Research Program was to construct a laser polarimeter to make measurements of electrooptical materials at one particular laser line. I was to be responsible for writing the necessary software as well as the interfacing of various hardware components. Proper calibration was also a necessary part of my duties.

III. Background

Polarimetry is the optical discipline concerned with measuring the polarization state of a light beam and the polarizing and retarding properties of materials. A polarimeter is an optical instrument used for the determination of the polarization state of a light beam. Given the knowledge of how the polarimeter itself acts on the light, the polarization change produced by inserting a sample into the polarimeter may be determined. We describe here a polarimeter which operates in the infrared wavelength region and uses the Mueller matrix polarization formulation to process data and express results.

Our polarimeter is designed to be operated over the 3 to 14 μm spectral region using various sources. This spectral region is of great interest for evaluation of materials used in elements of optical processing systems or thermal imaging systems, yet polarization studies of only a few prominent materials have been made. The work discussed in this paper was all done with a CO_2 laser source at 10.6 μm.

We chose a data processing prescription that has been used in ellipsometry and is described by Azzam[1] and by Hauge[2]. This scheme uses two fixed polarizers and two rotating waveplates in a configuration described in the next section of this paper. Mueller matrix elements and Stokes vectors are used to represent the polarization elements and polarized light, respectively. We use the Mueller matrix formulation because it is preferable for experimental work where scattering and depolarization measurements are required. Waveplates are rotated at different but harmonic rates and a modulation of the detected intensity results. The Mueller matrix of the sample is found through a relationship between the Fourier coefficients of a series representing the modulation and the elements of the sample matrix.

IV. Optical Configuration and Element Description

Figure 1 shows a block diagram of the polarimeter. This configuration is typical of automatic *rotating compensator* Mueller matrix ellipsometers. The system can be divided into five sections, the source, the polarizing optics, the sample, the analyzing optics, and the detector.

The polarizing optics consist of a fixed polarizer and quarter wave plate both mounted in computer controlled rotating stages. The sample region is followed by the analyzing optics which consist of a quarter wave plate followed by a fixed polarizer. The source may be polarized, partially polarized, or unpolarized. Polarization sensitivity of the detector is not important since the orientation of the final polarizer does not change.

The instrument is detailed in Figure 2. The source is a CO_2 laser operating at 10.6 μm. The power output of the laser is more than enough to overcome attenuation of all the polarimeter elements. In fact, three zinc selenide (ZnSe) beamsplitters were needed to reduce the power of the beam to a level acceptable to the detector. The configuration shown

transmits 0.1% of the total power emitted by the laser to the polarizing optics. The first beamsplitter provides a convenient place to monitor the power output of the laser. This proved to be an important consideration and was accomplished with a pyroelectric detector. The beam is then chopped using a rotating wheel with apertures. It continues on to pass through the polarimeter elements including the sample, and then is focused on the detector by a ZnSe lens. The detector element is mercury cadmium telluride (HgCdTe) and is mounted in a dewar which is filled with liquid nitrogen and has a hold time of several hours. A preamp provides a bias voltage to the detector and outputs a maximum signal of 10 volts.

The polarizer P_1 is a Brewster angle window polarizer with a specified extinction ratio of 10,000:1. The quarter wave plates are cadmium sulfide zero order waveplates giving nominally $90^o \pm 2^o$ phase shift between orthogonal polarization states at 10.6 μm. The analyzer P_2 is a wire grid polarizer with a specified extinction ratio of 1,000:1.

V. Alignment and Calibration

The optical elements were aligned using a HeNe laser. The CO_2 laser was aligned first using infrared indicator material, then actually maximizing the signal from the detector. The more difficult calibration of the instrument involved finding the orientations of the polarizers and retarders. Although nominal orientations are given by the manufacturers, we must have reference orientations established after the elements are mounted. The sensitivity of the instrument to this misalignment is large and could lead to rather large errors (discussed in the simulation section below). Reference orientations were found experimentally.

Two sources were used in the calibration; a blackbody, and the CO_2 laser. It was found that the blackbody was more stable and allowed minima and maxima to be found with a greater degree of precision in the alignment of the

polarizers. For measurements, the first polarizer was to be placed in the beam oriented with the transmission axis parallel to the known laser polarization (vertical, hereafter defined as 0°). The second polarizer was placed in the beam and minima and maxima were found.

A quarter wave plate was then placed in the beam between the polarizers at 45° and the second polarizer was oriented at 90°. The quarter wave plate is highly wavelength dependent and passes the blackbody radiation with varying degrees of retardation, but the crossed polarizers do not transmit light that is not retarded approximately one-quarter wave and so a maximum with the quarter wave plate at 45° is found. The second quarter wave plate was similarly oriented. The polarizers were then made parallel and both waveplates were placed in the beam at 45°. For monochromatic light this configuration would completely extinguish the beam; for polychromatic light, the result is a minimum. The retarders were tuned together and separately to further refine the orientation of the fast axes. The blackbody was replaced with the laser and the result was confirmed within the limits of the laser stability.

VI. Element Control and Data Acquisition

The polarimeter is completely under computer control. All four polarizing elements, the two linear polarizers and two quarter wave retarders, are mounted in computer controlled rotary stages. These are connected to a stage controller which is itself programmable, but in order to tie together the functions of stage control and data acquisition, the stage controller is connected to a computer. All the software necessary for calibration procedures, data acquisition, and processing has been stored on this computer. The computer is easily programmed in BASIC to control the rotary stages.

Data acquisition takes the form of measuring voltages from two detectors, a pyroelectric detector which monitors

the power level prior to the polarimeter elements, and the HgCdTe detector which detects the modulated intensity from the polarimeter elements. Both of these detectors are monitored by multimeters which are connected directly to the computer via a IEEE 488 data bus.

The computer is then programmed in BASIC to rotate the waveplates and query the multimeters. The second waveplate is rotated five times the rate of the first. Data is typically collected for every two to six degrees of rotation of the first waveplate. The stages are stopped completely after each incremental rotation. The resulting data set is a modulated waveform which is then processed according to the algorithm given by Azzam. The waveform is expressed as a Fourier series

$$a_o + \sum_{n=1}^{12} \left(a_n \cos n\omega_1 t + b_n \sin n\omega_1 t \right)$$

where the Fourier coefficients are functions of the sample Mueller matrix elements, as follows:

$a_0 = M_{11} + M_{12}/2 + M_{21}/2 + M_{22}/4$

$a_1 = 0$	$b_1 = M_{14} + M_{24}/2$
$a_2 = M_{12}/2 + M_{22}/4$	$b_2 = M_{13}/2 + M_{23}/4$
$a_3 = -M_{43}/4$	$b_3 = -M_{42}/4$
$a_4 = -M_{44}/2$	$b_4 = 0$
$a_5 = 0$	$b_5 = -M_{41} - M_{42}/2$
$a_6 = M_{44}/2$	$b_6 = 0$
$a_7 = M_{43}/4$	$b_7 = -M_{42}/4$
$a_8 = M_{22}/8 + M_{33}/8$	$b_8 = -M_{23}/8 + M_{32}/8$
$a_9 = M_{34}/4$	$b_9 = -M_{24}/4$
$a_{10} = M_{21}/2 + M_{22}/4$	$b_{10} = M_{31}/2 + M_{32}/4$
$a_{11} = -M_{34}/4$	$b_{11} = M_{24}/4$
$a_{12} = -M_{22}/8 - M_{33}/8$	$b_{12} = M_{23}/8 + M_{32}/8$

These expressions are then inverted to give the Mueller matrix elements as functions of the Fourier coefficients:

$M_{11} = a_o - a_2 + a_8 + a_{10} + a_{12}$
$M_{12} = 2a_2 - 2a_8 - 2a_{12}$
$M_{13} = 2b_2 + 2b_8 - 2b_{12}$
$M_{14} = b_1 - 2b_{11} = b_1 + 2b_9$
$M_{21} = -2a_8 + 2a_{10} - 2a_{12}$
$M_{22} = 4a_8 + 4a_{12}$
$M_{23} = -4b_8 + 4b_{12}$
$M_{24} = -4b_9 = 4b_{11}$
$M_{31} = -2b_8 + 2b_{10} - 2b_{12}$
$M_{32} = 4b_8 + 4b_{12}$
$M_{33} = 4a_8 - 4a_{12}$
$M_{34} = 4a_9 = -4a_{11}$
$M_{41} = 2b_3 - b_5 = -b_5 + 2b_7$
$M_{42} = -4b_3 = -4b_7$
$M_{43} = -4a_3 = 4a_7$
$M_{44} = -2a_4 = 2a_6$

The measured Mueller matrix is output together with the modulated waveform.

VII.System Simulation and Error Analysis

An integral part of the calibration and error analysis of the instrument is the mathematical simulation of the optics. The simulation provides a data base from which adjustment of the orientation of the optics is determined. The simulation also shows in what manner and to what extent limitations in the calibration procedure produce error. Perhaps most importantly it provides insight to the response of the instrument as various parameters are changed.

The simulation is performed on a personal computer. The optics are simulated using the Mueller calculus with as many parameters included as possible involving the orientation and properties of the optical elements. The polarized output beam of the CO_2 laser is represented by a Stokes vector for an unpolarized beam followed by the Mueller matrix for an ideal polarizer oriented along the plane of

polarization of the laser beam. This produces no demands on the model within the required accuracy and simplifies the simulation somewhat. Mueller matrices representing the polarizers, retarders, and a sample are multiplied in the proper order. The polarizers are assumed to be ideal. This assumption is proved valid in experiment - it produces negligible error.

The matrices representing the action of the retarders are functions of the orientation of the fast axis. Since the second retarder is rotated at five times the rate of the first, any initial error in the orientation of the second waveplate is magnified by a factor of five. A variable representing an initial misalignment of the fast axis in relation to the polarizers allows the effects of any misalignment to be seen. In addition, deviations from an exact value of 90 degrees retardance is also modeled.

The sample in almost all cases is assumed to be the identity matrix which, in the Mueller calculus, represents no change in the incident light beam and thus *no sample*. A few simulations have been run with matrices for known optical elements to test the algorithm used and to compare theoretical intensity values with those found experimentally.

The simulation finds the output Stokes vector from the last polarizer. The first element of the Stokes vector is examined as the intensity data that the detector actually sees. The angular increments of the retarders are 5° (stepped through 180°) and 25° resulting in 36 intensity readings. This intensity information is then run through a routine to calculate the Fourier coefficients of the modulated output signal. The relations between the Fourier coefficients and the Mueller matrix elements as described by Azzam are then employed to calculate the sample matrix.

In short, we start with a known sample, use the data reduction algorithm as it will be used in practice, and calculate the sample matrix. An error matrix is then

computed to show the difference in the matrix we started with and the computed result. Through the error matrix, the result of small misorientations of the optical elements are easily seen. The simulation also plots the intensity modulation as the angle of the retarders is changed. Some examples of the simulated Mueller and error matrices with small misalignments are shown in Table 1. Table 2 includes the effect of deviations in the retarders from the ideal retardance of 90 degrees.

Several interesting results are seen. The fourth row and fourth column, except for the M_{44} element, are not affected by changes in the alignment of the elements. A given misalignment or combination of misalignments produces changes only in certain elements of the Mueller matrix. Different combinations affect different elements by differing amounts as is obvious in Table 1. If the transmission plane of the second polarizer is misaligned by a small positive angle, the M_{13}, M_{23}, and M_{32} elements are affected whereas a small misalignment in the orientation of the fast axis of the first retarder causes errors in the M_{31}, M_{23}, and M_{32} elements.

These error matrices and Mueller matrices are tabulated and are used to calibrate the orientation of the optical elements in the experimental setup to a high degree of accuracy. A comparison of the computed Mueller matrix and the Mueller matrix calculated from measured intensity data indicates how the elements should be moved to reduce the error matrix. The various combinations are clearly numerous, but several iterations reduces the experimental error matrix to acceptable values.

VIII. Mueller Matrix Processing and Results

The polarimeter was exercised with three samples. The first sample was the trivial case of no element at all while the other two were a linear polarizer and a half wave plate. The experimental modulated intensity pattern for all three

samples is shown in Figure 3 together with the simulation results in Figure 4. It is clear from these plots that the experimental results are virtually identical with those predicted by our simulation. The experimental Mueller matrix which the data processing program produced was also clearly recognizable as the matrix representing the optical element under scrutiny. (At this stage of the development of our instrument, matrix element error is on the order of 5%.)

IX. Issues

There are several issues to be considered in the construction of a Mueller matrix polarimeter. Every effort must be made to increase the signal to noise ratio in a system that is inherently noisy. The stability of the CO_2 laser and the noise inherent in the detector must be addressed. The number of optical elements and the number of measurements necessary to calculate the Mueller matrix also increases the possibility of error, either systematic or random.

In a measurement in which the modulation of the intensity of the beam is recorded, the stability of the laser is paramount to finding accurate data. Stability has been briefly discussed as problematic in finding the proper orientation of the optical elements. A blackbody was used to assist in this calibration, but this technique is not applicable in taking data. Thus every attempt was made to reduce and then monitor the power fluctuations. A warmup period of one to two hours is required to allow the laser to settle into a single mode. Adequate ventilation and cooling provide thermal stability after warmup. Even with these precautions, fluctuations occur but may be monitored by a pyroelectric detector. While the response of the pyroelectric detector and the HgCdTe detector are not one to one, the fluctuations are proportional. These changes are measured and the Mueller matrix measurement is discarded if the power level change is greater than a predetermined

amount.

Most changes in the laser power involve fairly long time periods. Any reduction in the time needed to make the total number of measurements reduces the effect of any fluctuations that occur. The greatest expense of time involves the rotation of the retarders to the angles θ and 5θ. Since there is no restriction on its value, θ was chosen to reduce the time involved. Since there is a certain amount of overhead in starting and stopping the stages and making the actual measurement, the larger the angle the better.

The detector is subject to environmental noise, and the preamp generates a certain amount of electronic noise. The net result is a non-zero reading for a zero signal. It is easy to correct for this noise bias simply by subtracting the zero signal reading from each intensity reading. This reading is found either by blocking the laser beam or crossing the polarizers. Both methods produce the same reading to the accuracy of our multimeter.

Other factors may introduce fluctuations in the detector's response, such as air currents or stray reflections. Air currents are reduced by utilizing a cover over the optics bench. Care must be taken, however, to allow adequate ventilation for the laser, which is also on the optics bench. Stray reflections are blocked through the use of apertures placed strategically along the optic axis.

X. Recommendations

From the eight weeks experience we have with the polarimeter, there are several modifications which would definitely improve the operation and quality of data. 1.) A more stable laser is needed. This might be done by providing the existing laser with a water-cooled plate to replace the existing forced air cooling. If this fails, a replacement laser will be found. 2.) Additional polarizers which do not deviate the beam are needed. We feel the difficulty with the

calibration of elements might be avoided with all wire grid type polarizers. Polarizers from Molectron are due to be delivered for this purpose. 3.) Another HgCdTe detector to monitor the laser output power would greatly assist the data reduction process. The output from this detector would be used to normalize the intensity data from the final detector, thereby eliminating not only long term drift effects but even the short term laser fluctuations.

We have constructed and demonstrated operation of a laser polarimeter operating in the infrared. We hope to use this instrument for the evaluation of electrooptical materials for modulator use. With further development, it should prove a valuable tool for this purpose.

XI. References

1. Azzam, R. M. A., "Photopolarimetric measurement of the Mueller matrix by Fourier analysis of a single detected signal", Optics Letters, **2**, 6 (1978).
2. Hauge, P. S., "Mueller matrix ellipsometry with imperfect compensators", Journal of the Optical Society of America, **68**, 11 (1978).

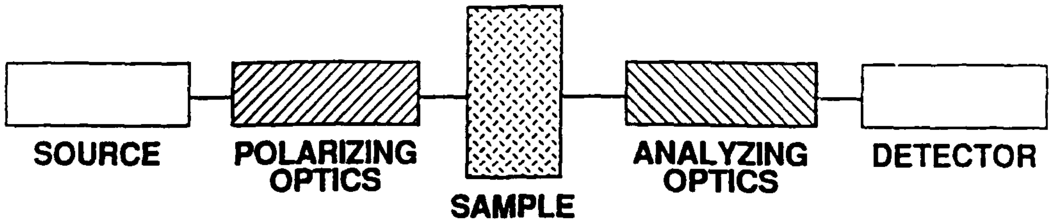

Figure 1: Polarimeter Block Diagram

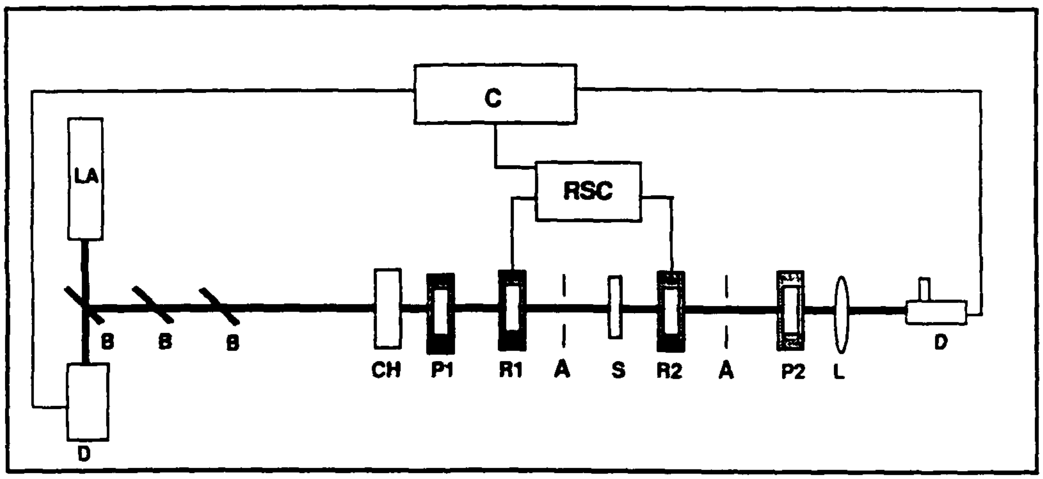

LA	LASER
D	DETECTOR
P1,P2	POLARIZERS
R1,R2	RETARDERS
S	SAMPLE
CH	CHOPPER
L	LENS
B	BEAM SPLITTER
A	APERTURE
C	COMPUTER
RSC	ROTARY STAGE CONTROLLER

Figure 2: Polarimeter Optics

α	β	γ	Mueller matrix	Error matrix
1	0	0	$\begin{pmatrix} 1 & 0 & .035 & 0 \\ 0 & 1 & -.035 & 0 \\ 0 & .035 & 1 & 0 \\ 0 & 0 & 0 & 1 \end{pmatrix}$	$\begin{pmatrix} 0 & 0 & .035 & 0 \\ 0 & 0 & -.035 & 0 \\ 0 & .035 & 0 & 0 \\ 0 & 0 & 0 & 0 \end{pmatrix}$
0	1	0	$\begin{pmatrix} 1 & 0 & 0 & 0 \\ 0 & 1 & -.07 & 0 \\ -.035 & -.07 & 1 & 0 \\ 0 & 0 & 0 & 1 \end{pmatrix}$	$\begin{pmatrix} 0 & 0 & 0 & 0 \\ 0 & 0 & -.07 & 0 \\ -.035 & .07 & 0 & 0 \\ 0 & 0 & 0 & 0 \end{pmatrix}$
0	0	1	$\begin{pmatrix} 1 & .03 & -.171 & 0 \\ 0 & .94 & .342 & 0 \\ 0 & -.342 & .94 & 0 \\ 0 & 0 & 0 & .985 \end{pmatrix}$	$\begin{pmatrix} 0 & .03 & -.171 & 0 \\ 0 & -.06 & .342 & 0 \\ 0 & -.342 & -.06 & 0 \\ 0 & 0 & 0 & -.015 \end{pmatrix}$
.5	1	0	$\begin{pmatrix} 1 & 0 & .017 & 0 \\ 0 & 1 & -.087 & 0 \\ -.035 & .087 & 1 & 0 \\ 0 & 0 & 0 & 1 \end{pmatrix}$	$\begin{pmatrix} 0 & 0 & .017 & 0 \\ 0 & 0 & -.087 & 0 \\ -.035 & .087 & 0 & 0 \\ 0 & 0 & 0 & 0 \end{pmatrix}$
1	0	1	$\begin{pmatrix} 1 & .024 & -.137 & 0 \\ 0 & .951 & -.309 & 0 \\ -.309 & 0 & .951 & 0 \\ 0 & 0 & 0 & .99 \end{pmatrix}$	$\begin{pmatrix} 0 & .024 & -.137 & 0 \\ 0 & -.049 & -.309 & 0 \\ -.309 & 0 & -.049 & 0 \\ 0 & 0 & 0 & .01 \end{pmatrix}$
0	5	1	$\begin{pmatrix} 1.03 & -.03 & -.171 & 0 \\ -.03 & 1 & 0 & 0 \\ -.171 & 0 & 1 & 0 \\ 0 & 0 & 0 & .97 \end{pmatrix}$	$\begin{pmatrix} .03 & -.03 & -.171 & 0 \\ -.03 & 0 & 0 & 0 \\ -.171 & 0 & 0 & 0 \\ 0 & 0 & 0 & -.03 \end{pmatrix}$
3	3	1	$\begin{pmatrix} 1 & 0 & -.07 & 0 \\ -.015 & 1 & .035 & 0 \\ -.104 & -.035 & 1 & 0 \\ 0 & 0 & 0 & 1 \end{pmatrix}$	$\begin{pmatrix} 0 & 0 & -.07 & 0 \\ -.015 & 0 & .035 & 0 \\ -.104 & -.035 & 0 & 0 \\ 0 & 0 & 0 & 0 \end{pmatrix}$

Table 1: Simulated Mueller matrices with orientation errors.

α	β	γ	δ_1	δ_2	Mueller matrix	Error matrix
0	0	0	88	88	$\begin{pmatrix} 1 & .034 & 0 & 0 \\ .034 & .931 & 0 & 0 \\ 0 & 0 & .931 & 0 \\ 0 & 0 & 0 & 1 \end{pmatrix}$	$\begin{pmatrix} 0 & .034 & 0 & 0 \\ .034 & -.069 & 0 & 0 \\ 0 & 0 & -.069 & 0 \\ 0 & 0 & 0 & 1 \end{pmatrix}$
1	0	0	92	92	$\begin{pmatrix} 1 & -.036 & .036 & 0 \\ -.036 & 1.07 & -.037 & 0 \\ 0 & .037 & 1.07 & 0 \\ 0 & 0 & 0 & 1 \end{pmatrix}$	$\begin{pmatrix} 0 & -.036 & .036 & 0 \\ -.036 & .07 & -.037 & 0 \\ 0 & .037 & .07 & 0 \\ 0 & 0 & 0 & 1 \end{pmatrix}$
1	1	1	91	91	$\begin{pmatrix} 1 & 0 & -.143 & 0 \\ -.027 & 1 & .25 & 0 \\ -.029 & -.25 & 1 & 0 \\ 0 & 0 & 0 & .989 \end{pmatrix}$	$\begin{pmatrix} 0 & 0 & -.143 & 0 \\ -.027 & 0 & .25 & 0 \\ -.029 & -.25 & 0 & 0 \\ 0 & 0 & 0 & -.011 \end{pmatrix}$

Table 2: Simulated Mueller matrices with orientation and retardation errors.

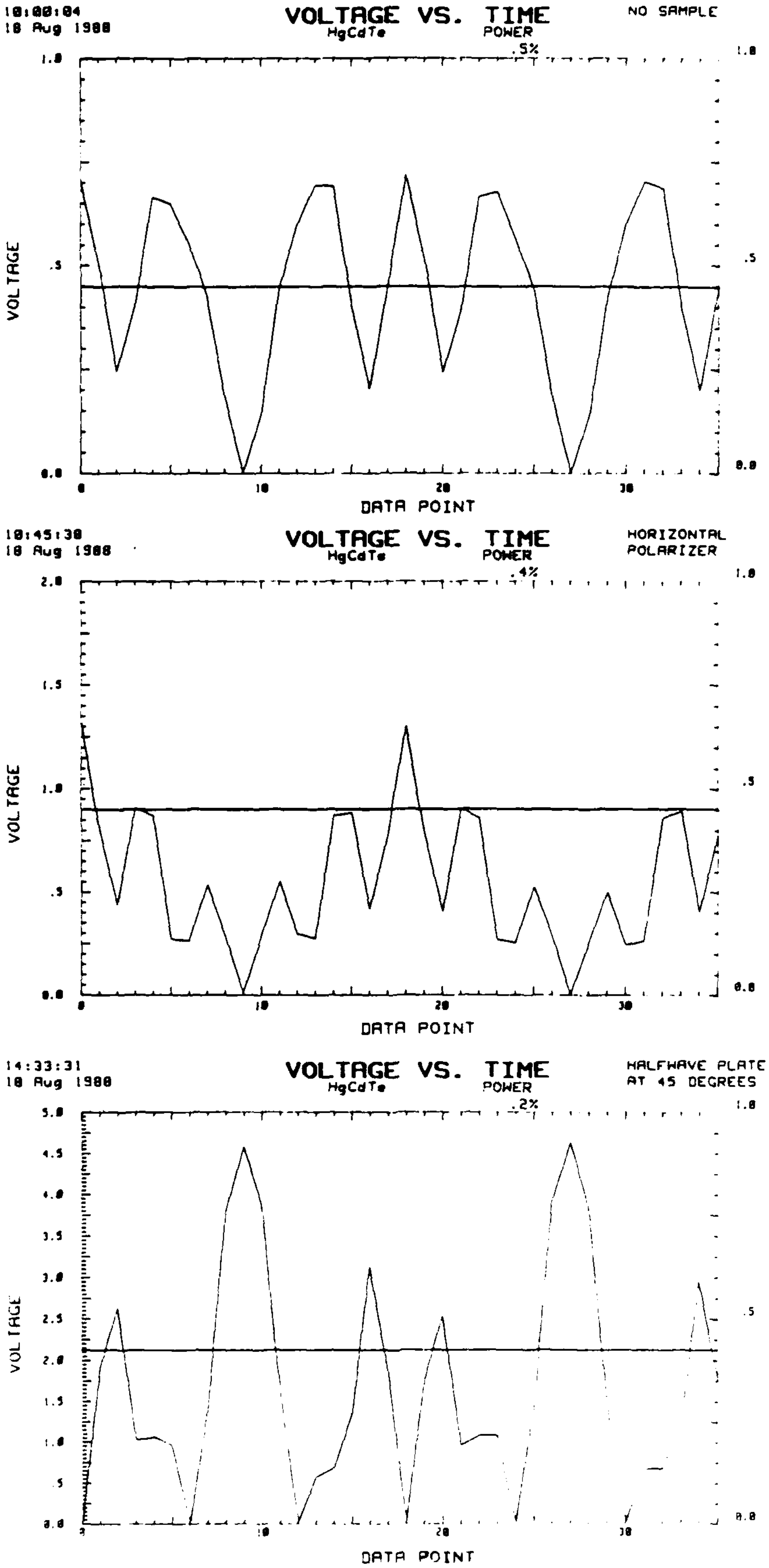

Figure 3: Experimental Intensity Modulation

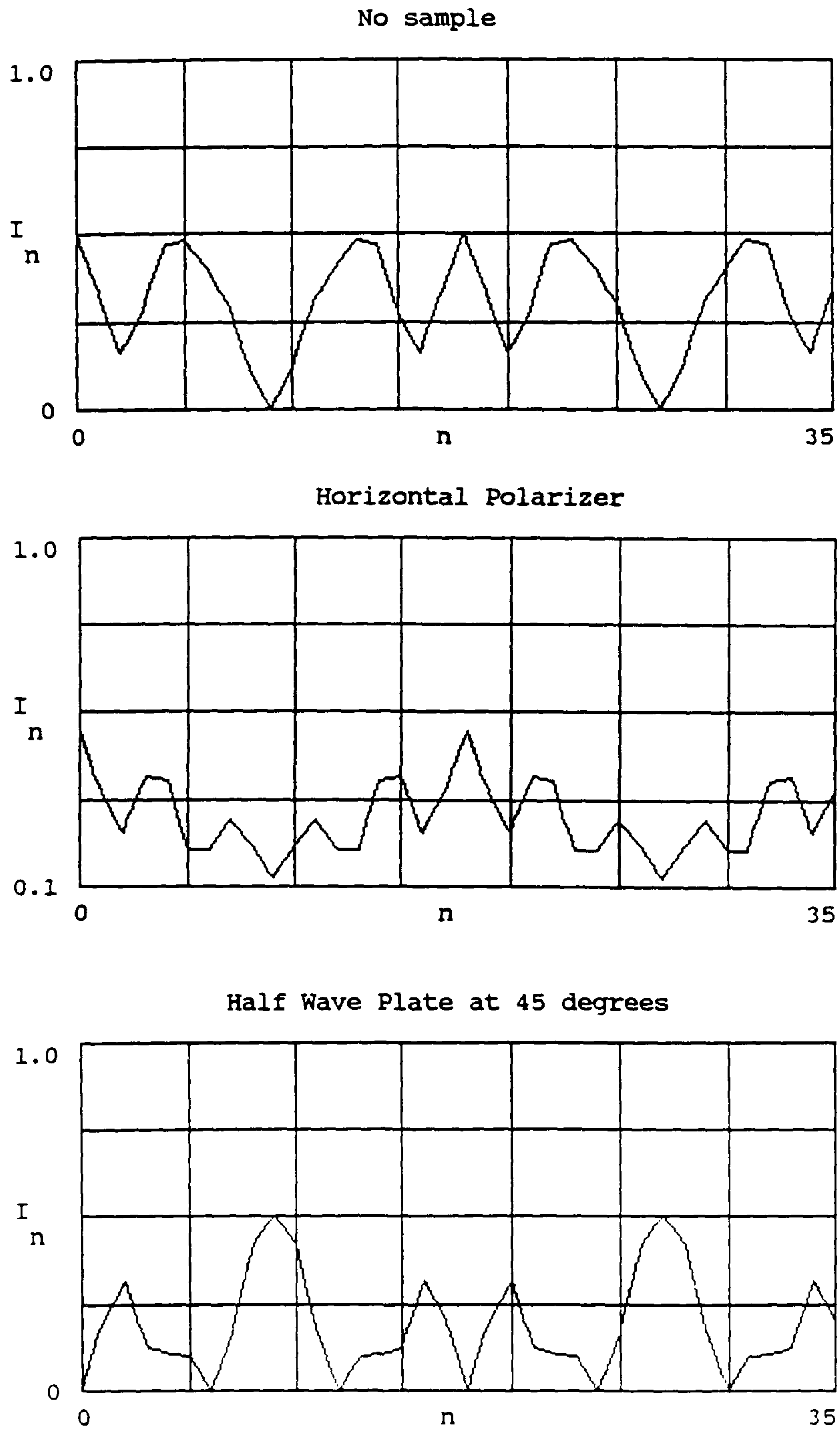

Figure 4: Simulated Intensity Modulation

1988 USAF-UES SUMMER FACULTY RESEARCH PROGRAM/

GRADUATE STUDENT SUMMER RESEARCH PROGRAM

Sponsored by the

AIR FORCE OFFICE OF SCIENTIFIC RESEARCH

Conducted by the

Universal Energy Systems, Inc.

FINAL REPORT

Determing the Aerodynamic Coefficients of High L/D Projectiles Using a Body-Fixed Coordinate System

Prepared by:	Thomas Harkins
Academic Rank:	Master's Student
Department and	Mechanical Engineering Department
University:	Louisiana State University
Research Location:	AFATL/FXA
	Eglin AFB, Florida 32542
USAF Researcher:	Mr. Gerald L. Winchenbach

Date:	September 30, 1988
Contract No.:	F49620-88-C-0053

Determining the Aerodynamic Coefficients of High L/D Projectiles Using a Body-Fixed Coordinate System

by

Thomas Harkins

ABSTRACT

The objective of this research effort was to develop a method of determining the aerodynamic coefficients of flexible aeroballistic models using a body-fixed coordinate system. The experimental data were obtained from spark range shadowgraph stations. A FORTRAN program was developed to provide a "best fit" to the data and thereby converge to a solution set containing the aerodynamic coefficients. The computer program used a Least Squares parameter estimation technique with differential correction. Analytical aerodynamic models for both rigid-body and flexible-body cases were included in the coefficient extraction program.

A test calculation for a missile with L/D of [illegible] was performed in which the aerodynamic coefficients for the flexible body were determined by comparison with the rigid body trajectory. The flexible body coefficients, in some cases, deviated by more than the expected probable error from the rigid body values. Further parametric calculations are currently under way to isolate the flexibility effects on specific coefficients.

ACKNOWLEDGEMENTS

The author would like to express his gratitude to the Air Force Office of Scientific Research, the Air Force Systems Command, and Universal Energy Systems, Inc. for providing the opportunity to participate in the Graduate Student Summer Support Program. The research done in aeroballistics at the Air Force Armament Laboratory, located on Eglin AFB, was highly educational and helpful in that it provided me with an interesting thesis topic.

Special thanks should go to the following people who personally made the summer's research particularly enjoyable and fulfilling: Chief Scientist Dr. Sam Lambert for arranging travel orders and housing; Branch Chief Carroll Butler for supporting the research effort and providing his technical advice; Section Chief Gerald Winchenbach for providing the necessary technical background information and for giving his excellent advice to the specific problems that were encountered; Project Engineer Greg Abate for his [illegible] help with the computer systems that were used; Air Force Captain James Kidd for his technical advice on matters concerning numerical computations and aeroelasticity.

Finally, the utmost thanks and appreciation should go to the author's Major Professor, Dr. Robert Courter, for giving me the opportunity to work with him and for being there whenever he was needed.

1. INTRODUCTION

Experimental methods are used to test the performance of a prototype or a scaled model. At the Aeroballistic Research Facility, located at Eglin AFB, testing of high fineness ratio penetrators has been performed. The free-flight ballistic range is instrumented with timers and two-plane (vertical and horizontal) shadowgraph stations that can measure the angular orientation and translational position of the ballistic model. The shadowgraph stations are located every fifteen feet along the 750 foot range. Currently, the data are reduced using a parameter estimation technique developed by Hathaway and Whyte (Ref. 1) which is a modified form of the Chapman and Kirk technique. This estimation technique compares trajectory data with analytical predictions and calculates the aerodynamic coefficients as a result. In free-flight aerodynamic data analysis, the reduction is not successful until the motion data can be reproduced using the calculated coefficients to a probable error which is equivalent to range measurement error.

This requirement dictates that the analytical model be an accurate representation of the physical behavior of the actual model. However, a measurable amount of aeroelastic flexing has been observed from the shadowgraphs of the high fineness ratio penetrators. This flexing raises certain doubts about the validity of using the current rigid body motion as the analytical model.

II. OBJECTIVES

The objectives of the summer research program are:

1. Develop a technique for determing the aerodynamic coefficients of a free-flight projectile using a body-fixed coordinate system.
2. Include flexible-body equations of motion in the analytical model and solve for the aerodynamic coefficients on this basis.

III. FLEXIBILITY ANALYSIS

The equations of motion are influenced by the elastic deformation of the body. These equations are derived by taking into account the change in the center of mass and moments of inertia. The rigid-body equations of motion are modified by adding "elastic inertia" terms. The elastic inertia terms are determined analytically by describing the dynamics of an arbitrarily deformed mass element [illegible].

Since the aerodynamic coefficients are not known before the model is tested, the loads on the model are indeterminate, and a forced vibration analysis of the penetrator cannot be performed. It is necessary to find a function of deformation with respect to time so that the elastic inertia terms can be calculated as the simulation program is integrated numerically.

The body is assumed to vibrate at its natural [illegible]

This frequency is calculated using a finite element computer program. The deformation of the body is then defined as

$$\xi = A*\sin(wt)*F(x,y,z)$$

where A is the amplitude of the flexing model, w is the natural frequency, and $F(x,y,z)$ is the mode shape.

It should be noted that for the case being considered, only bending deformations are taken into account and the torsional and axial deformations are neglected. Considering the flexibility of the projectile in bending compared with that in torsion or tension, the assumption is reasonable.

The dynamics of the elastic penetrator can now be determined by numerically solving the equations of motion of the elastic body, where the elastic inertia coefficients have been determined a priori with a free-free vibration analysis of the fundamental mode shape (Ref. 2). The details of the dynamic simulation are described in the next section.

IV. MODEL SIMULATION

The simulation program uses the fourth-order, Runge-Kutta integration algorithm. Physical characteristics of the model, as well as the aerodynamic coefficients, are read into the program from an input file. The initial position, time, and velocities are also read into the program. The program takes the "earth-fixed" initial data and transforms them into "body-fixed" values. The output of the program is in both body-fixed and earth-fixed coordinates.

The simulation can be performed using either rigid or flexible body equations of motion. Which equations are used

depends on whether the flexibility flag is set (See flow-chart Appendix A). The equations of motion are differential equations of the six state variables (X, Y, Z, ϕ, θ, ψ). However, the aerodynamic forces and moments are related to the acceleration and angular acceleration of the body-fixed coordinate system. The equations of motion as well as the force and moment equations are given in Reference 2.

V. MODEL REGRESSION

The data aquired in the ballistic range are compared with the trajectory simulation. The trajectory can be determined using either rigid or flexible body equations of motion as mentioned above. A set of residuals is calculated for each state variable at each shadowgraph station. The sum of the square of the residuals is calculated. Minimisation of the sum of squares is performed until the trajectory matches range data to the accuracy of measurement error.

In order to minimize the sum of squares, an iterative differential correction process (LSDC) is performed on the coefficients of regression. The coefficients are adjusted so that the simulated trajectory approaches the experimental data on each iteration. The coefficients of regression in this case are the set of aerodynamic coefficients read into the computer program. The advantages of the LSDC technique is the simplicity of the algorithm and fact that it can handle nonlinear models. The method for determining the differential correction step size is given

1. Determine the residuals of the state variables for all shadowgraph stations, $R_i = S_i - E_i$, where S_i is the state variable and E is the experimental measurement.
2. Sum the square of the residuals, $\Phi = \sum R_i * R_i$.
3. Calculate the state Jacobian by taking the partial derivative of each state variable with respect to each coefficient of regression. This process is done numerically for each data station using a forward difference technique. The resulting matrix has the column dimension that is equal to the number of data points with a row dimension that is the size of the number of coefficients that are regressed upon.
4. Send the state Jacobian to subroutine [illegible]. This subroutine uses orthogonal factorization to determine the differential step size, $\Delta\bar{C}$. This subroutine is a least squares type technique in that a Cholesky-type upper triangular matrix is updated successively by adding each observation vector [illegible]. The method is analogous to filter techniques used in control applications, and is numerically superior to classical filter and least squares techniques.
5. Set $\bar{C} = \bar{C}_i + \Delta\bar{C}$. Recalculate the residuals of the state variables.

6. Check for convergence. If not converged, go to Step 2. The convergence criteria is based upon the normalized differential correction step size $\Delta\vec{C}/\vec{C}$. If the sum of the square of these values are less than 10^{-9} , the regression is considered converged.

It should be noted that the computer program is written entirely in Double Precision so that accuracy can be maintained in the differential correction process. The forward difference approximation is 10^{-7} accurate.

VI. RESULTS

For a test case, a high length over diameter model was chosen (L/D=50). The overall length of the model is [illegible] inches with an amplitude of deflection of 0.25 inches. The natural frequency of the projectile is 534 cycles per second. The elastic inertia terms are as follows:

$$K_{\ell} = 0.0000[illegible]$$
$$L_{zz} = 0.000083$$
$$N_{zz} = 0.000069$$

Table I shows the results of the reduction of the flexible model as compared to rigid body aerodynamics. A marked change in the aerodynamic coefficients results from the single plane bending effect. Coefficients that were equal in magnitude in the rigid body start to separate in the flexible model.

TABLE 1: Flexible-Body Coefficients for L/D=50 Projectile

Coeff.	Coefficients for Rigid-Body Trajectory	Flexible-Body Coefficients to Match Rigid Body Traj.
C_{l_0}	0.8475	0.8253
C_{l_p}	-17.3140	-22.7337
C_{m_α}	-209.9372	-174.4763
C_{n_β}	209.9372	241.7058
C_{m_q}	-24014.1836	-23635.6641
C_{n_r}	-24014.1836	-25768.6855
C_{y_β}	-20.5404	-18.1432
C_{z_α}	-20.5404	-22.3196

VII. RECOMMENDATIONS

In addition to further testing of free-flight projectiles, the following recommendations are made.

1. A closure error analysis should be performed in the integration of trajectory. This will determine the optimum time-step size to be used.
2. A full statistical study of the data reduction scheme would provide the necessary uncertainty information of the regression coefficients.

FLOW CHART FOR COEFFICIENT EXTRACTION

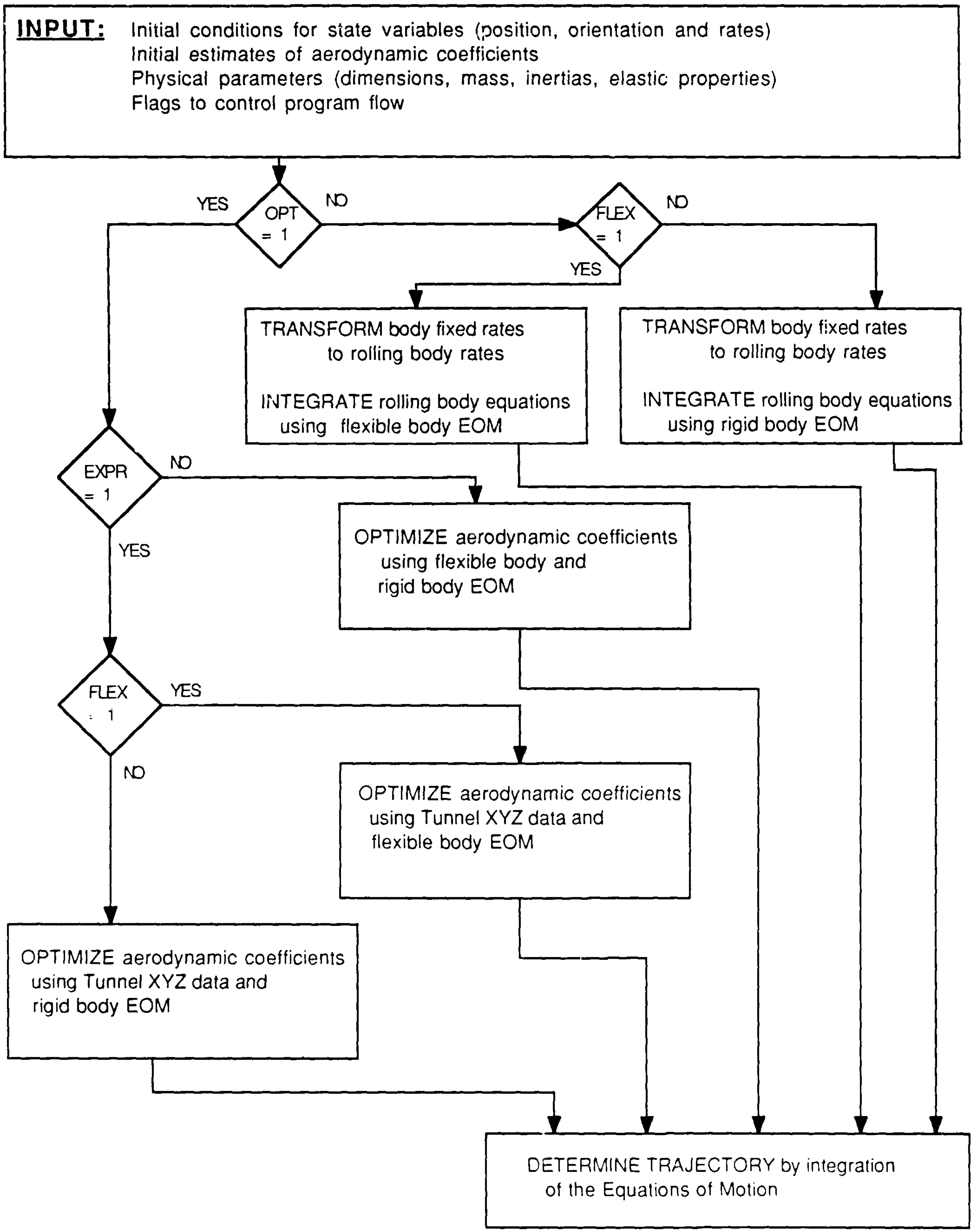

FLOW CHART FOR LEAST SQUARES - DIFFERENTIAL CORRECTION ALGORITHM

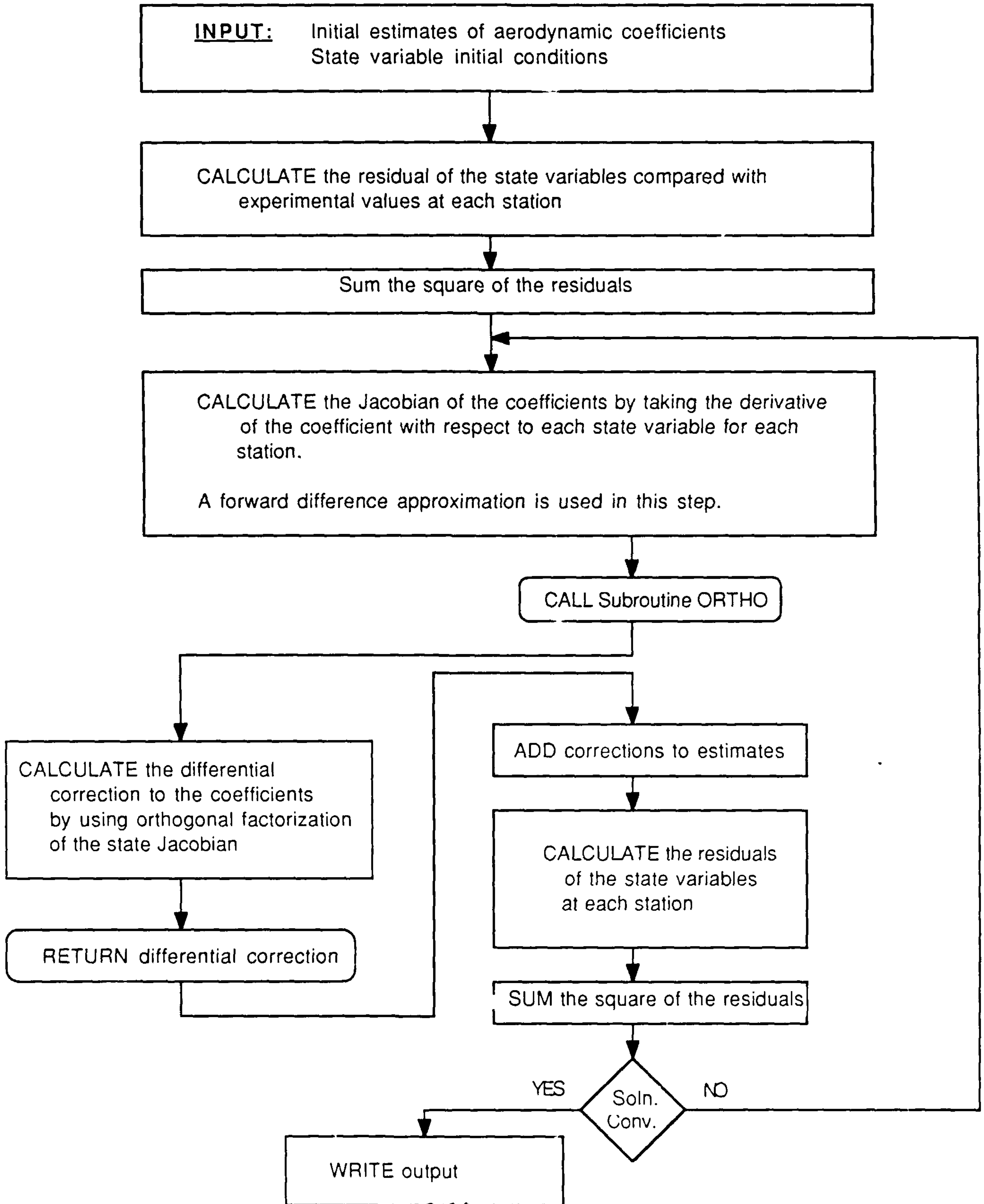

REFERENCES

1 Hathaway, W. and R. White, "Aeroballistic Range Data Analysis For Nonsymmetric Configurations", AFATL-TR-[illegible], September, 1976.

2 Courter, R. W., "The Effect of Model Flexibility on the Accuracy of Aerodynamic Coefficients Determined from [illegible] Flight Ballistic Tests", Final Report AFOSR/UES Summer Research Program, AFATL/FXA, Eglin AFB, Florida, [illegible], 1987.

1988 USAF-UES SUMMER GRADUATE STUDENT RESEARCH PROGRAM

Sponsored by the

AIR FORCE OFFICE OF SCIENTIFIC RESEARCH

Conducted by the

Universal Energy Systems, Inc.

FINAL REPORT

Prepare by:	Hisook L. Min, M.S.
Academic Rank:	Graduate Student
Department and University:	Physics Department East Texas State University
Research Location:	AFATL/MNF Eglin AFB, Fl. 32542-5434
USAF Researcher:	Capt. James Hawkins
Date:	16 Aug. 1988
Contract No.	F49620-88-C-0053

Filter Design and Signal Processing
in the Development of
Target-Aerosol Discrimination Techniques
for Active Optical Proximity Sensors

by

Hisook L. Min

ABSTRACT

Over a decade numerous efforts have been pursued by USAF in the development of all-weather Active Optical Proximity Sensors. The principal investigator (KSM) has undertaken an assignment of developing an alternate approach or new algorithms for this challenging objective. A few new techniques for the aerosol-target discrimination have been initiated and formulated by the principal investigator. The tasks of designing appropriate filters, comparing the effectiveness of several orthogonal basis functions in the filter design, coding, execution, and running simulations have been carried out by this writer. Programs were written in C-language and pascal for modularity. Extensive use of graphics are made for the relevant illustrations. Listings of the source codes are to be included in a proposed separate report to the AFATL (jointly with the PI). A proposal for a paper presentation at the upcoming IEEE International Conference on Acoustics, Speech, and Signal Processing (1989) has been submited based on this work.

Acknowledgements

I am grateful to the Air Force Systems Command and the Air Force Office of Scientific Research for sponsorship of this research. Sincere appreciation goes to Universal Energy Systems for their kind concern and all administrative arrangement of the program. It has been a rewarding and enlightening research experience at the Air Force Armament Laboratory at Eglin AFB. Dr. Sam Lambert, chief scintist of the laboratory, gave warm encouragement and guidance. Capt. James Hawkins and Mr. Robert Orgusaar provided a great deal of help during the course of this research. Warm hospitality of branch chiefs, Ron Boulet and Lanny Burdge are sincerely appreciated. Capt. Mike Caraway's expertise in C-language programming and his kind concern rendered me an invaluable help. I also wish to thank Mr. Bob Erdman and Mr. Scott Turner for facilitating the environment for my computational work.

I. INTRODUCTION

Some years ago, the writer developed her research interests in the discipline of image processing, a branch of applied mathematics. Theoretical analysis as well as practical implementation of several techniques in the area of image enhancement have been explored during past three years. Among these techniques are edge detection and image smoothing both in frequency and spatial domain and contrast enhancement in the spatial domain based on histogram analysis and modification. This summer, the PI(KSM) has been assigned to examine the algorithms currently in use and develop, if possible, new techniques in separation of aerosol signals from those of a target. A few new techniques have been initiated and promising results have been obtained.

All of these techniques are based on signal processing principles. Some of them extensively utilize transformation by orthogonal basis functions, design of filter transfer functions, and related techniques that the writer has been exposed to in the course of her previous studies in image enhancement techniques.

II. OBJECTIVES OF THE RESEARCH

In his summer research at AFATL the PI (KSM) initiated three new techniques for aerosol-target signal separation. They are: (1) correlation technique using multi-sensor array, (2) digital filtering separation using orthogonal transforms, and (3) wave form separation technique. The assignments to the writer were mainly for the second method. The fllowing are the tasks carried out for this method.

1. Development and implementation of a Fast Fourier Transform suggested by the PI.

2. Implementation of Triangular Transform developed by the PI.

3. Implementation of Hartley Transform and Cosine Transform.

4. Design and implementation of low- and high-pass filter transfer functions.

5. Running simulation with the algorithms implemented.

6. Evaluation of the transforms and filter functions in relation to aerosol-target separation.

III. ORTHOGONAL TRANSFORMS

To achieve the goal of developing a desirable filter transfer function which will separate target signals from those of aerosol, four orthogonal transforms are studied. The definitions of their basis functions are given as follows:

Discrete Triangular Transform (DTT)

The orthogonal basis functions of DTT is based on two triangular wave forms, say, $Ct(x,u)$ and $St(x,u)$, defined as follows.

$$Ct(x,u) = \begin{cases} 1 - 4ux/N & \text{if } 0 \le x < T/2 \\ -3 + 4ux/N & \text{if } T/2 \le x \le T \end{cases}$$

$$S(x,u) = \begin{cases} 4xu/N & \text{if } 0 \le x < T/4 \\ 2 - 4xu/N & \text{if } T/4 \le x < 3T/4 \\ -4 + 4xu/N & \text{if } 3T/4 \le x \le T \end{cases}$$

where T is a period; u, a frequency; x, a data point; and N, a total no. of data points.

These wave forms do not form an orthogonal set. To maintain orthogonality they are modified in the following way. Let $Tc(x,u)$ and $Ts(x,u)$ denote the modified $Ct(x,u)$ and $St(x,u)$ respectively. They are defined as follows:

1. If u is a power of 2:

   $Tc(x,u) = \sqrt{3/N}\, Ct(x,u)$ and

   $Ts(x,u) = \sqrt{3/N}\, St(x,u)$

2. If $u = p^k \cdot 2^n$ for $k = 1, 2, 3 \ldots$, p a prime no. and $n = 0, 1, 2 \ldots$

Let $q = p^{k-1} 2^n$ Then $u = p \cdot q$

$$Tc(x,u) = \sqrt{3/N}\sqrt{p^4/(p^4-1)}\ [Ct(x,u) - (1/p^2)\ Ct(x,q)]$$

$$Ts(x,u) = \sqrt{3/N}\sqrt{p^4/(p^4-a)}\ [St(x,u) - (a/p^2)\ St(x,q)]$$

for $a = (-1)^b$ where $b = (p-1)/2$.

3. If $u = p \cdot q \cdot 2^n$ where $n = 0, 1, 2 \ldots$ and p and q are prime nos. such that $p \neq q$

$$Tc(x,u) = \sqrt{u^4/(u^4-a\cdot p^4-b\cdot q^4+1)}\ [St(x,u) - (1/q^2)St(x,(p\cdot 2^n)) - (1/p^2)\ St(x,(q\cdot 2^n)) + (1/u^2)\cdot Ct(x,2^n)]$$

$$Ts(x,u) = \sqrt{u^4/(u^4-a\cdot p^4-b\cdot q^4+1)}\ [St(x,u) - (a/q^2)St(x,(p\cdot 2^n)) - (b/p^2)\ St(x,(q\cdot 2^n)) + (1/u^2)\ Ct(x,2^n)]$$

where $a = (-1)^K$ for $k = (q-1)/2$ and

$b = (-1)^m$ for $m = (p-1)/2$.

An N x N *Triangular transform matrix* [A] is defined as

$$A(i,j) = \begin{cases} \sqrt{1/N} & \text{if } i = 0 \\ Tc(u,j) \quad \text{for } u = (i+1)/2 & \text{if } i \text{ is odd} \\ Ts(u,j) \quad \text{for } u = i/2 & \text{if } i \text{ is even.} \end{cases}$$

The N x N inverse transform matrix [B] is a transpose of [A].

<u>Discrete Cosine Transform</u> (DCT)

The kernel of the one-dimensional DCT is defined as

$$f(x,0) = \sqrt{1/N}$$

$$f(x,u) = \sqrt{2/N}\ \cos\ ((2x + 1)\cdot u\pi\ /(2N)) \qquad \text{(C-1)}$$

where x is a data point, u a frequency and N is the total no. of the data points. The transform F(u) of f(x) can be expressed

$$F(0) = \sqrt{1/N}\sum_{x=0}^{N-1} f(x)$$

$$F(u) = \sqrt{2/N} \sum_{x=0}^{N-1} f(x) \cos[(2x + 1) u\pi/(2N)]$$

for $u = 0, 1, 2, 3, \ldots, N-1$

The inverse kernel is of the same form as in Eqs.(C-1) and the inverse DCT is define as

$$f(x) = \sqrt{1/N}\, F(0) + \sqrt{2/N} \sum_{u=1}^{N-1} F(u) \cos[(2x+1)u\pi/(2N)]$$

for $x = 0, 1, 2, \ldots, N-1$

<u>Discrete Hartley Transform</u> (DHT)

The kernel of the one-dimensional DHT is given by the relations

$$f(x,0) = \sqrt{1/N}$$

$$f(x,u) = \sqrt{1/N}\, (\cos[2\pi ux/N] + \sin[2\pi ux/N]) \qquad \text{(H-1)}$$

The transform F(u) of f(x) is given by

$$F(0) = \sqrt{1/N} \sum_{x=0}^{N-1} f(x)$$

$$F(u) = \sqrt{1/N} \sum_{x=0}^{N-1} f(x)(\cos[2\pi ux/N] + \sin[2\pi ux/N])$$

for $u = 0, 1, 2, \ldots, N-1$

The inverse kernel is of the same form as in Eqs.(H-1) and the inverse DHT is given by

$$f(x) = \sqrt{1/N}\, F(0) + \sqrt{1/N} \sum_{u=1}^{N-1} F(u)(\cos[2\pi ux/N] + \sin[2\pi ux/N])$$

for $x = 0, 1, 2, \ldots, N-1$

<u>Fast Fourier Transform</u> (FFT)

There exist a number of FFT algorithms. The algorithm described here is suggested by the PI (KSM) and implemented by the writer.

The discrete Fourier transform F(u) of a function f(x) is defined as

$$F(u) = \sqrt{1/N} \sum_{x=0}^{N-1} f(x) \exp[-j2\pi ux/N]$$

$$\text{for } u = 0, 1, 2, \ldots, N-1 \qquad \text{(F-1)}$$

and the inverse transform $g(x)$ of $F(u)$ is given by

$$g(x) = \sqrt{1/N} \sum_{u=0}^{N-1} F(u) \exp[j2\pi ux/N]$$

$$\text{for } x = 0, 1, 2, \ldots, N-1$$

For convenience let $w^n = \exp[-j2\pi n/N]$

For N=4 Eq. (F-1) can be written

$$\begin{aligned}
F(0) &= f(0)w^0 + f(1)w^0 + f(2)w^0 + f(3)w^0 \\
F(1) &= f(0)w^0 + f(1)w^1 + f(2)w^2 + f(3)w^3 \\
F(2) &= f(0)w^0 + f(1)w^2 + f(2)w^4 + f(3)w^6 \\
F(3) &= f(0)w^0 + f(1)w^3 + f(2)w^6 + f(3)w^9
\end{aligned} \qquad \text{(F-2)}$$

The matrix representation of Eqs. in (F-2) is

$$\begin{bmatrix} F(0) \\ F(1) \\ F(2) \\ F(3) \end{bmatrix} = \begin{bmatrix} w^0 & w^0 & w^0 & w^0 \\ w^0 & w^1 & w^2 & w^3 \\ w^0 & w^2 & w^4 & w^6 \\ w^0 & w^3 & w^6 & w^9 \end{bmatrix} \cdot \begin{bmatrix} f(0) \\ f(1) \\ f(2) \\ f(3) \end{bmatrix} \qquad \text{(F-3)}$$

To perform the matrix computation of (F-3), N multiplications and N(N-1) additions are required. However, the no. of multiplications can be reduced in the following way.

Let S be a set of whole nos. Since n and N are in S, there is a K and a R in S such that

$$n = K\,(N/2) + R \qquad \text{for } n > N/2 \text{ and } R < N/2$$

Then $w^n = (-1)^K w^R$ which reduces Operation (F-3)

$$\begin{bmatrix} F(0) \\ F(1) \\ F(2) \\ F(3) \end{bmatrix} = \begin{bmatrix} 1 & 1 & 1 & 1 \\ 1 & w & -1 & w \\ 1 & -1 & 1 & -1 \\ 1 & -w & -1 & w \end{bmatrix} \cdot \begin{bmatrix} f(0) \\ f(1) \\ f(2) \\ f(3) \end{bmatrix} \qquad \text{(F-4)}$$

The examination of the signs of the elements in the transform matrix of (F-4) yields the following operations.

$$\begin{bmatrix} F(0) \\ F(2) \end{bmatrix} = \begin{bmatrix} 1 & 1 \\ 1 & -1 \end{bmatrix} \cdot \begin{bmatrix} f(0) + f(2) \\ f(1) + f(3) \end{bmatrix} \qquad \text{(F-5)}$$

$$\begin{bmatrix} F(1) \\ F(3) \end{bmatrix} = \begin{bmatrix} 1 & w \\ 1 & -w \end{bmatrix} \cdot \begin{bmatrix} f(0) - f(2) \\ f(1) - f(3) \end{bmatrix} \quad \text{(F-6)}$$

Rearranging the factor w in Operation (F-6)

$$\begin{bmatrix} F(1) \\ F(3) \end{bmatrix} = \begin{bmatrix} 1 & 1 \\ 1 & -1 \end{bmatrix} \cdot \begin{bmatrix} f(0) - f(2) \\ w\,(f(1) - f(3)) \end{bmatrix} \quad \text{(F-7)}$$

Operations (F-5) and (F-7) yield

$$\begin{aligned} F(0) &= f(0) + f(2) + f(1) + f(3) \\ F(1) &= (f(0) - f(2)) + (f(1) - f(3)) \\ F(1) &= (f(0) + f(2)) - w\,(f(1) + f(3)) \\ F(1) &= (f(0) - f(2)) - w\,(f(1) - f(3)) \end{aligned} \quad \text{(F-8)}$$

Thus the no. of multiplications is reduced from 16 in operation (F-3) to 2 in Eqs. (F-8). For brevity, the case for N=4 is examined above. However, the algorithm can be extended for any matrix size N, if N is a power of 2.

IV. Filter Design

Two types of filter transfer functions are examined for separation of aerosol-target signals.

Ideal Filter

The transfer function L(u) of an Ideal Lowpass Filter (ILPF) is given by:

$$L(u) = \begin{cases} 1 & \text{if } u \leq C \\ 0 & \text{if } u > C \end{cases} \quad \text{(I-1)}$$

where $C > 0$ is a user defined integer.

Its counter part highpass filter (IHPF) transfer function H(u) is defined as

$$H(u) = \begin{cases} 1 & \text{if } u \geq C \\ 0 & \text{if } u < C \end{cases} \quad \text{(I-2)}$$

for $C > 0$, an arbitrary integer.

AD-A204 243 UNITED STATES AIR FORCE GRADUATE STUDENT RESEARCH PROGRAM PROGRAM TECHNIC..(U) UNIVERSAL ENERGY SYSTEMS INC DAYTON OH R C DARRAH ET AL. DEC 88 2/9

UNCLASSIFIED AFOSR-TR-89-0041 F49620-85-C-0013 F/G 5/1 NL

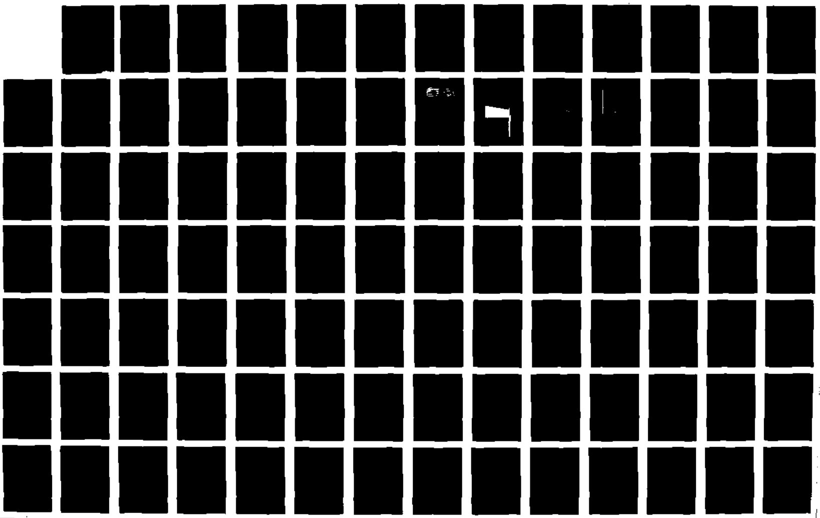

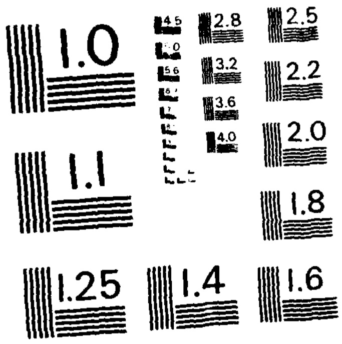
1.0
1.1
1.25
1.4
1.6
1.8
2.0
2.2
2.5
2.8
3.2
3.6
4.0
4.5
5.6

The locus of the cut-off frequency, C, is crucial in determining the behavior of the filter. The effective choice of this locus depends on the spectrum distribution of a given signal.

Trapezoidal Filter

The transfer function, L(u), of a Trapezoidal Lowpass Filter (TLPF) with cut-off frequency, C, is given as follow:

$$L(u) = \begin{cases} 1 & \text{if } u \leqslant C \\ (u - E)/(C-E) & \text{if } C < u \leqslant E \\ 0 & \text{elsewhere} \end{cases} \qquad \text{(T-1)}$$

where E is an arbitrary no such that $0 < E < C$.

Its counterpart highpass filter (THPF) transfer function, H(u), with a cut-off frequency, c, is defined:

$$H(u) = \begin{cases} 1 & \text{if } u \geqslant C \\ (u-E)/(C-E) & \text{if } E \leqslant u < C \\ 0 & \text{elsewhere} \end{cases} \qquad \text{(T-2)}$$

where E is an arbitrary no. such that $0 < E < C$.

Unlike ILPF and IHPF transfer functions, these transfer functions have a gradual transition line between passed and filtered frequencies. The magnitude of the slope of this line contributes significantly to the performance of the filter.

V. Application to Signal Separation

The following steps are taken to separate target signals from aerosol signals.

1. A spectrum distribution is constructed after performing transformation operation to input signals, using each of the four orthogonal basis function sets mentioned above. For the

signal models, the equation formulated by the PI (KSM) is used by applying various parameters.

2. Based on the spectral distribution, an appropriate cut-off frequency locus -- also the magnitude of the slope of a transition line in case of a trapezoidal filter -- is determined for each of the low- and high-pass filters.

3. Filtering operations are applied to the transform coefficients of the input signal.

4. The results are inverse transformed to reconstruct the separated signals.

Fig.1 - Fig.4 illustrate the results of applying ILPF and IHPF to signal separation for each of the four orthogonal basis function sets. Fig. 5 shows the application of TPLF and THPF. Points C and E in Eqs. (I-1), (I-2), (T-1) and (T-2) are denoted by pt0 and pt1 respectively in the figures.

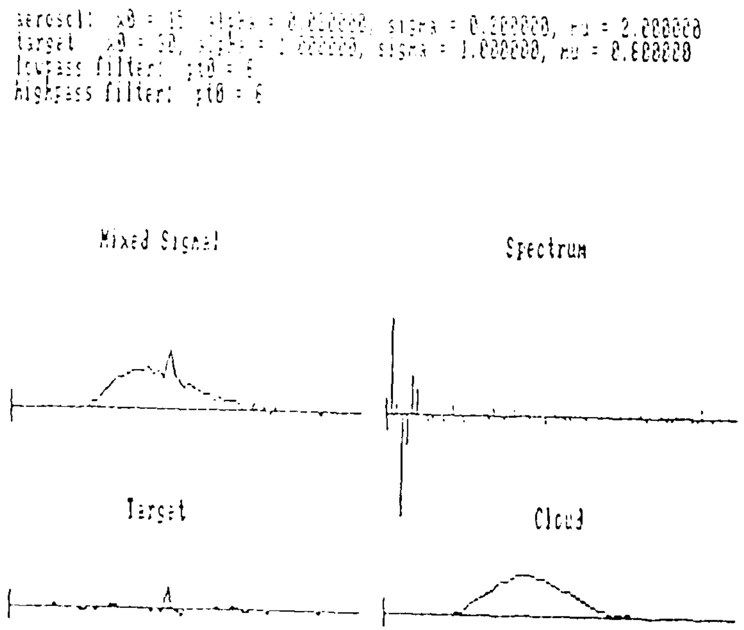

Figure 1. Signal Separation by Spectral Extraction. DCT. Ideal filter.

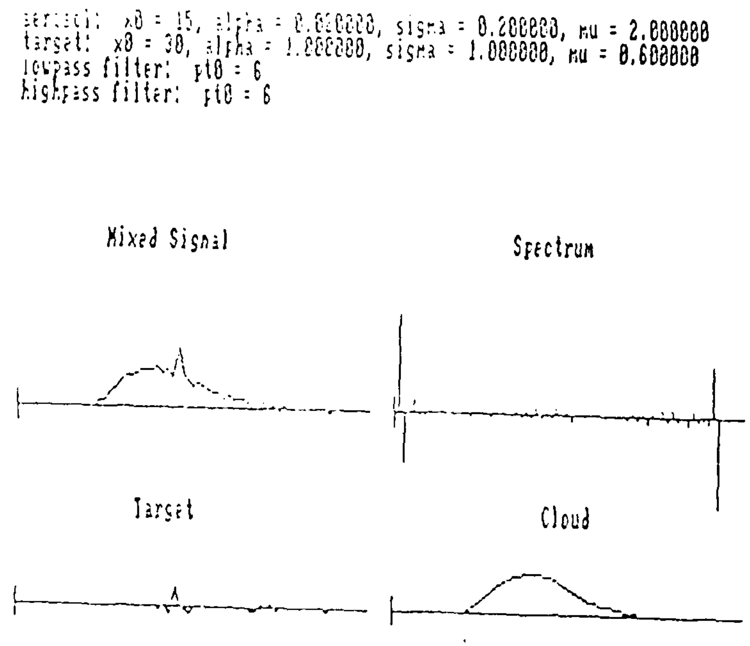

Figure 2. Signal Separation by Spectral Extraction. DHT. Ideal Filter.

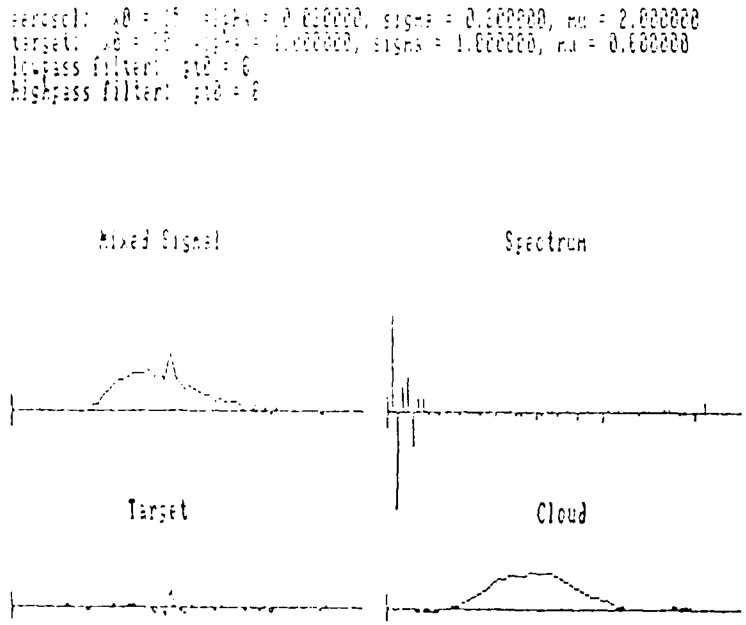

Figure 3. Signal Separation by Spectral Extraction. DFT. Ideal Filter.

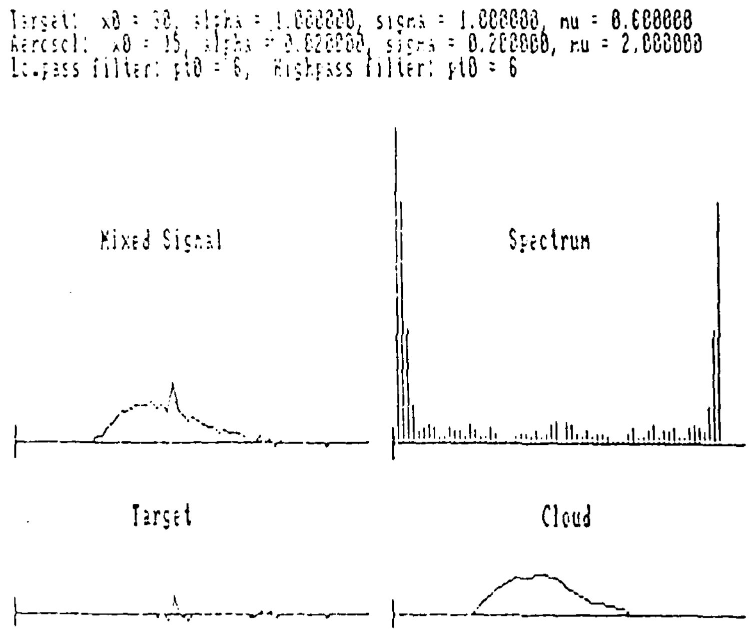

Figure 4. Signal Separation by Spectral Extraction. FFT. Ideal Filter.

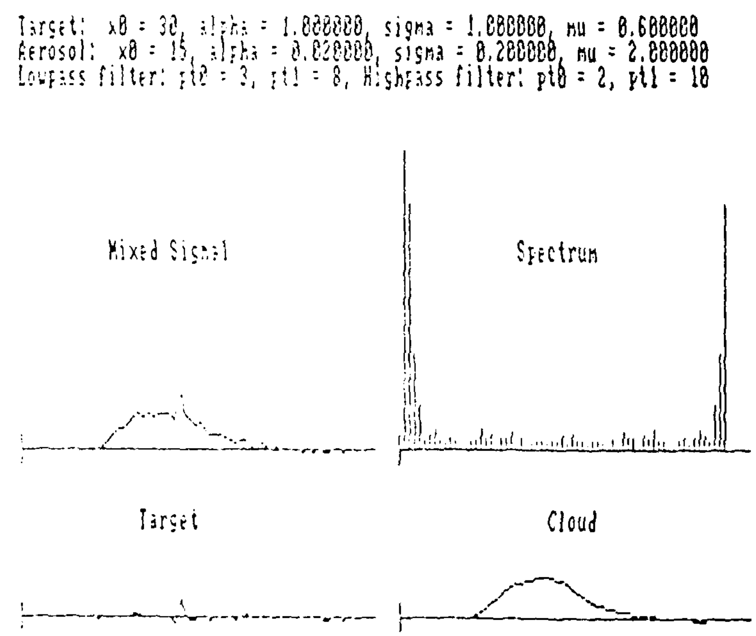

Figure 5. Signal Separation by Spectral Extraction. FFT. Trapezoidal Filter.

VI. CONCLUSION

Four orthogonal transforms and two different types of filter transfer functions are examined in this paper. They all produced favorable results in separation of aerosol-target signals. Also some subtle differences are noted in the way they have reacted to input signals. These points are summarized as follows:

1. The FFT was very effective in execution time, memory space, and ability to reonstruct a signal very close to the original. The reason is that, since the complex form of the Fourier transform was used, for the same amount of the input data points the number of frequencies involved in this transform is twice as much as that of the other transforms.

2. Cosine, Hartley and Triangular transforms produce somewhat coarsely reconstructed signals. However, lower density in the spectral distribution of these transforms brought forth easier analysis in transform domain.

3. Triangular transform is effective for signals with sharp spikes. While other transformation show some blurring effects on the reconstructed signals, the triangular basis functions could preserve the original sharpness.

4. An Ideal filter produces more ringing effects than a trapezoidal filter, especially for the high-pass filtered signals. This is due to the sharp discontinuity between passed and filtered frequencies.

VII. RECOMMENDATIONS

The results obtained during the summer research demonstrate that the aerosol-target signal discrimination of Ladar returns is feasible in several different ways within the limit of modest signal processing schemes. It is strongly urged that continued efforts be made in the following direction.

1. A study of parallel implementation of different methods is needed. To obtain a more dependable sensor, two or more algorithms could be implemented in parallel for target detection confirmation.

2. Automation of a filter design: Repeated testing and simulation have shown that the effectiveness of spectral extraction method heavily depends on a filter transfer function. A filter function workable for a certain type of aerosol-target signal is not always effective for a different type. Filter functions need to be taylored to each different input signal in order to avoid a false alarm or to accurately detect a target signal. Automation of a filter operation which can gear itself to detection of any given signal is needed and would be an extremely challenging study.

It is urged to have this study continued with the support from Mini Grant Program.

REFERENCES

1. D.E. Ruch and L.H. Koski: Target Descrimination Techniques for Optical Proximity Sensors, AFATL-TR-76-82, Air Force Armament Laboratory (Delco Electronics), 1976
2. G. Benjamin Hocker & Paul Nachman: Self-Detecting Sensors for Fuzes, AFATL-TR-80-64, Air Force Armament Laboratory (Honeywell), 1980
3. J. E. Gallagher and S.M. Borowko: Self-Detecting Optical Proximity Sensor (SDOPS), AFATL-TR-85-58, Air Force Armament Laboratory (McDonnell Douglas), 1985.
4. Missile Fuze Section Engineering Staff: Near Infrared Fuze Technology (NIFT), AFATL-TR-88-99, Air Force Armament Laboratory (Motorola), 1988
5. Dennis W. McGuire, Michael Conner, and Theodore H. Hopp: Aerosol Discrimination by Electronic High- and Low-pass Filtering, HDL-TR-1939, Harry Diamond Laboratories, 1981.
6. Dennis W. McGuire and Michael Conner:The Deconvolution of Aerosol Backscattered Optical Pulses to Obtain System-Independent Aerosol Signatures, HDL-TR-1944, Harry Diamond Laboratories, 1981.
7. K. Min et al., "A Fast Triangular Transform and Its Applications," Proc. IEEE International Conference on Acoustics, Speech, and Signal Processing, 1987 pp. 1811-1814. 1987.
8. K. Min et al., " Automated Two Speaker Separation System", Proc. IEEE International Conference on Acoustics, Speech, and Signal Processing, 1988 pp. 537-540, 1988.

1988 USAF-UES SUMMER FACULTY RESEARCH PROGRAM/

GRADUATE STUDENT RESEARCH PROGRAM

Sponsored by the

AIR FORCE OFFICE OF SCIENTIFIC RESEARCH

conducted by the

Universal Energy Systems, Inc.

FINAL REPORT

VISCOUS GRID GENERATION ABOUT A TWO-STORE MUTUAL INTERFERENCE PROBLEM

Prepared By:	Thomas H. Olsen
Academic Rank:	Graduate Student-Master's
Department and University:	Aerospace Engineering Sciences University of Colorado/Boulder
Research Location:	AFATL/FXA Eglin AFB Fort Walton Beach, Florida 32543
USAF Researcher:	Dr. Dave M. Belk
Date:	September 29,1988
Contract No:	F49620-88-C-0053

Viscous Grid Generation

About a Two-Store Mutual

Interference Problem

by

Thomas H. Olsen

ABSTRACT

Studies of the mutual interference flow problem have shown that a viscous flow field exists. Therefore, due to the importance of this problem to the study of store/aircraft combatibility, viscous modeling of this flow field is necessary. The first step in the computational modeling of a viscous problem is the delvelopment of a viscous grid. In this study, a computational mesh for a two-store mutual interference problem was generated using patched grids. However, because of a problem with off-boundary spacing, a viscous grid was not obtained. Once the grid lines can be made to follow the body, a viscous grid will be obtained.

Acknowledgements

I wish to thank the Air Force Systems Command and the Air Force Office of Scientific Research for sponsorship of this research effort. Universal Energy Systems must also be mentioned for their concern and help to me in all administrative and directional aspects of this program

My experience as a participant in the Graduate Student Research Program was enriching and rewarding due to many different influences. Dr. Dave Belk provided constant support and encouragement. The help of Dr. Lawrence Lijewski was invaluable in generating the configuration for the grid. Captain Jon S. Mounts's interest in every phase of this project served as an excellent source of stimulation. Bruce Simpson, Lt. Montgomery C. Hughson, Rudy Johnson, Lynn Lewis, Yen Tu, John Cipolla, and Bill Riner must also be mentioned for their help and encouragement. I would also like to thank the Air Force Armament Laboratory as a whole for providing me a truly enjoyable working atmosphere

I. INTRODUCTION

Today's high-speed military aircraft are intended to carry stores either externally or semi-submerged and are rated as to their ability to deliver these stores to their targets accurately without loss of aircraft performance or agility. However, store-induced aerodynamic drag can significantly downgrade aerodynamic performance, while aerodynamic interference may cause the released stores to scatter, run into each other, or impact the aircraft. Therefore, it is necessary to develop reliable methods to predict the aerodynamics of the store/aircraft interaction before and during separation.

The Computational Fluid Dynamics Section of the Aerodynamics Branch of the Armament Laboratory at Eglin Air Force Base is particularly interested in store aircraft combatibility. Therefore, the mutual interference problem between stores is an important flow field to study. Experimental data for mutual interference flow was initially collected for code validation (ref. 1). However, examination of experimental data and numerical data showed this mutual interference flow field to be dominated by viscosity (ref. 2). The numerical data was obtained using the EAGLE numerical grid generation code (ref. 3,4) and the EAGLE Euler code (ref. 5). The inviscid solutions obtained from the Euler code proved to be inadequate in modeling the mutual interference flow field. Viscous calculations, using a chimera grid scheme by Benek, have shown good qualitative results for a two- and three store mutual interference configuration (ref. 6). A closer study to quantitatively determine the aerodynamic interference is needed.

Due to the importance of the mutual interference problem, a viscous adaptation of the EAGLF flow solver is being developed by Simpson (ref. 7) and Mounts (ref.

8) at the Armament Laboratory. With the thin-layer Navier-Stokes code, viscous flow field solutions on blocked grids should be attainable for this mutual interference problem. Before viscous solutions can be obtained, however, a viscous grid for this mutual interference problem must be developed.

II. OBJECTIVES OF THE RESEARCH EFFORT

My research goal as a participant in the 1988 Graduate Student Research Program (GSRP) was to develop a viscous grid for a configuration consisting of two unfinned, axisymmetric stores using the EAGLE numerical grid generation code (ref. 3,4). The geometry of this configuration was designed to simulate the two-store case used in the wind tunnel experiment (ref. 1). This configuration was chosen to allow for the further study of the mutual interference flow field in the transonic regime.

III. APPROACH

In order to generate the computational mesh for the two-store configuration, one store is generated adjacent to a reflection plane to take advantage of symmetry. The separation distance between the store and the reflection plane is one-half the desired separation distance between the two stores. Therefore, with reflective boundary conditions applied in the flow solver (ref. 8), the geometry of the problem is identical to the geometry used in the wind tunnel experiment (ref. 1).

Due to the complexity of the configuration, a multi-block grid was designed. The first decision in the gridding process was which type of grids to use. There are basically four types of grids to choose from. These are O-grids, C-grids, H-grids and blocked, or Cartesian, grids. The O-grid has grid lines wrapped around the

body with a branch cut defined, as shown in figure 1a. The C-grid also has grid lines which wrap around the body, but with a physical branch cut along the wake, as shown in figure 1b. An H-grid has grid lines that extend to an infinite space with an internal branch cut, as shown in figure 1c. This branch cut causes a singularity at the leading edge of the body. The Cartesian grid is a simple blocked grid without any branch cuts, as shown in figure 1d.

The chosen arrangement consists of a C-grid around the body, an inner Cartesian grid in front of the C-grid, and an outer Cartesian grid surrounding part of the inner Cartesian grid and C-grid. The C-grid was used around the body to ensure that the tight concentration of grid points, needed for the viscous grid, only occurs around the body and to avoid the singularity at the leading edge. The physical branch cut for the C-grid occurs at the back boundary of the grid. The arrangement of the C-grid and the Cartesian grids is shown in figure 2. This figure shows how the inner Cartesian grid is positioned in front of the C-grid in order to square-off the front boundary and accurately resolve the flow field in front of the body. This figure also shows that the outer Cartesian grid only extends from the upper surface of the C-grid and the inner Cartesian grid, while the lower surface of the C-grid and inner Cartesian grid make up the reflection plane. The reflection plane can be seen in greater detail in figure 3, which is the back plane of the grid. This figure shows how the outer Cartesian grid wraps around part of the C-grid and contributes to the reflection plane.

The EAGLE numerical grid generation code (ref. 3,4) uses patched grids to map complex configurations. Therefore, since the C-grid and the inner Cartesian grid each contribute one-fourth of their outer boundaries to the reflection plane, these grids were each divided into four blocks. This was done in order to keep

consistent block sizes instead of using two blocks of different sizes. Since the outer Cartesian grid only surrounds three of the four blocks of the inner grids, only three blocks were used. However, the outer Cartesian grid was also subdivided into a fore and aft outer Cartesian grid. Therefore the total grid was composed of fourteen blocks.

The dimensions of the computational regions are as follows:

Four blocks of C-grid:	140x24x13	(1-4)
Four blocks of inner Cartesian grid:	25x15x13	(5-8)
Three blocks of outer Cartesian grid (fore):	25x13x13	(9-11)
Three blocks of outer Cartesian grid (aft):	128x13x13	(12-14)

These dimensions are thought to be adequate to resolve the viscous interference flow field. However, flow field solutions may show that a more refined mesh is necessary.

IV. RESULTS

Preliminary flow field solutions were not obtained due to problems with the off-boundary spacing. In order to obtain the viscous grid, spacing in the j-direction was specified to provide a high concentration of computational points close to the body of the store. However, the preliminary grid showed that the grid lines were separating away from the body in blocks 1-3 of the C-grid but not in block 4 as shown in figure 4. Efforts to resolve this phenomena have led us to believe that this is a problem with the blending function used in the transfinite interpolation process. The transfinite interpolation process interpolates values of the Cartesian coordinates for the grid points between already specified values on the section boundary. This interpolation may either be a linear interpolation, or an interpolation based on arc length. In blocks 1-3, this interpolation appears to be defaulting to the linear type. If an interpolation based on arc length can be used, a viscous grid may be obtained.

In order to obtain the grid shown in figures 2, 3, and 5, the spacing in the j-direction was increased by a factor of ten. This spacing allowed the grid lines to follow the body as shown in figure 5. However, this spacing is not tight enough around the body to give a viscous grid. Therefore, until the problem with the grid lines and the desired spacing is resolved, only an inviscid grid may be obtained

V. RECOMMENDATIONS

Due to the problems of the off-boundary spacing, the primary recommendation would be to determine why the grid lines are not following the body in the viscous grid. If this is a problem with the blending functions for interpolation, then it should be determined why linear interpolation is used, instead of an interpolation based on arc length. Once this problem is solved, a viscous grid may be obtained with the required off-boundary spacing

After this is accomplished, preliminary flow field solutions should be obtained to show where a higher concentration of grid points is desired. Once a final grid is developed, and good qualitative and quantitative results are obtained, the viscous flow field may be studied in greater detail.

In order to study the two-store mutual interference problem in greater detail, one should look at the effects of Mach number and separation distance on the flow field. Mach numbers that should be examined are 0.6, 0.85, 0.95, 1.05, and 1.20. The separation distance should be varied from 0.8 to 0.4 or when the onset of choking occurs.

The relative merits of blocked grids, used by the EAGLE code (ref. 3,4), and overset chimera grids (ref. 9) should also be explored. Also, a comparison between

the viscous adaptation of the Eagle flow solver (ref. 8) and the F3D flow solver (ref. 10) should be made. By running each of the flow solvers on both types of grids, a comparison can be made of the two different gridding techniques and the two flow solvers.

REFERENCES

1. Mrdeza, M. N., "CFD Unfinned Mutual Interference Wind Tunnel Experiment," AEDC-TSR-85-P21, November 1985.

2. Cottrell, C. J., and Martinez, A., "Experimental and Numerical Data for Transonic Mutual Interference Around Unfinned Bodies," AFATL-TR-86-75, October 1986.

3. Thompson, J. F., "Program EAGLE Numerical Grid Generation System User's Manual, Volume II: Surface Generation System," AFATL-TR-87-15, Vol. II

4. Thompson, J. F., "Program EAGLE Numerical Grid Generation System User's Manual, Volume III: Grid Generation System," AFATL-TR-87-15, Vol. III.

5. Mounts, J. S., Belk, D. M., and Whitfield, D. L., "Program EAGLE-Users Manual, Volume IV: Multi-block, Implicit, Steady-State Euler Code," AFATL-TR-88-117, September 1988.

6. Benek, J. A., Donegan, T. L., and Suhs, N. E., "Extended Chimera Grid Embedding Technique with Application to Viscous Flows," Computational Fluid Dynamics Conference, Honolulu, HI, 1987, AIAA 87-1126-CP.

7. Simpson, L.B., Three Dimensional Unsteady Navier-Stokes Solutions on Blocked Dynamic Grids, Ph.D Dissertation Mississippi State University, to be published December 1988.

8. Mounts, J. S., A Multi-Block, Implicit, Steady-State Thin-Layer Navier-Stokes Algorithm for Advanced Fluid Dynamic Applications, Master's Thesis, University of Florida, to be published December 1988.

9. Dougherty, F. C., Development of a Chimera Grid Scheme with Applications to Unsteady Problems, Ph.D. Thesis, Department of Aeronautics and Astronautics, Stanford University, June 1985.

10. Steger, J. L., Ying, S. X., and Schiff, L. B., "A Partially Flux-Split Algorithm for Numerical Simulation of Compressible Inviscid and Viscous Flow," Workshop on CFD, Institute of Nonlinear Sciences at UCD, 1986.

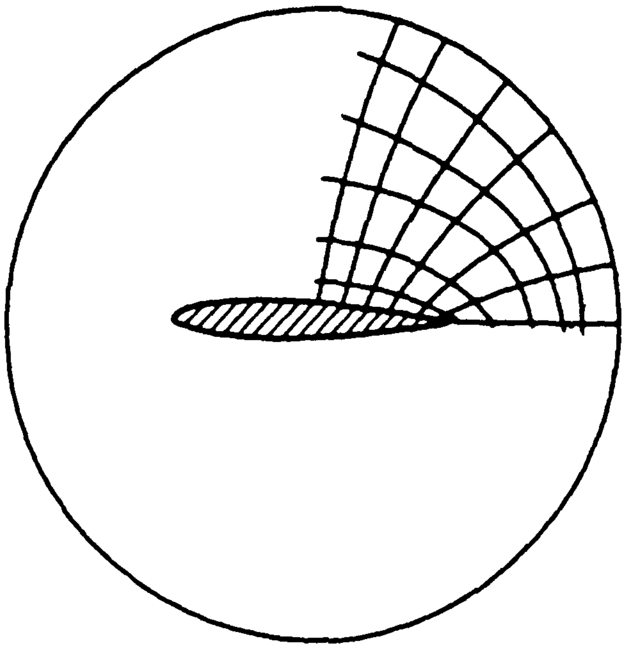

Figure 1a. O-Grid

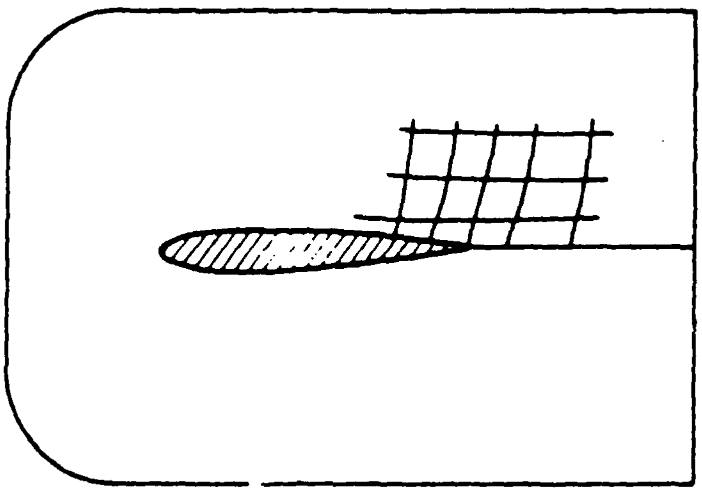

Figure 1b. C-Grid

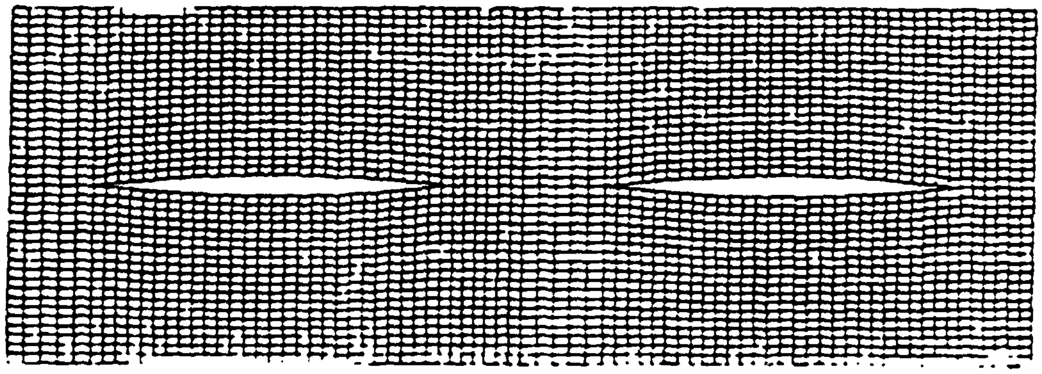

Figure 1c. H-Grid

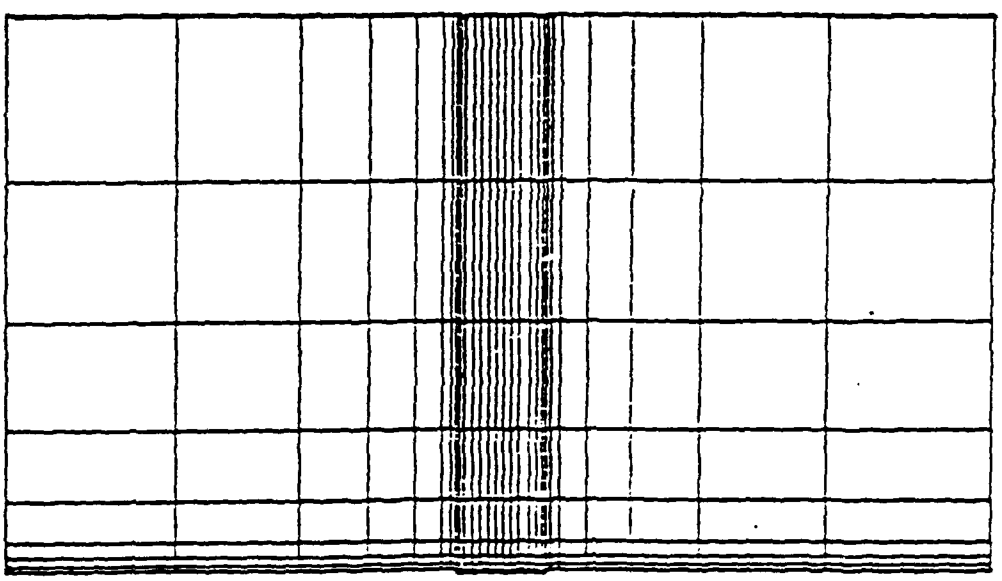

Figure 1d. Cartesian Grid

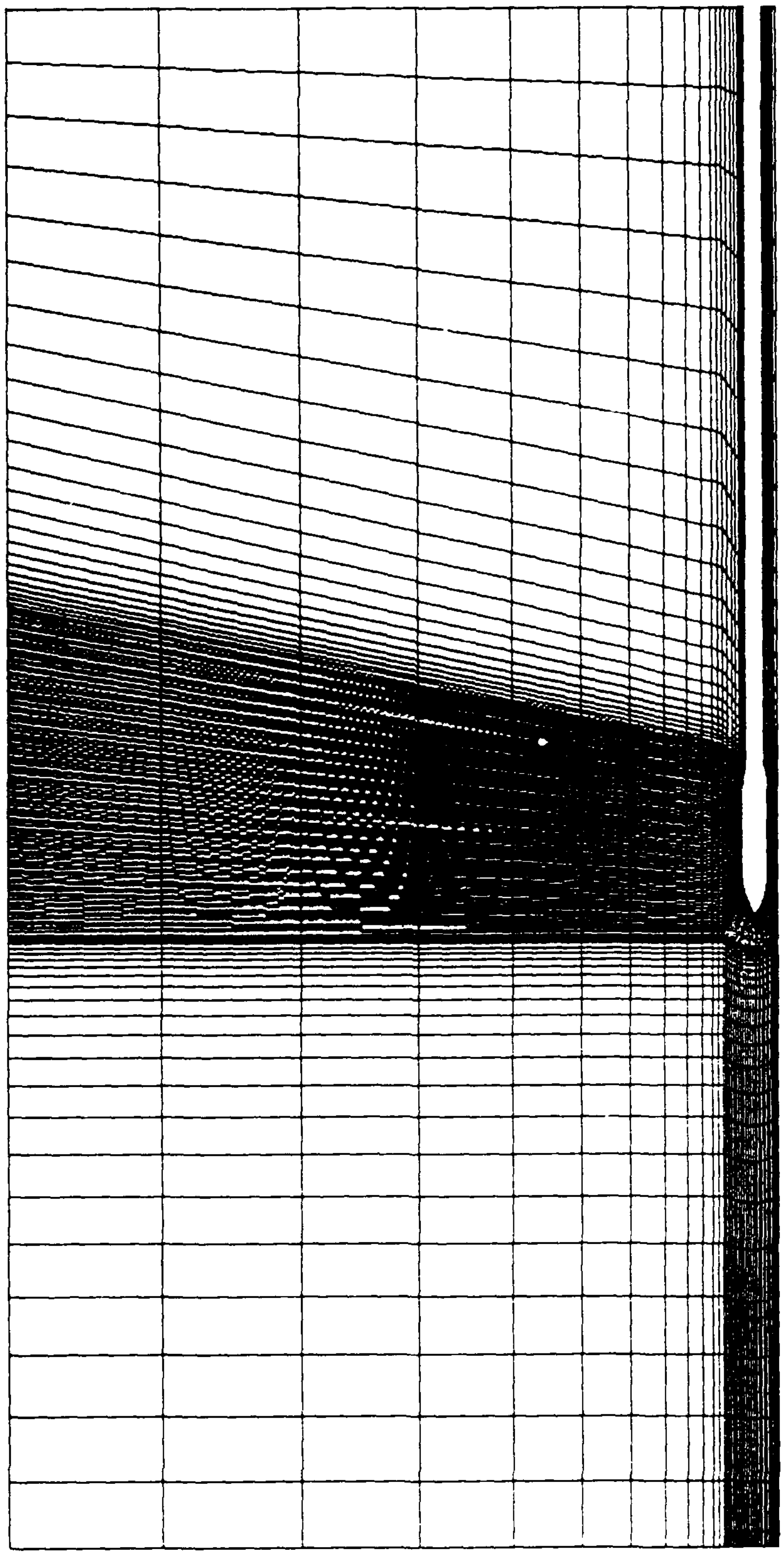

Figure 2. Side View of Computational Mesh

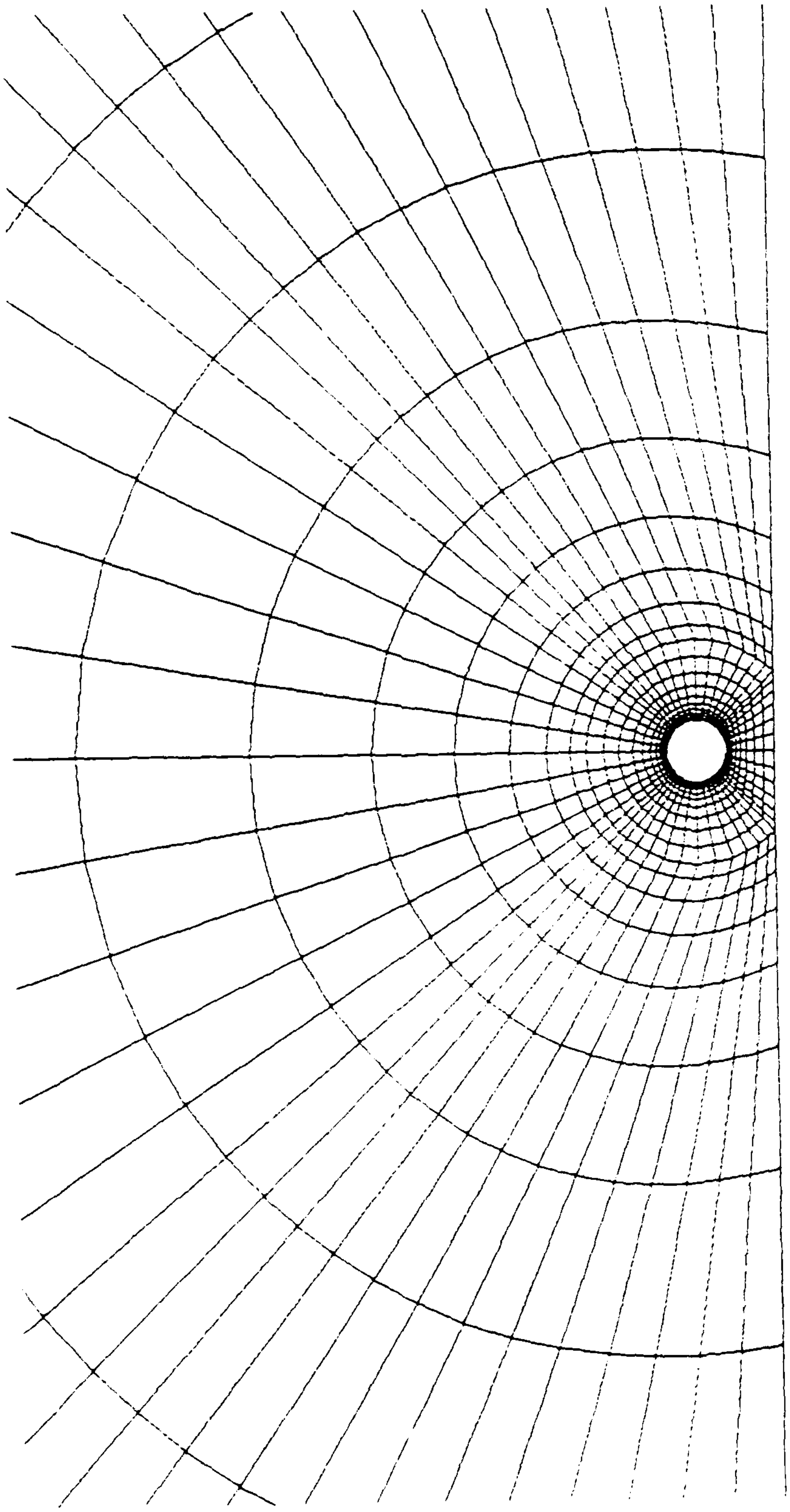

Figure 3. View of Back Plane of Computational Mesh

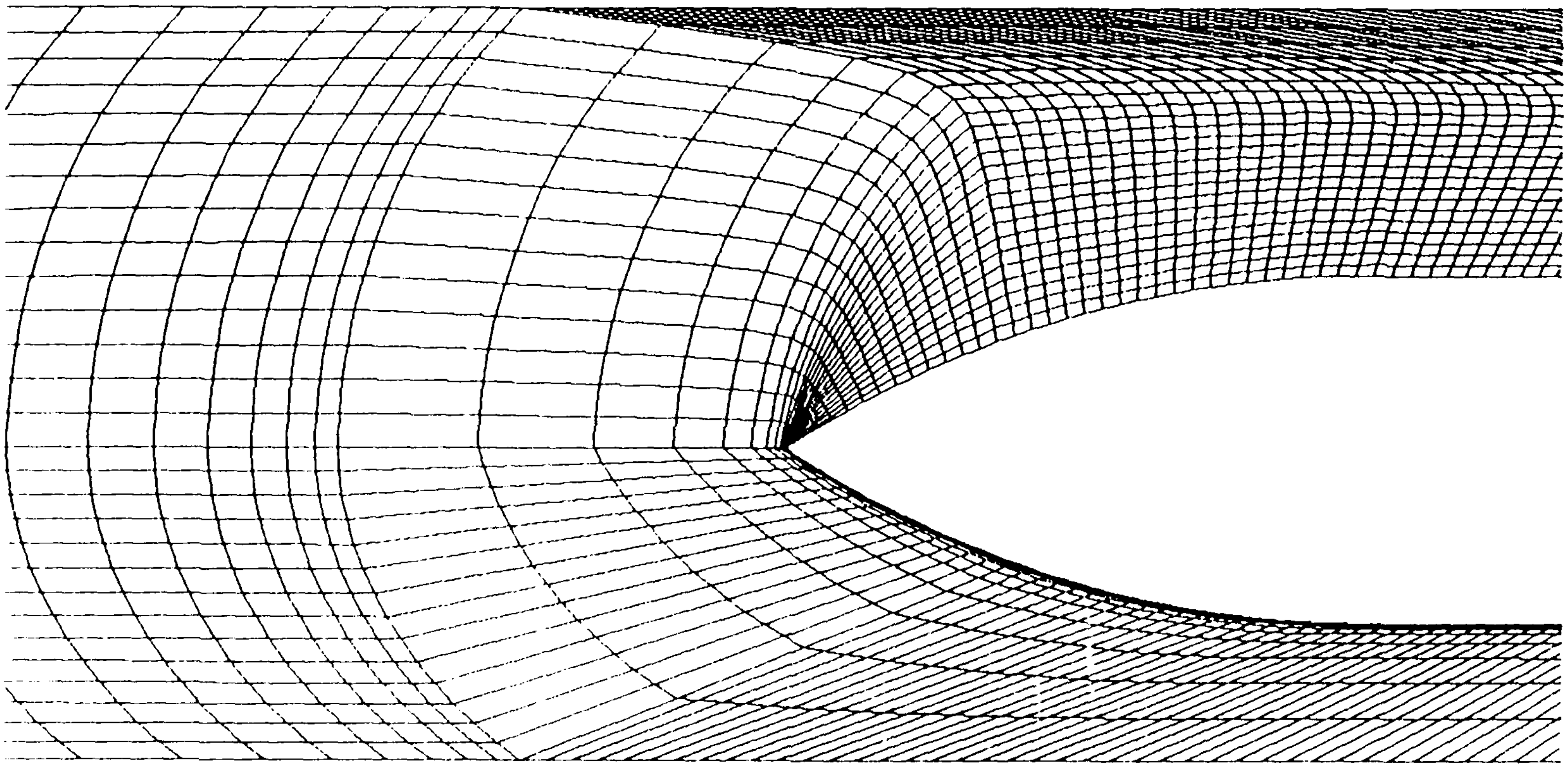

Figure 4. Close-up of C-Grid

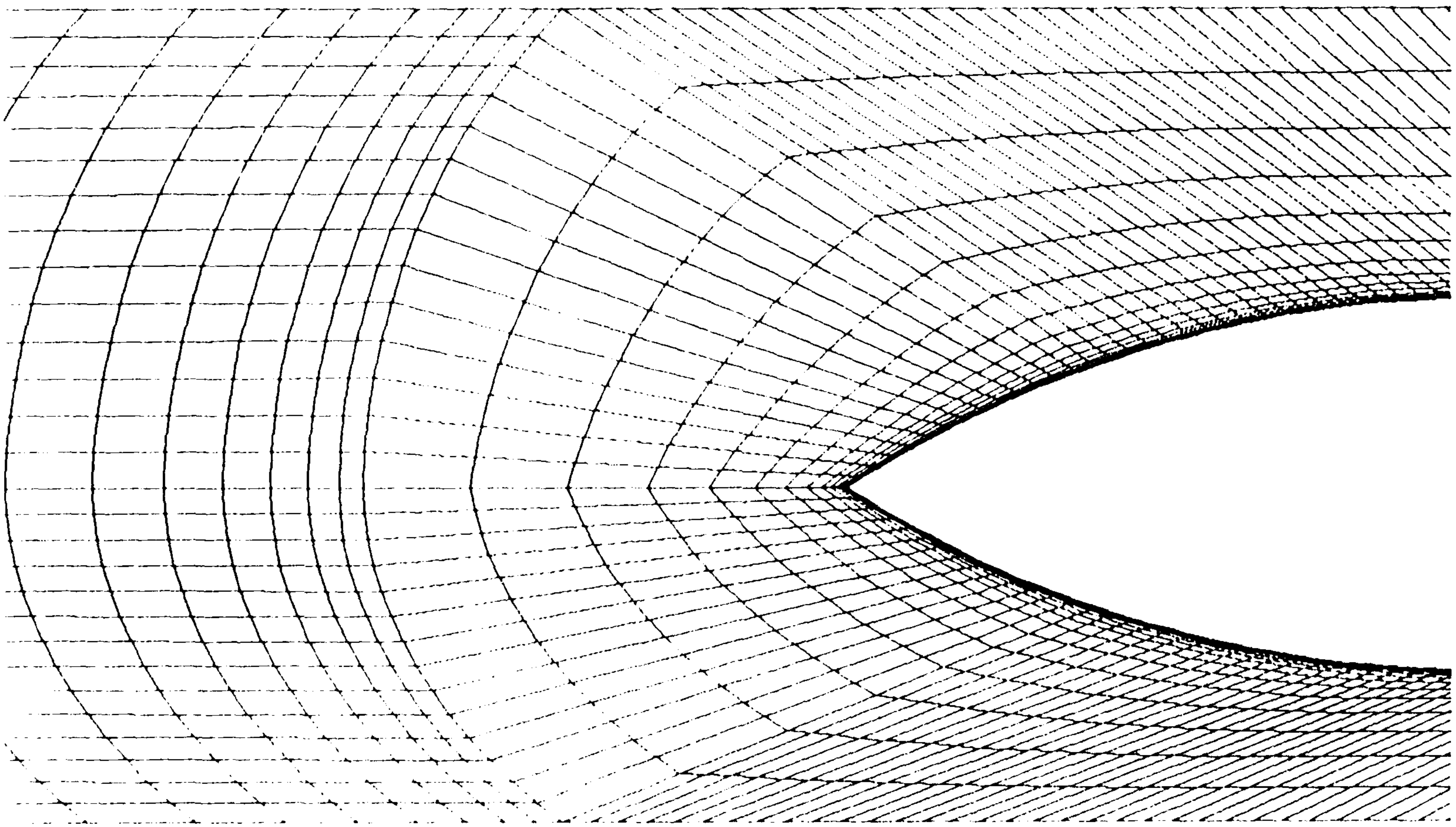

Figure 5. Close-up of Inviscid C-Grid

1988 USAF-UES SUMMER FACULTY RESEARCH PROGRAM

GRADUATE STUDENT RESEARCH PROGRAM

Sponsored by the

AIR FORCE OFFICE OF SCIENTIFIC RESEARCH

Conducted by

UNIVERSAL ENERGY SYSTEMS, INC.

FINAL REPORT

Arima Modeling of Residuals in AD/KR TDOP Models

Prepared By:	Shawky E. Shamma and Anne L. Siegman
Academic Rank:	Professor and Graduate Student
Department and University:	Department of Mathematics University of West F orida/Univ. of Miami
Research Location:	Directorate of Computer Science Armament Laboratory Eglin AFB, FL
USAF Researcher:	John Lindegren

Date:	1 August 1988
Contract No.	F49620-88-C-0053

SAME REPORT AS
DR. SHAMMA
ARMAMENT LABORATORY # 7

1988 USAF-UES SUMMER FACULTY RESEARCH PROGRAM/

GRADUATE STUDENT RESEARCH PROGRAM

Sponsored by the

AIR FORCE OFFICE OF SCIENTIFIC RESEARCH

conducted by the

Universal Energy Systems, Inc.

FINAL REPORT

MULTIGRAPH Kernel for Transputer Based Systems

Prepared by:	Ben Allen Abbott
Academic Rank:	Graduate Student
Department and University:	Electrical Engineering Department, Vanderbilt University
Research Location:	AEDC/DOTR Arnold AFB TN 37389-5000
USAF Researcher:	Lt. Ted Bapty
Date:	8 Sept. 1988
Contract No:	F49620-88-C-0053

MULTIGRAPH Kernel for Transputer Based Systems

by

Ben A. Abbott

ABSTRACT

Development of a multi-Transputer distributed real-time kernel for signal processing and control applications was started. The resulting system will be a parallel execution environment allowing a large grain data-flow graph to be built and scheduled in a dynamic fashion. This execution environment hides the underlying hardware structure (a virtual machine) so as to allow knowledge based system builders to create and dynamically adapt a real-time system.

Acknowledgements

Many thanks to the Air Force Systems Command and the Air force Office of Scientific Research for sponsoring this research. Universal Energy systems has my gratitude for their concern and help to me in all administrative and directional aspects of this program. Thanks as well to AEDC/DOTR for the much needed use of equipment and space.

There is no doubt the summer would not have been successful without the patience and insight of Lt. Ted Bapty. Good luck in your continuing work. As always, thanks are required for the crew at Vanderbilt, Janos Sztipanovits, Gabor Karsai, and Csaba Biegl without whom there would be no MULTIGRAPH.

I. INTRODUCTION:

The testing of complex systems such as jet engine turbines demands super computer power for the evaluation of results. The computational requirements are so immense that even the largest Cray systems are not capable of processing the information in real-time. The use of multi-processor systems offers the power needed. However, development of such parallel processing systems is extremely difficult. In light of this difficulty, the Electrical Engineering department of Vanderbilt University has on going research and development to provide tools that ease the burdens involved in multi-processor system development.

AEDC/DOTR is involved in building a parallel processing platform based on the INMOS Transputer building block. This system will be used for real-time analysis and display of test cell data. Such a system requires special purpose programming of very low level parallel processing features (no operating system is provided) as well as development of the higher level signal processing concepts. The work accomplished thus far has proven both the power and unwieldiness of such a system. Therefore, this system is a great candidate to utilize the tools developed by Vanderbilt.

Development of real-time instrumentation systems requires the cross-over of two distinct engineering fields: Signal processing and Computer Engineering. The high level problem is that of the signal processing issues, yet the computational complexity of parallel processing causes numerous low level computer engineering issues to emerge. The goal of Vanderbilt research has been to free the development of the signal processing concepts from the issues involved in computer implementation of the system.

Past work at Vanderbilt in this area has produced several extremely high level development environments [1],[2],[3]. These environments combine the use of symbolic programming and other techniques developed in the artificial intelligence research field with the classic numerical

approach for solving instrumentation problems. The result is a graphical editing environment where the signal flow graph is developed. This environment is set up to allow hierarchical design of the graph components. That is, an item such as a spectrum analyzer may be built up from some previously developed lower level items (bandpass filters, square-law devices, low pass filters, etc.). This spectrum analyzer may then in turn be used to built up even higher level components. The lowest level of the hierarchy (primitives) are implemented in standard numerical languages such as Fortran and C. When design of the top level signal flow graph of the hierarchy is completed, a mapping process converts it first to the lowest level components of the hierarchy and then maps the result into a parallel execution environment, the Multigraph Kernel, where it is then executed. The resulting execution program is inherently parallel. As well, it has been automatically generated from the high level description. Thus, the goal of easing the computer engineering portion of the burden is accomplished.

The implementation of this environment is a layered architecture (see figure 1) at the bottom of which in HARDWARE is a heterogeneous platform of computing elements. Above this rides a SYSTEM LAYER providing multitasking, synchronization, and communication among various components. The MODULE LAYER lies above the SYSTEM LAYER and provides a virtual machine for the basic numerical calculations and the interactions or synchronization among these components. This is done by providing functions to dynamically build up and schedule large-grain data-flow graphs. The KNOWLEDGE-BASED LAYER (sometimes called the system builder) is the top layer and provides functions such as declarative and graphical language descriptions of the system to be provided by the user. This declaration is then transformed into a data-flow graph in which each of the nodes is a numerical computing element. The connections of the graph itself establish the scheduling requirements for this parallel algorithm. The system builder then maps the built up graph down to the MODULE LAYER where it may be executed by the graph scheduling facilities provided. It is important to note that the MODULE LAYER hides the lower levels and thus porting to another hardware platform requires only development of the SYSTEM and MODULE LAYERS.

Previous implementation of this environment have been on multi-VAX systems, SUN workstations, IBM 9000, and HP workstations.

My research interests are in the area of parallel processing hardware and software. The problems generated by providing such a high level of user application environment without over taxing the computational requirements produce many interesting parallel processing issues.

II. OBJECTIVES OF THE RESEARCH EFFORT:

The main goal of this research effort was to explore the feasibility of porting the MULTIGRAPH kernel execution environment to a multi-Transputer based system. To accomplish this goal, several objectives were established early on and then later modified as needed. The first objective involved exploration of the multi-tasking facilities of the Transputer, evaluating each for efficiency, power, and flexibility. Once this information was known, a reasonable approach to the Transputer implementation could be taken. This initiated effort on the second objective of my summer work, porting the MGK to a single Transputer (watching for issues of the eventual multi-Transputer implementation). The third objective of the work involved specific tailoring of the MGK scheduling functions to take advantage of the Transputer's hardware support of concurrency. The forth objective was to spread the single Transputer based MGK across a set of Transputers using the serial links provided to produce a virtual machine. This objective produced a spin off objective requiring generation of a message routing system flexible enough to work across many different Transputer configurations (an end system might use the INMOS crossbar switch to dynamically reconfigure the actual architecture to match the specific problem being solved). The fifth objective (worked in parallel with the others) was to set up a UNIX based host for the set of Transputer-MGK components. This host will then provide symbolic computation through Kyoto Common Lisp [KCL]. In an end system the KCL/Host is to provide the functions of building and monitoring an application program while the Transputer-MGK components provide the work force. All aspects of the work as well as its daily status were discussed with Lt. Ted Bapty as well as my advisor at Vanderbilt, Janos Sztipanovits.

III. EXPLORATION OF MULTI-TASKING FACILITIES OF THE TRANSPUTER:

As stated previously, the first objective was to explore the multi-tasking facilities of the Transputer, evaluating each for efficiency, power, and flexibility. A 'C' compiler produced by 3L Ltd. was chosen due to availability. 3L provides parallel processing extensions to the Kernighan and Ritchie language with synchronization methods of both the classic processes/semaphores model as well as the communicating sequential processes model used by OCCAM [4]. Benchmark information fulfilling the first objective was compiled using two methods. First in the case of semaphore timing and process creation it proved easiest to disassemble the 3L runtime library and count the clock cycles used by each of these routines. For memory allocation benchmarks a uniform random number generator was used to randomly allocate and free 1000 blocks each with a random size between 10 bytes and 1k bytes. The benchmark information is shown in Table I.

The results of these benchmarks made it clear both channels and semaphores require very little overhead. The semaphores tend to be a more desirable choice for two reasons: 1) they do not require copying the data structures but rather allow a pointer to a structure to be passed between processes and 2) they facilitate asynchronous types of synchronization. Of course, the only way to communicate with another Transputer is through a channel. The only discouraging information gained through these benchmarks was the extremely slow dynamic memory management times. The approach adopted due to this problem was to note it and ultimately hand code a faster algorithm.

CHANNEL INPUT / OUTPUT:

Supported by a single machine instruction. Execution time is 2w+19 clock cycles (w is the number of 32 bit words to transfer). For channel I/O to another Transputer, an independent DMA controller is used for each physical link. Physical links transfer at 10 mega bit per second.

SEMAPHORES:

initialization	16	(clock cycles)
wait	17 or 37 if blocked	(clock cycles)
signal	22 or 40 if re-start	(clock cycles)

PROCESSES (THREADS):

priority check	9 (clock cycles)
stop	16 (clock cycles)
start*	206 + (37 per parameter passed in) (clock cycles) * This number does not include time for workspace allocation.
restart	17 (clock cycles)

DYNAMIC MEMORY MANAGEMENT (malloc, free):

allocate	sometimes > 10 milli-seconds
free	sometimes > 8 milli-seconds

T414 used: 2 Meg of 3 cycle RAM, 20 MHz processor.

TABLE I. Synchronization benchmarks for INMOS T414 with 3L Ltd C.

IV. PORTING MGK TO A SINGLE TRANSPUTER:

The second objective, porting the MGK to a single Transputer, progressed smoothly. Previous versions of the MGK were coded in 'C' in a transportable fashion. Even with this portable code, problems were expected since Transputer compilers are new products. The task ended up simply as some editing to remove the LISP portions of the kernel from the Transputer version, chasing some word size compatibility errors, and finding a set of I/O compatible routines.

V. TAILORING MGK SCHEDULING TO FIT THE TRANSPUTER:

During the third objective, tailoring the scheduler to use the Transputer scheduling functions, a scheduling issue arose. The Transputer hardware scheduler supports only two priorities of processes in its job scheduler. Past MULTIGRAPH systems have used many different levels of priority of the underlying scheduler to allow the target system to respond in a real-time manner. A decision was made at this time to use a multiple priority scheduler so as to allow the application system to have this added flexibility. The trade-off, of course, is the added overhead of a software scheduler verses the hardware scheduler. Benchmark testing at this point showed the extended scheduler added less than 5 percent overhead. In order to allow control over event response times, the parallel scheduler was set up in a fashion allowing the maximum number of nodes executing concurrently (hardware time sliced) to be limited. This keeps the processor resources from becoming flooded even when a large number of nodes could be executed simultaneously. The original node swapping scheduler (used for standard hardware) was left in the code so graph flow could be single stepped when debugging application systems.

VI. SPREAD MGK ACROSS A SET OF TRANSPUTERS:

The forth objective, spreading the MGK across a set of Transputers, has one large issue. Centralized or Decentralized control? This is a classic decision to be made in distributed computing systems. Work on this objective reached only preliminary stages. The time spent was used to establishing the issues. Due to the point to point communication nature of the Transputer, as well as the need to always store and forward messages rather than establishing a circuit or using global shared memory, it was deemed necessary to have decentralized control. With centralized control, message passing through the master's four communication links poses an inevitable bottleneck. Decentralized control of a graph computational model is not a difficult issue since the graph may be broken into sub-graphs each of which may be scheduled independently. The connections between these sub-graphs require external synchronization, but not in a centralized fashion. Obviously, to implement this multi-Transputer version of MGK an underlying communication system must be generated, this is the subject of the fifth objective, developing a flexible message routing system. Thus, the fifth objective, a spin off, took precedence. Another issue involved in this objective is the need for a dynamic linking loader to allow portions of the graph to be built up while others are already built. To allow structurally adaptive systems [5], this linking loader should be flexible enough to allow redistribution of an executing graph. 3L Ltd was not willing to provide the necessary interface information to allow this work to be easily done. Therefore, CSA (the compiler vendor) was contacted in hopes of a trade for the Logical Systems 'C' compiler. Logical systems provides full source code for their compiler and run-time environment. Results of this trade are still pending.

VII. DEVELOP A FLEXIBLE MESSAGE ROUTING SYSTEM:

The fifth objective, develop a flexible message routing system, was worked heavily during the end of the summer appointment. The basic goal was to provide the minimum system necessary to continue with the spreading of MGK across multiple Transputers. To keep from losing work, an effort was made to identify those items that would be desirable for a robust message routing system. In this way hooks were left to allow for graceful expansion of the message routing system when time provides. The issues established and the reasoning around them may be found in Table II. The basic message routing system provides the capability to make a remote procedure call from any node to any other node. Results of the call are always returned. Work on the message system was in an integration with the MGK phase when the summer appointment ended.

o Transport mechanism -

"Store and forward"
- Processing overhead will be minimized by DMA .
- Does not lower bandwidth due to bursty message nature.
- Order consistency is the biggest problem.
- Routing overhead is costly and repeated.
- Buffering wastes memory but send/acknowledge allows control.
- Datagram over packet-switch due to rebuilding overhead.
- To simplify buffer management and routing a form of packet will proceed each message.
- Messages will have the ability to lock a service so as to force consistency and inseparable operations (accomplished with remote procedure call).

o Routing mechanism
- Provide a distributed approach only.
- Provide self routing messages as a minimum.
- Allow tables with addresses later.

o Buffer management
- MGK dynamic memory (build type as specified by sender).

o Flow control
- The basic return code mechanism of MGK calls provides a "send/acknowledge protocol".

Table II. Key message passing system issues from "Multicomputer Networks" [6] pages 138+ applied to MULTIGRAPH - Transputer system.

VIII. PROVIDE A UNIX HOST:

The sixth object, to provide a Unix host, was worked in parallel with the other objectives. Previous system builder functions have been developed in a Kyoto Common Lisp (KCL) / Xwindows environment. AEDC is planning to use a PC 386 clone running Unix for the host functions. The tasks then were to install KCL with the Xwindows interface and develop a Unix driver providing communication with the Transputer network. The KCL was successfully installed, but the Xwindows interface still does not work. In order to investigate the problems associated with the Unix driver and to provide graphics support under MS-DOS, time was spent modifying the INMOS Afserver (a MS-DOS host driver).

IX. RECOMMENDATIONS:

A Transputer based MULTIGRAPH system is not only possible but gives every indication of being an extremely flexible yet powerful computing platform. With such a computing platform, real-time processing will be able to meet challenges presently unobtainable. Synchronization efficiency and inter-processor communication facilities of the Transputer meet the requirements of the MGK. Preliminary work porting the MGK to the Transputer has progressed smoothly. The most useful tools and information gained from this research will come only after a full version of a Transputer based MGK is in place. In light of this, future research should proceed in the following stepwise fashion:

1) Complete a basic message routing system.
2) Interface the MGK with this message routing system.
3) Set up a UNIX/KCL based host (includes driver and loader issues).
4) Interface the system builder functions to the Transputer platform.

After a full version of a Transputer based MULTIGRAPH system is completed, further use and research may branch in several directions. One important direction then available, is the use of the system builder to aid in development of specific application systems such as the real-time analysis of test cell data for AEDC. Further research possibilities include:

1) Exploration of the fault tolerance issues of this platform.
2) Use of this platform for performance measurement and comparison of the graph computational model.
3) Surveying and testing the feasibility of various message routing paradigms as they compare with the graph computational model.
4) Exploration of the issues around systems that dynamically restructure their software and hardware architectures in real-time.

REFERENCES

1. Sztipanovits, J., Biegl, C., Karsai, G., Bourne, J., Mushlin, R., Harrison, C.: "Knowledge Based Experiment Builder for Magnetic Resonance Imaging (MRI) Systems," Proc. of the 3rd IEEE Conference on Artificial Intelligence Applications, Orlando, FL, pp. 126-133, 1987.

2. Karsai, G., Biegl, C., Sztipanovits, J., Bourne, J., Mushlin, R., Harrison, C.: "Experiment Design Language for Intelligent MRI Systems," Proc. of the 8th Annual IEEE/EMBS Conference, Dallas, TX, pp. 803-807, 1986.

3. Sztipanovits, J., Biegl, C., Karsai, G.: "Graph Model-Based Approach to Representation, Interpretation and Execution of Real-Time Signal Processing Systems," International Journal of Intelligent Systems, 1988 (in press).

4. D. Pountain, A tutorial introduction to OCCAM programming, INMOS Limited, March 1987.

5. J. Sztipanovits: "Toward Structural Adaptivity," Proc. of the 1988 IEEE International Symposium on Circuits and Systems, Espoo, Finland, 1988. (in press).

6. Reed, D. and Fujimoto, R., Multicomputer Networks Message-Based Parallel Processing, Cambridge, Massachusetts, MIT Press, 1987.

1988 USAF-UES SUMMER FACULTY RESEARCH PROGRAM/

GRADUATE STUDENT RESEARCH PROGRAM

Sponsored by the

AIR FORCE OFFICE OF SCIENTIFIC RESEARCH

Conducted by the

Universal Energy Systems, Inc.

FINAL REPORT

PERFORMANCE ANALYSES OF AN IR LASER SCANNER SYSTEM UTILIZING BRAGG CELL DEFLECTORS AND MODULATOR FOR WRITING DIRECTLY ON FPAs UNDER TEST

Prepared by:	Keith Alan Krapels
Academic Rank:	Doctoral Intern
Department and University:	Electrical Engineering Dept. Memphis State University
Research Location:	Arnold Engineering Development Center, Von Karman Facility, Space Systems Branch Arnold AFB, TN 37389
USAF Researcher:	P. David Elrod

Date:	19 August 1988
Contract No:	F49620-88-C-0053

FINAL REPORT IS NOT PUBLISHABLE AT THIS TIME

1988 USAF-UES SUMMER FACULTY RESEARCH PROGRAM

GRADUATE STUDENT RESEARCH PROGRAM

Sponsored by the

Air Force Office of Scientific Research

Conducted by

Universal Energy Systems, Inc.

<u>FINAL REPORT</u>

Test of a Locally Implicit Method for the Euler Equations and an Artificial Dissipation Scheme

Prepared By:	Robert W. Tramel
Academic Rank:	Graduate Research Assistant
Department and University:	Mathematics University of Tennessee, Tullahoma
Research Location:	Arnold Air Force Station Tullahoma, TN 37389
USAF Researcher:	K. C. Reddy
Date:	12 August 1988
Contract No.	F49620-88-C-0053

TEST OF A LOCALLY IMPLICIT METHOD FOR THE EULER EQUATIONS AND AN ARTIFICIAL DISSIPATION SCHEME

by

Robert W. Tramel

ABSTRACT

A locally implicit method for the solution of the unsteady one dimensional Euler equations of fluid mechanics is considered as well as a new artificial dissipation scheme based on the Hamiltonian structure of Eulerian fluid mechanics. The method is also tested with Jameson-type artificial dissipation terms. The method is tested both without and with artificial dissipation on the standard test problem proposed by Sod(1978). Results are reported for each case.

I. INTRODUCTION:

The scope and magnitude of the problems that the working engineer wishes to solve using the methods of computational fluid dynamics grow constantly. Thus, there is a very important need for more efficient algorithms for solving large scale problems.

The computational fluid dynamics group of Calspan Corporation, Arnold Engineering Development Center Branch are actively engaged in this effort. They need efficient, robust methods for the solution of fluid flow problems about bodies of various configurations.

My own research interests include the development of new methods for the efficient solution of the equations of fluid motion and the use of these methods in the elucidation of the behaviour of fluid systems. My research interests also include dynamical systems theory. In this context, I attempted to develop a new artificial dissipation scheme based on the Hamiltonian method of fluid dynamics.

II. OBJECTIVE OF THE RESEARCH EFFORT:

The main objective of my research effort for the 1988 Summer Faculty Research Program (SFRP) is to work on the development of a locally implicit scheme for the solution of the Euler equations of fluid mechanics. The scheme is to be tested on a version of the Reimann problem proposed by Sod(1978) as a standard test. A sucessful scheme would be one which accurately predicts the time evolution of a flow field which includes both shock and rarefaction waves.

My secondary objective for the SFRP is to develop a new artificial dissipation scheme based on the Hamiltonian method of conservative fluid mechanics. An additional term is added to the Hamiltonian of the system. This perturbation term is supposed to add stablity in regions in which the numerical method being tested produces spurious oscillations.

III.

a. The Euler equations can be written in the form (1)

$$\frac{\partial \vec{Q}}{\partial t} + \frac{\partial \vec{F}}{\partial x} = \vec{0} \qquad (1)$$

where $\vec{Q}$ is the vector ($\rho, \rho u, e$) and $\vec{F}$ is the vector ($\rho u, \rho u^2 + p, u(e+p)$). Here ρ is the density, u is the velocity, e is the energy per unit volume, and p is the pressure. The pressure is related to the other variables for a perfect gas by the relation $p = (\gamma - 1)(e - \frac{1}{2}\rho u^2)$.

The locally implicit scheme based on central difference spatial approximations is written as follows. For details see the paper by Reddy and Jacocks(1987).

$$\frac{1}{\Delta t}\left(\vec{Q}_i^{n+1}-\vec{Q}_i^{n}\right)+\frac{1}{2\Delta x}\left(\vec{F}_{i+1}-\vec{F}_{i-1}\right)=\vec{0} \tag{2}$$

$\vec{Q}_i^{n+1}$ is the value of the vector $\vec{Q}$ at the Ith lattice point at time step n+1. $\vec{Q}_i^{n}$ is the value of the vector $\vec{Q}$ at the Ith lattice point at time step n. $\vec{F}_{i+1}$ is the value of the vector at the I+1 lattice point and $\vec{F}_{i-1}$ is the value of the same vector at the I-1 lattice point. Both the vectors are evaluated using the values of the vector $\vec{Q}$ at time step n+1. Δt is the lattice spacing in the time direction, and ΔX is the lattice spacing in the spatial direction. From one time step to the next, the system of equations (2) is solved by the following iterative method. A modified Gauss-Seidel iteration is made from the inital lattice point to the final point. The process is then repeated with the sweep going from the final lattice point to the inital point. Several such symmetric iteration sweeps are made at each time step. The latest estimate for the value of the vector $\vec{Q}$ at the Ith lattice point at time step n+1 is denoted by $\vec{Q}_i^{*}$. At each lattice point it is updated by the formula (3).

$$\vec{Q}_i^{*}=\vec{Q}_i^{*}+\frac{win}{c}\left(\vec{R}es_i\right) \tag{3}$$

C is given by the formula $c=\frac{1}{\Delta t}+\frac{1}{\Delta x}\left(|u_i|+a_i\right)$ where a_i is the local speed of sound at the Ith lattice point at time step n+1. Win is called the inner iteration parameter. $\vec{R}es_i$ is the so called residue defined to be $-\frac{1}{\Delta t}\left(\vec{Q}_i^{*}-\vec{Q}_i^{n}\right)-\frac{1}{2\Delta x}\left(\vec{F}_{i+1}^{*}-\vec{F}_{i-1}^{*}\right)$. $\vec{Q}_i^{n}$ is the fixed value of the vector $\vec{Q}$ at the Ith lattice point at

time step n. The vector $\vec{F}_i^*$ is evaluated using the values of the vector Q_i^* . After several symmetric sweeps are made, the value of the vector $\vec{Q}_i$ at time step n+1 is fixed at the value given by formula (4).

$$\vec{Q}_i^{n+1} = \vec{Q}_i^* + \left(\vec{Q}_i^* - \vec{Q}_i^n\right) * Wout \qquad (4)$$

The entire process is then repeated at the next time step. $Wout$ is called the outer relaxation parameter. For time accurate calculations, $Wout$ should be equal to 1.0.

b. This method is tested on the Reimann problem with the following initial conditions.

$$(\rho_L, u_L, P_L) = (1.0, 0.0, 1.0) \;;\; (\rho_R, u_R, P_R) = (0.125, 0.0, 0.1) \qquad (5)$$

This problem, first introduced by Sod(1978), has become a standard test problem. One hundred lattice points are used with a step size of 0.1. A CFL number of 0.8 is used to obtain the time step. The value of Win is taken to be 0.67 and the value of $Wout$ is taken to be 1.0. The locally implicit method without artificial dissipation can not solve the problem from the initial data as the sharp interfaces involved cause the method to predict negative pressures. However, if the method is started with the true solution at four time steps or larger it is found to be stable even without dissipation. The method is seen to produce no oscillations in shock regions. This appears to be a major advantage of the method. The method does produce oscillations at the end of the rarefaction region. Results for the computation from four to sixty time steps are presented in graphs 1-4. The method is also tested with Jameson type

artificial dissipation terms. For details on this method see the papers by Jameson(1985) or Reddy and Jacocks(1987). Using this dissipation model the locally implicit scheme is able to solve the problem from the initial conditions. The spurious oscillations produced in the rarefaction region are also eliminated. Results using this method are shown in graphs 5-8. The run shown is started from the initial conditions and carried out to sixty time steps.

IV.

a. It is a well known fact that most central difference methods will produce oscillations when they are applied to problems which contain sharp interfaces between regions with discontinuities in the relevant variables. The method of controlling these oscillations dates back to the influential paper of Von Neumann and Richtmyer(1950). In this paper, the authors introduced an artificial viscosity term into the eqns of motion. The effect of this term is to suppress the oscillations as well as limiting the shock region to a few mesh points. In another paper, Von Neumann(1944) , Von Neumann has conjectured that the oscillations are the result of heat energy generated by the irreversible action of the shock. In this spirit, I attempt to develop a new artificial dissipation scheme based on the Hamiltonian formalism of fluid mechanics. For a description of the Hamiltonian method for infinite dimensional conservative system see Holm and Kupershmidt(1983). A perturbation term which is a function

of the spatial deriviative of the entropy is added to the Hamiltonian (i.e. the energy density of the fluid). The extra term is chosen in such a manner that it would have no effect in regions in which the flow is isentropic, but would decrease the energy density in regions which contain an entropy gradient. A new set of equations of motion are then generated.

b. The set of equations generated using the perturbed Hamiltonian are also approximated with a central difference scheme. These equations are then tested on the standard problem as described in section III. The shock regions are already smooth as described above, but the method is unsucessful in suppressing the oscillations at the end of the rarefaction region.

V. RECOMMENDATIONS

a. The locally implicit method should be further tested in order to gain better insight into the oscillations produced at the end of the rarefaction region.

b. Once the above stated goal is reached a more sophisticated dissipation term should be added to the Hamiltonian method. This model should be one which will reduce the oscillations at the rarefaction region and be negligible elsewhere.

ACKNOWLEDGEMENTS

The support of this research by the Air Force Systems Command and the Air Force Office of Scientific Research is greatly appreciated. Universal Energy systems is also to be commended for their effective administration of the program.

I would like to thank Dr. John Benek of Calspan corpration for providing me with a very hospitable work environment. The technical advise of Dr. K. C. Reddy has also been an invaluable asset. Dr. Bill Thomson is also due many thanks for his advice on all matters relating to the computer systems used in the course of this research.

REFERRENCES

Holm, D.D., B.A. Kupershmidt., Poisson Brackets and Clebsch Representations for Magnetohydrodynamics, Multi-fluid Plasmas, and elasticity. Physica 6D, 1983, pp.347-363.

Jameson, A., Numerical Solution of the Euler Equations for Compressible invisicid Fluids. Numerical Methods for the Euler Equations of Fluid Dynamics, Ed. Angrand, et al., SIAM, 1985, pp. 199-245.

Neumann, J.V., Proposal and Analysis of a New Numerical Method for the calculation of Hydrodynamical shocks. Vol VI, Collected Works. London, Pergamon, 1963, pp. 361-380.

Neumann, J.V., R.D. Richtmeyer., A Method for the Numerical Calculation of Hydrodynamical Shocks. J. Appl. Phys., 1950, Vol. 21, pp. 232-237.

Reddy, K.C., J.L. Jacocks., A Locally Implicit Scheme for the Euler Equations. Proceedings of the AIAA 8th Computational Fluid Dynamics Conference, Honolulu, 1987. pp.470-477.

Sod, G.A., A Survey of Several Finite Difference Methods for Systems of Hyberbolic conservation laws. _J. Comp. Phys._ 1978, Vol. 27, pp. 1-31.

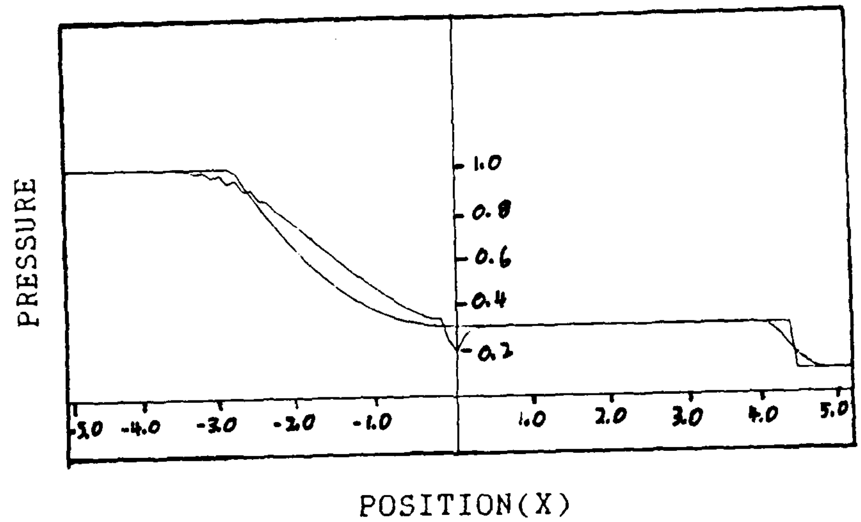

FIGURE 1

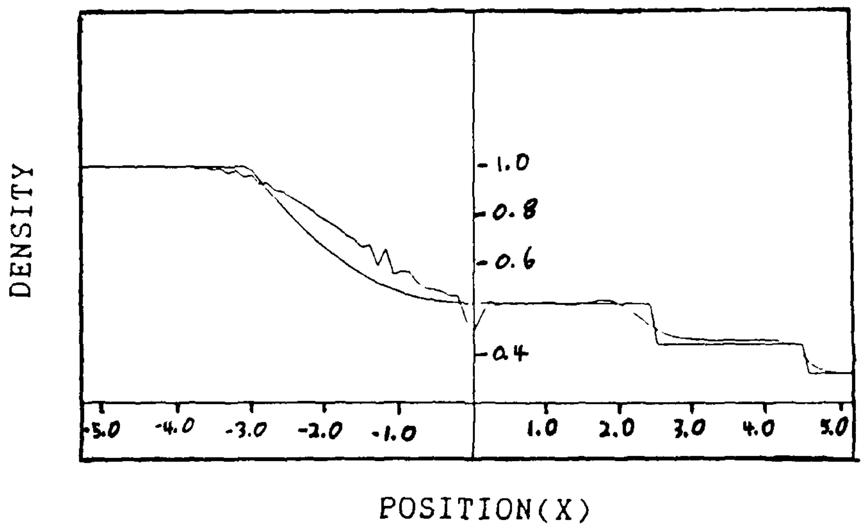

FIGURE 2

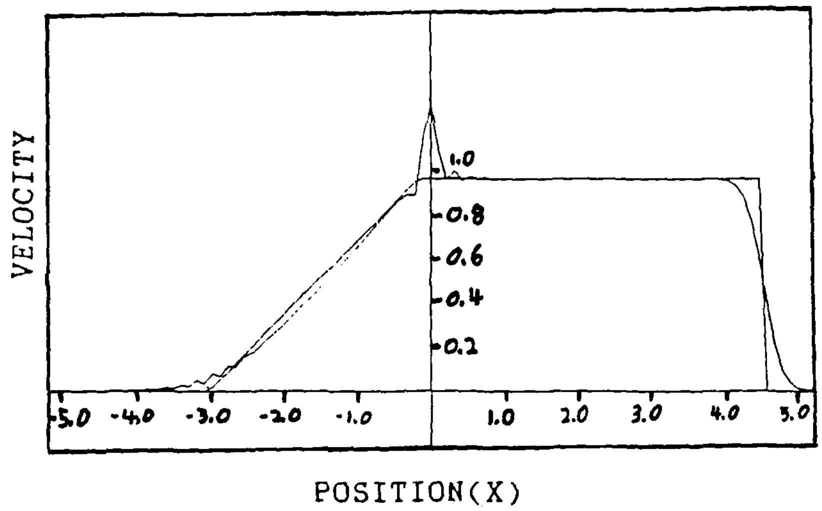

FIGURE 3

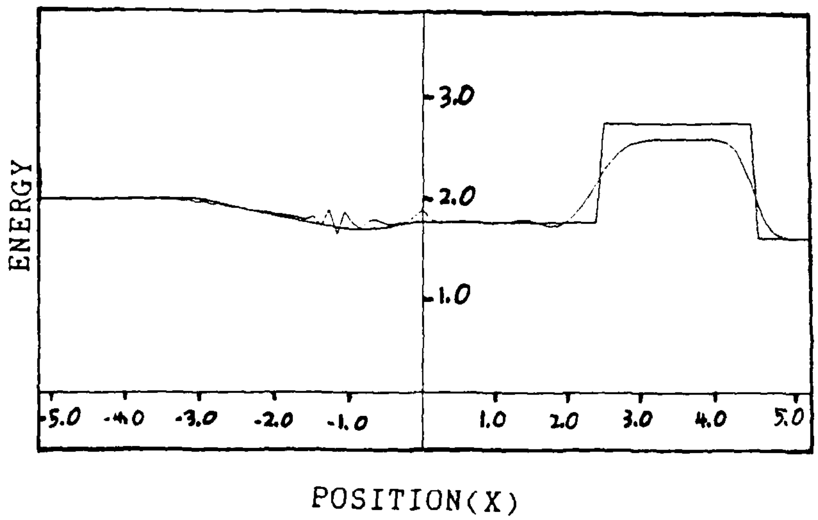

FIGURE 4

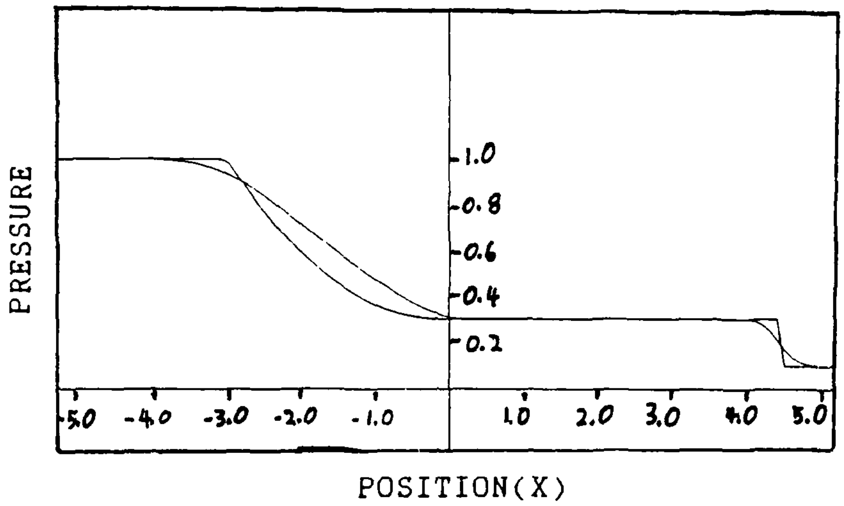

FIGURE 5

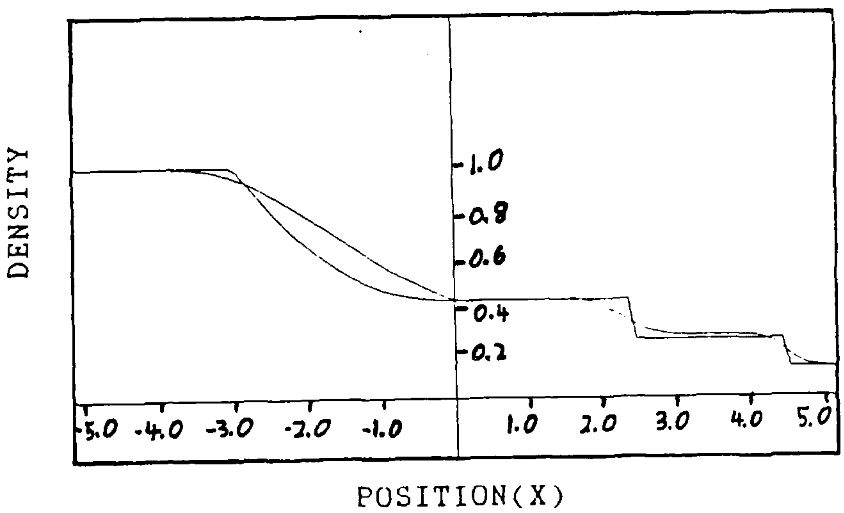

FIGURE 6

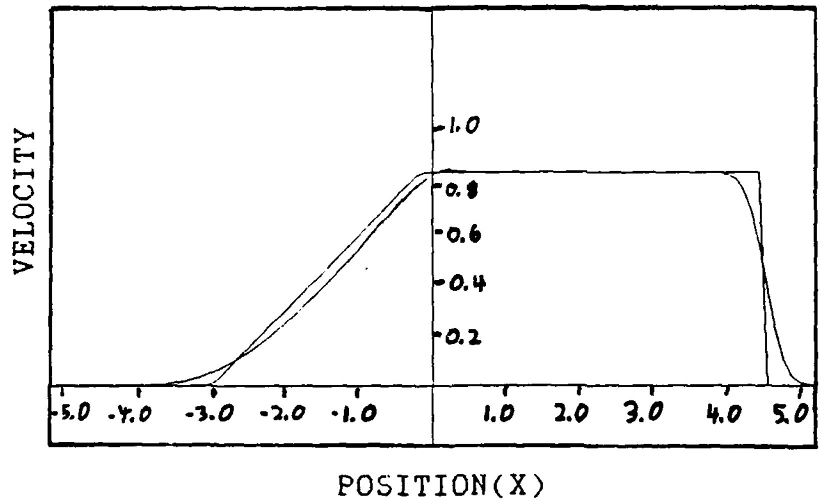

FIGURE 7

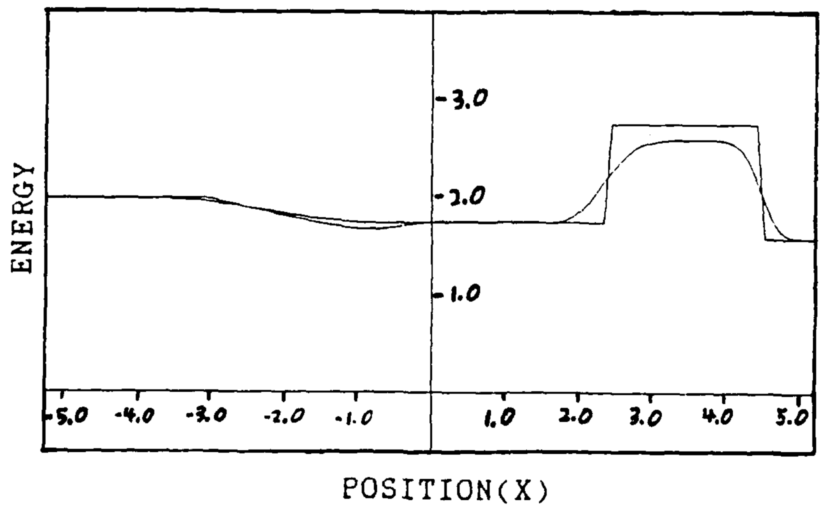

FIGURE 8

1988 USAF-UES SUMMER FACULTY RESEARCH PROGRAM/

GRADUATE STUDENT RESEARCH PROGRAM

Sponsored by the

AIR FORCE OFFICE OF SCIENTIFIC RESEARCH

Conducted by the

Universal Energy Systems, Inc.

FINAL REPORT

Ground-Based Experimental Control Techniques

for Space-Based Structures

Prepared by:	Joel L Berg
Academic Rank:	Doctoral Student
Department and	Engineering Science and Mechanics
University:	Virginia Polytechnic Institute and State University
Research Location:	USAF/AL Astronautics Laboratory Edwards AFB, CA 93523
USAF Researcher:	Dr. Alok Das

Date:	12 Sep 88
Contract No	F49620-88-C-0053

Ground-Based Experimental Control Techniques for Space-Based Structures

by

Joel L Berg

ABSTRACT

This report addresses the effects of gravity in ground-based experiments for space-based structures and also presents a procedure to take them into account. The method of computer simulations which allows one to determine the control actuator requirements is outlined. In addition, this report demonstrates that computer speed limitations have an effect on the choice of sensor quantity and actuator quantity for the equipment available and the grid structures constructed by the Air Force, and that the number of participatory modes affects the tradeoff between sensor quantity and actuator quantity.

ACKNOWLEDGMENTS

I wish to thank the Air Force Systems Command and the Air Force Office of Scientific Research for their sponsorship which made this research possible. Also, I wish to thank the professional staff of Universal Energy Systems for conducting their business in such an efficient manner.

I greatly appreciate the support of the Rocket Laboratory of Edwards Air Force Base. In particular, I wish to thank Dr. Alok Das for securing the necessary hardware and Mr. Waid Schlaegel for serving as liason between human and computer. They made the project much more easier and enjoyable.

I INTRODUCTION:

As space-based structures are becoming larger and remaining as light as possible, the problems of structural vibrations become very real. Equipment pointing errors, orbit destabilization, and structural failure are obvious problems which may occur when vibrations get out of hand. Guarding against vibrations may not be possible because vibrations arise from a multitude of conditions: uneven heating, thermal shock, atmospheric drag, solar pressure, gravity torques, sublimation forces, moving parts, etc. Clearly, flexible space structures need to incorporate some type of control as a means of introducing added damping into the system.

The United States Air Force has an interest in controlling the structural vibrations of various space-based structures, including a proposed space-based platform, which is to serve as a versatile foundation for supporting equipment and possibly human habitats. Because of the obvious expense, any required testing on space-based structures such as the Air Force space platform needs to be carried out on Earth (i.e., ground-based testing). This fact is unfortunate, because Earth's gravitational forces are not balanced by orbital kinematics and therefore influence ground-based tests.

The Air Force has constructed two test structures (grids) for ground-based testing of the space-based platform concept. The first requirement prior to testing the grids is to establish the effects of gravity. After gravity has been accounted for, various tests can be performed thru simulations and on the platform including tests to accomplish my major objective: to explore the controlling capabilities of the hardware involved so that we are able to define the required space-based hardware.

My coursework concentrated on Space Dynamics throughout my Masters program at the University of Wisconsin -- Madison. I have since worked as a Strength Engineer at McDonnell Douglas Corp. in St. Louis, Missouri. Presently, I am working toward my Doctorate at Virginia Polytechnic Institute with research interests in the area of structural dynamics and controls.

II OBJECTIVES OF THE RESEARCH EFFORT:

The Air Force has constructed two "grids" to allow ground-based testing to be conducted on the space platform concept (see Figure 1). The two grids are geometrically the same with the exception that one is constructed of 2-inch width aluminum strips which overlap, while the second grid is constructed of a single sheet of aluminum with square holes cut from the sheet. My assignment was, in part, to investigate what needs to be done so that the control aspects of the space platform can be tested with the grid structures. In particular, I looked into the effects of gravity, determined the requirements of the torquer type actuators, and then in preparation for the control tests, I determined the capacity of the available hardware for controlling the structure given a certain number of sensors and actuators.

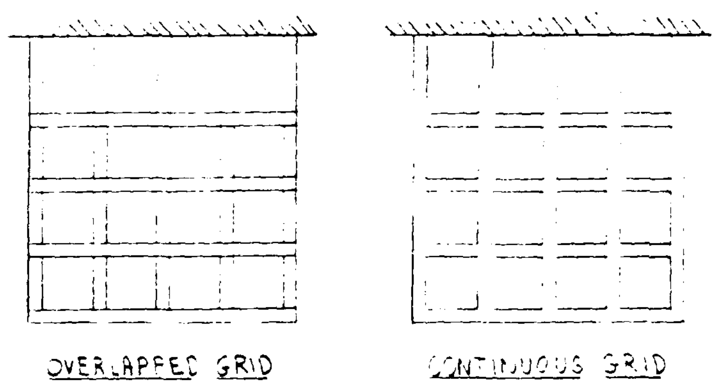

Figure 1

III

Gravity affects both the test structures and the tests themselves. The effect on the test structures is in the form of differential stiffening which is due to the structures' distributed weight. This stiffening changes the test structures' natural modes, which are of prime importance because our controls work relies heavily on the validity of representing our test structures' displacement vectors by a superposition of calculated eigenvectors. The validity of this assumption depends on the accuracy of the calculated eigenvectors. The eigenvectors, along with the eigenvalues, are determined thru an eigensolution routine within NASTRAN. If the NASTRAN models have mass and stiffness distributions which correspond well with the actual structures, the NASTRAN eigensolutions should approximate the actual eigenvectors and eigenvalues of the structures. An easy method to check this correspondence is to measure the eigenvalues of the actual structures and compare them to the eigenvalues found thru NASTRAN.

NASTRAN models are characteristically stiffer then the structure they model because the restraints within the model elements cause the degrees of freedom to be finite (as opposed to infinite in the actual structure). For this reason, we would expect the eigenvalues found for the NASTRAN model of a structure to be greater than the actual eigenvalues of the structure. The existing NASTRAN models for the grid structures gave eigenvalues which were generally <u>less</u> than the tested values, which leads us to believe that something may be wrong with the models. One possibility is that the existing models ignore the effects of differential stiffening which is present due to gravity acting upon the grids which is a distributed mass system. To account for the differential stiffening effects, I used NASTRAN (solution 13) to find the eigensolutions of the models. Solution 13 is similar to the solution routine

commonly used (solution 3) except that it allows for differential stiffening. Clearly, we would expect the eigenvalues for solution 13 to exceed those of solution 3 and we hope that they exceed, but fall close to, the tested values. Figures 2, 3 display the results for the three methods.

CYCLIC FREQUENCIES -- OVERLAPPED GRID STRUCTURE

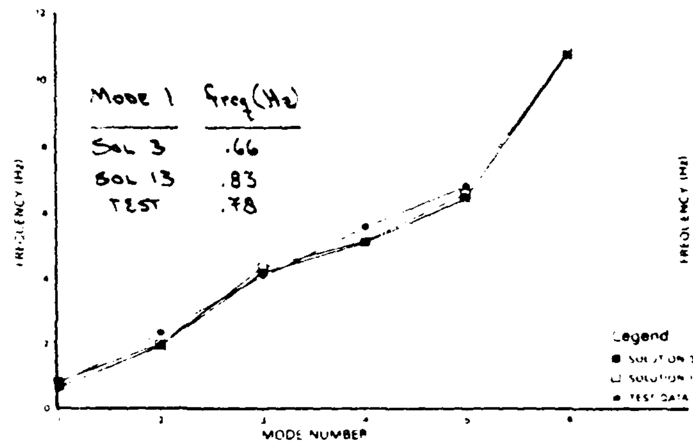

Figure 2

CYCLIC FREQUENCIES -- CONTINUOUS GRID STRUCTURE

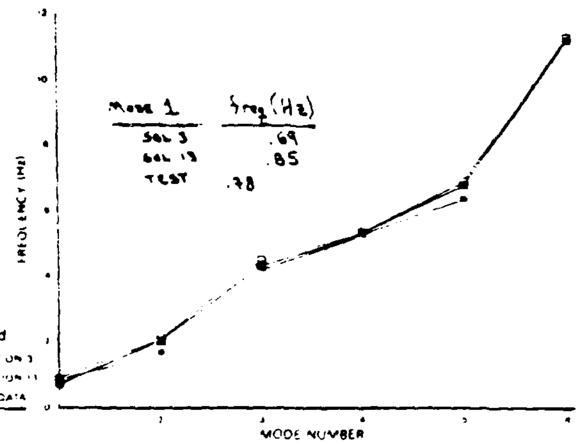

Figure 3

A few observations worth noting concern the two previous figures. First of all, as we would expect, the natural frequencies increased once we accounted for differential stiffening (solution 13 frequencies fall above solution 3 frequencies); and the effect of differential stiffness is very much the same for both grids. If one were to lay figure 3 onto figure 2, one could see that the NASTRAN natural frequencies for the overlapped grid are less than those of the continuous grid. This variance is to be expected because the only difference between the two models is that the overlapped grid NASTRAN model has added mass at the nodes to account for the overlapping strips of material. There is, of course, a stiffness difference between the actual grids; this shows up clearly in the torsional modes if the two figures are superimposed. In other words, the test data displays the increased torsional stiffness which occurs when the grid is constructed by overlapping; this

increase in torsional stiffness would be very difficult, if not impossible, to model and therefore we did not. In conclusion, the continuous grid NASTRAN model represents the continuous grid better than the overlapped grid NASTRAN model represents the overlapped grid.

IV

The second effect of gravity that concerns us will show itself in the testing process. The sensors used in the tests are null-balance accelerometers, meaning that any bias acting on the accelerometer (i.e., constant acceleration) is balanced out so as not to show up in the readings. Therefore, if our tests simply acted in translation, the gravity field would remain constant and there would be no concern. However, because our displacements generally consist of rotations as well as translations, the acceleration field becomes dynamic in nature and therefore influences the accelerometer readings. In short, the accelerometer readings are different from the accelerations that we seek.

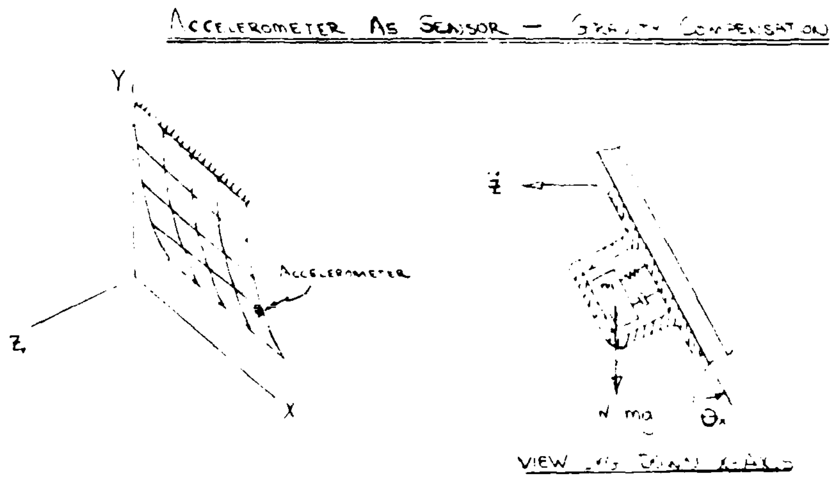

Figure 4

Figure 4 illustrates how gravity effects the accelerometer readings. A positive accelerometer reading could be interpreted as a compression in the spring within the accelerometer. The gravity component ($g \cdot \sin(\theta x)$) would relieve the spring somewhat and therefore lower the reading as shown here for the i^{th} accelerometer, which is located at the j^{th} node:

$$y_i = \ddot{z}_j - g \cdot \sin(\theta_{xj}) \approx \ddot{z}_j - g \cdot \theta_{xj} \tag{Eq. 1}$$

;i = accelerometer index
;j = nodal index (in the modeling sense)
;y_i = reading of the i^{th} accelerometer
;$\ddot{z}_j$ = translational acceleration of the j^{th} node
;θ_{xj} = rotational displacement of the j^{th} node in the x direction

Our goal is to describe the reading of the i^{th} accelerometer in terms of the modal state vector ($\underset{\sim}{q}(t)$) and the controller inputs ($\underset{\sim}{u}(t)$).

$$y_i = \ddot{z}_j - g \cdot \theta_{xj}$$

;$\ddot{z}_j = [0 \cdots 0 \ \underset{\uparrow \, j^{th} \text{ element}}{1} \ 0 \cdots 0]\underset{\sim}{\ddot{z}} = (\underset{\sim}{S}_j)^T \underset{\sim}{\ddot{z}}$

;$(\underset{\sim}{S}_j)^T \equiv j^{th}$ Standard unit vector, transposed

;$\theta_{xj} = (\underset{\sim}{S}_j)^T \underset{\sim}{\theta}_x$

Let the modal matrix be sectioned as:

$$\Phi = \begin{bmatrix} \emptyset_1 \\ \emptyset_2 \\ \emptyset_3 \end{bmatrix} \begin{matrix} \}\text{nodal } z \text{ displacements} \\ \}\text{nodal } \theta_x \text{ rotations} \\ \}\text{nodal } \theta_y \text{ rotations} \end{matrix} \tag{Eqn 2}$$

This sectioning allows us to represent the configuration displacements and rotations in terms of the modal matrix (Φ) and the modal amplitudes ($\underset{\sim}{\eta}(t)$):

$$\begin{matrix} \underset{\sim}{z}(t) \\ \underset{\sim}{\theta}_x(t) \\ \underset{\sim}{\theta}_y(t) \end{matrix} = \begin{bmatrix} \emptyset_1 \\ \emptyset_2 \\ \emptyset_3 \end{bmatrix} \underset{\sim}{\eta}(t)$$

$$y_i(t) = (\underset{\sim}{S}_j)^T \emptyset_1 \underset{\sim}{\ddot{\eta}}(t) - g \cdot (\underset{\sim}{S}_j)^T \emptyset_2 \underset{\sim}{\eta}(t) \tag{Eqn 3}$$

The modal equation of motion permits us to substitute into Eqn 3 the following form of the modal acceleration:

$$\ddot{\underset{\sim}{\eta}}(t) = -\Lambda\, \underset{\sim}{\eta}(t) - Z\, \dot{\underset{\sim}{\eta}}(t) + b\, \underset{\sim}{u}(t)$$

$;\Lambda$ = diagonal matrix of eigenvalues
$;Z$ = diagonal damping matrix

$$y_i(t) = \left[\{-(\underset{\sim}{S}_j)^T\, \varnothing_1 \Lambda - g\cdot(\underset{\sim}{S}_j)^T\, \varnothing_2\} \quad -(\underset{\sim}{S}_j)^T\, \varnothing_1\, Z\right] \begin{bmatrix} \underset{\sim}{\eta}(t) \\ \dot{\underset{\sim}{\eta}}(t) \end{bmatrix} + (\underset{\sim}{S}_j)^T\, \varnothing_1\, b\, \underset{\sim}{u}(t)$$

$$y_i(t) = C_i\, \underset{\sim}{q}(t) + D_i\, \underset{\sim}{u}(t) \qquad \text{(Eqn 4)}$$

$;C_i = [\{-(\underset{\sim}{S}_j)^T\, \varnothing_1 \Lambda - g\cdot(\underset{\sim}{S}_j)^T\, \varnothing_2\} \quad -(\underset{\sim}{S}_j)^T\, \varnothing_1\, Z]$
$;D_i = (\underset{\sim}{S}_j)^T\, \varnothing_1\, b$
$;\underset{\sim}{q}(t)$ = modal state vector = $[\underset{\sim}{\eta}(t) \quad \dot{\underset{\sim}{\eta}}(t)]^T$
$;\underset{\sim}{u}(t)$ = control vector

The steps required to account for the gravity effects on the accelerometer readings are as follows:

- Section the modal matrix as shown in Eqn 2
- For each accelerometer, construct the standard unit vector which corresponds to the nodal location of that accelerometer. For example: if an accelerometer is located at node 12, then the 12th standard unit vector would be used.
- Construct the C and D matrices row by row, with the ith row corresponding to the ith accelerometer, as shown in Eqn 4.

V

The previous two sections addressed the gravity effects on the structure and the accelerometers. We now have a better estimate of the modal dynamical equations because the differential stiffening has been accounted for in the NASTRAN eigensolution. Also, we understand what the accelerometer readings are truly representing and can express them in terms of the modal state vector and the control inputs. Now we need to design the control system on the computer so that we can perform computer simulations prior to real-time operations. The ease of running

simulations for different parameters is invaluable for determining the actuator requirements. Figure 5 illustrates the closed-loop control system which is assumed for the simulations.

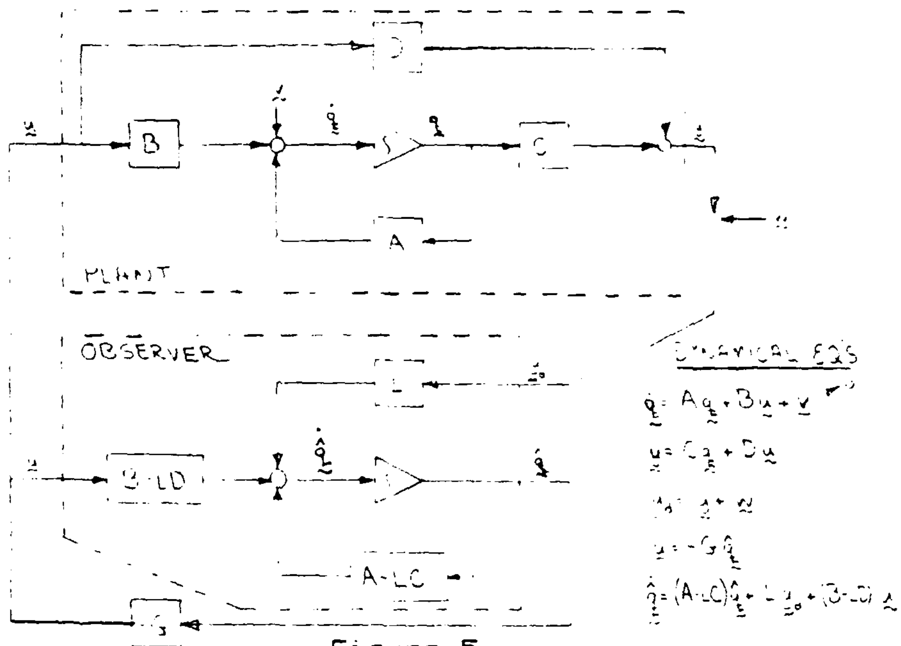

Figure 5

VI

Our objective is to control the structure by controlling its modes. There are two types of modal control laws to choose from: Independent Modal Space Control (IMSC), and Coupled Control. The difference between the two can be better understood by first looking at the modal equation of motion.

$$\ddot{\eta}_r(t) + 2\zeta_r\omega_r\dot{\eta}_r(t) + \omega_r^2\eta_r(t) = b^T \underset{\sim}{u}(t) \equiv f_r(t) \qquad \text{(Eqn 5)}$$

Equation 5 is the modal equation of motion for the r^{th} mode. The forcing function ($f_r(t)$) is obviously in terms of the control input ($\underset{\sim}{u}(t)$), but if we turn back to the block diagram of Figure 5, we see that the forcing function is ultimately in terms of the estimated modal state of the structure. Nothing says that we are required to use the total state vector in defining the forcing function and one

may opt to use only those elements of the state vector which correspond to the mode we are attempting to control.

$$f_r(t) = f_r(\eta_r(t), \dot{\eta}_r(t)) \qquad \text{(Eqn 6)}$$

$$f_r(t) = f_r(\eta_1(t), \dot{\eta}_1(t), \eta_2(t), \dot{\eta}_2(t), \ldots) \qquad \text{(Eqn 7)}$$

; $\eta_r(t)$ = the modal amplitude of the r^{th} mode.

; $\dot{\eta}_r(t)$ = the modal rate of the r^{th} mode.

Equation 6 allows the modes to remain uncoupled and the control law is referred to as Independent Modal Space Control. The uncoupling is an attractive feature of IMSC; however, this requires as many actuators as the number of controlled modes if we expect a good degree of accuracy. Equation 7 recouples the modal equations of motion and the control law is referred to as Coupled Control. This is our choice of a control law because it allows us to control multiple modes with a single actuator.

VII

The simulation actuators are, of course, purely mathematical and can supply any force or torque that we request of them. What we need to know now is whether the available actuator in the laboratory, which is a torquer type actuator, is capable of controlling the actual structure. To answer this question, we need to determine the torque and power requirements for a single torquer to successfully control each of the first 6 modes independently. Successful control is defined here as creating enough closed-loop damping so that the poles of the mode of concern have a real component no larger than -0.03.

Our strategy is to first inspect the eigenvectors to find favorable torquer placements for each mode to be controlled. During this inspection, we must keep an eye on how well the other modes are damped in order to guard against any unintended excitation. Once the torquer placement has been decided for a particular mode, that is, the best nodal

location and orientation (the spin axis pointing either along the x-axis or y-axis; see Figure 1), the controller gains need to be found such that the closed-loop poles of the mode in question fall to the left of -0.03. Next, we need to calculate a reasonable initial offset for the mode in question so that a simulation can be performed. This was done for each of the first 6 modes and the first mode turned out to be the critical case. The procedure and results of the first mode follows:

- Actuator Type: Torquer

  This is all that is available in the laboratory at this time.

- Placement of Actuator: Node 21 in the X direction

  Node 21 is the lower left hand corner of the grid. I assumed only the first 6 modes are participatory, so prior to deciding on the actuators placement, I cross-checked the effect of that placement on controlling the other 5 modes. I do not want any unintended excitation of the other modes to go uncontrolled.

- Control Gains of the Actuator: k=0; c=0.17

  It can be shown that the displacement gains (k) have little effect on the closed-loop damping, whereas the rate gains (c) have a substantial effect. For this reason, it is safe to simplify the job of determining the control gains by assuming that k=0.

- Initial Conditions: $\eta_1(t)=-0.1995$

  This corresponds to an initial displacement for node 21 of 5 inches.

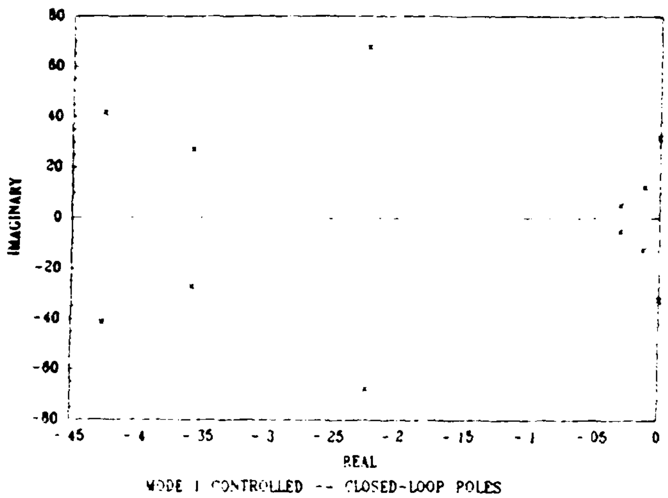

Figure 6

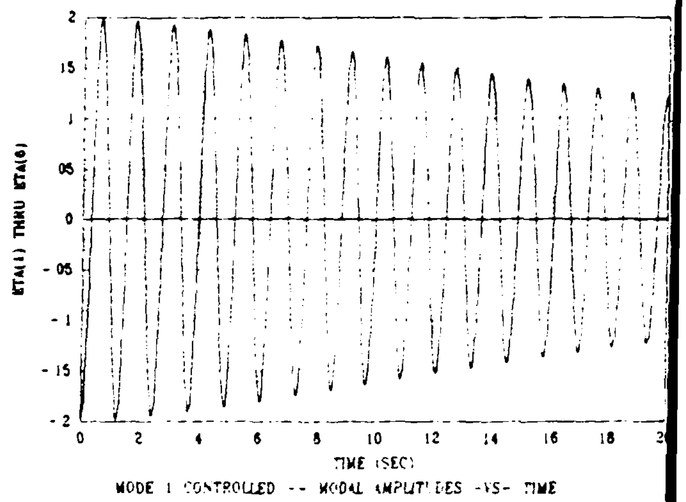

Figure 7

Figure 6 shows the closed-loop poles for the above control gains. As can be seen in Figure 7, the closed-loop damping affects the first mode. The open-loop system assumes zero damping which means that all of the damping is due to the control gains. In the actual structure, there does exist a combination of structural and aerodynamic damping; however, this open-loop damping was found to be relatively small, especially for the lower modes.

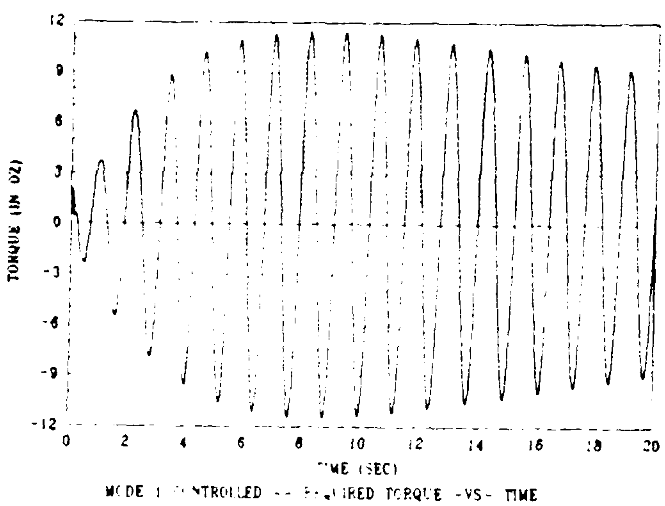

Figure 8

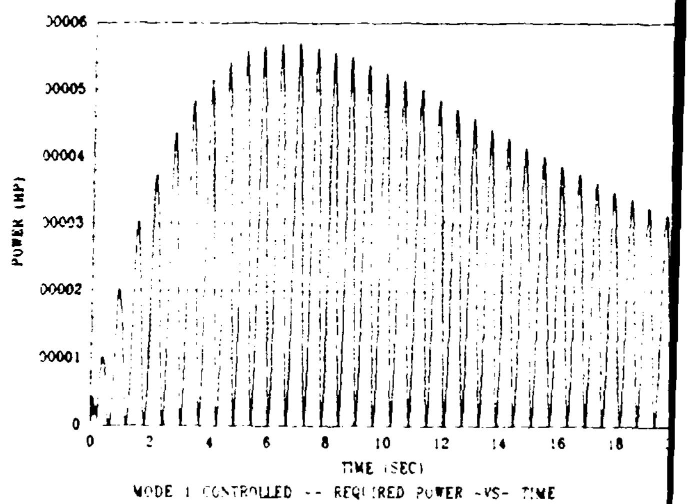

Figure 9

Figure 8 displays the required torque for the initial conditions given and Figure 9 displays the required power. The required power presents no problems; however, the required torque is about 5 times higher than the particular torquer that we have in the laboratory.

VIII

The computer within the control loop largely determines the limitations in the control process. The computer accepts the sensor readings in terms of voltage and then performs two steps prior to using those readings. First, the computer must offset the voltage readings by any D.C. bias supplied by the electrical components between the accelerometers and the computer. Next, the computer must factor the corrected readings so that they are in terms of meters/seconds^2. Now the accelerations are ready to be used along with the control inputs by the computer to calculate the estimated state of the structure and the updated control inputs. Prior to sending the updated control inputs to the actuators, the computer factors them so that they are in terms of voltage. All of these steps take time and as the number of sensors or actuators or the number of assumed participatory modes increase, the time it takes for the computer to complete a cycle increases; i.e., the sampling time increases. In addition, an increase in the assumed number of participatory modes requires the sampling time to decrease if accuracy is to be maintained.

I ran several tests to define the limitations of the computer within the laboratory. By varying the number of sensors and the number of actuators for a certain number of participatory modes, I found the minimum sampling time the computer was capable of maintaining. Figures 10 and 11 display the tradeoff that must be considered when choosing the number of sensors or actuators. Assume that it has been

determined that only the first 5 modes are participating significantly in the response of the structure. Figure 10 displays the number of actuators the computer is capable of supporting for 4, 5 and 6 sensors. In order to accurately sense and control the 5^{th} mode, the maximum sampling time needs to be $1/10^{th}$ to $1/6^{th}$ the period of the 5^{th} mode. This translates to a sampling time that is less than 0.0244 seconds (or maybe as low as 0.0146 seconds, depending on how conservatively the tests are performed). Figure 10 shows that the computer can easily handle this time, even for 6 sensors and 5 actuators. There would be no reason to go beyond 5 actuators, because with 5 participating modes, 5 actuators will allow you to control the structure with IMSC. Now if the number of participatory modes were to increase to 6, we are not so fortunate. If the computer is to recognize and control the 6^{th} mode, the sampling time must fall below an upper limit of 0.0089 to 0.0148 seconds. Again, this limit depends on which rule of thumb we follow: $1/10^{th}$ the period or $1/6^{th}$ the period. Note in Figure 11 that the computer may have trouble controlling the structure with IMSC if we desire to use 6 sensors and if we required the sampling time to be less than $1/10^{th}$ the period of the 6^{th} mode, the computer would not even be able to support 1 actuator with 6 sensors. Certainly we have the option of reducing the number of sensors in order that the computer can handle a desired number of actuators. This illustrates the tradeoff that may need to be considered if the number of participatory modes, which is inherent to the structure, becomes too large for the computer being used to handle. As an added note, if we desire to record any of the sensor readings, state values, or actuator signals, more operations are demanded of the computer and the curves in Figures 10 and 11 are effectively shifted to the right.

HIGHEST PARTICIPATORY MODE -- 5

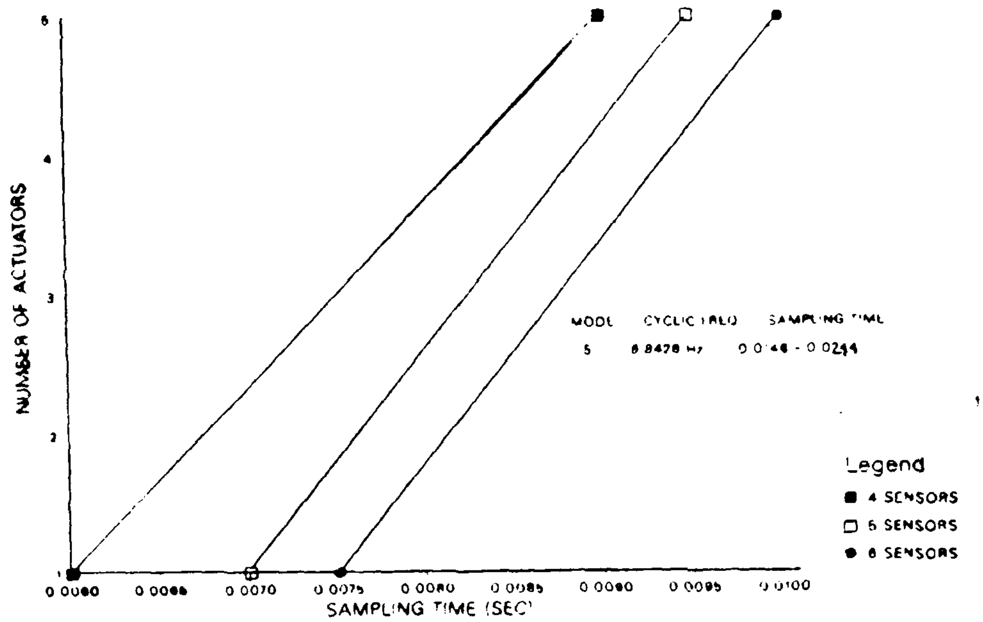

Figure 10

HIGHEST PARTICIPATORY MODE -- 6

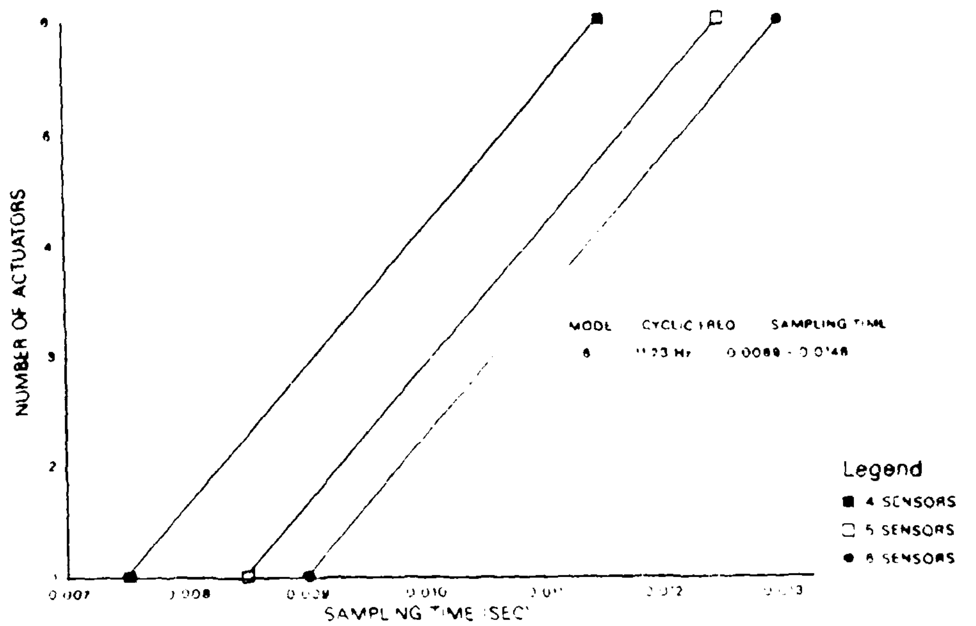

Figure 11

IX RECOMMENDATIONS

We have accomplished our goal of testing a space-based structure in a ground-based laboratory. Now we need to determine how to optimize (in the general sense of the word) the vibrational control of the space-based structure given the hardware limitations.

The next clear objective is to successfully control the grid structure; I suggest that all future experiments be performed on the continuous grid because of the accuracy difference between the NASTRAN models. We know the torquer requirements for a single torquer to control each mode of the structure independently, so I propose that an attempt be made to find or build a set of torquers to fit the requirements. If that is not feasible, then I suggest we concentrate on controlling the grids with multiple actuators.

Once the test structure has been successfully controlled, we have the opportunity to study the differences between coupled and uncoupled control laws, spillover effects and methods to counter them, optimal sensor and actuator placement, real-time eigenvector modifications by using the spillover or thru parameter identification.

REFERENCES

Chen, Chi-Tsong, Linear System Theory and Design, CBS College Publishing, 1984

Doebelin, E.O., Measurement Systems, Application and Design, McGraw-Hill, Inc., 1975

Herzl, G.C., Tubular Spacecraft Booms, J.W. Stacey, Inc., 1970

Meirovitch, L.. Computational Methods in Structural Dynamics, Sijthoff and Noordhoff International Publishers B.V., 1980

1988 USAF-UES SUMMER FACULTY RESEARCH PROGRAM

GRADUATE STUDENT RESEARCH PROGRAM

Sponsored by the

AIR FORCE OFFICE OF SCIENTIFIC RESEARCH

Conducted by the

Universal Energy Systems, Inc.

FINAL REPORT

Prepared by: Lance H. Carter

Academic Rank: Graduate Student

Department and University: Aerospace Engineering Department, Virginia Polytechnic Institute and State University

Research Location: AFAL/VSSS
Edwards AFB
Edwards, CA

USAF Researcher: Alok Das

Date: 9 September 1988

Contract No: F49620-88-C-0053

An Observer Design for the AFAL Grid

by

Lance H. Carter

Abstract

A Luenberger observer was designed for use in the AFAL grid experiment. The observer produces modal state estimates based on accelerometer outputs and a discretized mathematical model. The design includes the effects of gravity on the accelerometers and noise. The observer performance was then experimentally evaluated using free and forced response grid data. Results show that an observer of this type can be successfully used in a grid control system as long as there exists careful structural modeling and observer pole placement.

Acknowledgements

I wish to thank the Air Force Systems Command and the Air Force Office of Scientific Research for sponsorship of this research. I also thank Universal Energy Systems for their efficient and helpful handling of the program.

Thanks additionally go to Wayne Roe and Alok Das for the opportunity to participate in this research at the AFAL. The whole staff there proved to be very accommodating and helpful. Lastly, I wish to thank Mark Norris for his unending patience and direction in support of this research.

I. Introduction

Current and future space applications often require the use of large space structures (LSS) in orbit. A large space structure is characterized by long, thin members and low natural frequencies.

The Air Force Astronautics Lab (AFAL) at Edwards Air Force Base is concerned with the dynamic response and control of LSS. Specifically, their grid experiment uses a five foot by five foot thin aluminum grid structure to simulate the types of LSS found in actual applications.

My academic interests are in the areas of structural dynamics and controls, and the AFAL Grid Experiment provided an ideal arena in which to conduct research in these areas.

II. Objectives of Research Effort

Large space structures are often subjected to various loadings (such as propulsive forces) that can excite their natural modes of vibration. Since for some applications it is imperative that the structure be quickly damped, an active control system may be necessary to suppress these vibrations. The distributed nature of these structures makes it difficult to apply most existing control theory which assumes a discrete system. One control theory proposed for distributed structures is the independent modal space control (IMSC) method. The idea here is to

control the structure by controlling its modes, which can be found based on a discretized mathematical model of the structure.

To experimentally test such theories, the AFAL has a large, aluminum grid mounted to a concrete monolith. Various loading and control actuators can be applied, and the resulting response is collected using a data acquisition system.

My research for the 1988 Summer Graduate Student Research Program (GSRP) consisted of designing a state estimator to be used in a control system for the AFAL grid. I then evaluated the performance of the design by collecting free and forced response data from the grid to be used in computer simulations.

III. State Estimator Choice

In order to control the grid, the modal displacements and velocities must be known. Since sensors measure nodal states, the modal coordinates must be extracted from these. Two common approaches to this end are the use of spatial modal filters and asymptotic (Luenberger) observers. A Luenberger observer is a dynamical system that uses both the mathematical model of the system and sensor data to generate an estimate of the state [illegible] modal filtering is [illegible] based on [illegible] of the structure [illegible] modal [illegible]

the type and number of sensors are no object, then modal filters are generally a much better way of reconstructing the state. This is because the orthogonality of the modes is taken into account, which eliminates observation spillover. Furthermore, implementation involves only simple computations, which makes the estimates virtually instantaneously available. It is often the case, however, that a limited number of sensors can be used. In addition, the modal filter assumes nodal displacements and velocities (as opposed to accelerations) are measured. For these reasons, the grid modal states will be estimated using a Luenberger observer in conjunction with acceleration sensors (accelerometers).

IV. Equations of Motion

A finite element discretization of the grid leads to the differential equation

$$M\ddot{X} + KX = F(t) \qquad (1)$$

where M and K are the symmetric mass and stiffness matrices of order N respectively, X(t) is the Nx1 nodal displacement vector, and F(t) is the actuator force vector. These equations are transformed into modal space by solving the eigenvalue problem and forming the modal matrix

$$\Phi = [\phi_1 \vdots \phi_2 \vdots \cdots \vdots \phi_N] \qquad (2)$$

where each column is an eigenvector corresponding to an eigenvalue, which are ordered from lowest to highest.

Assuming the (not yet developed) damping matrix is diagonalizable and normalizing Φ such that modal masses equal one, the equations of motion are transformed to principal coordinates using the transformations:

$$\begin{aligned} M' &= \Phi^T M \Phi = I \\ K' &= \Phi^T K \Phi \\ \eta(t) &= \Phi^T X(t) \\ f(t) &= \Phi^T F(t) \end{aligned} \qquad (3)$$

where prime denotes modal matrices and T denotes the transpose. The result of the transformations is the uncoupled equations of motion

$$\ddot{\eta} + \Lambda \eta = f(t) \qquad (4)$$

where Λ is a diagonal matrix consisting of the eigenvalues, and f(t) is the modal forcing vector, both of order N. It is desired, however, to control the first n modes, where n < N. The last (N-n) modes are truncated with respect to the control system design, so the actual states are now assumed to be a linear combination of only the first n modes. It was originally necessary to include higher modes to ensure the accuracy of the nth order truncated system. Next damping is added to the system by specifying the modal damping ratios, ξ_r. These were obtained experimentally by fitting an exponential decay curve to the amplitude envelope of free response data. Unwanted modes and noise were filtered out using Fourier transforms. Thus the discretized, truncated equations of motion in modal space become

$$\ddot{\eta}_r + 2\omega_r \xi_r \dot{\eta} + \omega_r^2 \eta_r = f_r(t) \qquad (5)$$

where r = 1,2,...,n, ω_r = natural frequency, and n < N.

V. State Space Representation

To design a Luenberger observer, it is convenient to express the equations of motion and the sensor outputs in the form

$$\dot{q} = Aq + Bu \qquad (6)$$

$$y = Cq + Du \qquad (7)$$

where A, B, C, and D are real constant matrices. Letting $q = [\eta^T \vdots \dot{\eta}^T]^T$ and U = F(t) equation (5) can be represented in state-space form by defining

$$A = \begin{bmatrix} 0 & I \\ -\Lambda & -\mathcal{C} \end{bmatrix} \qquad B = \begin{bmatrix} 0 \\ T \end{bmatrix} \qquad (8)$$

where:

I = nxn identity matrix

Λ = previously defined

$\mathcal{C}$ = nxn diagonal modal damping matrix

T = nxm matrix containing a row of eigenvectors where m = number of actuators and each eigenvector corresponds to the nodal location of each actuator. Note the system represented in state space form is of order 2n. The sensor output must now be represented in the form given by (7), where

$$y_s = \ddot{x}_s + g x_s \qquad (9)$$

where $\mathbf{x_s}$ = vector of order s, the number of accelerometers, and g = gravitational constant. The second term of equation (9) is due to the gravitational component measured by the accelerometers. To get this in the form of (7), the configuration space outputs must be

transformed to modal space:

$$y = \Phi' \ddot{\eta}_s + g\Phi'' \eta_s \qquad (10)$$

Φ' and Φ'' represent two different transformation matrices made up of certain elements of the global modal matrix. Next the $\ddot{\eta}_s$ term is eliminated using the modal equation of motion giving,

$$y = \Phi'\left(-\zeta\dot{\eta} - \Lambda\eta + f(t)\right) + g\Phi''\eta \qquad (11)$$

Letting $q = [\eta^T \vdots \dot{\eta}^T]^T$ and $U = F(t)$ results in the final form of the output equation (7) where

$$C = \left[-\Phi'\Lambda + g\Phi''\right] \qquad D = \left[\Phi' * T\right] \qquad (12)$$

VI. Observer Form

Once A, B, C, and D are specified it is possible to construct a Luenberger observer. Since the number of controlled (and observed) modes is relatively small, a full order identity observer is chosen of the form

$$\dot{\hat{q}} = A\hat{q} + L(y - C\hat{q} - Du) + Bu \qquad (13)$$

where L = observer gain matrix. Collecting terms gives:

$$\dot{\hat{q}} = (A - LC)\hat{q} + L(y - Du) + Bu \qquad (14)$$

The solution of this differential equation gives the desired estimated modal velocities and displacements to be implemented in a control law. Especially since the modal equations of motion are uncoupled, one question is why not just solve those equations instead of the ones shown above? This type of "open loop" approach has two problems. First, the correct initial conditions must be known, which is rarely the case. Second, since the model

of the system differs from the actual structure, and the model may have unstable poles, small variations from the actual response may grow large in time. It should be stressed that we desire to control the structure, not the model, and the closed loop given in (14) alleviates both of these problems.

The next step is to specify the gain matrix L such that the estimated states converge to the actual ones. Defining the error to be

$$\text{error} = e = \hat{q} - q \tag{15}$$

or the difference between the actual and estimated states. This implies

$$\dot{e} = \dot{\hat{q}} - \dot{q} \tag{16}$$

Substituting (15) and (16) into equations (6) and (14) gives

$$\dot{e} = (A - LC)e \tag{17}$$

The solution of this equation reveals that the estimation error goes to zero if the poles of (A-LC) are in the left half plane. The observer gain matrix should be chosen such that this is true. The further the poles are placed in the left plane, the faster the convergence speed, but also the observer becomes more noise sensitive. Especially for the multi-variable case, there are no set rules for pole placement. Since a Luenberger observer is dual to a modal controller, one criteria is to solve the problem dual to the optimal quadratic regulator. Since the design of observer gains can be viewed as a trade-off between state reconstruction speed and measurement noise,

we may choose L so as to minimize the mean square error, or,

$$\mathrm{Min}\, J = E\|(\hat{q} - q)\|^2 \tag{18}$$

where E is the expectation operator. The error is now dependant on measurement and actuator noise. Letting w = the input disturbance, G = the input disturbance matrix, and v = the sensor noise, the state equations become

$$\dot{q} = Aq + Bu + Gw \tag{19}$$

$$y = Cq + Du + v \tag{20}$$

It can be easily shown that the error equation now becomes

$$\dot{e} = (A - LC)e + Gw - Lv \tag{21}$$

It is obvious that a L is increased, the measurement noise is amplified. The solution of this optimization problem involves the solution of a Riccatti equation. Fortunately, computer software was readily available that automatically computed the optimal (Kalman) gains given the input and measurement noise intensities, where all disturbances are assumed to have a Gaussian distribution and a zero mean. The noise intensities were calculated for each sensor by reading a "zero" signal and summing the square error over the time domain. The mean square error is inputted as the noise intensity of each sensor, or

$$Q_{yy}\delta(t - \tau) = E[v(t)v^T(\tau)] \tag{22}$$

where Q_{yy} is the measurement noise intensity and δ is the Dirac delta function. The input noise intensity, Q_{xx}, is similarly defined as

$$Q_{xx}\delta(t - \tau) = E[Gw(t)w^T(t)\,G^T] \tag{23}$$

Since for this experiment the actuator noise was

negligible compared to the sensor noise, Q_{xx} was arbitrarily assigned a value about two orders of magnitude smaller than Q_{yy}. Q_{xx} can not be zero or the observer will indicate a zero response for the free response case. With these parameters specified, a computer algorithm was used to compute the gain matrix. With the observer now completely described, modal state estimates can be generated from available outputs. It should be mentioned that the system must be observable. There are various equivalent criterion to determine observability, one being that the matrix defined as

$$\gamma = [C^T \vdots A^T C^T \vdots \cdots \vdots (A^T)^{n-1} C^T]^T \qquad (24)$$

must have full rank. Before implementing the observer in the control system of the grid, its accuracy was tested as described in the next section.

VII. Observer Accuracy

In the absence of noise, the error equation (as stated earlier) is

$$\dot{e} = (A - LC)e \qquad (17)$$

With properly placed observer poles, the estimated state should asymptotically approach the actual state. For our observer this is not precisely the case, and the above equation can be misleading. In deriving the error equation, it was assumed that the sensor output, y, is equal to $Cq + Du$. The sensors measure accelerations, and the output equation relates these accelerations to a

linear combination of the modal displacements and velocities via the equations of motion. Since the governing equations will never completely and accurately describe the actual system, the observer may not perfectly approach the actual system even in the total absence of noise.

VIII. Results

a. To investigate the effect of having different model and system dynamics, a simple two d.o.f. mass spring system was simulated. As described, the damping factors for the grid model were computed using experimental data. Since in reality damping is a nonlinear function of velocity, this was only an approximation. To isolate this effect, a simulated mass spring system was constructed such that the observer and plant had the exact same dynamics except that the simulated system contained damping, whereas the observer system did not. Figures (1) and (2) show the actual system output (Y) and observer estimate ($\hat{Y}$) for this case along with the case that the observer also includes damping effects. The observer response converges for both cases, but when damping is not included the estimation takes longer and exhibits a slight phase shift. Note that in the actual grid system this effect will be magnified since modes dynamics are implicit in the sensor matrix.

b. Next the observer performance was tested using actual free response grid data. The observer dynamics assumes that four out of the 120 modeled modes participate in the response. Input and sensor noise intensities were calculated as previously described. Four accelerometers were placed on the grid as shown in figure (3). Two additional accelerometers were also placed to compare output estimates at nodes not included in the observer inputs. The grid was excited at the first mode, and the resulting data was used in the observer to estimate the modal states and system outputs. Figure (5) shows the actual and estimated accelerometer output at position one. The estimated output (dotted line) proves to be quite close to the actual output (solid line). Figure (6) shows the first four estimated modal displacements, which are ultimately needed for state feedback. The large amplitude line is the first mode, which should indeed dominate the response. The first six seconds represent the transient response of the observer, after which the plot shows the expected damped behavior. Note that the modal estimates are relatively noise free. Figures (7) and (8) show the estimated and actual outputs at accelerometer locations not included in the observer inputs.

c. To further evaluate the observer performance, the grid was given a harmonic excitation at a frequency close to the first natural frequency. Figure (4) shows the four accelerometer locations and the location of the shaker.

Data was acquired once steady state conditions had been reached. Figure (9) shows the actual and estimated outputs at the fourth nodal location. The observer shows a good convergence. The first four modal displacements are shown in figure (10). As expected, the first mode dominates the response, but in the time shown the observer has not yet reached steady state.

d. To investigate the effect of varying the observer gains, the sensor noise intensity matrices were changed in the cost function. Figure (11) shows the same forced observer response as figure (9) except that Θ_{yy} was made very large. The optimizer then puts more weight on the mathematical model resulting in very small observer gains. Note that the observer takes a long time to give an inaccurate estimation because the available outputs are essentially not used, so the observer relies wholly on the mathematical model which includes a transient response and phase shift. Next the sensor noise intensity matrix was made very small, resulting in very large observer gains. The output estimation is again poor because the sensor noise term in equation (21) is amplified, and the observer never converges.

IX. Conclusions and Recommendations

a. Since model dynamics implicit in the sensor matrix and noise hamper observer performance, the specification

of observer gains is critical to observer accuracy.

b. Prudent structural modeling and careful observer pole placement should make it possible to use a Luenberger observer of this type in a grid control system.

c. To test the above conclusions, it is recommended that the observer be implemented into an actual real time control system to experimentally evaluate its real time performance.

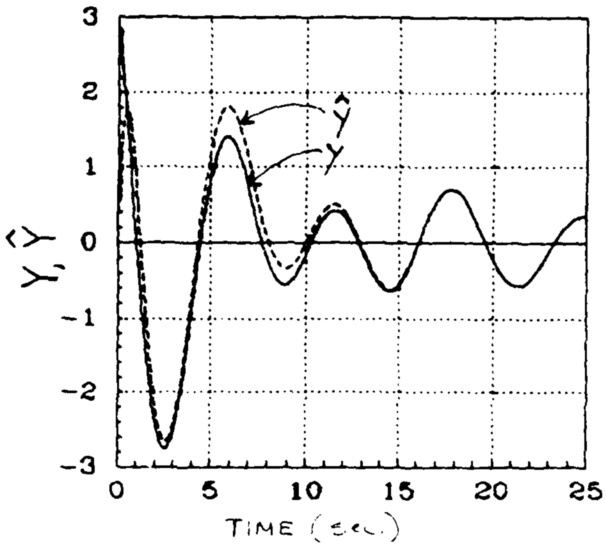

Figure 1
Y and Ŷ vs. time for mass spring system, observer and model include damping

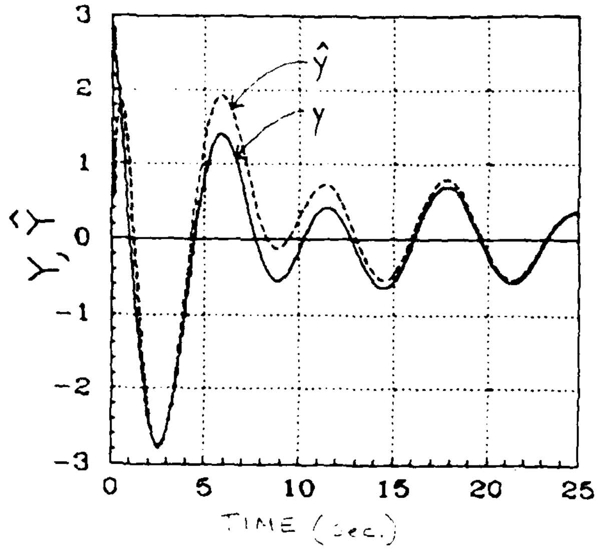

Figure 2
Y and Ŷ vs. time for mass spring system, observer does not include damping

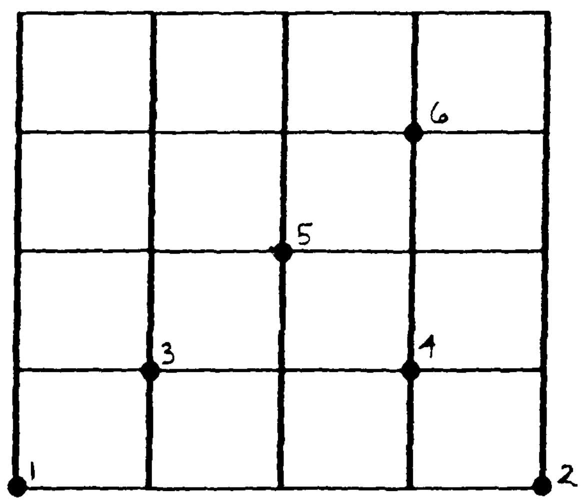

Figure 3
Free response accelerometer locations

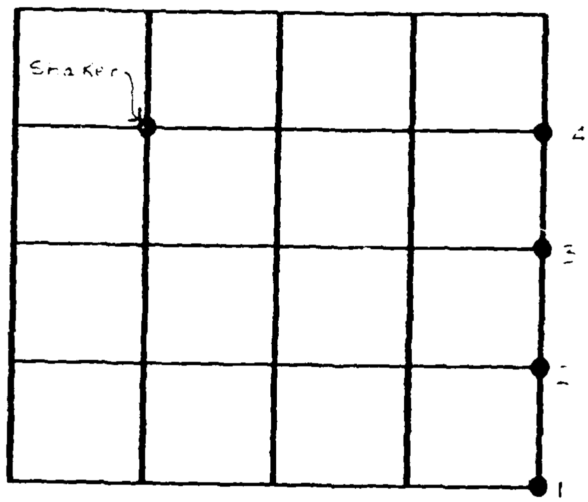

Figure 4
Forced response, accelerometer and shaker locations

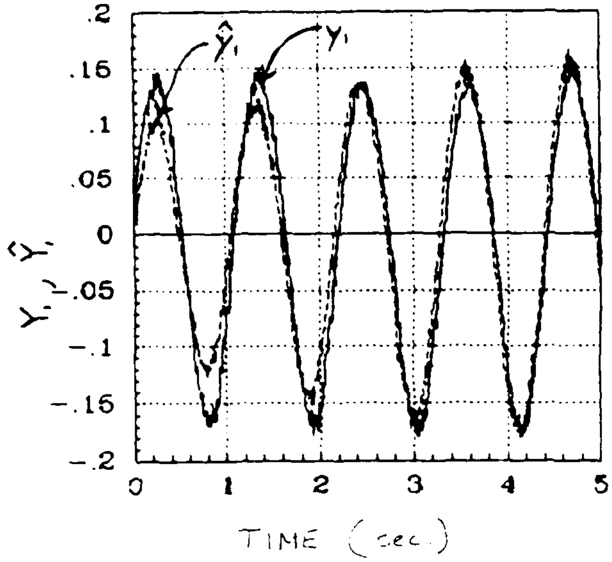

Figure 9
Y_1 and $\hat{Y}_1$ vs. time for grid forced response

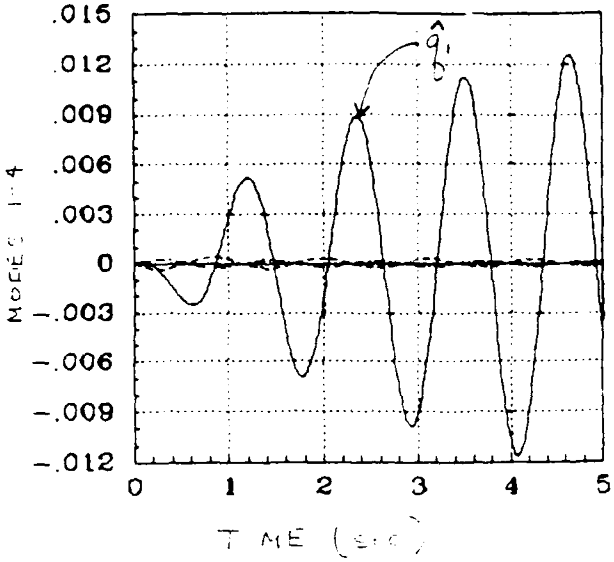

Figure 10
Modal displacements 1-4 vs. time for grid forced response

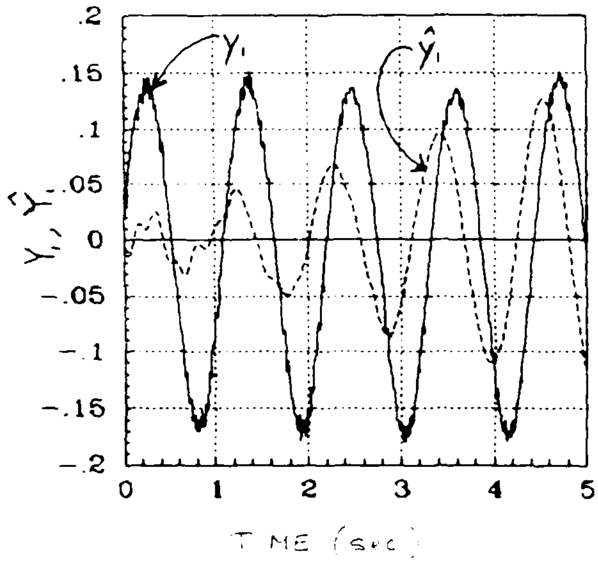

Figure 11
Y_1 and $\hat{Y}_1$ vs. time, Q large, observer gains small

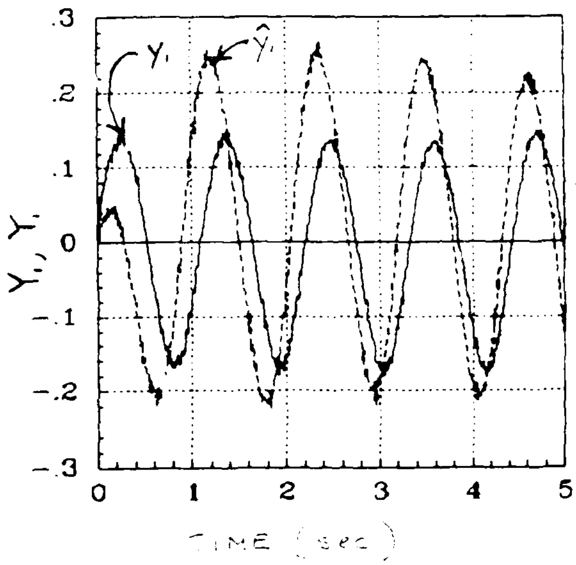

Figure 12
Y_1 and $\hat{Y}_1$ vs. time, Q small, observer gains large

AD-A204 243 UNITED STATES AIR FORCE GRADUATE STUDENT RESEARCH 3/
PROGRAM PROGRAM TECHNIC..(U) UNIVERSAL ENERGY SYSTEMS
INC DAYTON OH R C DARRAH ET AL. DEC 88
UNCLASSIFIED AFOSR-TR-89-0041 F49620-85-C-0013 F/G 5/1 NL

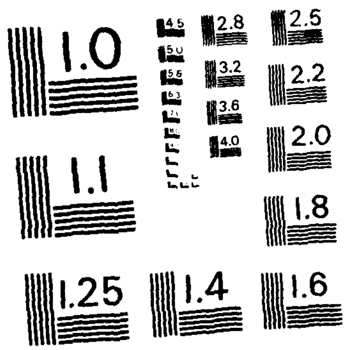
1.0
1.1
1.25
1.4
1.6
1.8
2.0
2.2
2.5
2.8
3.2
3.6
4.0
4.5
5.0
5.6
6.3

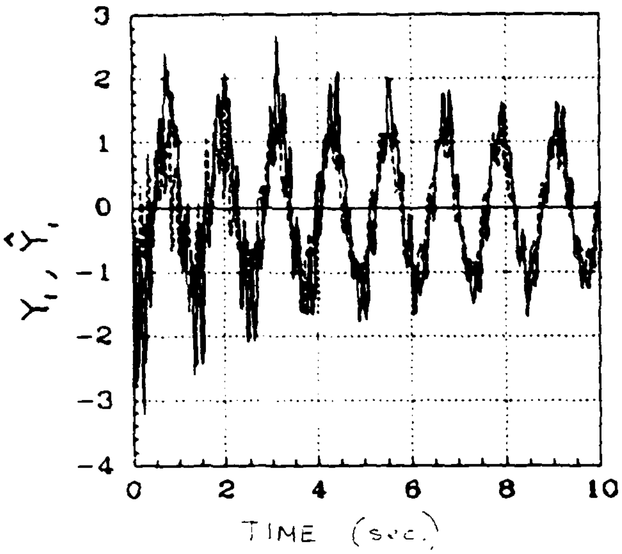

Figure 5
Y_1 and $\hat{Y}_1$ vs. time for grid free response

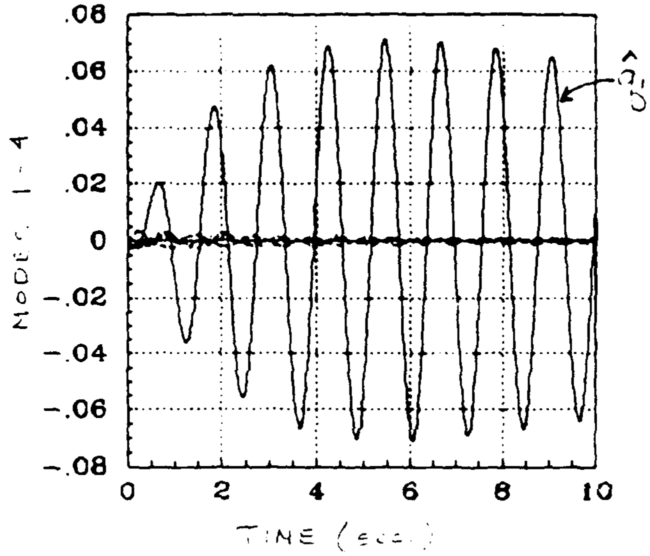

Figure 6
Modal displacements 1-4 vs. time for grid free response

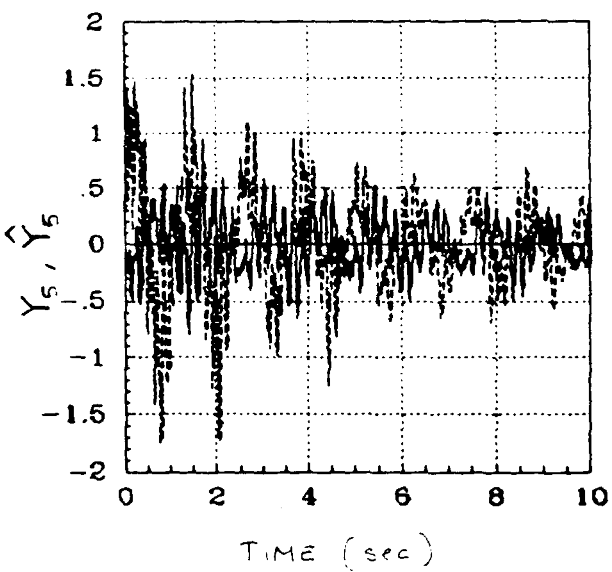

Figure 7
Y_5 and $\hat{Y}_5$ vs. time for grid free response

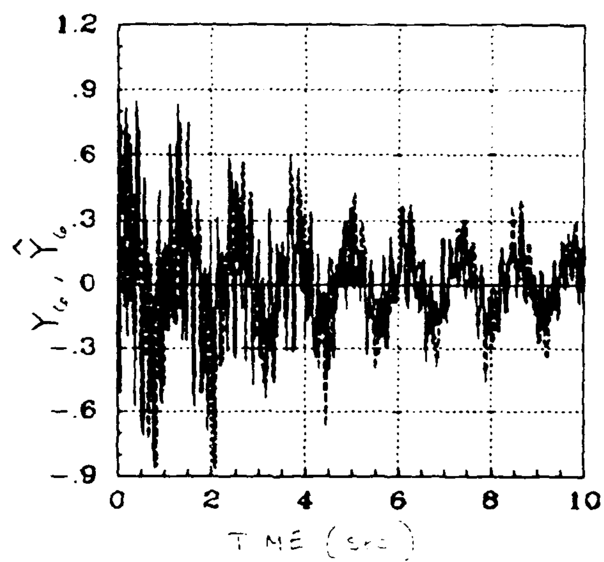

Figure 8
Y_6 and $\hat{Y}_6$ vs. time for grid free response

References

1. Brogan, William L., Modern Control Theory, Englewood Cliffs, New Jersey, Prentice-Hall Inc., 1985.

2. Craig, Roy R., Structural Dynamics, An Introduction to Computer Methods, New York, New York, John Wiley & Sons, Inc., 1981.

3. Kailath, Thomas, Linear Systems, Englewood Cliffs, New Jersey, Prentice-Hall Inc., 1980.

4. Meirovitch, L., Anderson, L.R., Kim, Z., "An Investigation of Methodology for the Control of Flexible Structures," Virginia Polytechnic Institute & State University.

5. Meirovitch, L., Baruh, H., "The Implementation of Modal Filters for Control of Structures," Journal of Guidance and Control, Vol.8, No.6, Nov.-Dec. 1985.

6. Meirovitch, L., "Modeling and Control of Distributed Structures," Virginia Polytechnic Institute & State University.

1988 USAF-UES SUMMER FACULTY RESEARCH PROGRAM/

GRADUATE STUDENT RESEARCH PROGRAM

Sponsored by the

AIR FORCE OFFICE OF SCIENTIFIC RESEARCH

Conducted by the

Universal Energy Systems, Inc.

FINAL REPORT

Rheometrics Stress Rheometer Applications

Prepared by:	William Geisler
Academic Rank:	Graduate Student
Department and University:	Polymer Science Department University of Akron
Research Location:	USAFAL/RKPL Edwards AFB Edwards, CA 93523
USAF Researcher:	Capt. D.M. Husband

Date:	1 August 1988
Contract No.:	F49620-88-C-0053

Rheometrics Stress Rheometer Applications

by

William Geisler

ABSTRACT

A method of training AFAL-RKPL personnel in the use of the Rheometrics Stress Rheometer (RSR) was needed to reduce the large amount of time required to train an individual to operate the RSR. The report serves as a guide to the RSR for the newcomer. By working with the laboratory's technicians I was able to determine what information needed to be provided to the newcomer immediately and which information could easily be obtained from the RSR's operations guide.

ACKNOWLEDGEMENTS

I wish to thank the Air Force System Command, the Air Force Office of Scientific Research, and UES for the opportunity to research in the Air Force Astronautics Laboratory at Edwards AFB.

I would especially like to thank Capt. D.M. Husband, Daniel Schwartz, and SSgt. David E. Foxx for the support and advice they provided during my stay at AFAL-RKPL.

I. INTRODUCTION:

The method of rheological characterization of highly filled polymer systems varies greatly from manufacturer to manufacturer and even between research groups working with similar materials. Different methods of evaluating highly filled suspensions, and even the testing schedule of a sample can yield rather disparate results from experimenter to experimenter for a single material.

The Solid Propellant Laboratory of the USAF Astronautics Laboratory at Edwards Air Force Base is concerned with the development, preparation and testing of solid propellants. Of particular interest in the testing of propellants' rheological properties is continuity and reproducibility of test measurements. The Propellant Laboratory makes use of two Rheometrics, Inc. apparatus in characterizing propellants -- the mechanical spectrometer and the stress rheometer. The Propellant Laboratory has developed a training and operations manual for the mechanical spectrometer and is in need of a simple and effective way to train personnel in the use of the stress rheometer.

My research interests in rheology have been in the area of characterization of highly filled and polymeric systems through constant stress measurements and variable strain testing. In developing programmed control of a stress rheometer I learned a great deal about the operation,

control and testing uses of stress rheometers which has aided me in in this summmer effort.

II. OBJECTIVES OF THE RESEARCH EFFORT:

The goal of my research effort at the AFAL Propellant Laboratory is twofold -- the development of a training and troubleshooting guide for the laboratory's Rheometrics Stress Rheometer (RSR); and the initiation of an NK series solid propellant (R-45M based) characterization study. In order to make full use of the laboratory's equipment it is necessary to have an effective way to bring new personnel up to speed on the operation of equipment so that research does not lag. Of particular concern is the number of duties and frequent rotation of tasks placed on the laboratory's technicians. The difficulty then lies in retrieving meaningful data when several operators are involved with the same study. The report emphasizes the most important and basic operations of the RSR -- leaving detailed description of the device's components operation to Rheometrics' standard operations guide.

III. BACKGROUND:

S.L. Smith's (1985) final report, 'The Rheometrics Mechanical Spectrometer (RMS) Solid Propellant Manual' (AFRPL TR-85-Ø12) provides an excellent starting point for introduction to rheology. The 'Rheometrics Stress Rheometer RSR-86ØØ Operations Manual' (1987) is the primary source of

apparatus and operations specifications, as well as calibration procedures, for the RSR. The RSR is used to examine materials' strain response to a constant or varied applied stress. Several types of fixtures are available to use in testing -- parallel plates, cone and plate, and torsion rectangular test fixtures. The parallel plates and cone and plate are used primarily for testing liquids and suspensions, whereas the torsion rectangular fixtures are used to test solid rectangular specimens.

The report is organized according to the path one takes through average testing procedures. The intent is to present the apparatus to the user in a way that promotes the recognition of recurring themes of operations procedures, as well as highlighting crucial testing concerns. Therefore, this is NOT a step-by-step operations guide, but is intended to be a 'friendly' (?) tour guide to the RSR. Some descriptions of operations may seem to be overly simplified or obvious -- but I have found that they are necessary for those who are not familiar with using personal computer (PC) controlled equipment.

IV. OPERATING CONDITIONS:

Make sure that all equipment has been turned on and warmed up for several hours before beginning. The air compressor supplying the RSR's air bearing should not ever be turned off, unless repairs are necessary. Letting the air run continuously to the air bearing seems to reduce the

need for cleaning of the air bearing and is reccommended by Rheometrics, Inc. The compressor tank and air lines should be drained of water daily.

If the RSR will not turn on or powers down during operation check the fuses on the back of both the computer control box and the test station. It is important that any damaged fuses be replaced with the appropriate size of fuse. Also, attempt to determine the source of strain on the equipment. If repairs are beyond your ability, pursue a course of repair with your supervisor.

V. FORMATTING A DISK:

Before running the RSR's programming it will be necessary to format a data storage disk. Insert the DOS disk in drive A (the top one) and the disk to be formatted in drive B. Turn on the switch on the side of the computer, and the switch on the video screen. When you get the A> prompt, type FORMAT B: and then press the ENTER key (NOTE: all commands are followed by striking the ENTER key). Follow the instructions given by the format program.

VI. MAKING A BACKUP DISK:

It is important to make sure that there is always a backup copy of your computer programming. The RSR's programming is contained on a disk labeled 'Recap II RSR Composite Disk v 1.31'. If you look through the boxes of disks in the lab you should be able to find a backup copy of

this programming. If there ever comes a time when the RSR disk goes bad and won't run the programming, it will be necessary to make a copy of the backup disk. To do this, boot up the DOS disk, (described in V) type DISKCOPY A: B:. Insert the 'Recap II RSR Composite Disk v 1.31' backup disk (the SOURCE disk) in drive A, and a blank formatted disk in drive B (the TARGET disk). The DISKCOPY program will instruct you in copying the backup copy of the RSR's composite disk. Properly label the newly copied disk.

VII. SUBMENU USE (Setting up a Notebook):

Place the 'Recap II RSR Composite Disk v 1.31' in drive A. To reboot the system with this diskette, depress the CTRL, ALT, and DEL keys simultaneously. The IBM will ask you for the date and time. The current time must be typed in in military format. After inputting the date and time the Rheometrics logo is printed on the screen, quickly followed by the main menu.

The Recap program makes use of menus and submenus to control experiments, print and plot data, analyze data and the like. Before running an experiment it will be useful to see how the menus work and practice using them. Submenus may be selected in one of three ways: using the appropriate function keys (F1, F2, F3, etc.) located on the top row of the keyboard; by highlighting the submenus with the up or down arrow keys followed by pressing the ENTER key; OR by

pressing a key which corresponds to the appropriate yellow shaded letter.

RSR experiments are stored in notebooks on the data diskette. The notebooks allow you to segregate experiments by project -- each project's experiments will be stored in its own notebook. So, our first order of business will be to setup a notebook for storing future experiments. Press F1 to 'Select Notebook'. A list of notebooks will be presented -- you will note at the bottom of the screen that pressing 'C' is used to create a notebook. So, go ahead and press 'C'. Type in your notebooks name -- try to be descriptive so that you will be able to tell what is contained in the notebook three years hence.

Practice using the three methods of selecting submenus to see what they contain and formulate a mental picture of the organization of the Recap II program. If you find yourself in a submenu with no apparent way out (e.g. when entering 'Terminal Mode') simply press F10 -- this action returns you to the previous menu.

VIII. CHECKING UTILITIES SETTINGS:

From the main menu select F7 -- 'Utilities'. Highlight the option, 'Change the default file settings' and select it by pressing ENTER. The important note to make here is that the Engineering units are setup in SI units. It seems that if cgs units are selected the program will compute the data

in cgs units but label the data in SI units! So, be careful when using cgs units.

If your data disk ever becomes full or you need to use another disk make sure that you read the index off of the disk. To do this, select 'Change data disk and read the new index' from the Utilities submenu.

The Utilities submenu contains other useful options. Familiarize yourself with them by looking through the submenu.

IX. CALIBRATING THERMOCOUPLES:

Thermocouples and the PRT (Platinum Resistance Thermocouple) should be calibrated periodically. The PRT is used by the computer's temperature controller to meet the setpoint dialed in on the TEMP thumbwheel when the oven is activated. The Rheometrics RSR Operations manual gives a well organized breakdown of calibration in section 6-3.

X. TEMPERATURE CONTROL:

Temperature control is fairly simple when using the RSR. If you wish to run a test at a temperature lower than room temperature, liquid nitrogen is used. If an elevated temperature is desired, air heating is used.

Before heating or cooling the chamber the appropriate thermocouple should be selected. Tests involving parallel plates or the cone and plate fixture should make use of the thermocouple located underneath the bottom fixture.

Rectangular torsion tests use the thermocouple just to the right of the lower fixture. The thermocouples are plugged into the test station on the front left panel.

XI. COOLING:

1. Have your fellow technicians or supervisor check you out on the filling and operation of the indoor nitrogen storage tank. The inside tank is filled from the large outdoor nitrogen reservoir. The vapor pressure in the outdoor tank should not be allowed to get so great (50-60 psig) that the tank's blow off valve is activated.

2. Open the liquid valve on the indoor tank. Make sure that the valve is not fully opened -- as the valve might stick in the open position. When a valve has been fully opened turn it back 1/4 turn. Open the gate valve on the line leading to the RSR's small nitrogen dewar.

3. Close the doors of the oven -- enclosing the upper and lower fixtures. The oven will not operate with the oven doors open. Depress the 'LN2/GAS' switch on the environmental control box so that 'LN2' lights. Set the temperature thumbwheel to a higher temperature than will actually be used. Press the oven 'ON' button on the RSR test station, wait a few minutes, and then dial in your desired temperature. By doing this you have avoided a rapid temperature dive.

4. Wait for the lines and dewar to fill with liquid nitrogen (5-10 minutes). When this has been accomplished

the 'LN2 READY' light will come on. If this procedure takes an excessive amount of time, check the inside tank pressure and level, and the liquid nitrogen lines for leaks.

XII. HEATING:

1. Make sure liquid nitrogen line valves are closed.
2. Put the 'LN2/GAS' switch in the 'GAS' position.
3. Lower the upper fixture so that it will fit in the oven.
4. Shut the oven door. Set the temperature thumbwheel at a setpoint lower than the desired temperatures.
5. Press the oven 'ON' switch, wait a few minutes and dial in the desired temperature.

XIII. MAKING A 'CAL. CURVE':

Basically, a Cal. Curve is a plot of the resistance of the air bearing versus position. While running a test the RSR compensates for error in readings by accounting for friction losses and non-uniform laminar flow in the air bearing. Cal. Curves may be used for experiments 50 C above or below the temperature at which a Cal. Curve was measured. For example, a Cal. Curve measured at 100 C may be used when testing a material at 120 C. Naturally, if you are making very sensitive readings it may be necessary to make Cal. Curve measurements at the temperature of your test. It must be kept in mind that Cal. Curves are fixture dependent -- you shouldn't use a Cal. Curve made with the 50 mm parallel plates to run a test with a cone and plate. For

normal operating conditions, Cal. Curves should be remeasured every few months.

To make a Cal. Curve, lower the upper fixture until it will fit inside the oven. Close the oven doors. Bring the oven to temperature for 20-30 minutes. Setup a notebook for storing your Cal. Curves. Press the 'TRACK' button and wait for the 'POSITION LOCKED' light to come on. Press 'CAL'. The computer will take its torque measurements during the following 15-20 minutes. When the 'CAL' light turns off the Cal. Curve test is finished. The Cal. Curve needs to be stored on your data disk. From the main menu select 'CALIBRATION' (F8). Store the Cal. Curve in the 'CALIBRATION' submenu by following the directions given by the 'Store Cal. Curve' (F1) option. Note that Cal. Curves are retrieved and deleted through the CALIBRATION submenu. When loading a Cal. Curve remember to select your calibration notebook before retrieving a Cal. Curve. It is important to check which Cal. Curve has been loaded into the computer before beginning an experiment.

XIV. PLATE GAP:

Setting the zero plate gap takes a bit of practice. The zero gap is the position of the fixtures when they initially meet. The zero gap should be set before each experiment. If the zero gap is set incorrectly, experimental results are thrown off -- so you should recheck the zero gap several times before testing a material.

The quill is lowered and raised with the hand crank located on the top of the test station. Lower the quill -- as the top fixture gets close to the bottom, watch the 'ZERO GAP INDICATOR' on the test station carefully. Lower the upper fixture a few microns at a time. When the needle on the gap indicator deflects the plates have come into contact. Adjust the quill height until you find the position where the plates just meet. To set the gap gauge to zero, adjust the thumbscrew under the gauge so that both needles read zero. Raise the quill and recheck your zero gap several times.

Gap readings are made in millimeters. On the RSR gap gauge there are two needles to be read when determining the gap height. The small gauge in the middle is read first and is read in millimeters -- the small tick marks on this gauge each represent 0.2 mm. The gauge with the large needle is read next. Each small tick mark on the larger gauge represents 0.002 mm (2 microns). One trip around the larger gauge represents 0.2 mm. A numbered mark like 40 on the larger gauge is read as 0.040 mm (40 microns). Figure 1 shows some examples of gauge settings.

XV. TORQUE CALIBRATION:

Due to the organization of this guide it will be helpful to try some practice experiments (see XVI) before attempting to calibrate the RSR. However, I feel it is important to be presented with the torque calibration

FIGURE 1 - Example readings of RSR gap gauge.

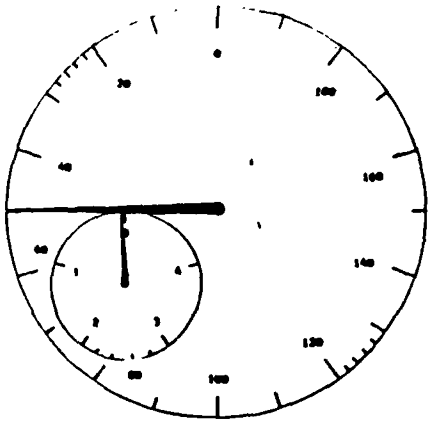

0.050 mm (50 microns)

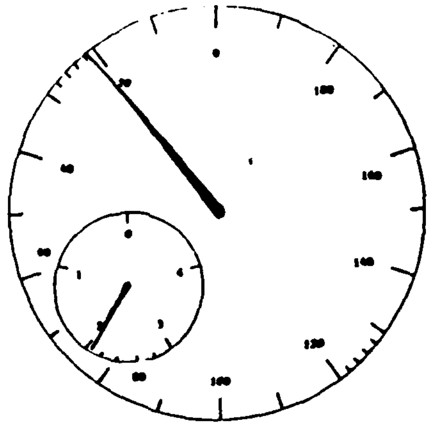

2.022 mm

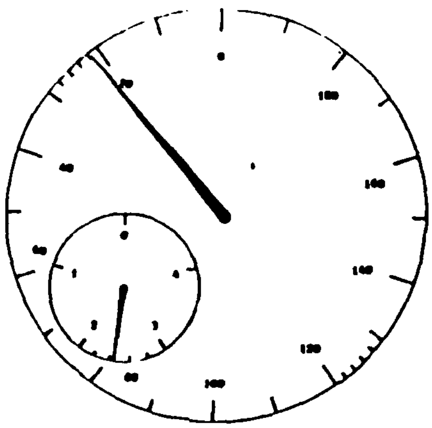

2.422 mm

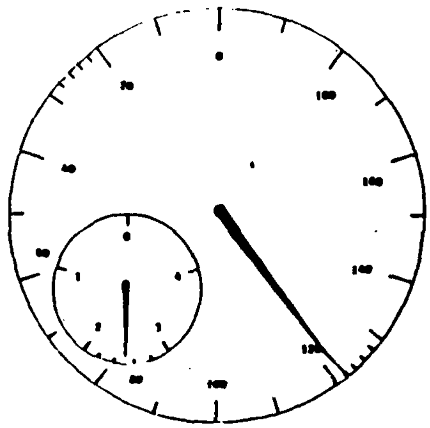

2.522 mm

procedure before you begin to perform experiments. Hopefully, after reading this section you will remember that the RSR will need to be calibrated periodically.

Rheometrics' operations manual gives an easy to follow breakdown of the calibration procedure in section 6-1.2. It is important to go through this procedure several times (at least three) before making a decision on whether or not to calibrate the RSR. Plate gap and temperature control should be carefully set during this procedure. You should not expect to match the viscosity given on the oil standard bottle exactly. If your viscosity measurements are within 5% of the value given by the manufacturer you are doing great and the RSR isn't in need of calibration. If the RSR's results are consistently more than 10% high or low you will need to continue with the calibration procedure. Again, make sure that you make several measurements of the oil's viscosity, and that you get consistent results before you calibrate the torque. If you are not sure of the age of your oil standard or the oil's purity, get a new standard oil.

XVI. STRESS MODE EXPERIMENTS:

Through stress mode experiments the operator may run constant stress tests. In this section I will demonstrate the use of the 50 mm parallel plates. The use of the other fixtures is similar and a small amount of instruction is

given for the cone and plate and torsion rectangular fixtures in the latter part of the section.

When running a stress mode experiment you will often have to determine the stress level input that will yield reasonable results. The RSR's experimental limiter is rotational rate. If a fixture is turning too slowly the RSR's transducers cannot pickup any movement. Rate limitations are listed in Tables 4-1 and 4-2 of the RSR's operations manual.

I will use a propellant to demonstrate the use of the parallel plates. NK-33A is an 85% solid filled propellant. When testing solid propellants it is desirable to test them immediately following mixing. Nk-33A was mixed at about 60 C -- so I stabilized the oven temperature at 60 C prior to the end of the mix (see XII). While waiting for the mix I checked and rechecked the plate gap (see XIV). Next, I set the 'TEST GEOMETRY' and 'TEST PARAMETERS':

1. From the main menu select 'Terminal Mode' (F6).
2. Press the 'TEST GEOMETRY' button on the computer control box.
3. Enter 'Y' for 'DISC & PLATE' and 'N' for the other plate choices.
4. I will set the 'GAP' for my test at 2.000 mm. The plates I am using have a 25 mm radius.

If you make a mistake while entering information there are two ways to correct the misinformation -- begin the

process over, or while you are on the line where the error has occurred, press the CTRL and K keys simultaneously.

5. Press the 'TEST PARAMETERS' button.

6. Answer the 'USE EXTERNAL INPUT?' question with 'N'.

7. Answer 'Y' to the 'STRESS MODE' question.

The RSR has 8 command zones -- ZONES 1-4 are designated as stress zones, while 5-8 are recovery zones. The user inputted stress is applied to the test material during stress zones. During a recovery zone, no stress is applied and the RSR measures movement of the upper fixture caused by the material's recovery. The total length of time an experiment may run can not exceed 32,760 seconds. If you exceed this time limit, you will not be able to analyze the data taken during the test.

8. I entered 50 dynes/sq. cm as a stress, for 600 seconds in ZONE 1. Zeroes were entered for the other zones.

Before loading the sample, press the 'TRACK' button. When the 'POSITION LOCKED' light comes on, raise the fixture and load your sample. Press 'START' to begin testing.

When the experiment ends, return to the main menu (F10). To store the experiment, select 'Store Experiment on Disk' (F3). The program will ask you to title your experiment and provide a space to type in any observations you made about the test. After typing your notes, press the ESC key to continue with the data storage procedure.

Printing and plotting menus are also selected from the main menu (F5). Before printing or plotting data, run through the printing or plotting parameters submenus (F3, F4). Your answers will vary according to the type of test being performed. If you have not used a printer or plotter before, ask one of your fellow technicians to explain the use of the printer and/or plotter. The 'Printing Parameters Selection' (F3) option is fairly straightforward -- simply answer each of the questions the program poses. When filling in t 'Axes Range Selection' portion of the 'Plotting Parameters Selection' (F4) option, you will find the high and low data points listed in the 'Actual Window Value' box. To turn on or off the ability to send information to the printer or plotter press Alt F2 or Alt F3 respectfully.

A straight line, least squares fit can be made to any range of data by selecting 'Least Square Fit Analysis' (F5). Viscosity measurements are determined by using option (F1) 'Stress Zone'. Use the data at the end of a stress zone which is fairly linear to determine a steady state viscosity.

Cone and plate experiments are performed in an analogous fashion to the parallel plate experiments. A few methods are different however -- the gap of the 25 mm, 0.1 radian cone angle fixtures are set at 0.050 mm (50 microns); and tests must be performed at constant temperatures to maintain the appropriate gap.

The torsion rectangular fixtures are used to study rectangular solid samples. The thermocouple located underneath the bottom fixture will need to be removed temporarily during experimentation. The dimension of samples are measured with calipers and are repoted in terms of millimeters.

XVII. STRESS RAMP EXPERIMENTS:

Stress ramp experiments are selected from the 'Terminal Mode' (F3) with the 'TEST PARAMETERS' button. Simply answer 'N' to the 'STRESS MODE' question and 'Y' to the 'STRESS RAMP' option. You will be asked for the maximum applied stress and the duration of the experiment. When the test is run, a linear ramp of stress will be inputted over the duration of the experiment. The stress ramp test may be used to determine a materials yield stress.

XVIII. RECOMMENDATIONS:

Due to the short visit I was afforded to the propellant laboratory, several areas of this report are slightly less than I had hoped they would be. In particular it would have been nice to work through some actual experiments in the body of the report. However, time and the twenty page format limited the inclusion of detailed example experiments. Due to the nature of vacation seasons, I was unsuccessful in scheduling propellant mixes with the mixing laboratory during my five week stay at AFAL-RKPL.

However, I do feel that the report will be a useful starting point in the training of personnel on the use of the RSR. I have stressed the need for cautious and mindful experimentation.

REFERENCES

Rheometrics, Inc., 'Rheometrics Stress Rheometer RSR-8600 Operations Manual', 1987.

Smith, S.L., 'The Rheometrics Mechanical Spectrometer (RMS) Solid Propellant Manual', AFRPL TR-85-012, 1985.

1988 USAF-UES SUMMER FACULTY RESEARCH PROGRAM

GRADUATE STUDENT RESEARCH PROGRAM

Sponsored by the

AIR FORCE OFFICE OF SCIENTIFIC RESEARCH

Conducted by the

Universal Energy Systems, Inc.

<u>FINAL REPORT</u>

<u>Stability of Jets Under the Supercritical State</u>

Prepared by:	David L. Graham
Academic Rank:	Graduate Student
Department and University:	Mechanical Engineering Northwestern University
Research Location:	AFAL/RKLA Edwards AFB, CA 93523
USAF Researcher:	1Lt Angela Bartholomew

Date:	12 Sep 88
Contract No:	F49620-85-C-0013

Stability of Jets Under the Supercritical State

by

David L. Graham

ABSTRACT

A high pressure system was constructed to study straight and impinging jets of carbon dioxide. In the next few weeks, carbon dioxide above supercritical pressure and at sub/supercritical temperatures will be injected into a windowed high pressure chamber containing supercritical nitrogen. The jets will be photographed by a laser shadowgaph, to examine the stability of the shear layer and the transition to turbulence. The experiment is modelled to liquid rocket geometry, with the objective of a better understanding of fine spray in rocket and other high pressure conditions.

Acknowledgements

Thanks to all of the people at the Air Force Astronautics Laboratory who contributed to my project. I would like to specifically mention Lt. Bartholomew, Tully Becker, Clinton Jones, Capt. Seidemann, Delbert Surrett, Bob Wiswell, Wayne Roe, Mike Powell, Jolaine Lamb, Tom Coultas, Dick Ritell, and Mike Dieckhoff. Many others in XR, TO, and RK helped me as well, more than I could possibly list, but their assistance is not forgotten.

Thanks also to my advisor at Northwestern, Prof. Siavash Sohrab.

This research was sponsored by a AFOSR grant to Universal Energy Systems.

I. Introduction

A current design issue for liquid rockets is the whether to pre-heat the fuel to a gaseous state prior to injection. This involves taking a fuel such as Liquid Hydrogen and circulating it around hot engine components to raise its temperature above the critical temperature[1], and then injecting it into the combustion chamber.

The more traditional design is to inject the fuel as a liquid, at a supercritical pressure and subcritical temperature as it leaves the injector, vaporizing to a gas in the supercritical temperature combustion chamber. The theory for this is well developed from studies of rocket, turbine, and reciprocating engines. For fuels preheated well above the supercritical temperature and the supercritical pressure, the theory for this type of injection, gas into gas, is also fairly well defined. However, relatively little is known about the actual physical behavior and appearance of jets injected in the vicinity of the supercritical temperature and pressure, where the single-phase injected fluid combines gaseous and liquid behavior. The relative dearth of physical knowledge from experiments has made creation of empirical models difficult.[2]

The Air Force Astronautics Laboratory at Edwards Air Force Base is the main Air Force center for this type of rocketry-related research, in my case the Launch Vehicle Propulsion (RKLA) section's in-house spray research project. My research project developed from my thesis advisor's (Prof. Sohrab) 1985 and 1986 summer work at AFAL and his subsequent AFOSR mini-grant on supercritical phenomena.

II. Objectives of Research Effort

The goal of my research project is to achieve more understanding of the physical behavior and the stability of jets in the region of the critical point, and to explore the vanishingly small surface tensions occurring above the critical point for production of fine sprays. The current evidence, gathered mainly in burning tests, suggests that the transition from liquid to gaseous behavior is fairly gradual, with purely gaseous injection theory not accurate until the injection pressure is 130 percent of the critical pressure[3] and/or the temperature is about six degrees C above the critical temperature[4] The approach is to observe the more basic mechanisms of jet stability, atomization, and vaporization, avoiding combustion by using CO2 as a fuel simulant.

The experimental apparatus, shown in Figure 1, is designed to simulate rocket combustion chamber pressures, allowing pressures up to 2000.psi can be studied. The main objective of my work at AFAL was to design and construct the experimental system (Figs 1, 2, 3) , and then bring it back to Northwestern University for the actual testing and laser shadowgraph photography. The test matrix will include examination of the effects of temperature, pressure, injection pressure drop, and jet geometry (see Figures 3a and 3b). At the current time, all necessary components have been acquired, and assembly of the system is nearly complete. Pressure tests should be underway in about a week. The tests will be completed in November and a final report will be sent to AFAL in December 1988.

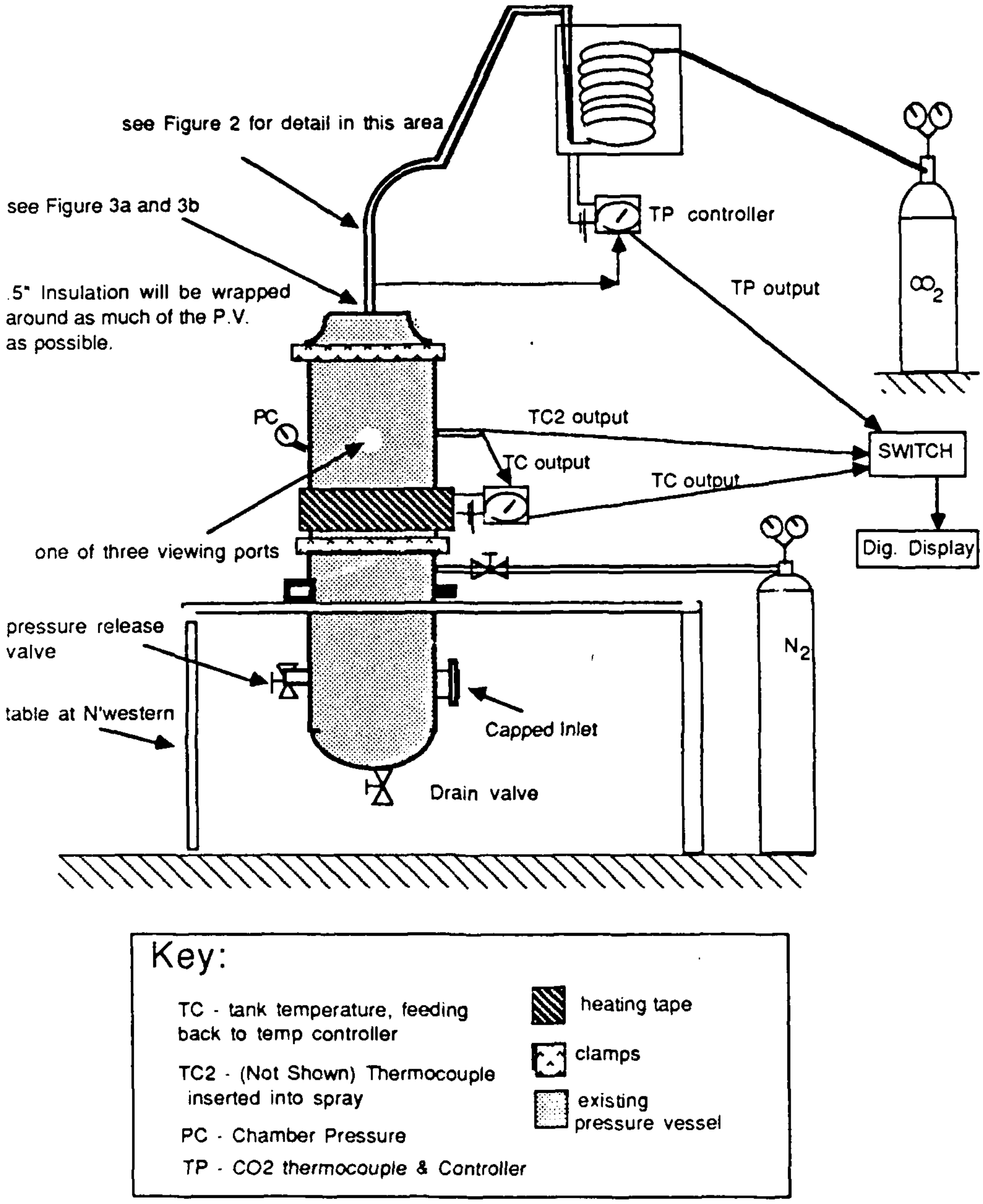

Figure 1. Schematic of Apparatus

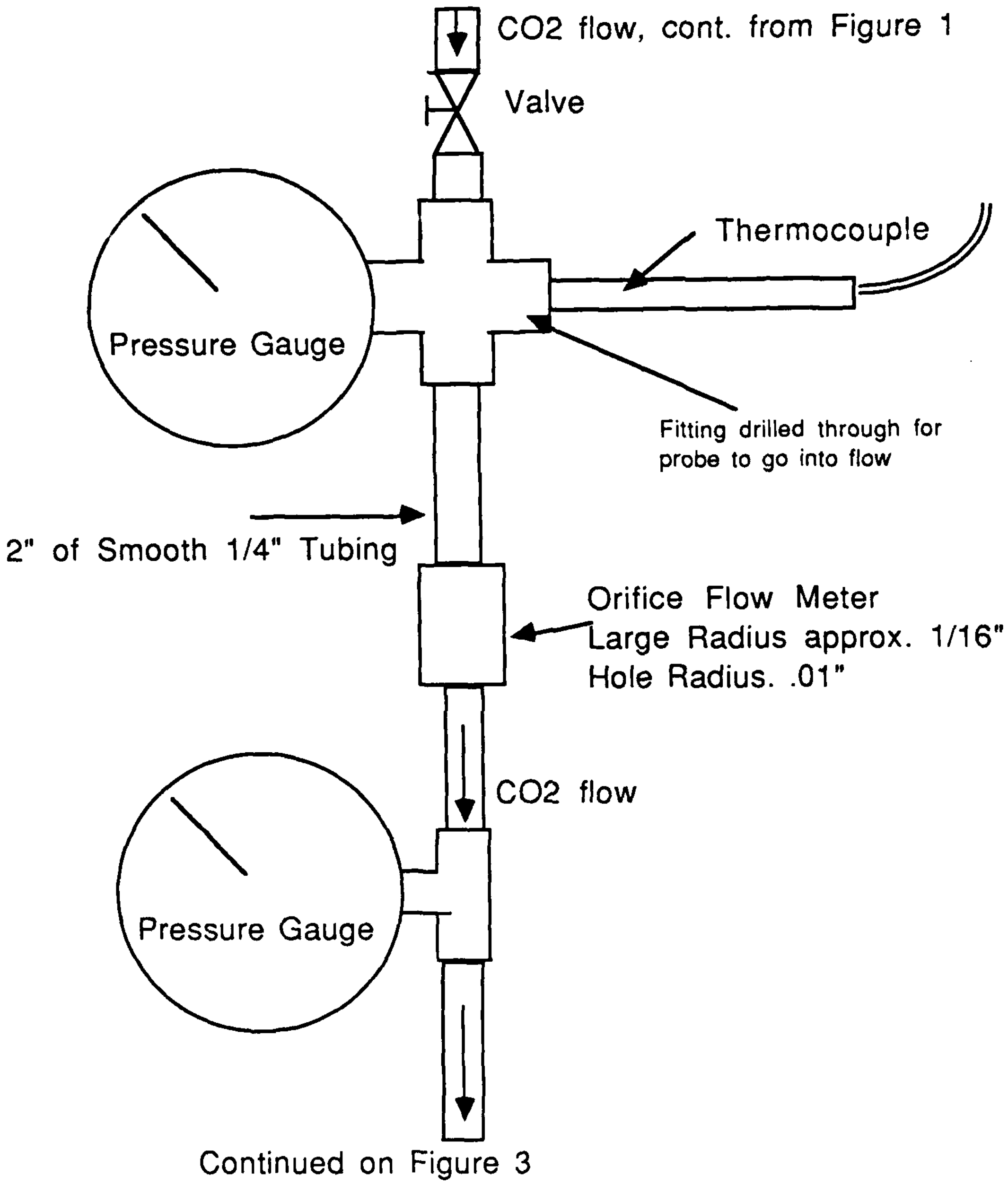

Figure 2. Detailed Schematic of Instrumentation

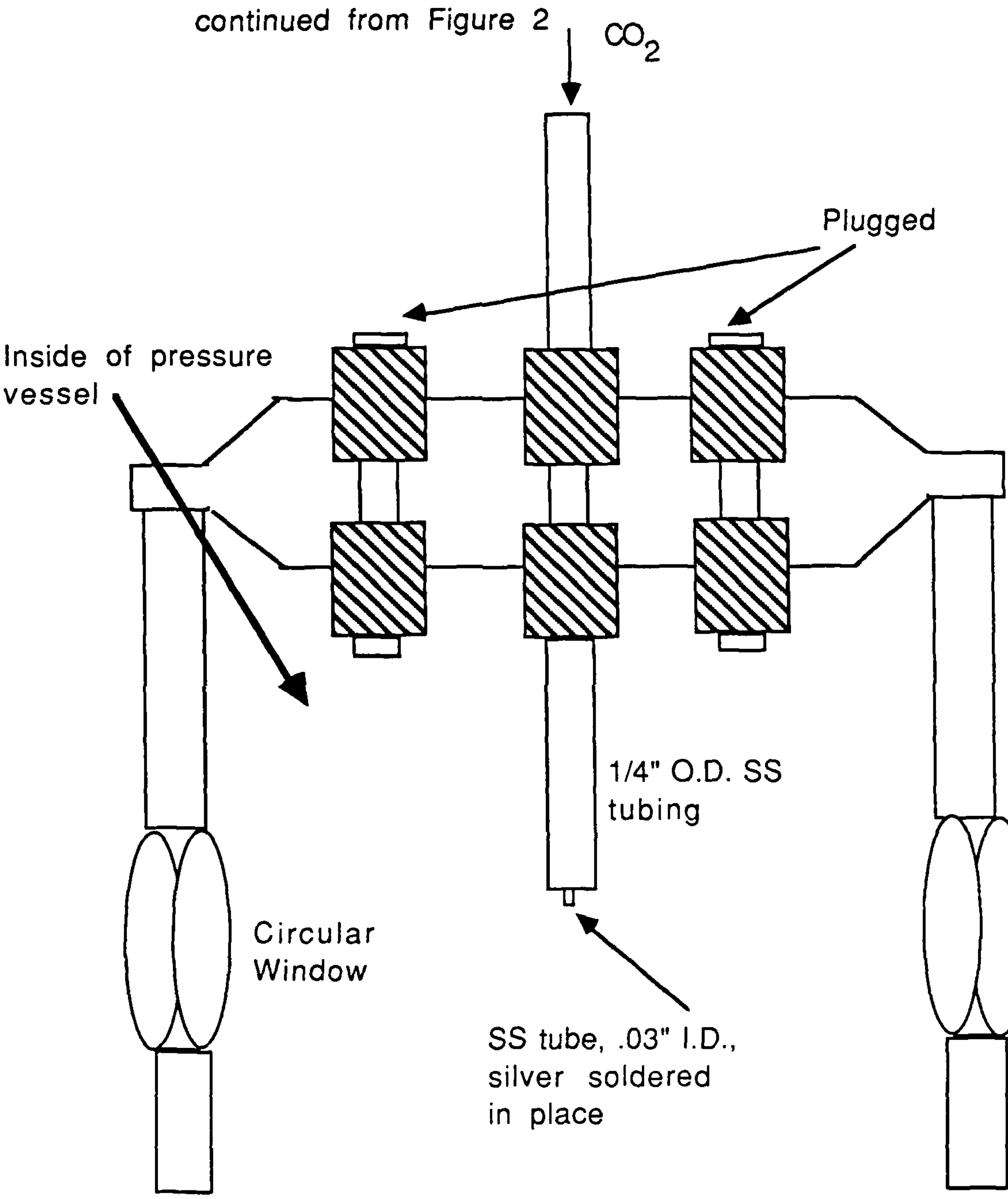

Fig. 3a. Straight Jet Setup

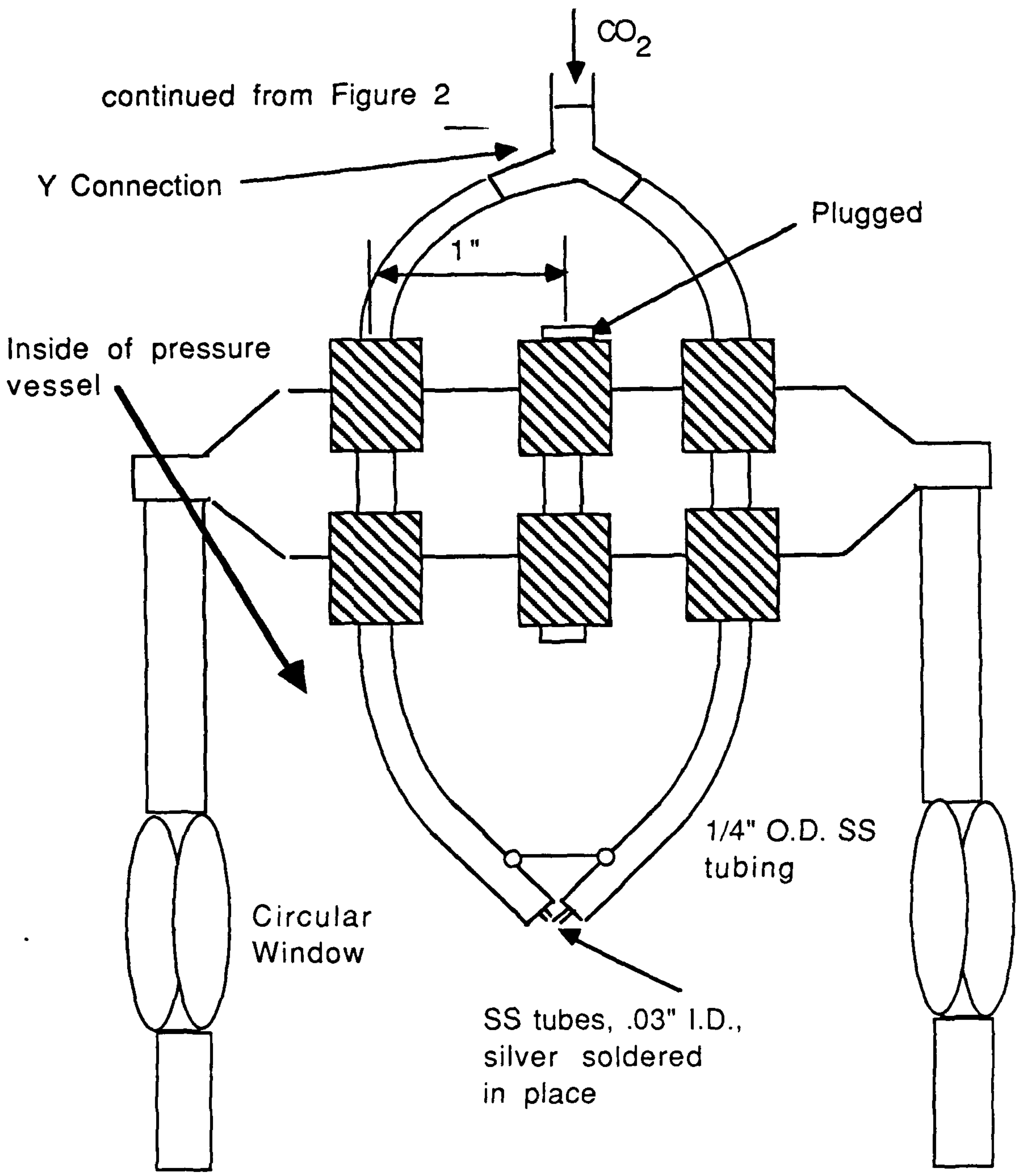

Fig. 3b Impinging Jet Setup

III. Details of Experimental Approach

In a typical experiment, a jet(s) of carbon dioxide at a pressure of 80 atm and a temperature of 28° C, compared to the critical points (P_c = 72.9 atm, T_c = 31°C), will be injected into a stagnant 75 atm. nitrogen environment . The jets will be gradually heated to 40° C, well above the supercritical temperature. Current experimental evidence suggests that evaporation of the supercritical CO_2 will be rapid, but more than simply a "puff" into a gaseous state[5].

Using a He-Ne laser sheet light, produced by the passage of the cylindrical laser beam through a cylindrical lens, the nature of the jet flow may be observed due to the changes in the indices of refraction. If necessary, the jet could also be dyed. The objective is to photograph and compare the stability of the shear layer at the jet boundary under supercritical/subcritical conditions and also the transition between laminar and turbulent jets.

In addition to the supercritical jet behavior study, condensation under sudden expansion into the saturated state will be examined. Here, two jets of supercritical fluid impinge and subsequently expand to lower pressures.

IV. Background on the Supercritical State

a. The use of the term "supercritical" applies to the liquid/gaseous state of the fluid and should not be confused with another use of the term, which applies to situations where the flow is choked.

For each gas, there is a **critical temperature** which is the upper limit for inducing liquefaction. The **critical pressure** is the pressure that is required to liquefy the gas at the **critical temperature**. Above this temperature, no

amount of pressure can induce liquefaction. The volume occupied by a gas at its **critical pressure** and **critical temperature** is the **critical volume**. At this **critical point,** there is no distinction between liquid and gaseous behavior, in density, index of refraction, or molar volume.

As the figure[6] below shows, the lower the temperature; the lower the liquefaction pressure. The left side of the graph is liquid; the area under the hump is vapor (a term used for any gas below its critical temperature) and liquid in mutual equilibrium, with the horizontal lines representing the saturated vapor pressure of the liquified gas; the right side of the hump is gas. At the very top of the hump is the supercritical point.

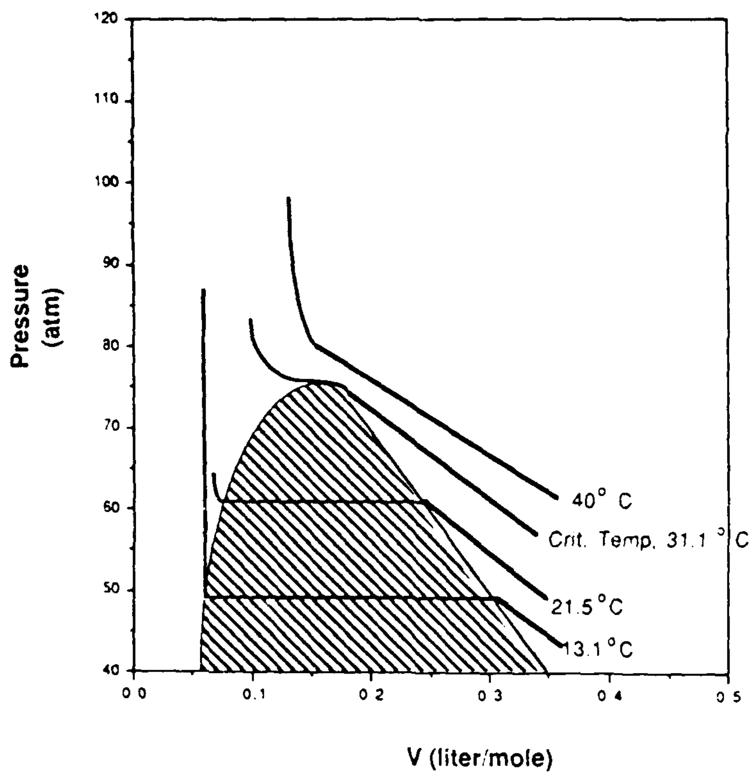

Figure 4. P-V Curve for Carbon Dioxide

b. There are numerous empirical models for fluid viscosity and surface tension as a function of temperature. Most bring both values to zero at the supercritical temperature. One such relationship[7] is:

$$\frac{d}{dT}\left[\gamma(M/\rho)^{.66}\right] = -k \qquad (1)$$

where (M/ρ) is the molar volume and $(M/r)^{.66}$ is proportional to the surface area. The product $g(M/\rho)^{.66}$ is called the surface Gibbs free energy. Taking $g = 0$ at T_c and integrating gives

$$g(M/\rho)^{.66} = k(T_c - T) \qquad (2)$$

The surface tension actually vanishes at about 6 degrees above the critical temperature, according to Ramsey and Shield. The best these formulas can be is a guide, since they apparently break down at the supercritical temperature.

V. Recommendations

It is difficult to make a recommendation at this point, sinee experimental results will not be available for several weeks. However, successful experiments should have applications to the production of fine sprays and more complex problems involving chemically active supercritical flows, including rocket, turbine, and diesel combustion.

REFERENCES

1. Section III includes more detail on supercritcal phenomena and the supercritical state of carbon dioxide in particular.

2. Liang, P.Y. and Jensen, R.J. "Modeling of dense sprays from LOX/H2 coaxial injectors under supercritical conditions" A 1985 Rocketdyne study, related to the Space Shuttle Main Engine design, which gives some basic empirical models.

3. From Discussion with Mr. Tom Coultas.

4. Liang and Jensen

5. Ibid.

6. Fried, Hameka, and Blukis Physical Chemistry (MacMillan:New York 1977)

7. Ibid.

1988 USAF-UES SUMMER FACULTY RESEARCH PROGRAM

GRADUATE STUDENT RESEARCH PROGRAM

Sponsored by the
AIR FORCE OFFICE OF SCIENTIFIC RESEARCH
Conducted by the
Universal Energy Systems, INC

FINAL REPORT

IN-PLANE FRACTURE IN 2-D CARBON-CARBON

Prepared by:	Gary Griesheim
Academic Rank:	Graduate Student
Department and University	Civil Engineering and Mechanics Southern Illinois University
Research Location:	USAFAL/VSSC Edwards AFB Edwards, CA. 93523
USAF Researcher:	Dr. Peter Pollock
Date	10 Aug 1988
Contract No:	F49620-88-C-0053

IN-PLANE FRACTURE IN 2-D CARBON-CARBON

by

GARY GRIESHEIM

ABSTRACT

Experimental results are reported from an on-going program studying in-plane fracture in 2-D carbon-carbon. The material used in this study was a laminated 2-D carbon-carbon composite containing WCA carbon cloth as the reinforcement. Compact tension specimens were extracted from the laminated composite and tested for their fracture behavior. Initial cracks were machined into the specimens using both V-notches and Chevron notches. Crack opening displacement measurements were taken during each fracture test.

The experimental fracture behavior of 2-D carbon-carbon is compared with assumptions which are fundamental to the theory of linear elastic fracture mechanics. Specific issues which are discussed include: effect of notch sharpness on fractue strength, relation of specimen compliance to crack length, effect of very small crack length on fracture strength, and the role played by nonlinear material behavior in the development of crack tip stresses.

I. INTRODUCTION: Compreheasive investigations are being made into the fracture behavior of 2-D carbon-carbon composites. The comprehensive investigation includes both interlaminar and in-plane fracture behavior. The investigation has been initiated due to the limited amount of research that has been conducted on this relatively new composite. Carbon-carbon is one of very few materials which can withstand the harsh enviroments of exit cones for rocket engines, re-entry space vehicles, and other space structures. Although cabon-carbon can withstand such high temperatures, it has a number of problems. One problem in particular is its low structural properties.

Knowledge of in-plane fracture behavior in 2-D carbon-carbon is becoming more desirable due to the increased number of cylindrical products. These products include carbon-carbon tubes, struts, and exit cones to name a few. The cylindrical structures when loaded will generally fail due to in-plane fracture rather than delamination.

The investigation into in-plane fracture was also conducted to observe how the crack actually propagates through the carbon-carbon material. Another reason for the investigation was to determine if linear elastic fracture does apply to 2-D carbon-carbon composites.

This paper presents results from the three series of experiments conducted on two different types of carbon-carbon material. The first series of experiments were the compact tension fracture experiments. From the compact tension experiments there were a number of additional experiments conducted. These additional experiments include notch sharpness comparison on fracture specimens, Chevron notch vs. razor blade notch comparison and also a comparison of fracture strength between the two types of material. The second series of experiments from the investigation was the tensile tests on the two materials. The final series of experiments was the compression tests. Low compressive strength is a characteristic of some carbon-carbon composites which prevented the three point bending experiments from being conducted. A detailed description

is given on the compression and tension procedures A number of specimens were polished and viewed under the microscope. The stereoscope was used during an experiment to observe the crack tip as it propagated This was necessary to fully understand and observe what was actually happening at the crack tips during loading.

II EXPERIMENTAL TESTING: The carbon-carbon composite specimens were machined out of two different material types The two materials were from Kaiser Aerotech, which are referred to as material A and material C. the materials were graphitized and had WCA carbon cloth with a phenolic-baked, pitch/furfural impregnated matrix.

The series of experiments were all conducted using a MTS hydraulic actuated loading machine, using displacement control. The data was gathered on a data acquisition system and plotted on a screen during the test.

III. COMPACT TENSION TESTS: Compact tension specimens were machined with specifications from the ASTM manual (1) on compact tension experiments. These specimens were nominally 2 inches by 1.8 inches by .25 inches thick. Figure 1. shows the compact tension specimen and how it is oriented with respect to the warp and fill fibers From the figure it can be seen that the fill fibers are broken when the crack propagates The fill direction is weaker than the warp direction due to less fibers per bundle and the fact that the fill fibers are not perfectly straight Loading fixtures were also designed to ASTM specifications From the compact tension experiemnt the load, and the crack opening displacement (C.O.D.) are plotted over time. Figure 2. shows the M.T.S., amplifier for C.O.D. gage, and data acquisition system used for these experiments. The crack was measured from a 14X cathetometer which was mounted on the MTS machine It was found that the most accurate method of crack propagation was that of monitoring the C.O.D output on the screen. This was because of

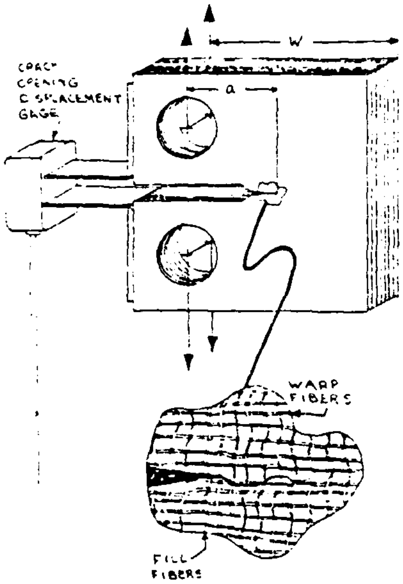

FIGURE 1.

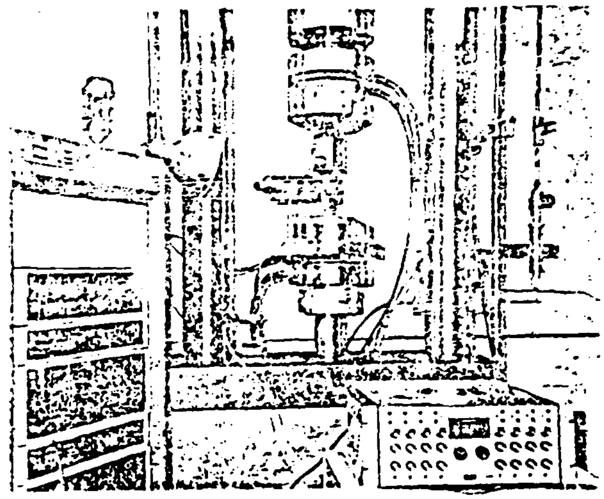

FIGURE 2.

the sensitivity of the gage making it far superior than that of the 14X cathetometer. After the specimens were loaded and the crack was measured, the specimen was unloaded down to about 15% or 20% of the fracture load and loaded again to find a new fracture load at this new crack length (a). This is continued for about two or three more times depending on the material properties. As a result of the above procedure fracture curves were generated from the specimens.

IV. <u>TENSION TESTS:</u> Ten tensile specimens were machined from the two material types. The specimens were approximately .25 inches thick, by .75 inches wide (dogboned) by 6 inches long, each specimen was reinforced at the ends with aluminum tabs glued with super glue and pinned. Two of the specimens failed because of the end tabs slipping. A shackle fixture was used to ensure that there

was no bending moment introduced while loading. While the specimens were loaded, the strain difference was monitored to ensure proper loading. An extensometer was mounted on both sides of the dogboned specimen, which is able to measure the longitudinal strains on the two opposite faces of the specimen. The data acquisition system was again used and tensile strength in warp and fill directions as well as moduli of elasticity were obtained.

V <u>COMPRESSION TESTS:</u> The compression blocks were formed by using commercial super glue to bond square pieces of the materials together in the same direction to form rectangular blocks. From these blocks density calculations were produced. As a result the density of material A was 1.486 gr/cc. and the density from material C was 1.514 gr/cc. Compression specimens were tested from the two materials in both warp and fill directions. The extensometer used was a biaxial extensometer similar to the one used in the tensile tests. The extensometer also gave the Poisson's strain across the specimen. Again the data acquisition system was used to determine Poisson's ratio, maximum compressive strength in the warp and fill directions, and a modulus of elasticity.

VI <u>NOTCH SHARPNESS:</u> One of the first criteria to determine with the compact tension experiment was the initial crack geometry and how it affects the fracture behavior. Different notch sharpnesses or radii of curvature of the initial crack were chosen to help determine this criteria. Nine compact tension experiments with an (a/W) of .5 were machined. At the tip of the notches different radii of curvature were machined. The radii of curvature were: .021, .031, .040, .049, and .061 inches. Graph 1 shows the fracture load vs. (a/W) for the different radii of curvature. From the data obtained it was obvious that the smaller radii of curvature gave the smaller and most desirable value of fracture load. It is also evident that above a radius of curvature of about .031 inches the distribution of the data is somewhat scattered.

The radom data distribution might be explained by the observation that above a radius of curvature of say the unit cell the fracture may propagate to the nearest bundle, rather than at the point of

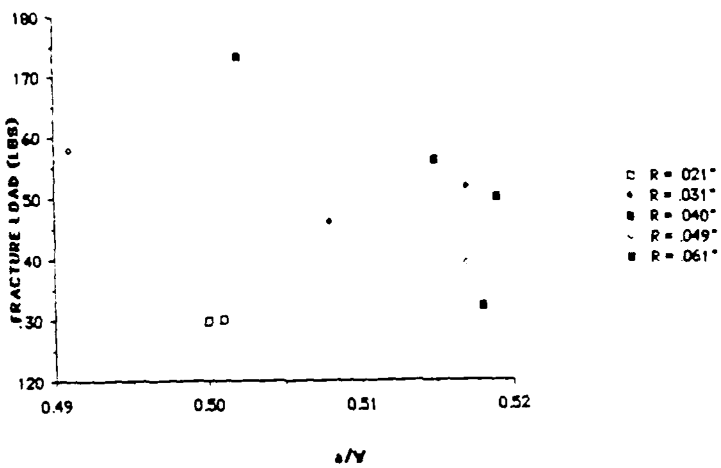

GRAPH 1.

maximum stress concentration at the back of the circle. This phenomena is being more closely studied by a series of microscopy studies on the crack fronts. From Graph 2. there are four specimens which also have different radii of curvature. These

specimens also behave similarly to the other material.

The previous series of experiments concluded that a very small radius of curvature was necessary for the most accurate results. The next series of experiments included the comparison between the straight through (V-notch) with a razor blade notch and the Chevron notch. The specimens were machined on a numerical mill to ensure that all the dimensions were accurate. The Chevron notch was estimated to have a machined radius of curvature of about 1/1000th of an inch. The radius of curvature from a razor blade notch was estimated to be 1/10000th of an inch. By observations of the crack tip it was obvious that some of the Chevron notched specimens didn't have straight crack propagation, which is necessary for accurate results. The razor blade notches on the other hand propagated approximately straight along the specimens. The comparison of this experiment is illustrated in Graph 2. The Chevron notched specimens are shown in Graph 2. It is obvious that the razor blade notched specimens are found to produce the most accurate results.

After the initial loading and the first crack was measured, the specimens were unloaded and loaded as previously described. This second loading can be seen in Graph 2., it is referred to as (AC) or "after static load crack". These specimens have natural cracks rather than Chevron or razor blade notches. The data points are shown as Chevron (AC) and V-Notch (AC). From the data shown it can be seen the the natural cracks actually have a higher fracture load than that of the razor blade notches. There are two possible explanations for this. One is that the razor blade notch is actually sharper than that produced by the natural crack. The other is the natural crack is not straight from one face to the other face. This non-linearity would cause the fracture load to be higher than if the crack was straight through the specimen. By using a razor blade it is guaranteed that the crack is exactly straight from one face to the other. This phenomena can be clearly seen again in a fracture load vs. (a/W) from material A in Graph 2.

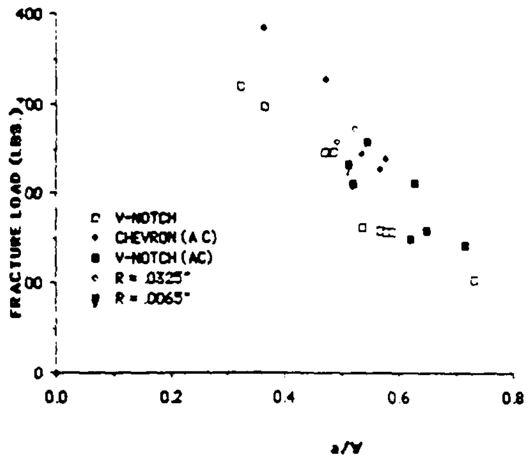

GRAPH 2.

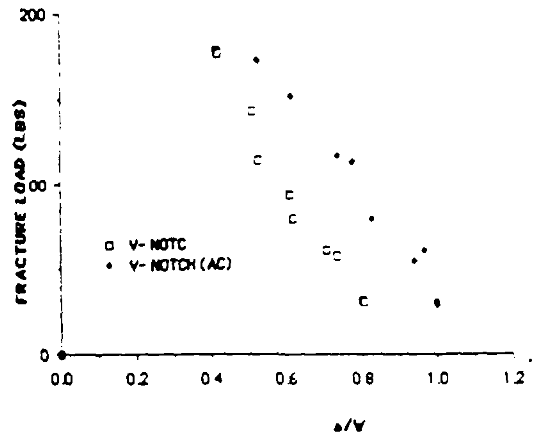

GRAPH 3.

VII. FRACTURE CURVE: Fracture curves generated from the specimens have a considerable amount of data. From Graph 4., it is

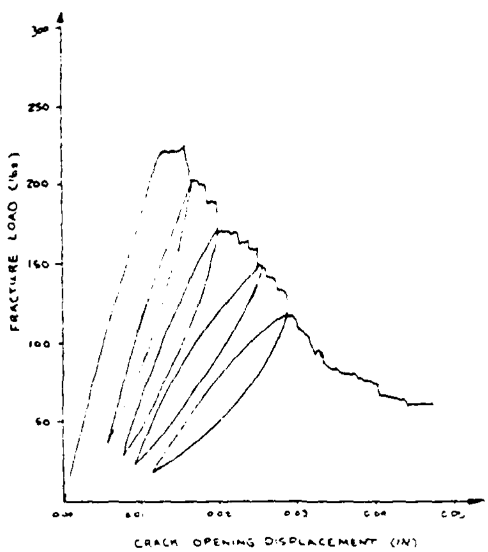

GRAPH 4.

apparent that they are relatively complex curves. It is obvious that the graph is nearly linear all the way up to the initial fracture load. This linear relationship implies there is no plasticity in this material. Also because of this linear relationship even in the fill direction, the J integral test is not necessary. A characteristic which is being investigated further is the hysteresis loops, which appeared when one particular specimen was loaded and unloaded before initial fracture. From the fracture curves the hysteresis loops were very obvious during the loading and unloading part of the experiment. Hysteresis loops are characteristically in graphite materials, which explains their presence in carbon-carbon material. A final observations in some of the fracture curves was the stepping effect present on the back side of the curves. Referring to Graph 4 this can be seen between hysteresis loops. The stepping effect might be caused by actual fiber bundles breaking. The problem with observing this in 2-D carbon-carbon is that the plies are not stacked perfectly on top of one another, and therefore plies are not broken simutaneously. A 3-D carbon-carbon experiment is going to be conducted to study the stepping effect. The 3-D carbon-carbon specimens are used because of the fibers in the third direction. Therefore these specimens are guaranteed to have the plies perfectly aligned, which will ensure simutaneous bundle breakage. From the fracture curves the following in-plane fracture toughnesses were generated for the fill direction. These values came from equation 1.

EQUATION 1 $$K_{IC} = \frac{\text{LOAD}}{BW^{1/2}} \cdot f\left(\frac{a}{W}\right)$$

WHERE $$f\left(\frac{a}{W}\right) = \frac{\left(2+\frac{a}{W}\right)\left[0.886+4.64\left(\frac{a}{W}\right)-13.32\left(\frac{a}{W}\right)^2+14.72\left(\frac{a}{W}\right)^3-5.6\left(\frac{a}{W}\right)^4\right]}{\left[1-\left(\frac{a}{W}\right)\right]^{3/2}}$$

For meterial C, Kic = 6374 lbs in**1/2 , while meterial A has a Kic = 4108 lbs in**1/2.

VIII. CRACK PROPAGATION: While reading the crack tips, there

was some question as to where the crack tip actually was located. With some specimens there was a clearly defined crack tip. While some specimens had crack tips which ran along the fiber bundles. High intensity lights were mounted to aid in the observations of the cracks. Another reason for the difficulty in reading the crack tips was the fact that the specimens were black, and the crack also appears black. Brittle coating or a white coating was not used because this coating would cover up the bundles which aided in tracking the crack tip.

Specimens were polished for observation under the microscope. From the specimens it was found that the cracks propagated both around bundles and actually through the bundles. It was noted that under the microscope there were very small and short cracks which periodically branched off from the main crack. This implies there might be a small radius of damage aroung the crack tips.

Stiffness vs. (a/W) graphs were generated for both materials C and A, using the razor blade notched specimens. These graphs can be used to check and confirm the cathetometer readings of (a). Stiffness is defined as the slope of the initial section of the fracture curve. Graph 5 shows the stiffness vs. (a/W) for material C. Graph 6 shows the stiffness vs. (a/W) for material A. The determination of the accuracy of the cathetometer readings can be accomplished as follows. From the fracture curve it is necessary to calculate the stiffness from the lower linear region of the hysteresis loop. From this stiffness, go to the stiffness vs. (a/W) curve, and read off an (a/W) value. From this (a/W) value a crack length (a) can be backed out, knowing the value for W. This calculated (a) can be compared with the (a) from the cathetometer readings. The error for both plates was around 4%, which is acceptable.

IX TENSION AND COMPRESSION RESULTS The tensile properties for the material might be slightly off, due to the location of the fracture in some of the specimens. The fracture occured close to one end of the tabs rather than in the exact center for some of the

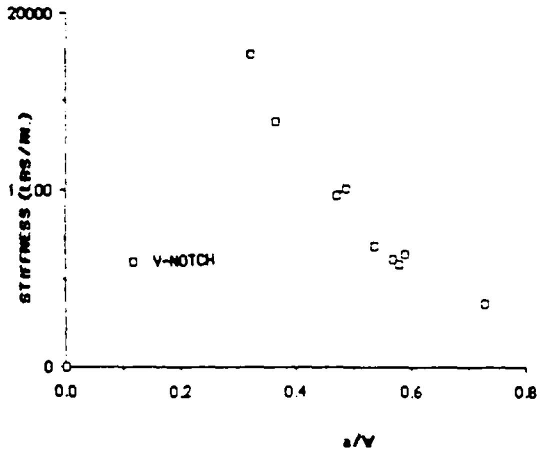

GRAPH 5.

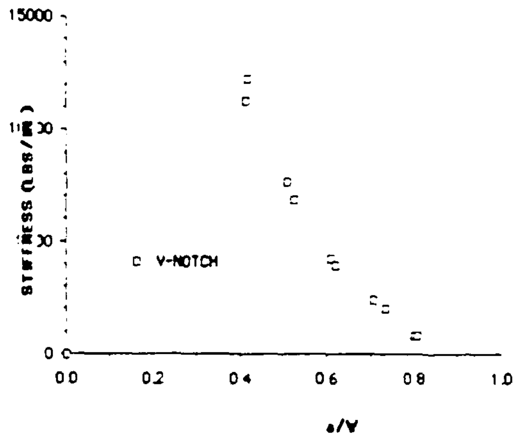

GRAPH 6.

specimens. The following properties were obtained from material C: Warp direction = 12750 psi., Fill direction = 10000 ps..(high). Material A was found to have these properties: Warp direction = 8950 psi., Fill direction = 5900 psi.

The compression test produced properties similar to those of the tensile tests. The angle of fracture on the specimens from each material were individually very consistent. The angles between the two materials were slightly different. Material A had an angle of about 40 degrees from the loading axis, while material C had an angle of about 25 degrees. The following compressive properties were obtained from material C: Warp direction = 14500 psi., Fill direction = 12200 psi. Material A was found to have these properties: Warp direction = 9500 psi., Fill direction = 7500 psi.

X. RECOMMENDATIONS:

A) There is a considerable amount of information which could be obtained from microscopy studies. This information includes observations on crack propagation and how it propagates through the bundles. It might help explain why the Chevron notch specimens didn't propagate straight through. It might also explain why the crack initiated at different locations in the radii of curvature experiments.

B) Experiments should be conducted on the two materials to determine fiber volume fractions.

C) The hysteresis loops observed in the fracture curves could be studied in greater detail. There is a considerable amount of information on hysteresis loops in graphite, which could be studied. This information could or could not apply to carbon-carbon materials.

D) A detailed series of experiments should be conducted on 3-D carbon-carbon to see if fiber bundles can be observed breaking by the stepping effect on the fracture curves. This could be accomplished very effectively with the compact tension experiment with a video recorder, to monitor the crack as it propagates.

E) The study of in-plane fracture of carbon-carbon limits one to only a few experiments. One which is successful is the compact tension experiment. Other fracture experiments will also work but there are some problems with them. Again low compressive strength is a limitation to the types of fracture experiments which can be conducted. Therefore more standardized experiments should be designed for composite materials.

XI ACKNOWLEDGEMENTS: I wish to thank the Air Force Astronautics Laboratory and the Air Force Office of Scientific Research for sponsorship of this research. Universal Energy Systems must also be mentioned in there honest concern to ensure that all adminastrative tasks ran smoothly.

This summer was a truly rewarding summer for myself. The components lab personnel provided an excellent working atmosphere which gave me considerable enthusiasm while I worked on my project. I would like to mention my patient supervisor Dr. Peter Pollock who was invaluable to me while I was at the Astronautics Lab. I would also like to mention Ernie Butler the machinest who was a considerable help to my project, as was Stan Shetos the mechanic and Bruce Hinds a fellow researcher.

VII. REFERENCES:

1) Ewalds,H.L., Wanhill,R.J.H., Fracture Mechanics, Bedford Square, London, 1986 ,p 75-116

2) Plane-Strain Fracture Toughness of Metallic Materials, Annual Book of ASTM Standards, Easton, M.D., 7-P Publications, 1985 p 547-582.

1988 USAF-UES SUMMER FACULTY RESEARCH PROGRAM

GRADUATE STUDENT RESEARCH PROGRAM

Sponsored by the

AIR FORCE OFFICE OF SCIENTIFIC RESEARCH

Conducted by

Universal Energy Systems, Inc.

FINAL REPORT

Experimental Verification of Identification Spillover for Distributed Structures

Prepared by:	Steven P. Kahn
Academic Rank:	Graduate Student
Department:	Engineering Science and Mechanics
University:	Virginia Tech
Research Location:	USAF AFAL/VSSS Edwards AFB Edwards, CA 93523
USAF Researcher:	Dr. Alok Das

Date:	5 August 1988
Contract No:	F49620-88-C-0053

Experimental Verification of Identification Spillover for Distributed Structures

by

Steven P. Kahn

ABSTRACT

Identification spillover is verified with the "Grid Experiment" using a modal identification technique [1]. The effects of spillover on the identified eigenvalues, eigenvectors, and natural frequencies are examined, and it is shown that the inclusion principle holds. Comparisons are made with the actual system parameters of interest and those obtained from the Ibrahim Time Domain method.

Acknowledgements

I would like to extend a sincere thank you to my graduate faculty advisor Dr. Mark Norris for his guidance, support, and patience throughout the research period. His knowledge and understanding in the field has enriched the educational value of the past ten weeks. Additionally, I would like to thank Dr. Alok Das for all of his support in the use of the facilities. Finally, I wish to thank Dr. Roger Thompson, Waid Schlaegel, Joel Berg, and Lance Carter for all the help they have provided.

I. Introduction

The identification of parameters in distributed structures is currently of great interest. In reality, these structures have an infinite number of degrees of freedom, while experimentally they must be modeled as finite systems, or lumped-systems. Therefore, certain modes of vibration can participate in the system response that are not included in the lumped-system. The effect of these extraneous modes on the identified parameters is called identification spillover.

The identification technique involved uses the temporal and spatial orthogonality properties of distributed-parameter systems to form a pseudo-Rayleigh quotient. Since the inclusion principle holds for this method [2], it can be used to predict a satisfactory model. In other words, the order of the model is increased until convergence is obtained. The experimental setup for the "Grid" is shown in Figure 1.

II. Objectives

My main objective for the summer research period was to experimentally verify the existance of identification spillover. Additionally, however, there were some minor goals that included: (1) compared the modal identification technique and the Ibrahim Time Domain method in terms of identification spillover, (2) study the effects of spillover on eigenvalues and eigenvectors, (3) test the modal identification method with different pseudo-Rayleigh quotients, and (4) study the effects of noise and damping on the identified eigenvalues.

III. Equations of Motion

The governing equation for undamped distributed structures is given as [3]

$$\mathcal{L}u(P,t) + m(P)\ddot{u}(P,t) = f(P,t), \quad P \in D \tag{1}$$

where u is the displacement at the spatial position P at time t, m is the mass density, f is the external force density, $\mathcal{L}$ is a self-adjoint positive semi-definite differential operator of order 2p, and D is the domain of the system. The boundary conditions are expressed as

$$B_i u(P,t) = 0, \quad i=1,2,\ldots,p \quad P \in S \tag{2}$$

where B_i are differential operators of maximum order 2p-1 and S is the boundary of D. Functions satisfying the geometric boundary conditions, those in which the order of B_i is no greater than p, are called admissible functions [3].

IV. Modal Equations of Motion

For the case of free vibration, the eigenvalue problem associated with Eq.(1) is

$$\mathcal{L}\phi(P) = \lambda m(P)\phi(P) \tag{3}$$

where $\phi(P)$ are functions that satisfy the boundary conditions. The orthonormality conditions that are satisfied by the eigenfunctions of Eq.(3) are

$$\int_D m(P)\,\phi_r(P)\,\phi_s(P)\,dD = \delta_{rs} \tag{4}$$

and,

$$\int_D \phi_r(P)\,\mathcal{L}\phi_s(P)\,dD = \lambda_r\,\delta_{rs} \tag{5}$$

The displacement can be expressed as a linear combination of the eigenfunctions and the modal coordinates.

$$u(P,t) = \sum_{r=1}^{\infty} \phi_r(P)u_r(t) \tag{6}$$

Substituting Eq.(6) into (1) and considering (4) and (5), we obtain the modal equations.

$$\ddot{u}_r(t) + w_r^2 u_r(t) = f_r(t) \tag{7}$$

where $u_r(t)$ are the modal coordinates, w_r are the natural frequencies, and $f_r(t)$ are the modal forces.

V. Variational Characterization of the Eigenvalues

From Rayleigh's principle, it is known that the stationary values of Rayleigh's quotient are identical to the eigenvalues, w_r^2. In continuous form Rayleigh's quotient is given as

$$R(\quad(P)) = \frac{[\phi(P), \phi(P)]}{\int_D m(P)\,\phi(P)^2 dD} \tag{8}$$

where [,] represents an energy inner product associated with twice the potential energy of the system [4] and ϕ (P) need only be admissible. The stationary values occur every time ϕ (P) is identical to an eigenfunction.

VI. Temporal Filtering

The temporal inner product of two time-dependent functions a(t) and b(t) is defined as

$$< a(t), b(t) > = \lim_{T\to\infty} \frac{1}{T} \int_0^T a(t)b(t)\,dt \tag{9}$$

With $f_r(t)=0$ in Eqs.(7), the modal coordinates, $u_r(t)$, are independent so that distinct modes of vibration are mutually orthogonal. Hence, it can be shown that

$$< u_r(t), u_s(t) > = O_r \delta_{rs} \quad (10)$$

$$< \dot{u}_r(t), \dot{u}_s(t) > = w_r^2 O_r \delta_{rs} \quad (11)$$

and,

$$< \ddot{u}_r(t), \ddot{u}_s(t) > = w_r^4 O_r \delta_{rs} \quad (12)$$

VII. Spatial Filtering

Spatial filters are similar to temporal filters, except that in this case the spatial dependence is removed. We have

$$q(t) = \int_D \Psi(P) u(P,t) dD \quad (13)$$

where q(t) is a generalized coordinate. A more specific type of spatial filter relative to this study is the modal filter. From Eq.(6) and the orthogonality conditions (5), we have

$$u_r(t) = \int_D m(P) \phi_r(P) u(P,t) dD \quad (14)$$

where $u_r(t)$ are the modal coordinates. Note that if the test function, $\Psi(P)$, in Eq.(13) is represented by a linear combination of the mass density times the eigenvectors,

$$\Psi(P) = \sum_{r=1}^{\infty} v_r m(P) \phi_r(P) \ , \quad (15)$$

then the generalized coordinates can be written as a linear combination of the modal coordinates with the same coefficients.

$$q(t) = \sum_{r=1}^{\infty} v_r u_r(t) \tag{16}$$

VIII. Modal Identification

The object of modal identification is to obtain the natural frequencies and mode shapes of a structure from its free response. It is to this end that the temporal and spatial filters can be used. We define a pseudo-Rayleigh quotient based on generalized coordinates.

$$R(\Psi(P)) = \frac{< \ddot{q}(t), \ddot{q}(t) >}{< \dot{q}(t), \dot{q}(t) >} \tag{17}$$

Now using the result from the spatial filter, Eq.(16), we obtain

$$R(\Psi(P)) = \frac{\sum_{r=1}^{\infty} \sum_{s=1}^{\infty} v_r v_s < \ddot{u}_r(t), \ddot{u}_s(t) >}{\sum_{r=1}^{\infty} \sum_{s=1}^{\infty} v_r v_s < \dot{u}_r(t), \dot{u}_s(t) >} \tag{18}$$

Next we use the temporal filters given by (11) and (12) to get

$$R(v_i) = \frac{\sum_{r=1}^{\infty} v_r{}^2 c_r{}^2 w_r{}^4}{\sum_{s=1}^{\infty} v_r{}^2 c_r{}^2 w_r{}^2} \tag{19}$$

Hence, the temporal and spatial filters provides identically the Rayleigh quotient [1].

As mentioned before, distributed structures must be modeled experimentally as finite-order or lumped-systems. We choose the test functions in Eq.(13) to be approximated by

$$\Psi_r(P) = \sum_{r=1}^{n} v_r \, \delta(P-P_r) \tag{20}$$

Substitution of Eq.(20) into (13) and the result into (17) gives us the form of the pseudo-Rayleigh quotient desired

$$R(v_i) = \frac{\sum_{r=1}^{n}\sum_{s=1}^{n} v_r v_s \, k_{rs}}{\sum_{r=1}^{n}\sum_{s=1}^{n} v_r v_s \, m_{rs}} \tag{21}$$

where

$$k_{rs} = < \ddot{u}(P_r,t),\ddot{u}(P_s,t) > \tag{22}$$

and,

$$m_{rs} = < \dot{u}(P_r,t),\dot{u}(P_s,t) > \tag{23}$$

The problem of finding the stationary values of the pseudo-Rayleigh quotient given by (21-23) is equivalent to solving the eigenvalue problem

$$\lambda M \underset{\sim}{v} = K \underset{\sim}{v} \tag{24}$$

where M and K consist of the elements k_{rs} and m_{rs} respectively. Therefore, we need only formulate these matrices based on the free response data and solve Eq.(24) to obtain the eigenvalues. From this, it follows that the eigenvectors v_i are equal to the eigenvectors of the structure within a multiplicative constant.

IX. The Inclusion Principle and Identification Spillover

Consider the n^{th}-order approximation of the structure represented by the matrices $K^{(n)}$ and $M^{(n)}$ and the $(n+1)^{th}$-order approximation of the structure represented by $K^{(n+1)}$ and $M^{(n+1)}$. Note that for the higher-order approximation we need only calculate an additional row and column of the stiffness and mass matrices. The n^{th}-order approximation will yield n eigenvalues, while the $(n+1)^{th}$-order approximation will yield (n+1) eigenvalues. From the inclusion principle [4], we have

$$\lambda_1{}^{(n+1)} \leq \lambda_1{}^{(n)} \leq \lambda_2{}^{(n+1)} \leq \lambda_2{}^{(n)} \leq \ldots \leq \lambda_n{}^{(n)} < \lambda_{n+1}^{(n+1)} \qquad (25)$$

As the order of the approximation is increased, the estimated eigenvalues decrease monotonically and approach the actual eigenvalues of the system asymptotically from above. This implies that the effects of identification spillover on the eigenvalues should decrease with better approximations. The next section will discuss some results obtained from the "Grid Experiment" and experimentally verify the inclusion principle and identification spillover.

X. Results

Free response acceleration data obtained from piezoelectric accelerometers (Endevco Model 7751-500) was used for the identification purpose. Six accelerometers were placed on the grid structure. These acceleration profiles were then integrated once with respect to time to obtain the velocity profiles. The mass and stiffness matrices were then constructed according to Eq.(22) and Eq.(23). Finally, the eigenvalue problem given by (24) was solved to obtain the eigenvalues, eigenvectors, and natural frequencies. Once the mass and stiffness matrices had been constructed, identification spillover was examined by simply deleting a row and column from both matrices and resolving the new eigenvalue problem. The values of the first n identified natural frequencies are displayed in Table 1. The actual natural frequencies according to a NASTRAN model are also shown.

Table 1

Number of Identified Modes :	3	4	5	6	Actual
				6.44	5.22
			6.48		
		6.61		15.22	12.57
	7.99		16.24		
		16.55		27.48	28.84
	25.64		28.36		
		30.72		44.99	35.24
	40.06		45.14		
		48.44		53.64	44.48
			57.03		
				77.64	74.90

IDENTIFIED NATURAL FREQUENCIES
FOR THE MODAL IDENTIFICATION METHOD.

It is clear from Table 1 that the inclusion principle does hold experimentally. Also, we see that the identified natural frequencies converge to the actual natural frequencies as n approaches infinity. It is also worthwhile to note that convergence occurs sooner for the lowest modes. These results suggest that identification spillover is an important consideration in determining the accuracy of identified parameters.

Additionally, the first two mode shapes of the "Grid" were identified. These are displayed in Fig.3 and Fig.4 . There was only a moderaterate degree of success in identifying the mode shapes. This is likely due to: (1) only six accelerometers being used, (2) noise in the instrumentation, and/or (3) identification spillover. The exact effect of identification spillover on the eigenvectors was not determined. It is safe to say, however, that the effect is significant.

Finally, identification spillover was examined using the Ibrahim Time Domain method. These results are displyed in Table 2.

Table 2

Number of Identified Modes:	3	4	5	6	Actual
				0.00	5.22
			0.00		
		20.90		21.32	12.57
	13.01		5.41		
		39.43		38.50	28.84
	43.87		37.48		
		50.60		48.90	35.24
	70.48		61.31		
		62.77		56.65	44.48
			78.32		
				73.37	74.90

IDENTIFIED NATURAL FREQUENCIES
FOR THE ITD METHOD.

From these results, we see that the inclusion principle does not hold for the ITD method, the identified natural frequencies do not converge to the actual values, and the effect of identification spillover is not as clear. Therefore, the modal identification technique allows us to determine more easily the accuracy of the model.

XI. Conclusions and Recommendations

This report has given an experimental verifiction of identification spillover. Additionally, it was shown that the inclusion principle holds for the modal identification technique but it does not hold for the Ibrahim Time Domain method. The mode shapes of the "Grid" were identified, but the effects of spillover were not determined.

Future work in this area will concentrate on examining the effects of spillover on the eigenvectors more closely and in forming and testing new ideas associated with the modal identification method.

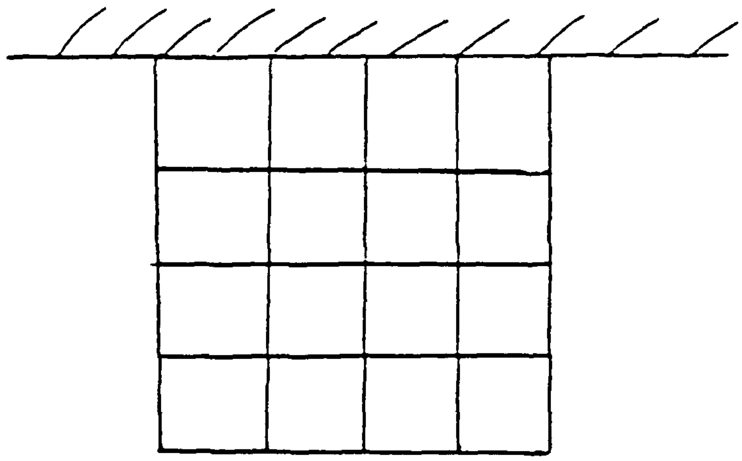

FIGURE 1. AFAL GRID STRUCTURE

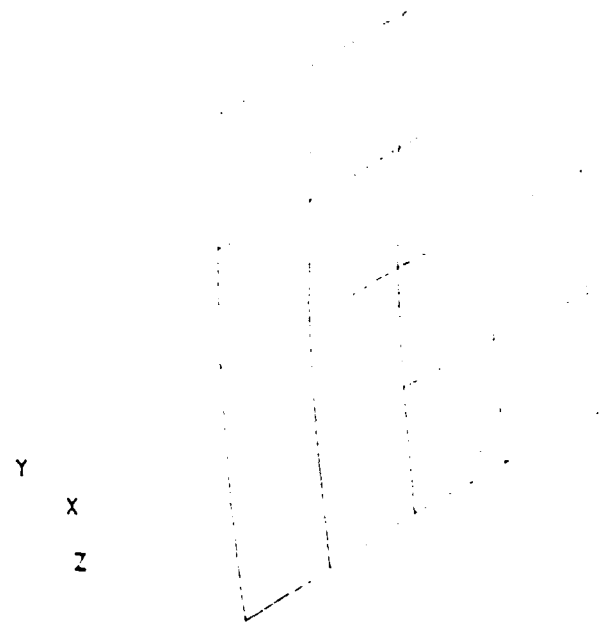

FIGURE 2: IDENTIFIED 1ST MODE SHAPE

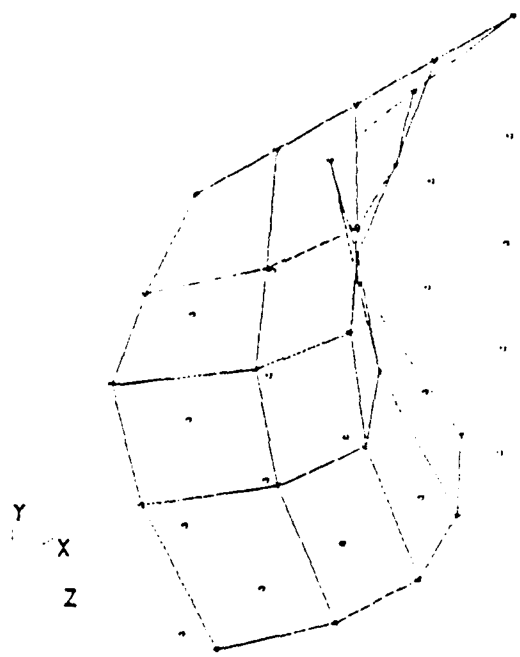

FIGURE 3. IDENTIFIED 2ND MODE SHAPE

XII. Refences

1. Norris, M. and Silverberg, L., ' Modal Identification of Self-Adjoint Distributed-Parameter Systems ', 23rd Annual Technical Meeting for the Society of Engineering Science, August 25-27, 1986; Buffalo, NY.

2. Norris, M. and Meirovitch, L., ' On the Inclusion Principle and Spillover Effect in the Identification of Distributed Structures ', USAF/NASA Workshop on Model Determination for Large Space Systems ', March 22-24, 1988; Pasadena, CA.

3. L. Meirovitch, **Analytical Methods in Vibrations**, The MacMillan Company, New York, NY, 1967

4. L. Meirovitch, **Computational Methods in Structural Dynamics**, Sijthoff & Noordhoff, The Netherlands, 1980..

1988 USAF-UES SUMMER FACULTY RESEARCH PROGRAM/

GRADUATE STUDENT RESEARCH PROGRAM

Sponsored by the

AIR FORCE OFFICE OF SCIENTIFIC RESEARCH

Conducted by the

Universal Energy Systems, Inc.

FINAL REPORT

THE EFFECTS OF ELEVATED TEMPERATURE EXPOSURE ON THE STRENGTH AND MICROSTRUCTURE OF 2-D CARBON-CARBON

Prepared by:	Christopher G. Kocher
Academic Rank:	Graduate Student
Department and	Civil Engineering and Mechanics
University:	Southern Illinois University at Carbondale
Research Location:	AFAL/VSSC
	Edwards AFB, CA 93523
USAF Researcher:	Dr. Peter B. Pollock
Date:	September 21, 1988
Contract No:	F49620-88-0053

THE EFFECTS OF ELEVATED TEMPERATURE EXPOSURE

ON THE STRENGTH AND MICROSTRUCTURE

OF 2-D CARBON-CARBON

by

Christopher G. Kocher

ABSTRACT

2-D carbon-carbon material fabricated from T-300 fibers and a CVD matrix as exposed to a heat treatment temperature of 2350C. Tension and Iosipescu shear tests were performed on both heat treated and as-received material to investigate the effects of the elevated temperature exposure on the mechanical properties of the composite. It was found that the material subjected to the elevated temperature experienced a roughly 25 percent decrease in tensile strength in both the warp and fill directions, and the fill shear strength decreased by approximately 50 percent. Optical microscopy revealed that the heat treatment significantly increased the number of microcracks within the fiber bundles.

Acknowledgments

I wish to thank the the Air Force Office of Scientific Research for sponsorship of this research.

I would also like to thank the entire staff of the Composites Lab of the Air Force Astronautics Laboratory, and in particular Dr. Peter B. Pollock of the University of Dayton Research Institute, whose helpful guidance and assistance provided me with an excellent atmosphere in which to learn.

I must also extend my sincere appreciation to Universal Energy Systems for providing the outstanding opportunity made available to myself and the other students and faculty around the country to gain experience working in such highly regarded research environments.

I. INTRODUCTION:

2-D carbon-carbon is currently used in high-temperature applications such as rocket nozzles, exit cones, and major components of space structures owing to the material's ability to retain its structural integrity at elevated temperatures, low coefficient of thermal expansion, and high strength-to-weight ratio. Very little is understood, however, regarding the effects of high temperature exposure on the mechanical properties of this refractory composite.

The Composite Structures Lab at the USAF Astronautics Laboratory at Edwards Air Force Base is currently involved in a major research thrust to develop and analyze structural carbons for use in rockets and space structures.

My research interests lie in both the mechanical testing and microscopic evaluation of composite materials, particularly carbon-carbons, so as to be able to determine the mechanical response of the material and relate the observed behavior to changes in microstructure. Previous work involved extensive microscopic characterization of carbon-carbon composite materials and the mechanical testing of various composite systems.

II. OBJECTIVES OF THE RESEARCH EFFORT:

Several methods are currently available for the manufacture of carbon-carbon composites. Among them is the impregnation of dry fibers with a matrix deposited by chemical vapor infiltration (CVI), a process which involves the deposition of a carbon matrix in the fiber bundles through the decomposition of a carbon-containing gas, such as methane, in a furnace. CVI-matrix carbon-carbon is currently being evaluated as a candidate material for components of advanced high-temperature turbine engines.

The efficiency of an engine increases as the operating temperature increases, so the requirement exists to formulate structural materials which are capable of sustained operation at temperatures far above those at which conventional aerospace materials (titanium, stainless steel,etc.) would deteriorate.

Before a new material can be applied to an area of technology, its mechanical behavior under a wide variety of conditions must be determined. As CVI-matrix carbon-carbon is a relatively new material, its mechanical properties are not well known, particularly after the material has been exposed to some elevated temperature similar to its anticipated operating environment.

As a participant in the 1988 Graduate Summer Research Program (GSRP), my assignment was two-fold. First, I was to expose CVI-matrix carbon-carbon to a temperature near 2400C then test the material along with material

that had not been heat treated to determine the effects of the elevated temperature exposure on the strength of the material. Second, both heat-treated and as-received samples of material were to be prepared for optical microscopy to determine the effects of the heat treatment on the microstructure of the material.

As a result of the mismatch of thermal coefficients of expansion between the warp and fill fiber bundles, microcracks are developed in the material during manufacture. It was believed that additional heating would serve to cause the initiation and propagation of additional cracks within the fiber bundles. These microcracks have been shown to contribute to a decrease in composite strength.

III.

a. Three CVI-matrix carbon-carbon plates 10" by 12" by 0.33" each were fabricated by HITCO. The plates consisted of 32 layers of T-300 3K PAN bi-directional cloth in a 8-harness satin weave. All layers were stacked at zero degrees, i.e. the warp bundles were laid parallel to the long axis of the plate. Prior to infiltration, the dry plies were heat treated to approximately 2400C. The stacked plies were then sandwiched between perforated graphite plates and infiltrated with a graphitic carbon matrix via the chemical decomposition of methane in a chemical vapor deposition (CVD) furnace for 125 hours. The plates were then removed and the top and bottom surface of the plates were machined off as to open any porosity that may have been sealed off during the

infiltration process. The infiltration /machining process was performed a total of 5 times with the machining being omitted after the fiftn infiltration. Successive infiltrations were used to maximize the density of the material.

b. In order to examine the effects of the heat treatment on material behavior, a plan was outlined in which specimens from each plate would be subjected to room temperature, 1500C, 2000C, and 2400C. These specimens would then be tested at room temperature to examine the material properties as a function of heat-treatment temperature. The Tsai-Hill failure criterion would be used to create for each temperature a curve of composite uniaxial strength versus fiber angle. Tests were performed on 0°, 30°, and 90° tensile specimens and 0° shear specimens to determine the shear strength of the warp fiber bundles. The Iosipescu shear test was used for the shear specimens.

Due to circumstances beyond my control, only the room temperature and 2400C specimens could be tested during my stay at the Composites Lab at AFAL.

The standard dog bone configuration was used for the tensile specimens. Owing to the limited amount of material available for the many tests needed, the tensile specimens were all sliced in the plane of the laminate to within 0.0005" along the entire length of each specimen so as to produce twice as many specimens, each with the same length and width but half the original thickness. The gauge section was approximately 0.75" wide and .125" thick. Aluminum end tabs were bonded

to the ends of each specimen; the ends were not pinned. To reduce the possibility of any bending moment being introduced into the tensile tests, a large clevis was inserted between the upper grip and the crosshead. This arrangement permitted the necessary freedom from constraint. Also, great care was taken to assure that the specimens were aligned properly in the grips. To effect a quasi-static loading situation, a loading rate of 0.001 in. per minute was used.

A special test fixture was required to perform the Iosipescu shear tests. Again, great care was taken to assure proper specimen alignment in the fixture.

An MTS tension-torsion machine under displacement-controlled loading was used for all tests. Extensional data was taken using clip-on extensometers whose amplified output was recorded by a computer data acquisition system. Load output was simultaneously fed into the computer which translated the inputs into stress and strain and stored the data on floppy disks.

b. Heat treating of the material was done in an Astrofurnace manufactured by Astro Industries under an inert gas atmosphere of helium preventing any possible oxidation of the material during heating. Prior to heating, the specimen chamber was evacuated to 10^{-5} torr and then purged four times with helium. The helium pressure at room temperature was roughly 10 psi. The material was taken to 2350C within a two-hour period, kept at that temperature for an hour, then cooled to ambient

temperature in 4 hours. It was thought that such a rapid heating rate would greatly increase the number of microcracks so a second run to the same temperature was done with a heating rate of approximately 100 C per hour. The same cooling rate was used.

The objective of heat treating the fibers prior to fabricating the composite was to eliminate the possibility of altering the fiber molecular structure during successive heat treatments. If the fibers had not been heat treated, then any additional heating above the highest temperature seen during the fabrication of the fibers would alter the microstructure of the fibers. As the heat treatment temperature increases, the graphite crystals in the fibers grow in size which increases their modulus but decreases their strength. Thus, with the fiber properties always being constant, any changes in the material from heating can be traced directly to a change in the matrix structure.

c. The stress-strain curves produced from the tensile tests of the warp and fill specimens were comparatively similar in initial moduli. One can conclude, therefore, that the curvatures of the fiber bundles are the same in both the warp and fill directions. This is not generally the case in 2-D woven composites. The relatively low compaction pressure applied to the plates during fabrication permitted the warp and fill bundles to reach similar states rather than the warp bundles being straighter than the fill, the condition that is more commonly observed.

The ultimate tensile strengths in the warp and fill directions were nearly equal. This observation is attributed to the fact that the bundle curvatures in both directions were similar. Thus, the warp and fill specimens exhibited similar stress-strain behavior.

The warp and fill stress-strain response was characterized by in initial linear region after which a sudden "yielding" occurred. This increase in strain is attributed to delamination onset and growth from the edge of the laminate inwards. After a period of high strain rate, the strain rate decreases and the load increases to failure.

In addition to delamination, a second damage mechanism exists: the initiation and propagation of microcracks. These cracks may contribute to an increase in strain rate as the transverse bundles are cracked parallel to the fibers (perpendicular to the applied load) thereby allowing significant extension of the transverse bundles. Optical microscopy has revealed that the warp and fill bundles are not well interlocked. The bundles are relatively straight along lengths on the order of several bundle widths. This provides ample mobility of the transverse bundles that are not constrained by interlocking bundles.

The 30^{o} tensile behavior was highly nonlinear to failure. This is accounted for by the freedom of adjacent layers to scissor owing to the fact that the bundles are not well interlocked. The failure mode was shear failure of the fill bundles as expected.

The shear behavior was highly nonlinear as well. Shear failure occurred parallel to the direction of the applied load indicating that shear failure of the warp bundles was the dominant mode of failure (rather than tensile failure of the matrix which would produce a failure crack at 45 ^{o} to the direction of the applied load).

The heat treatment to 2350C reduced the tensile strengths by roughly 25 percent and the shear strength by roughly 50 percent. The strain to failure of the shear specimens was increased significantly as a result of the heat treatment.

d. Optical microscopy of the as-received material showed that processing of the composite introduced a number of regularly-spaced microcracks within the fiber bundles. These cracks are typical of processing defects as they are oriented parallel to the fiber bundles in which they lie and perpendicular to the plane of the laminate.

Exposing the material to the elevated temperature increased the number of cracks, but preliminary investigations do not indicate a change in the crack spacing. The characteristic length needed for load transfer due to the mismatch in the coefficients of thermal expansion in the warp and fill directions remains constant.

IV. RECOMMENDATIONS:

a. A comprehensive experimental plan has been initiated to evaluate the effects of elevated temperature exposure on both the strength and microstructure of 2-D CVI-matrix carbon-carbon. Further heat treatments are needed within the low and high limits specified within this report to more accurately quantify the strengths as a function of heat treatment temperature.

b. Extensive microanalysis utilizing both optical and scanning electron microscopy must be undertaken to characterize the microcracks produced by the processing, additional heat treatment, and mechanical loading of the material. The crack densities under varying conditions must be studied and the characteristic lengths determined to relate these parameters to the thermomechanical loads experienced by the laminate.

c. Microanalysis of the tested specimens must also be performed to characterize the failure modes (delamination, matrix failure, fiber failure) of the composite.

1988 USAF-UES SUMMER FACULTY RESEARCH PROGRAM/

GRADUATE STUDENT RESEARCH PROGRAM

Sponsored by the

AIR FORCE OFFICE OF SCIENTIFIC RESEARCH

Conducted by the

Universal Energy Systems, Inc.

FINAL REPORT

COMPOSITE-EMBEDDED FIBER-OPTIC STRAIN SENSORS

Prepared by: David W. Jensen, Ph.D., Assistant Professor/
Michael J. Koharchik, Graduate Student

Departments: Aerospace Engineering/
Engineering Science and Mechanics

University: The Pennsylvania State University
University Park, PA 16802

Research Location: USAF Astronautics Laboratory
AFAL/VSSC
Edwards AFB, CA 93523-5000

USAF Researcher: Capt. Ted Doederlein

Date: Sept. 21, 1988

Contract No: F49620-88-C-0053

SAME REPORT AS
PROF. DAVID JENSEN
ASTRONAUTICS LABORATORY # 17

1988 USAF-UES SUMMER FACULTY RESEARCH PROGRAM

GRADUATE STUDENT RESEARCH PROGRAM

Sponsored by the

AIR FORCE OFFICE OF SCIENTIFIC RESEARCH

Conducted by

UNIVERSAL ENERGY SYSTEMS, INC.

FINAL REPORT

The Photochemistry of μ_3 - (n-Diethylacetylene)-Decacarbonyltriosmium in Solid Argon

Prepared By:	*Susan Collins and William Moran*
Academic Rank:	Assistant Professor and Master's Degree Candidate
Department and University:	Department of Chemistry California State University, Northridge Northridge, California 91330
Research Location:	Air Force Astronautics Laboratory Astronautical Sciences Division Applied Research in Energy Storage Office High Energy Density Matter Group
USAF Researcher:	Steve Rodgers/Pat Carrick
Date:	17 August 1988
Contract No.	F49620-88-C-0053

SAME REPORT AS
PROF. SUSAN COLLINS
ASTRONAUTICS LABORATORY # 16

1988 USAF-UES SUMMER GRADUATE STUDENT RESEARCH PROGRAM

Sponsored by the

AIR FORCE OFFICE OF SCIENTIFIC RESEARCH

Conducted by the

UNIVERSAL ENERGY SYSTEMS, Inc.

FINAL REPORT

INVESTIGATION OF SORPTION KINETICS

Prepared by:	Mark Brusseau
Academic Rank:	Masters Degree
Department and University:	Soil Sci. Dept., Univ. Florida
Research Location:	AFESC/RDVW Tyndall AFB, Florida
USAF Researcher:	Dr. Thomas Stauffer
Date:	22 August 1988

Contract No.:	F49620-88-C-0053

INVESTIGATION OF SORPTION KINETICS

by

MARK BRUSSEAU

ABSTRACT

The sorption process is very important regarding the transport and fate of organic contaminants in the subsurface. Generally, sorption has been assumed to be at local equilibrium, to be linear, and singular. These assumptions simplify the equations required to model sorption. However, under certain conditions, these assumptions may be invalid. Methods to investigate the kinetics of sorption are needed. A specific experimental and mathematical approach is explored in this work. An inverse correlation was found between the sorption rate coefficient and the sorbent-water partition coefficient for an homologous series of chlorinated benzenes.

ACKNOWLEDGMENTS

I would like to thank the Air Force Systems Command and the Air Force Office of Scientific Research for their sponsorship, and Universal Energy Systems for their administrative assistance. I would especially like to thank all those involved with my stay at Tyndall AFB. Everyone was most helpful in providing assistance. I benefited a great deal from the exciting and diverse research and development program that exists at RDVW.

Several individuals provided assistance and encouragement during my time at Tyndall. Dr. Richard Meyers deserves credit for constructing the experimental apparatus employed herein. Dr. Neil Hutzler provided helpful comments and suggestions; I would also like to thank him for the the valuable discussions we had on many subjects. Finally, I would like to thank Dr. Tom Stauffer for all of his help. My time here has been an invaluable experience, providing an opportunity to interact with the staff of RDVW, and with the permanent and visiting research faculty.

I. INTRODUCTION

The transport and fate of organic contaminants in the subsurface has recently become a subject of great interest.

Of the many processes that can influence transport and fate, sorption is one of the most significant as it controls the rate of transport. Sorption can also have an effect on other processes, such as biodegradation and chemical transformation. Several simplifying assumptions are often employed when modeling sorption. These are: 1. the rate of sorption is rapid such that local equilibrium conditions prevail; 2. sorption is linear; and 3. sorption is reversible. Several recent studies have shown that these assumptions may often be invalid.

In a recent review of sorption nonideality Brusseau and Rao (1989) concluded that sorption nonequilibrium is the major cause of nonideal behavior for hydrophobic organic compounds (HOCs). They identified two mechanisms, physical nonequilibrium (PNE) and intraorganic matter diffusion (IOMD), as the primary sources of nonequilibrium for HOCs. While PNE has been extensively studied, IOMD has only recently come under investigation.

Sorption nonequilibrium can have significant impacts on many aspects of groundwater contamination. The ability to accurately model and predict contaminant transport, as well as the ability to effectively plan and operate groundwater remediation systems, is dependent upon a clear understanding of sorption dynamics. Hence, the the processes responsible for sorption nonequilibrium and the conditions under which nonequilibrium is important require investigation.

II. OBJECTIVES OF THE RESEARCH EFFORT

The primary goal of this effort was to investigate the kinetics of sorption. The specific objects were as follows:

1. To evaluate the utility of the gas-purge desorption technique as a means to investigate sorption kinetics;

2. To evaluate the capability of a mathematical model to simulate the results of the gas-purge experiments.

3. To investigate the sorption kinetics of an homologous series of chlorinated aromatic compounds.

III. EXPERIMENTAL APPROACH

Previous approaches to investigating sorption kinetics usually involved the use of the bottle-point batch technique. This technique suffers from several limitations, including difficulty in providing data for early times and in producing a dense temporal array of data points. Recently, a new technique, called gas-purge desorption, has been developed that eliminates these limitations. The technique was first used by Karickhoff (1980). Since then, it has been used by a few other investigators (Karickhoff and Morris, 1985; and Coates and Elzerman, 1986).

To employ the technique, a reactor containing a pre-equilibrated slurry (sorbent, water, volatile solute) and a headspace is purged with a gas such as air or nitrogen. The gas stream strips the solute from the water phase, thus inducing desorption of sorbate. The effluent gas is analyzed to determine solute concentration. This is usually accomplished with the use of a trap device (e.g., tenax).

As described above, this technique provides data only for the kinetics of desorption. Wu and Gschwend (1986) modified this apparatus to allow determination of adsorption kinetics. The apparatus was constructed as a closed system to maintain a constant level of mass in the reactor. This construction, however, prevents the use of gas-purge Desorption.

The apparatus used for this work was constructed to allow operation in both closed and open modes. In this way, sorption/desorption kinetics could be investigated in the manner of Karickhoff (1980) and Wu and Gschwend (1986). A schematic diagram of the apparatus is given in Figure 1.

IV. MATHEMATICAL MODEL

Currently, a bicontinuum approach is most often used to model sorption kinetics. With this approach, sorption is divided into two components, a rapid (e.g, instantaneous) component and a rate-limited component. Several mathematical models have been developed to represent this conceptualization, including the so-called two-site model of Selim et al., (1976) and the two-region model of van Genuchten and Wierenga (1976). These models have been used to represent PNE and chemical nonequilibrium. The two-site model, when formulated in series, can also be used to represent IOMD (Brusseau and Rao, 1989). For the case of linear sorption, the nondimensional equations for the three models are identical. Hence, all three nonequilibrium mechanisms may be represented with the same model.

The model used in this work is based upon the bicontinuum model of Selim et al. (1976) and van Genuchten and Wierenga (1976).

Mathematical development may be found in these sources. These models were modified for use with the gas-purge desorption apparatus with incorporation of a gas-flux parameter. In model development it was assumed that mass transfer between the water and gas phases was instantaneous. This assumption will be valid as long as the rate of desorption is significantly slower than the rate of water-air mass transfer.

V. MATERIALS AND METHODS

The following chemicals were used: benzene, chlorobenzene, 1,2-dichlorobenzene, 1,2,4-trichlrobenzene, tetrachloroethene, and trichloroethene. The following sorbents were used: Belle Glade muck (organic carbon (OC) = approximately 18 %), Eustis sandy soil (OC = 0.4 %), and Ione aggregated paleosol (OC = 0.06 %).

A flow-through photoionization detector was employed to analyze solute concentration in the gas phase. The detector was housed in a Varian gas chromatograph. The detector was maintained at a temperature of 150 degrees to prevent vapor condensation. The detector output signal was recorded by a Linear chart recorder. The configuration of the experimental apparatus is diagrammed in Figure 1, as previously mentioned.

The typical experimental procedure was as follows: 1. Place measured quantities of sorbent, water, and solute in a 1 L round-bottom glass flask. 2. Place flask on a wrist action shaker for a period of 42 hours to establish equilibrium conditions. 3. Establish zero baseline for detector (the base line was established with humidified air passing through the detector). 4. After equilibration,

attach flask to apparatus and operate in closed mode to establish the equilibrium gas-phase concentration. 5. Operate system in open mode to effect gas-purge desorption.

Calibration curves were obtained for each of the compounds by monitoring the response of the system to known inputs of solute. Examples of the calibration curves are shown in Figures 2, 3, and 4. With these calibrations, the signal output from the detector recorded during the experiment could be converted to gas-phase concentrations. The model requires the data to be in terms of cumulative mass of solute removed from the reactor with time. The mass removed was obtained by trapezoidal integration of the concentration-time data.

The following parameters are required to run the model: partition coefficient, Henry's constant, gas flux, volume of water, volume of air, mass of sorbent, mass of solute, k (sorption rate constant), F (fraction of rapid sorption), and M (fraction of mass removed).

The partition coefficient for each solute-sorbent combination could be determined from knowledge of the equilibrium gas-phase concentration and the mass of soil, mass of solute, volume of water, and volume of air contained in the flask. The Henry's constants were obtained from Ashworth et al. (1988). The gas flux was measured by fluid displacement. The masses and volumes were measured.

M was obtained by dividing the total quantity of mass removed from the reactor by the mass input. Since in all cases the experiments were run until the baseline value (i.e., zero concentration) was reached, M represents the fraction of mass lost during the experiment. Considering the nature of the chemicals and

the short time frames involved, this loss is most likely a result of volatilization loss from the reactor. This loss was less than 10 % in all cases and closer to 2-3 % for most systems. This loss does not affect accurate determination of kinetic parameters since it is accounted for in the model.

With the above approach, all model parameters other than k and F are independently determined. These two kinetic parameters are determined by optimizing the fit of the model simulation to the experimental data.

VI. RESULTS AND DISCUSSION

The data obtained from gas-purge desorption of benzene, chlorobenzene, 1,2-dichlorobenzene, and 1,2,4-trichlorobenzene are given in Figures 5, 6, 7, and 8, respectively. The simulations provided by the model are also included in the figures. The kinetic parameters and the partition coefficient for the four chemicals are listed in Table 1. Data obtained from the literature for 1, 2, 3, 4-tetrachlorobenzene, pentachlorobenzene, and hexachlorobenzene are also included in Table 1. The sorption rate constant (k) was regressed against the partition coefficient (Kp); the results are plotted in Figure 9.

An inverse correlation between k and Kp is very evident. Such a correlation has also been observed by Karickhoff (1980), Karickhoff and Morris (1985), and Brusseau and Rao (1988). For the systems investigated herein, this inverse relationship is suggestive of IOMD-induced nonequilibrium (Brusseau and Rao, 1988). The addition of each successive chlorine atom to the benzene core results in an increase in

molar volume, which results in an increase in Kp. This, in turn, results in a decrease in the effective diffusion coefficient, which results in a lower k.

Experiments were also performed with Ione soil, which occurs in aggregated form. A purge was performed using the aggregates (>4.75mm diameter) and another was performed with the aggregates crushed (<1 mm). However, the data is uncertain as a result of problems encountered with the detector during the time period these particular experiments were performed. It is expected, however, that the effect of the aggregate structure would be to slow the desorption rate to some extent.

VII. RECOMMENDATIONS

The apparatus employed in this research appears to provide a useful technique for investigating the kinetics of sorption. The relationship observed between the sorption rate constant and the partition coefficient for the chlorinated benzenes suggests the possibility of being able to predict kinetic parameters for systems similar to those employed herein. This possibility should be further investigated. The applicability of parameters determined with this technique to other types of systems (e.g., column experiments) should also be investigated.

REFERENCES

Ashworth, R. A.; G. B. Howe; M. E. Mullins; and T. N. Rogers; 1988. Air-Water Partitioning Coefficients of Organics in Dilute Aqueous Solutions. J Hazard. Mat. 18, 25.

Brusseau, M. L. and P. S. C. Rao; 1988. Evidence for diffusional Mass Transfer within Sorbent Organic Matter as a Cause for Sorption Nonequilibrium. Envirn. Sci. Technol. (submitted).

Brusseau, M. L. and P. S. C. Rao; 1989. Sorption Nonideality During Organic Contaminant Transport in Porous Media. CRC Critical Reviews in Environmental Control, In Press.

Coates, J. T. and A. W. Elzerman; 1986. Desorption Kinetics for Selected PCB Congeners from River Sediments. J Contam. Hydrol., 1, 191.

Karickhoff, S. W.; 1980. Sorption Kinetics of Hydrophobic Pollutants in Natural Sediments. in Contaminants and Sediments, Vol. 2, R. A. Baker, ed. Ann Arbor Pub., Ann Arbor, MI.

Karickhoff, S. W. and K. R. Morris; 1985. Sorption Dynamics of Hydrophobic Pollutants in Sediment Suspensions. Environ. Tox. Chem., 4, 469.

Selim, H. H.; J. M. Davidson; and R. S. Mansell; 1976. Evaluation of a Two-Site Adsorption-Desorption Model for Describing Solute Transport in Soils. Proc. Summer Computer Sim. Conf., Wash. D. C.

Van Genuchten, M. Th. and P. J. Wierenga; 1976. Mass Transfer Studies

in Sorbing Porous Media: Analytical Solutions. Soil Sci. Soc. Am. J, 40, 473.

Wu, S. and P. M. Gschwend; 1986. Sorption Kinetics of Hydrophobic Organic Compounds to Natural Sediments and Soils. Environ. Sci. Technol., 20, 720.

AD-A204 243 UNITED STATES AIR FORCE GRADUATE STUDENT RESEARCH PROGRAM PROGRAM TECHNIC..(U) UNIVERSAL ENERGY SYSTEMS INC DAYTON OH R C DARRAH ET AL. DEC 88 4/

UNCLASSIFIED AFOSR-TR-89-0041 F49620-85-C-0013 F/G 5/1 NL

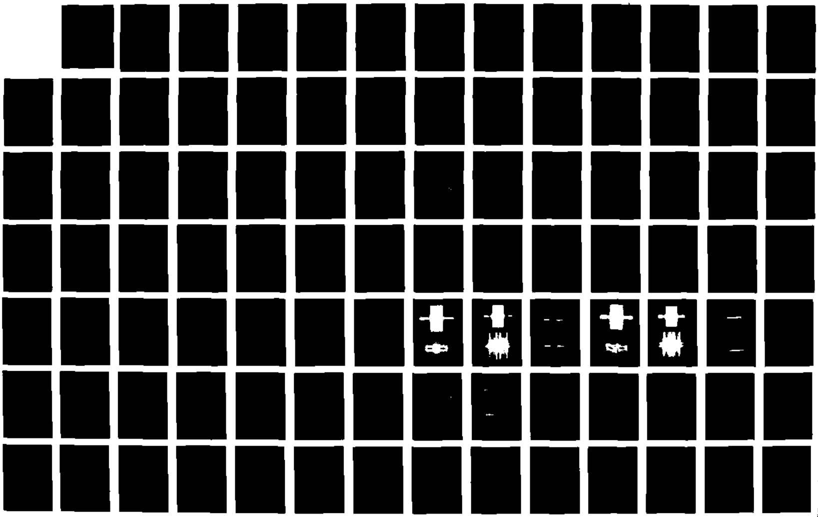

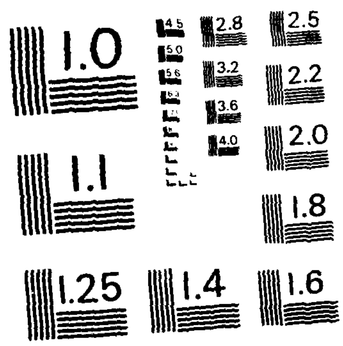

1.0
1.1
1.25
1.4
1.6
1.8
2.0
2.2
2.5
2.8
3.2
3.6
4.0
4.5
5.0
5.6

Figure 1. Experimental Apparatus

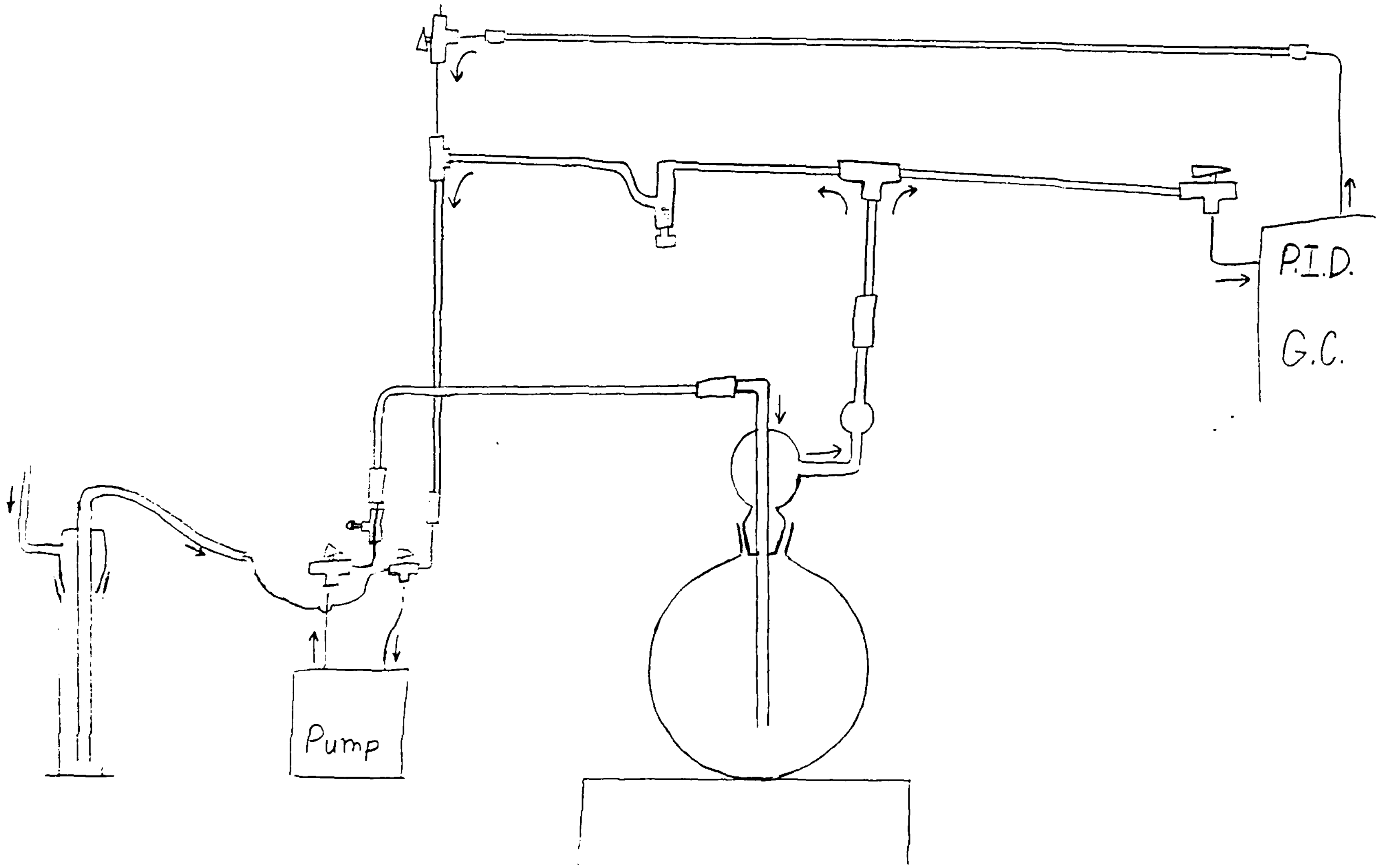

Figure 2.

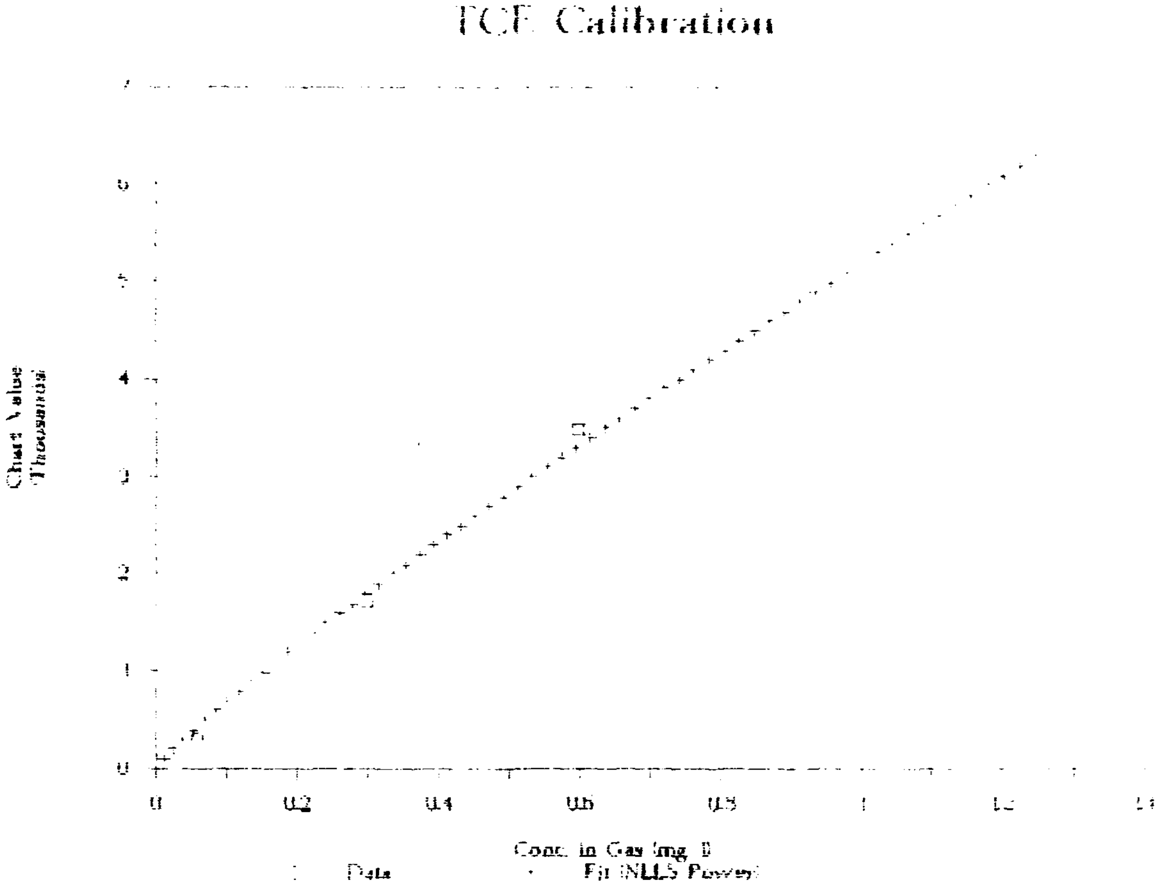

TCE Calibration
Chart Value (Thousands)
Conc. in Gas (mg/l)
Data
Fit (NLLS Power)

Figure 3. Calibration for Benzene

Figure 4. Calibration for Chlorobenzene

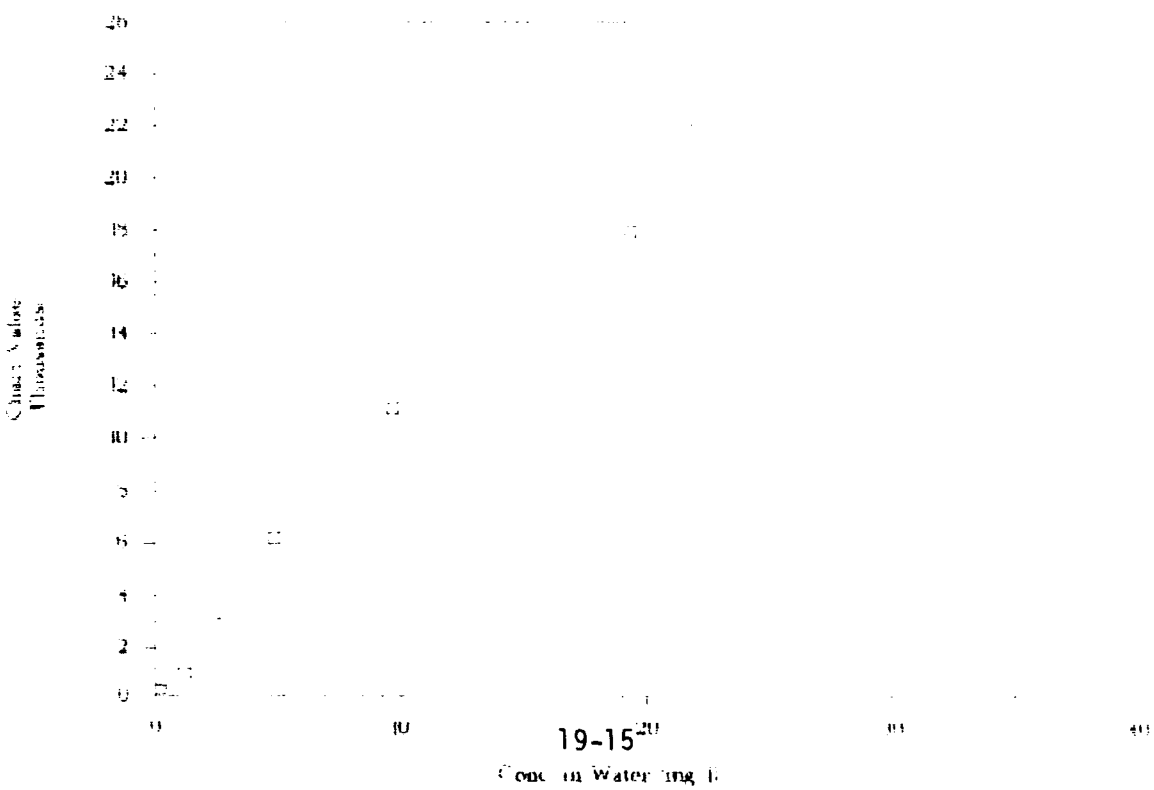

Figure 5.

Trichlorobenzene

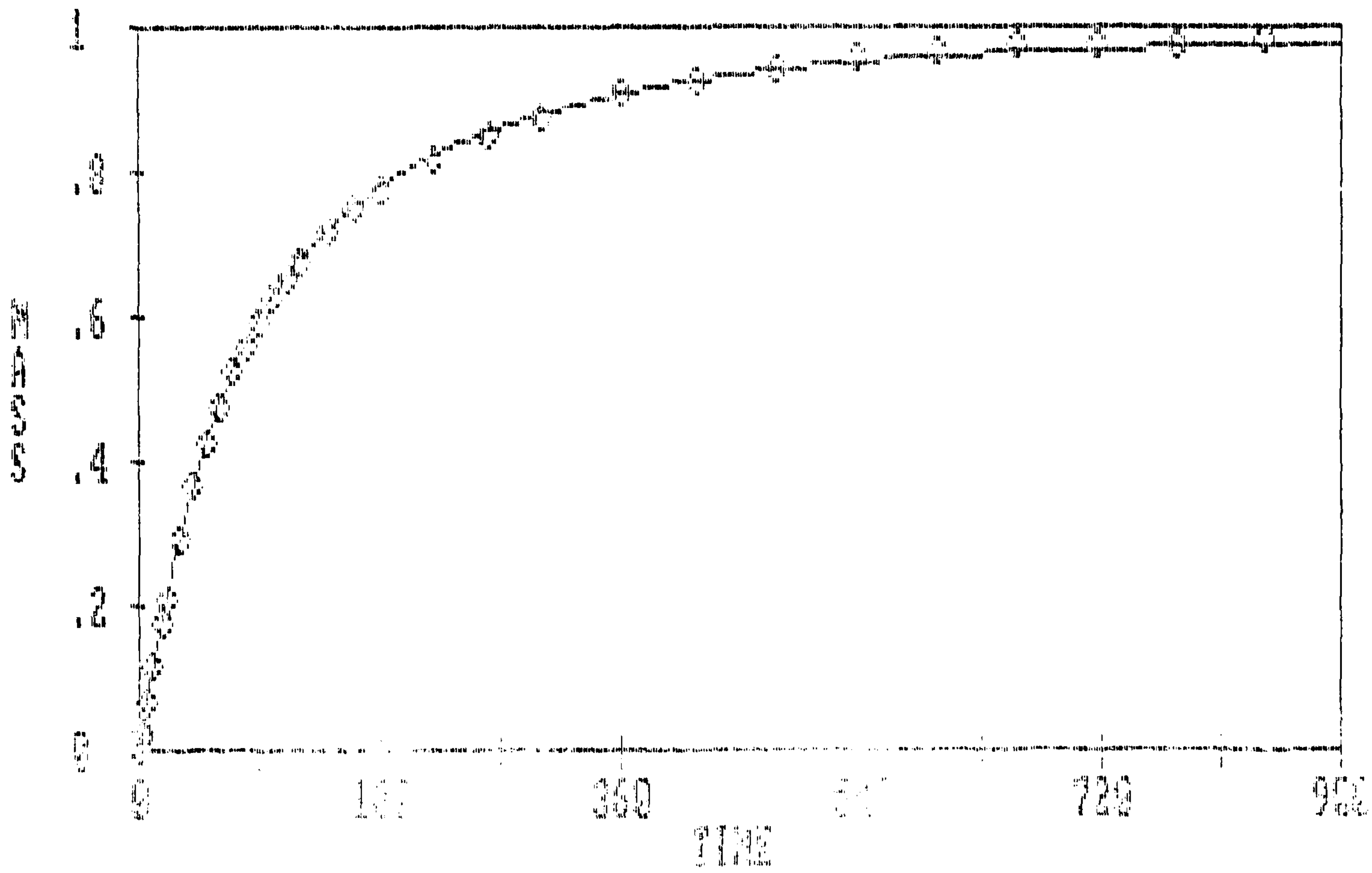

Figure 6.

Dichlorobenzene

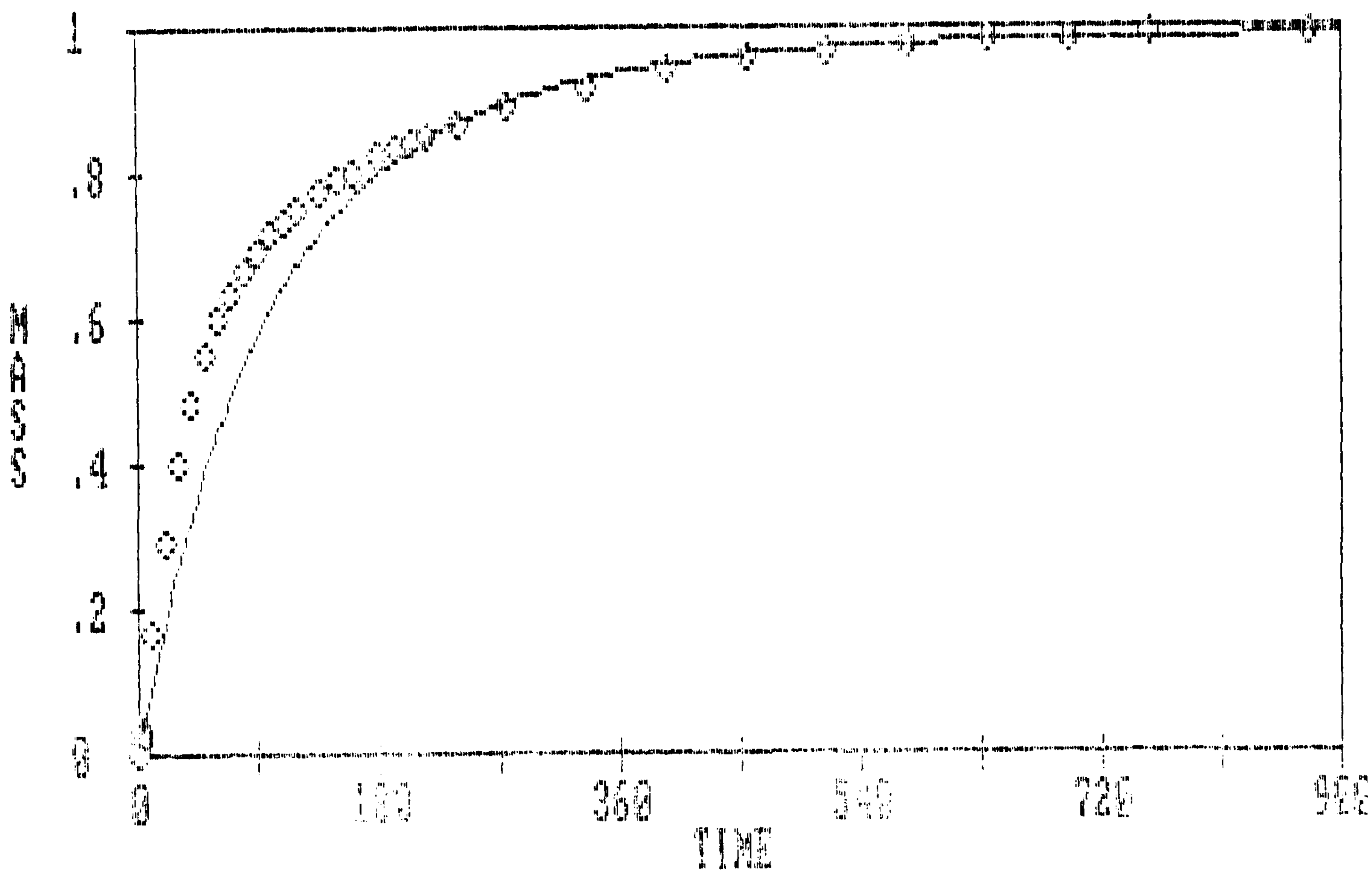

Figure 7.

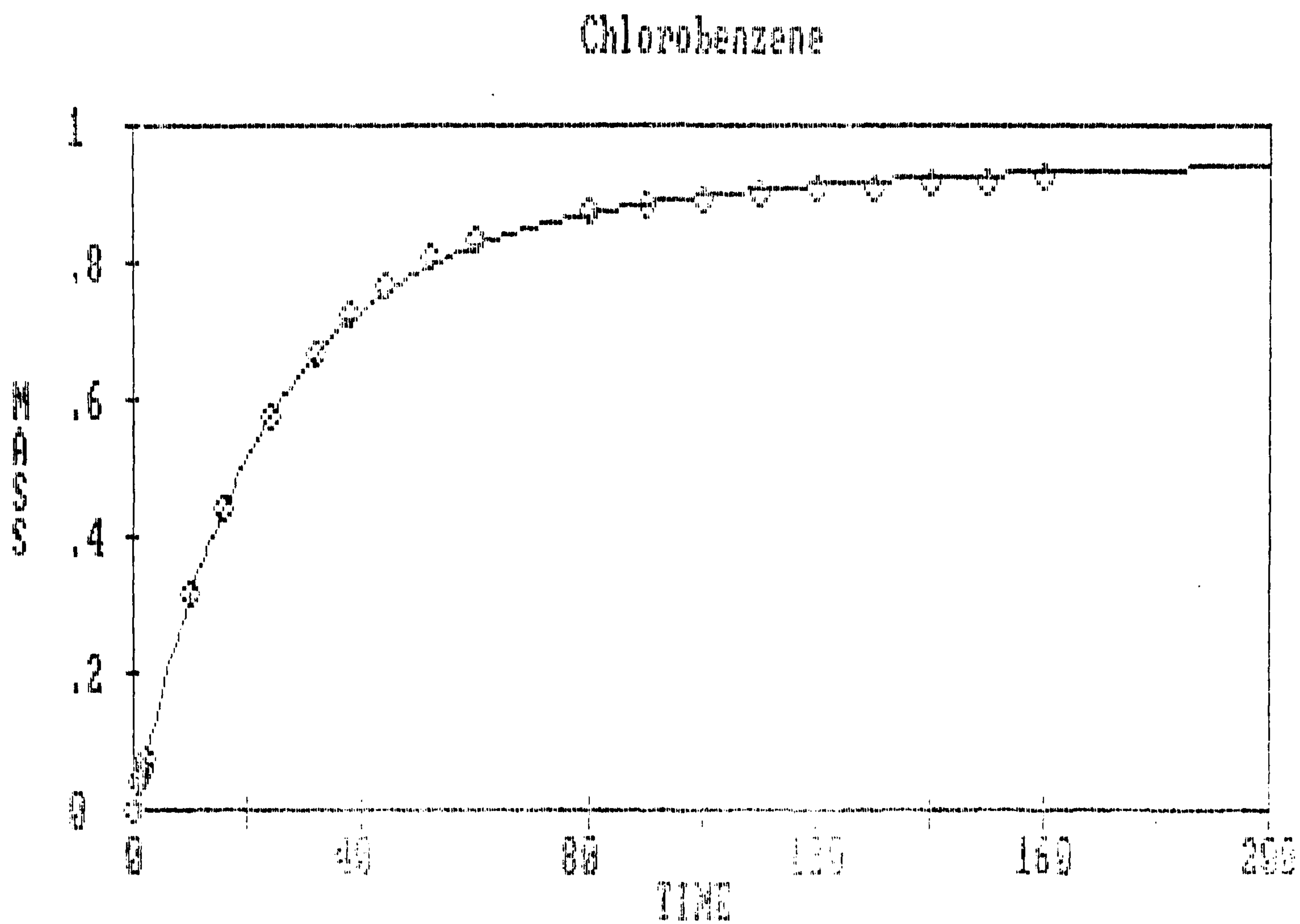

Figure 8.

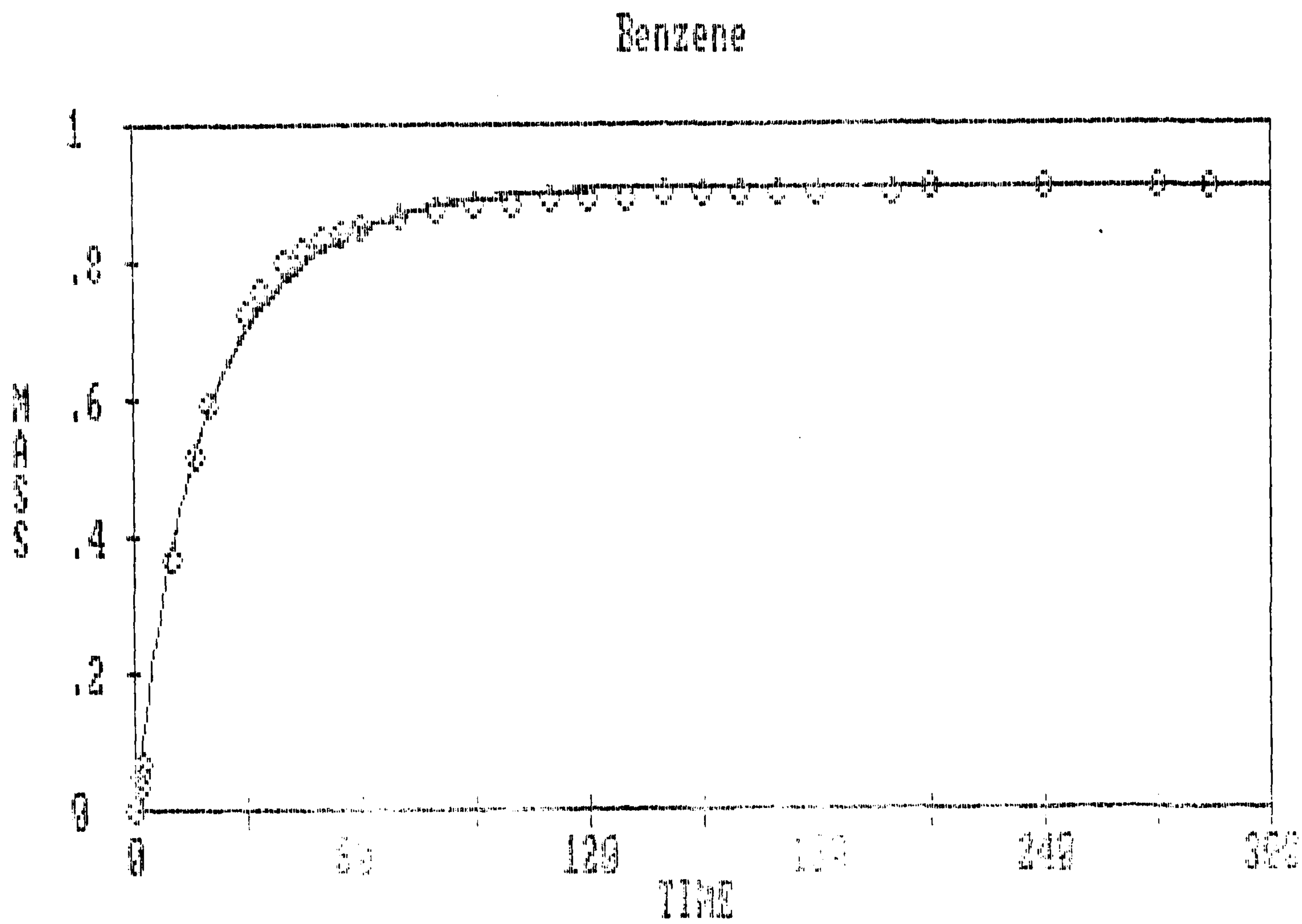

Figure 9. k vs Kp

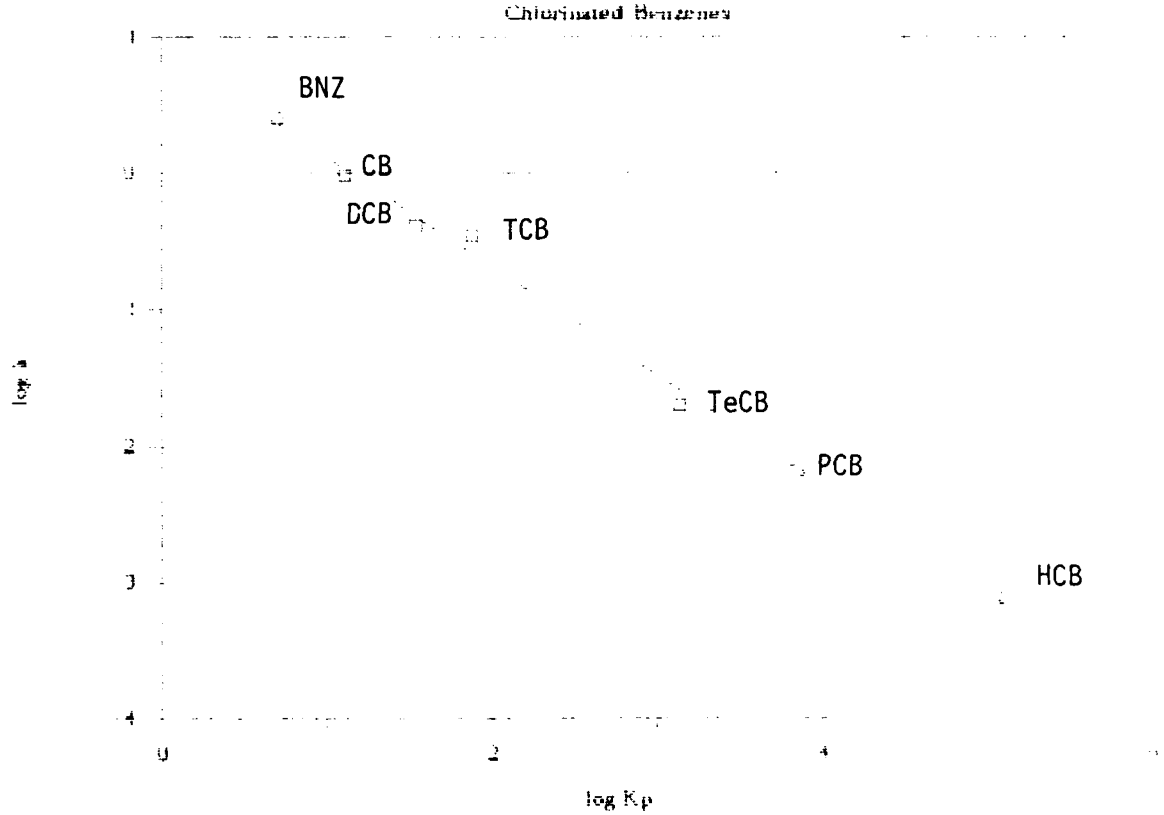

Table 1. Equilibrium and Kinetic Parameters

	Chemical	Kp (ml/g)	k (1/hr)	F	Source
BNZ	benzene	5	2.52	0.5	Exp.
CB	chlorobenzene	13	0.96	0.85	Exp.
DCB	1,2-dichlorobenzene	35	0.42	0.8	Exp.
TCB	1,2,4-trichlorobenzene	76	0.35	0.7	Exp.
TeCB	1,2,3,4-tetrachlorobenzene	1390	0.02	N.A.	Wu & G.
PCB	pentachlorobenzene	7100	0.0067	0.24	Karickhoff
HCB	hexachlorobenzene	130000	0.00075	N.A.	Oliver

1988 USAF-UES SUMMER FACULTY RESEARCH PROGRAM/

GRADUATE STUDENT RESEARCH PROGRAM

Sponsored by the

AIR FORCE OFFICE OF SCIENTIFIC RESEARCH

Conducted by the

Universal Energy Systems, Inc.

FINAL REPORT

ESTIMATION OF JET FUEL CONTAMINATION IN SOILS

Prepared by:	Deanna S. Durnford, PhD. and Douglas Hansen
Academic Rank:	Assistant Professor / Graduate Student
Department and University:	Agricultural and Chemical Engineering Colorado State University
Research Location:	USAFESC/RDVW, Tyndall AFB, Florida
USAF Researcher:	Jack Milligan

Date:	September 1, 1988
Contract No:	F49620-87-R-0004

SAME REPORT AS
PROF. DEANNA DURNFORD
ENGINEERING AND SERVICES CENTER # 27

1988 USAF-UES SUMMER FACULTY RESEARCH PROGRAM

GRADUATE STUDENT RESEARCH PROGRAM

Sponsored by the

AIR FORCE OFFICE OF SCIENTIFIC RESEARCH

Conducted by

UNIVERSAL ENERGY SYSTEMS, INC.

FINAL REPORT

Soil Vapor Extraction of Volatile Organic Chemicals

Prepared By:	Charles E. Lance, Ph.D. and David B. McKenzie
Academic Rank:	Associate Professor and Graduate Student
Department and University:	Civil Engineering Michigan Technological University
Research Location:	USAFESC/RDVW Tyndall AFB, FL 32403
USAF Researcher:	Dr. Tom Stauffer
Date:	18 August 1988
Contract No.	F49620-88-C-0053

SAME REPORT AS
DR. NEIL HUTZLER
ENGINEERING & SERVICES CENTER # 29

1988 USAF-UES SUMMER FACULTY RESEARCH PROGRAM/

GRADUATE STUDENT RESEARCH PROGRAM

Sponsored by the

AIR FORCE OFFICE OF SCIENTIFIC RESEARCH

Conducted by the

UNIVERSAL ENERGY SYSTEMS, INC.

FINAL REPORT

EVALUATION OF THE COMPUTER PROGRAM 'STRUCTURAL ANALYSIS FOR SEVERE DYNAMIC ENVIRONMENTS'

Prepared by:	J. Brian Normann
Academic Rank:	Graduate Student
Department and University:	Aerospace Engineering Department Virginia Polytechnic Institute and State University
Research Location:	AFESC/RDC Tyndall AFB Panama City, Florida 32403
USAF Researcher:	Captain Britt Bowen

Contract No.:	F 49620-88-C-0053

EVALUATION OF THE COMPUTER PROGRAM 'STRUCTURAL ANALYSIS FOR SEVERE DYNAMIC ENVIRONMENTS'

by

J. Brian Normann

ABSTRACT

The computer program 'Structural Analysis for Severe Dynamic Environments' is evaluated on the basis of accuracy and ease of use. The SDOF beam portion of the program was run with a number of input files, each designed to simulate typical elements in actual structures. A number of input files were also run in the slab/box portion of the program, each designed to simulate elements of an actual scale model structure tested in explosions by the Air Force at Tyndall Air Force Base. Output from the program is compared to an analytical/empirical model, allowing the Air Force some measure of confidence in the output from the program. Agreement of values calculated by the program with measured and hand calculated values is good and use of the program is found to be quick and simple.

ACKNOWLEDGEMENTS

I would like to thank the Air Force Office of Scientific Research for sponsoring this research. The personnel at the Engineering Services Center, specifically Captain Britt Bowen and Cheryl Garfield have been extremely helpful.

The people I have met and the amount of technical and organizational knowledge I have aquired on this assignment have been outstanding. My gratitude must also be expressed for the opportunity to do funded research granted to me by Universal Energy Systems.

I. INTRODUCTION:

The U.S. Air Force is currently conducting research and development in the area protective structures design including the development of accurate analysis techniques for protective structures subjected to conventional weapons. Shelters and protective structures must be evaluated and/or designed for effectiveness in resisting conventional and nuclear weapons effects in order to make decisions concerning choice and application of various designs.

The Structures division of the Engineering and Services Center at Tyndall Air Force Base is interested in analyses of this type. The structures' effectiveness is used to make decisions, based on cost, mobility and other factors, concerning application of designs. My role was to evaluate a computer program submitted to the Air Force on the basis of accuracy, simplicity of operation, and usefulness of code output.

The computer program deals with the dynamic analysis of beams and slabs subjected to localized loadings. My background in Aerospace structural dynamics is chiefly responsible for my selection as a summer fellow.

II. OBJECTIVES OF THE RESEARCH EFFORT:

In order for the Air Force to utilize computer codes supplied by private contractors, time must be spent acquainting personnel with the use of the codes, and the codes must be checked for accuracy, usefulness, simplicity of use, etc.

My assignment by the Universal Energy Systems, Inc. in the 1988 GSSRP was to perform an independent analysis of the computer program 'Structural Analysis for Severe Dynamic Environments,' by Theodor Krauthammer. Output from the program was to be compared to a simple analytical model and to experimental data reported in Reference 1.

III.

a. The author of the computer program, Theodor Krauthammer, prepared an exhaustive final report and a user's guide to supplement the submitted computer program. The contract was granted to Mr Krauthammer in order for the Air Force to have a means of predicting structural failure in a broad class of buildings and shelters. The program models beams, boxes, and slabs as single degree of freedom spring/mass/damper systems and predicts time, deflection, velocity, acceleration, etc. at the point of failure of the structure. The program then produces results in tabular as well as graphical formats. The forcing function input to the program may be either a bomb blast of specified distance and weight or a loading function with designated time/force points. In the former case, the program will model a multilinear forcing curve, and in the latter, points are joined on the forcing curve by straight line segments. Based on very specific data about the configuration and material properties of the beam or slab and reinforcements, the program generates three failure criteria to be used in its analysis. The three failure criteria are: crushing of concrete in compression, failure of steel in tension, and shear failure of the beam or slab. When failure occurs or a predetermined time is reached, computation is terminated and output format must be specified. An example input file, the graphical format of a modeled blast load, and output displacement vs. time are given in Figures 1, 2, and 3.

IV.

A variety of input files were compiled, designed to simulate structural elements and test the overall integrity of the program. The files were run through the program and output results were evaluated on the basis of

Figure 1

Figure 2

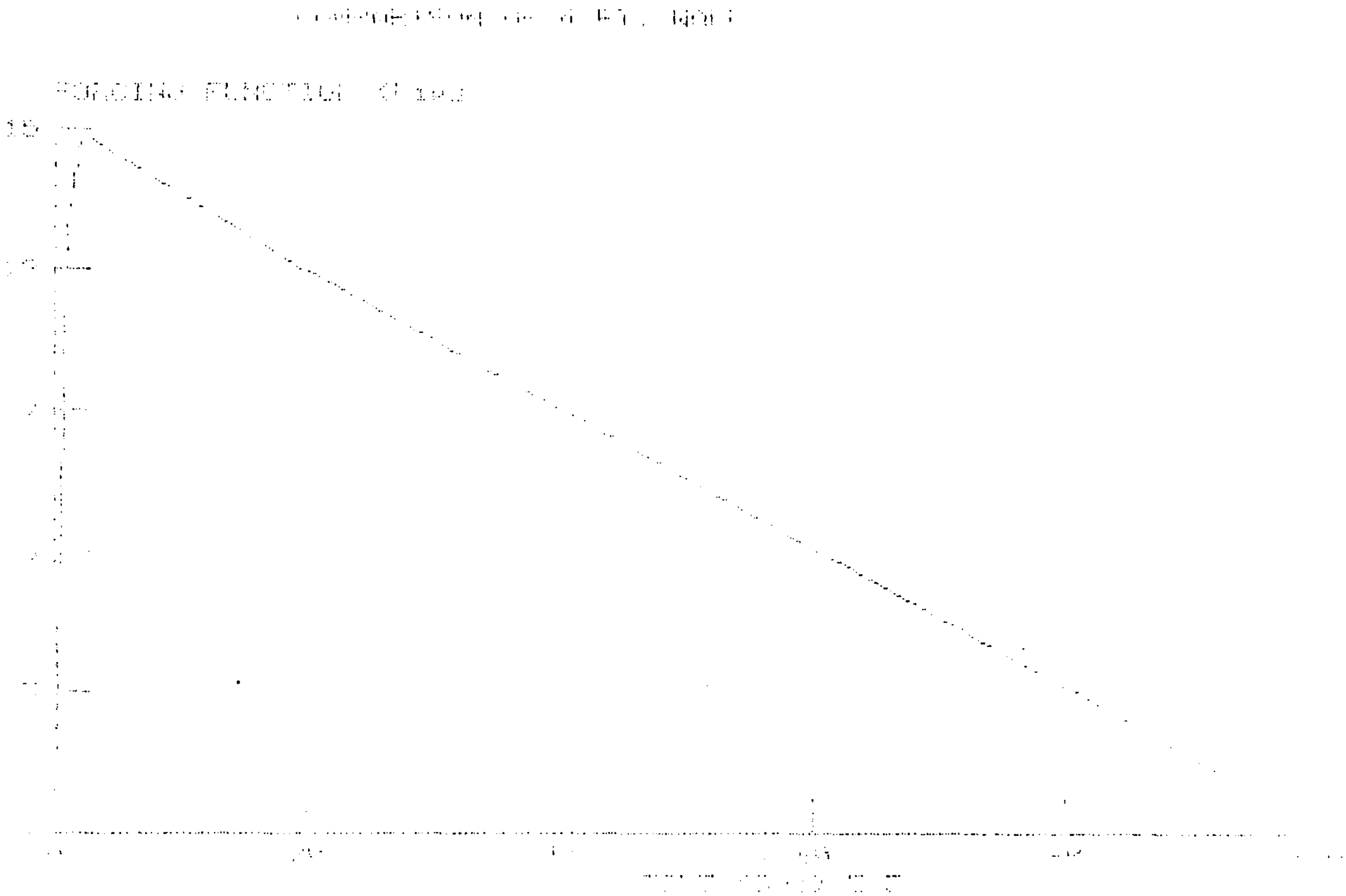

Figure 3

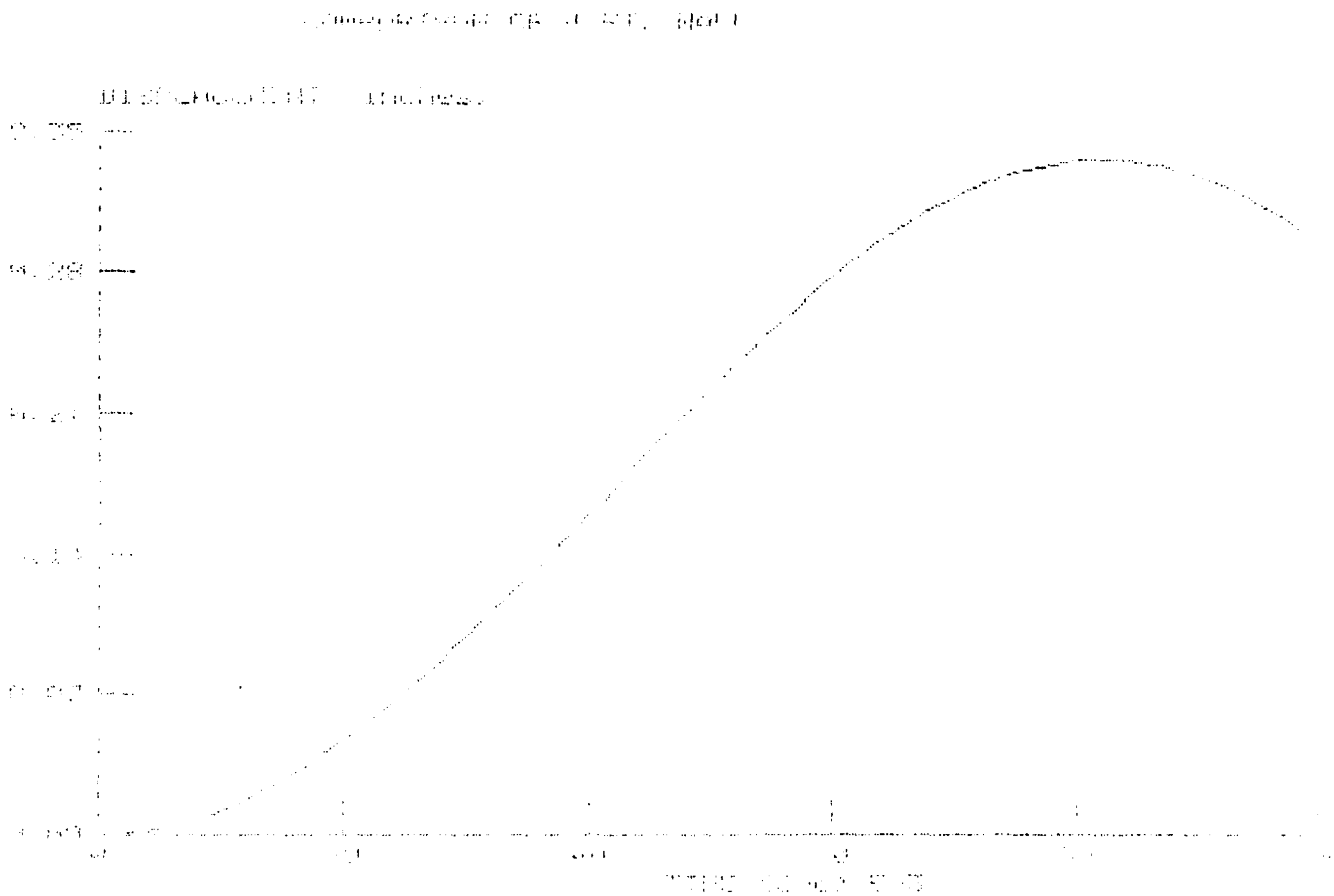

V. RECOMMENDATIONS:

a. For a given input file, values in each section should be varied so as to eventually find the most accurate output values. Specifically, in the load-deflection and SDOF input sections, tolerances, load increments, and time steps should be gradually reduced until the program terminates execution because of insufficient memory space. Prior to termination, accuracy of output values will probably be satisfactory for engineering applications. Automatic scaling of the number of divisions along with the element, load increments, and time step is not provided by the program, and would greatly simplify use of the program.

b. The slab portion of the program package is not as specific for input values as the beam portion. Load increments, boundary conditions on the slabs, and some reinforcing steel data are not required in the slab portion but are required inputs for the beam analysis. No explanation for the differences in input modules is given in the user's guide for the program. Also, no provision for air blasts on slabs seems to be taken in the slab/box analysis. Unburied slabs subjected to air blasts must apparently be modeled as beams to perform the analysis.

c. Overall, the accuracy of the program is good, as indicated by the example above and the agreement in outputs from example inputs in the program package and values measured in Reference 1. Use of the program is straight forward and a minimum amount of time may be invested by the user in learning to run the program.

accuracy and clarity of results. After gaining a feeling for input formats, and how the code reacts to extremes in inputs, an input file was set up to describe the example which follows:

> Dimensions: Width = 25.6 in. Length = 209.0 in. Depth = 25.6 in
> effective depth to centroid of tension steel = 24.85 in.
> side cover in tension and compression = 1.01 in.
> Number five bars, f_{sy} = 71458 psi at 5.0 in.
> Simply supported ends. 500 lb. bomb at 192 in.

Using equations in reference 3, maximum displacement was calculated to be 0.5 in. The computer program calculated the maximum deflection to be 0.35 in. The equivalent spring stiffness calculated by the program of 50,000.0 lb per inch also agrees with 36,000 lb/in, calculated using the approach given in reference 3. The frequency of oscillations is computed as 31 1/s , and is found to be 31.8 1/s by hand calculations. The input file, displacement versus time, and frequency of oscillations graphs are given in Figures 1, 2, and 3.

VI. REFERENCES:

1. Coltharp, D. R., K. P. Vitayaudom, S. A. Kiger, "Semihardened Facility Design Criteria Improvement," Final Report, October 1981-December 1984 U.S. Army Waterways Experiment Station, Vicksburg, MS, September, 1985.

2. Krauthammer, T., Shahriar, S., "A Computational Method for Evaluating Modular Prefabricated Structural Elements for Rapid Construction of Facilities, Barriers, and Revetments to Resist Modern Conventional Weapon Effects," Final Report, Department of Civil and Mineral Engineering, University of Minnesota, Minneapolis, MN, February, 1988.

3. Biggs, J. M., Introduction to Structural Dynamics, McGraw-Hill, New York, NY, 1964.

1988 USAF-UES SUMMER FACULTY RESEARCH PROGRAM

GRADUATE STUDENT RESEARCH PROGRAM

SPONSORED BY THE

AIR FORCE OFFICE OF SCIENTIFIC RESEARCH

CONDUCTED BY THE

UNIVERSAL ENERGY SYSTEMS, INC.

FINAL REPORT

PREPARED BY: WAYNE A. CHARLIE[1], PH.D., P.E. AND STEVEN J. PIERCE[2]

ACADEMIC RANK: ASSOCIATE PROFESSOR[1] AND GRADUATE STUDENT[2]

DEPARTMENT: CIVIL ENGINEERING

UNIVERSITY: COLORADO STATE UNIVERSITY

RESEARCH LOCATION: AIR FORCE ENGINEERING AND SERVICE CENTER
HQAFESC (RDCS)
TYNDALL AIR FORCE BASE
PANAMA CITY, FLORIDA

USAF RESEARCHERS: DR. ALLEN ROSS AND STAN STRICKLAND

DATE: 15 SEPTEMBER 1988

CONTRACT NO: F49620-87-0004

SAME REPORT AS
PROF. WAYNE CHARLIE
ENGINEERING AND SERVICES CENTER # 25

1988 USAF-UES SUMMER FACULTY RESEARCH PROGRAM

GRADUATE STUDENT RESEARCH PROGRAM

Sponsored by the

AIR FORCE OFFICE OF SCIENTIFIC RESEARCH

Conducted by the

Universal Energy Systems, Inc.

FINAL REPORT

Super Conducting Thin Films by Laser Evaporation of Bulk Material

Prepared by:	Bruce W. Bullard
Academic Rank:	Graduate Student
Department and	Electrical Engineering
University:	University of Colorado at Colorado Springs
Research Location:	Seiler Research Laboratory USAF Academy Colorado Springs CO 80840
USAF Researcher:	Dr. Ronald M. Sega

Date:	12 September 88
Contract No:	F49620-88-C-0053

SuperConducting Thin Films

by

Laser Evaporation of Bulk Material

by

Bruce W. Bullard

ABSTRACT

A system was setup to grow superconducting thin films by laser evaporation and deposition without post annealing in oxygen. The target material was a bulk superconductor, $YBa_2Cu_3O_{7-\zeta}$, that was ablated with a pulsed or Q-switched laser. The plasma plume produced was directed toward a dielectric substrate. The substrate was heated using a second laser. During the deposition, oxygen and ozone were flowed across the surface of the substrate. As of 26 August 1988, the final day of my GSRP, we had not produced a super conducting film.

I. INTRODUCTION:

Currently there is a large effort to produce high quality superconducting films. Many different approaches have been attempted and proved successful. Several examples are: electron beam evaporation, sputtering, and laser beam evaporation. The facilities at the Air Force Academy afford the opportunity to further refine and optimize the laser deposition process.

My research interest are in the areas of plasma processing and electromagnetics. Prior to working at the Air Force Academy, I worked in the Electromagnetics Laboratory at the University of Colorado at Colorado Springs. The work there entailed infrared detection of microwaves. Infrared detection is extremely useful in mapping the scatter, and absorption of electromagnetic waves from objects of varying size and composition.

II. OBJECTIVES OF THE RESEARCH EFFORT:

Prior to this project, there existed no method for producing high temperature superconducting thin films without post annealing in oxygen. Two problems encountered during annealing are substrate interaction, and random growth axis orientation. These deficiencies result in longer temperature transitions to the superconducting state, lower superconducting temperatures, lower critical current densities, and lower critical magnetic fields. The goals of this project were to produce superconducting films without post annealing, and to parameterize and optimize the laser deposition process. The parameters of interest are wavelength, intensity, pulse duration, and repetition rate.

III.

The experimental setup for depositing the first four films is shown in figure 1 below. A silicon wafer was used as the substrate. It was mounted 3cm from the target. Prior to deposition the target was cleaned to remove the carbonates and hydroxides that form on the surface of the bulk material when exposed to atmosphere. Cleaning was accomplished using the CW and then Q-switched modes of the laser. The first stage was CW mode with a power level of 3mW. The second and third stages are in the Q-switched mode at 100 Hz and 200 Hz with power levels 9mW and 18mW respectively. Films 001 and 002 were deposited in the Q-switched mode at 500 Hz with a power level of 960mW. The beam spot on target was elliptical with the shorter diameter equal to 1mm. Films 003 and 004 were deposited with the laser Q-switched at 1 KHz. An analysis of the substrates was done at the Space Vacuum Epitaxy Center at the University of Houston. No film was detectable on any of the four substrates. A suggestion for the deposition was to use a nitrated silicon substrate.

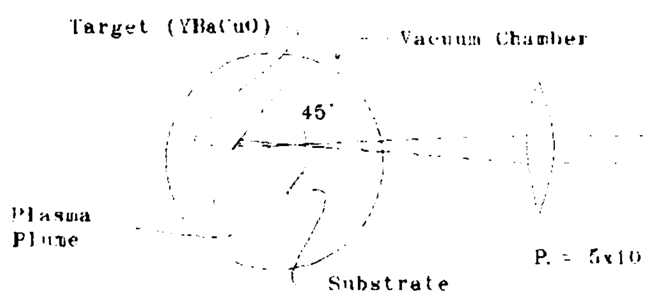

figure 1

Film five was deposited on a nitrated silicon wafer. The same experimental setup was used, however a neodymium: yttrium aluminum garnet (ND:YAG) laser was used for the target ablation. Cleaning was done by slowly increasing the

power of the laser in the Q-switched mode at 10 Hz. pulse width 35ps. A definite film was observed following deposition. The film did not adhere to the substrate and came off during analysis. A possible reason for the failure to adhere was that the substrate was not heated during deposition.

IV.

At this stage of the project, we made the decision to change substrates. The silicon based substrate is not well suited to growing superconducting films. Two substrates on which quality films have been grown are strontium titanate ($SrTiO_3$), and zirconium dioxide (ZrO_2). For films 006 and 007 a strontium titanate substrate was used. The substrate was heated with a CO_2 laser (P_0=0.57W). The spot size of the ablation laser (Nd:YAG 35ps pulse width, P_0=0.54W) on target was elliptical with the shorter diameter equal to 3mm. The experimental setup is shown in figure 2. Prior to deposition the substrate was shuttered and the target was cleaned. The substrate was then heated for one hour. No estimate of the substrate temperature was made. With the CO_2 laser still heating the substrate, a twenty minute deposition was accomplished. The two films adhered to the substrate. however the films were severely cracked. The problem appears to lie in the substrate heating.

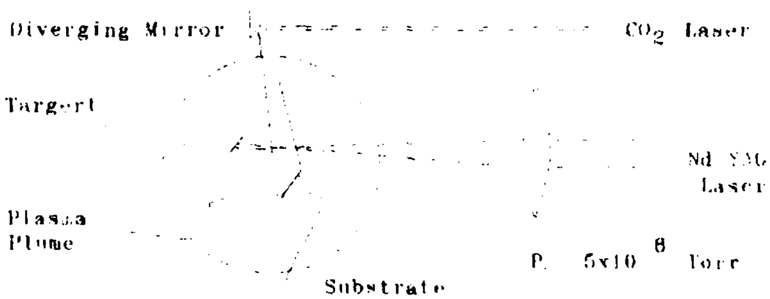

figure 2

Recent work[1] indicates that during deposition the substrate temperature should be greater than 400°C. This temperature is considerably lower than the 900°C required for post annealing. In order to achieve a higher substrate temperature we exchanged the CO_2 laser for a more powerful 7 W argon laser.

Films 008 and 009 were used to determine the effects of heating the substrate with the argon laser. The first film was deposited on a cold ZrO_2 substrate and the second on a heated ZrO_2 substrate. Previous measurements using a zirconium dioxide substrate indicated that the laser would not heat the substrate to 400°C. As expected, the heated film showed a smoother texture than the nonheated film. Analysis of the heated film showed cracking and large particles deposited on the film. The particles may be a result of the wavelength of the ablation laser (λ=1060 nm). A result that was not expected was that the film changed color during shipping (the films are sent to Houston for analysis). Originally the film was flat black similar to the bulk superconductor. Upon arrival however the film had changed to a yellowish gold color. This indicates that the film absorbed water, and the packaging of the film during shipping was faulty. As for the large deposits on the substrate, the frequency of the laser was doubled to produce light at λ= 532nm. By decreasing the wavelength we believe the size of the ablated particles will be decreased.

V.

The ultimate goal of this project was to produce a high quality superconductor without post annealing in oxygen. With that in mind film 010 was deposited in an oxygen background and film 011 was deposited in an ozone oxygen background. The experimental setup was similar to that used

in films 006 and 007 and is shown in figure 3. The last film (012) was made using the same experimental setup with the exception that a mechanical shutter was employed to reduce the repetition rate of the Nd:Yag laser. This allowed the laser to operate at its optimized frequency of 10 Hz while ablating the target at 1 Hz. By reducing the repetition rate, we allow more time for the excited atoms to combine with the extra oxygen in the system. It is possible that the time required for recombination is so short that a 10 Hz repetition rate is sufficient for total recombination.

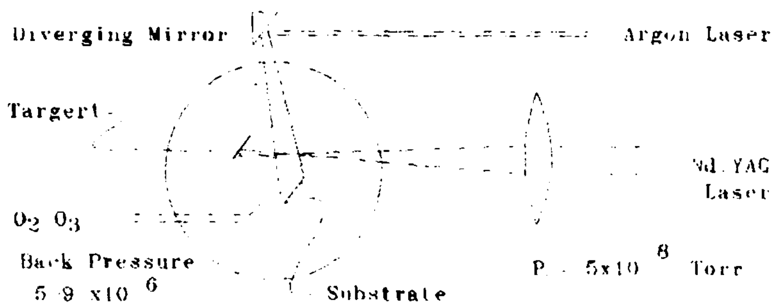

figure 3

Analysis of films 010, 011, and 012 showed that the films were moderately cracked and displayed signs of poor adhesion. The substrate may not have been at sufficiently high temperature for good deposition.

VI.

Between film depositions, a study of the plasma emitted during ablation was performed (figure 4). The wavelength of the ablation laser was $\lambda = 1060$ nm. Light emitted from the plasma during deposition was focused onto the aperture of an optical multichannel analyzer (OMA). Background light from the ablation laser did not interfere with the measurement as the wavelength is beyond the resolution of

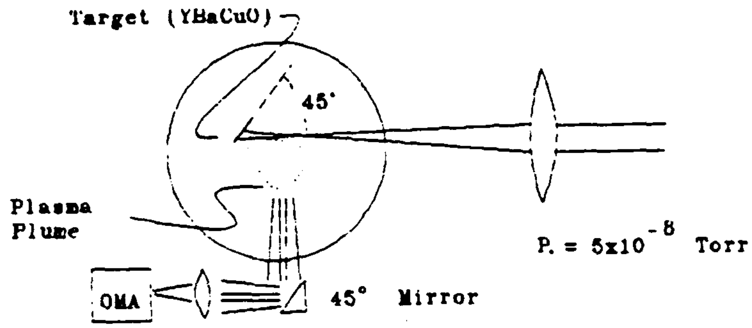

figure 4

the OMA. For the setup described the following spectra was obtained (figure 5).

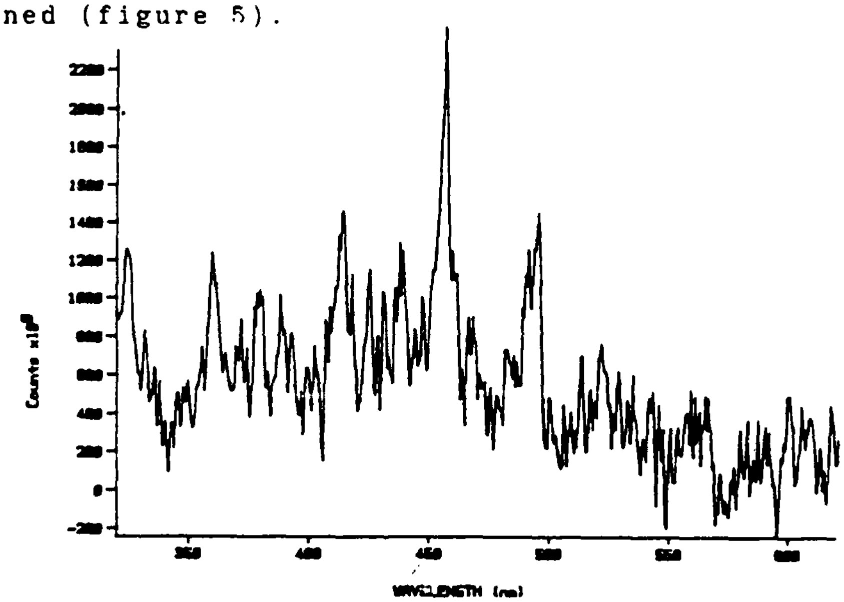

figure 5

The ablated gaseous species included Cu (325.364, 367.377, 515.404, and 521.766nm), Ba (413.649, and 455.915nm), Y (438.196, and 486.037)[2]. There are more species present than described however there was a definite absence of molecular emissions. The molecules of interest were CuO, BaO, and YO (peaks at 569.78 - 576.43nm, and 584.20 - 593.11nm).

The lack of molecular emission lines could be a result of several things: a) molecules were ejected in excited states,

but in low concentrations, b) the emission life times were less than those of atomic particles and our system was too slow to detect the emissions, or c) the particles were ejected in the ground state and no emission occurred.

VII RECOMMENDATIONS:

At this point in the project, the most logical recommendations to make would be those which contribute to producing quality films. The first recommendation is that a resistive heater be installed to permit finer control over substrate heating during deposition. The laser heating process now under consideration should be postponed until the heating characteristics are further understood. The second recommendation concerns the handling of the film following deposition. The film appears to react with the surrounding atmosphere. A system that would aid in handling would be a dry box. Such a system would allow the film to be removed from the vacuum in a nitrogen environment and thus eliminate atmospheric exposure.

Acknowledgements

I would like to thank the Air Force Office of Scientific Research for the sponsorship of this research. Universal Energy Systems has been very helpful in all administrative and directional aspects of this program.

I would also like to thank Dr. Ron Sega and Major Jim McNally, the project founders, for the opportunity to work with them on this project. Dr. Sega and Major McNally have done an excellent job of developing the project to the point it is at today. I feel certain that very shortly they will be successful in producing high quality films. The help of Duane Dunlap was invaluable in all aspects. His work with instrument setup, calibration, and ozone production was outstanding. Gary Petersen and Lieutenant Mike Dearborn were very enjoyable to work with.

Also extremely helpful and supportive were Lt Col Bill Thorpe, Lt Col Dick Cook, Major Bob Reilman, Major Jim Rotge', Captain Andy Motes, and George Brost.

References

[1] Applied Physics Letters, April - June, 1988

[2] Auciello, et. al., Spectroscopic analysis of electronically excited species in XeCl excimer laser-induced plasmas from high-temperature superconductor $YBa_2Cu_3O_7$, Applied Physics Letters Vol. 53 4 July 1988.

1988 USAF - UES SUMMER FACULTY RESEARCH PROGRAM/

GRADUATE STUDENT RESEARCH PROGRAM

Sponsored by the

AIR FORCE OFFICE OF SCIENTIFIC RESEARCH

Conducted by the

Universal Energy Systems, Inc.

FINAL REPORT

THE EFFECTS OF SODIUM CHLORIDE ON ROOM TEMPERATURE MOLTEN SALTS

Prepared by:	Jennifer A. Joyce
Academic Rank:	Graduate Student
Department and University	Department of Chemistry Texas A & M University
Research Location:	Frank J. Seiler Research Laboratory/NC United States Air Force Academy Colorado Springs, CO 80840 6528
USAF Researcher	Dr. John S. Wilkes

Date:	29 July 1988
Contract No:	F49620-88-C-0053

THE EFFECTS OF SODIUM CHLORIDE ON ROOM

TEMPERATURE MOLTEN SALTS

by

Jennifer A. Joyce

ABSTRACT

The effects of sodium chloride on a room temperature molten salt composed of aluminum chloride and 1-methyl-3-ethyl-imidazolium chloride (MEICl) were studied. The effects of adding sodium chloride to melts of various compositions were studied, and the solubility of sodium chloride in the melts was quantified. In addition, cyclic voltammetry was used to study the effects of the sodium chloride on the acidity/basicity of the melts. These tests showed that sodium chloride is soluble in an acidic melt to the point that the melt becomes neutral. The salt is, however, slightly soluble in basic melts.

It was also discovered that subsequent addition of MEICl to an acidic melt saturated with sodium chloride caused sodium chloride to precipitate from the melt and the melt to become basic.

ACKNOWLEDGEMENTS

I would like to thank the Air Force Systems Command and the Air Force Office of Scientific Research for sponsorship of this research.

A very special thank you must be extended to Dr. Tammy Melton who recommended me for this project and with whom I worked very closely throughout the research period.

It is also necessary to recognize the help of several individuals at the Frank J. Seiler Research Laboratory without whose help this project would not have been possible. Sincere gratitude is extended to: Dr. John S. Wilkes for his guidance throughout the project, Dr. Joseph Maloy and Dr. Richard Carlin for lending their expertise in the electrochemical aspects of the project, Mr. Lloyd Pflug for his assistance with ICP and NMR, and to Mr. Greg Godec and Mr. Fred Kibler for their technical assistance. Thanks are also extended to Dr. Ralph Hutchinson of the Department of Chemistry at the Air Force Academy for his assistance with atomic emmission analyses.

I. Introduction

Mixtures of aluminum chloride and 1-methyl-3-ethylimidazolium chloride have been shown to be molten salts at room temperature between apparent mole fractions of aluminum chloride (N_{AlCl_3}) of 0.333 and 0.667. (1,2) The Lewis acid-base characteristics of these melts vary according to the composition. A binary mixture with $N_{AlCl_3} < 0.5$ is basic due to the presence of chloride ion:

$$MEI^+Cl^- + AlCl_3 \rightleftharpoons MEI^+ + AlCl_4^- + Cl^- \quad (1)$$

Conversely, a binary mixture with $N_{AlCl_3} > 0.5$ is acidic due to heptachloroaluminate ($Al_2Cl_7^-$) :

$$AlCl_4^- + AlCl_3 \rightleftharpoons Al_2Cl_7^- \quad (2)$$

A neutral melt, that is, a melt of $N_{AlCl_3} = 0.5$ is composed principally of $AlCl_4^-$. However, it should be noted that the following equilibrium also occurs in these melts:

$$2AlCl_4^- \rightleftharpoons Al_2Cl_7^- + Cl^- \quad (3)$$

II. Objectives of the Research Effort

Various salts have been studied in these melts (3) including LiCl, which has been shown to form $LiCl_2^-$ and $LiCl_4^{2-}$ (4). There was an interest in examining the effects of sodium chloride in the melts, both basic and acidic in order to make comparisons with data on other salts. Many questions were raised as to the solubility of sodium chloride in basic and acidic melts and what effects the presence of the salt would have on the melt.

My initial goals for the research period were to quantify the solubility of sodium chloride in the melts at various N_{AlCl_3} values.

The next step, then, would be to determine the composition and structural aspects of the ternary melt. Also, and perhaps more importantly, it was desired to determine the effect of sodium chloride on the equilibria of the binary melt. This was to be done using cyclic voltammetry.

Additionally, it was desired to examine the effect sodium chloride would have on the conductivity of the melt. It would be useful to increase conductivity of the melt in this manner, as the binary melt has an expectedly low conductivity. (5)

Finally, the use of a sodium electrode to look at the possibility of a Na/Na^+ couple in a cell was considered.

III. <u>Determination of the Solubility of NaCl in Binary Melts</u>

All procedures were conducted in a helium atmosphere in a dry box system. Aluminum chloride and the imidazolium chloride were prepared following procedures established in this lab (1).

Several binary melts were prepared from apparent mole fraction of aluminum chloride of 0.33 to 0.667. Each melt was saturated with sodium chloride by adding small increments of salt and stirring on a stir plate until the melt became cloudy and had excess sodium chloride crystals present.

Upon saturation of the binary melts with sodium chloride, all melts (excluding that of N_{AlCl_3} = 0.667) were vacuum filtered and a given amount weighed into a volumetric flask. Dilutions were made, and sodium concentrations were determined via atomic emission

(Perkin-Elmer 306 Atomic Absorption Spectrometer). Aluminum content was determined as well using ICP (ARL 3510 ICP Spectrometer). Results of these tests are given in Table 1. (Variations in the values of sodium content in the basic melts are probably due to errors in the small quantities being measured.) Due to experimental difficulties, no data could be obtained for N_{AlCl_3} = 0.660 - 0.667.

Table 1

Nominal N_{AlCl_3}	Actual N_{AlCl_3}	Actual N_{MEICl}	Actual N_{NaCl}	mg NaCl per g binary melt
0.33	0.336	0.663	0.0010	0.41
0.40	0.400	0.600	0.0008	0.34
0.45	0.441	0.559	0.0019	0.49
0.50	0.507	0.493	0.0008	0.34
0.53	0.509	0.438	0.053	22.67
0.55	0.501	0.411	0.088	41.07
0.60	0.496	0.346	0.158	79.01

This data provided some rather interesting information: In an acidic melt, sodium chloride is soluble to the point that the mole fraction of aluminum chloride goes exactly to neutral (0.50). Upon further examination, this is not surprising as the addition of chloride ion shifts the equilibrium (equation 3) to the point that all heptachloroaluminate ($Al_2Cl_7^-$) is converted to tetrachoroaluminate ($AlCl_4^-$); this, by definition, is a neutral melt.

Thus the theoretical solubility of sodium chloride in an acidic, binary melt is that amount which would reduce the melt to neutrality. This does, then, provide a useful means of producing an exactly neutral melt for other purposes (assuming sodium ion would not be an interference).

One other interesting discovery was made (relevant to these solubility tests). Upon addition of an excess of sodium chloride to a melt of N_{AlCl_3} = 0.660 or 0.667, the melt solidified. This phenomenon is likely to be due to the fact that melts of these compositions are very near the phase limit, although no clear explanation has been determined.

The question, then, is this: If sodium chloride is soluble in acidic melts only to the point that the melt becomes neutral, why does any dissolve in a neutral or basic melt? While structural data on these ternary melts does not exist at this time, it is possible that the very small amounts which do dissolve in the basic melt exist as ion pairs, or discrete aggregates.

Cyclic voltammetry was used to provide data in support of the above conclusions. For all tests, a 250 micron tungsten wire working electrode, an aluminum wire counter electrode (separated from the melt by a coarse glass frit), and an aluminum wire in a N_{AlCl_3} = 0.60 melt reference electrode were used. A PAR 273 Potentiostat was used for all tests. Scan rate was 100 mV/s for each scan.

An acidic (N_{AlCl_3} = 0.52) melt was scanned by cyclic voltammetry for aluminum. Deposition and stripping peaks (of

heptachloroaluminate) were seen at -0.3 V and 0 V, respectively (Figure 1). Upon addition of sodium chloride (approximately enough to reach 2/3 saturation), the aluminum peak was greatly decreased under the same scanning conditions (Figure 2). Once the melt had been saturated, no aluminum peak could be seen, nor could a chloride peak be seen (Figure 3). It should be noted that in a slightly basic melt (N_{AlCl_3} = 0.495), a reversible chloride oxidation peak at +1.0 V could be readily detected. This is a very good indication that an acidic melt indeed goes only to the point of neutrality upon addition of sodium chloride.

IV. Solubility of MEICl in a NaCl Saturated Melt

The question was raised as to the nature of an exactly neutral ternary melt of this sort: Once the acidic melt has been saturated with the sodium chloride and presuming it is exactly neutral, will additional MEICl dissolve to produce a basic melt? To address this question, a N_{AlCl_3} = 0.52 melt saturated with sodium chloride was studied. A small amount (approximately 0.2 g) of MEICl was added to the melt. While initially it did not appear to be reacting with the melt, it did eventually dissolve. Cyclic voltammetry showed no change from the cyclic voltammogram of the saturated melt. However, upon addition of a quantity of MEICI sufficient to reduce the mole fraction to 0.495, the MEICl appeared to dissolve, and the melt became extremely cloudy (evidently caused by precipitation of sodium chloride). Cyclic voltammetry of the melt at this time showed a definite reversible chloride oxidation at +[illegible].24 V (Figure 4). This

indicates that MEICl can indeed be added to a neutral ternary melt to generate a basic melt.

While the solid precipitate produced has not yet been analyzed and quantified, it is presumed that all sodium chloride, save the small amount soluble in such a basic melt, is precipitated in this process.

V. Recommendations

While the previously described results contain some useful and interesting information, there are a number of other studies which seem pertinent in this system.

Certainly the conductivity of the ternary melts should be examined. The conductivity in binary melts has been well studied. (5) These studies demonstrated that conductivity is highest in a neutral melt. It is, however lower than expected in both basic and acidic melts; this is believed to be caused by hydrogen bonding between chloride ions and the hydrogen atoms on the imidazole ring which renders the chloride less mobile. If this is true, additional chloride ion in the melt (especially in an acidic melt in which sodium chloride is highly soluble) should cause conductivity to increase.

Another study which could prove to be useful is the possibility of a Na/Na^+ couple in the melt. It may be possible to devise a cell using a sodium chloride saturated melt and a sodium metal electrode.

Finally, I believe it would be interesting to determine the environment of sodium chloride in the melt. Both determination of the placement of the sodium chloride ions in the "lattice" of the neutralized acidic melt and in the basic melts would provide useful information in understanding the nature of these ternary melts.

Figure 1

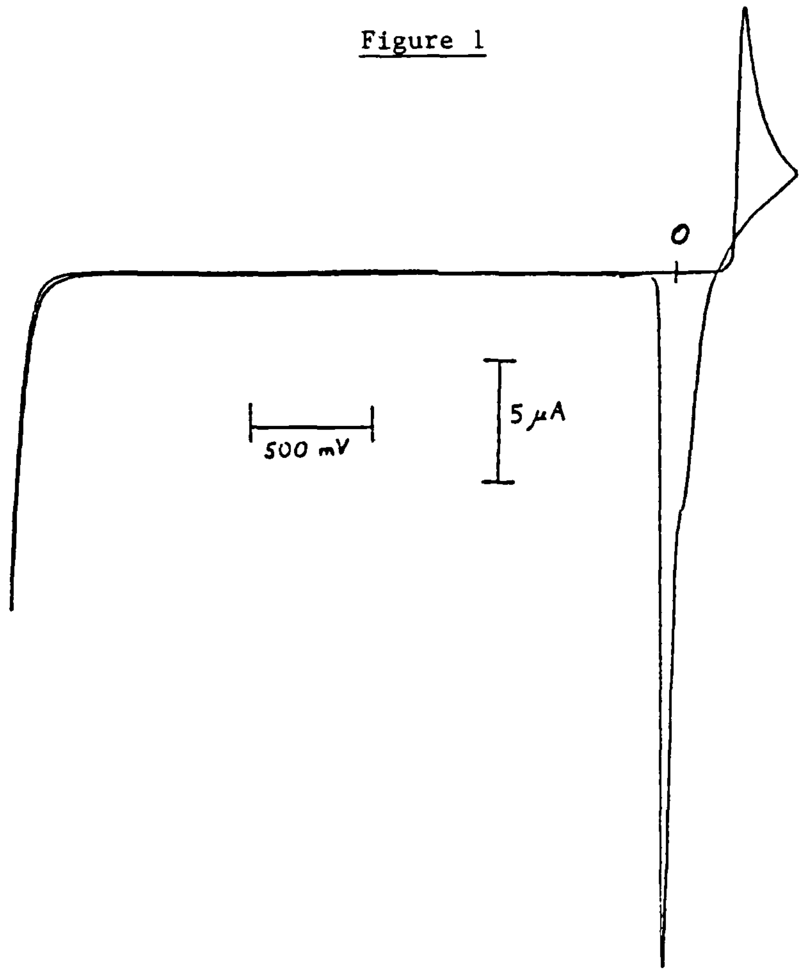

Figure 2

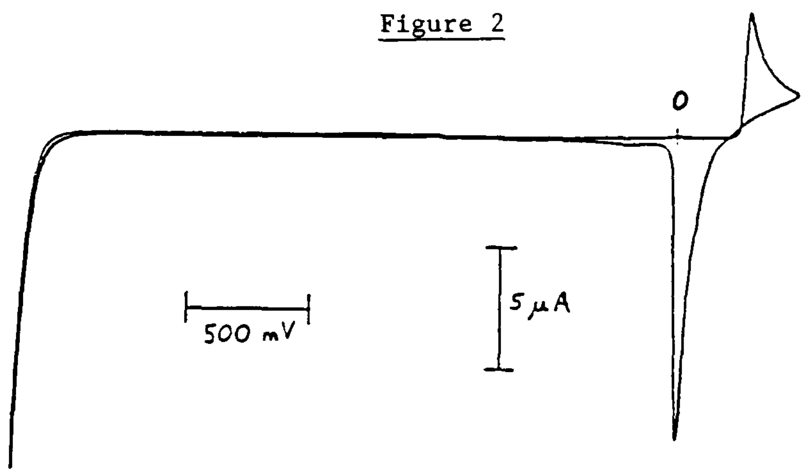

Figure 3

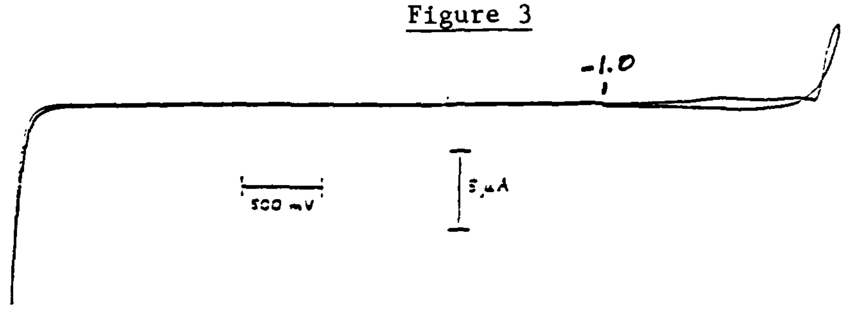

Figure 4

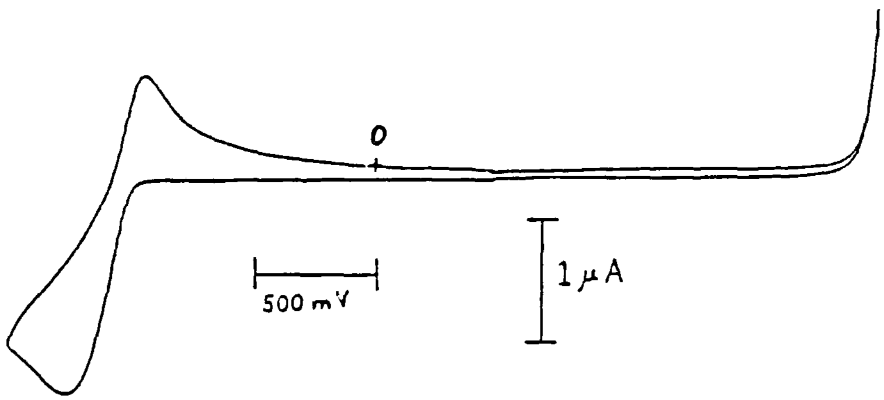

References

1. Wilkes, J.S., Levisky, J.A., Wilson, R.A., and Hussey, C.L., "Dialkylimdazolium Chloroaluminate Melts: A New Class of Room Temperature Ionic Liquids for Electrochemistry, Spectroscopy, and Synthesis," Inorg. Chem., 21, 1263 (1982).

2. Wilkes, J.S., Levisky, J.A., Pflug, J.L., Hussey, C.L., and Scheffler, T.B., "Composition Determinations of Liquid Chloroaluminate Molten Salts by Nuclear Magnetic Resonance Spectrometry." Anal. Chem., 54, 2378 (1982).

3. Piersma, B.J., and Wilkes, J.S., "Electrochemical Survey of Selected Cations and Electrode Materials in Dialkylimidazolium Chloroaluminate Melts," Frank J. Seiler Technical Report SRL-TR-82-0004m May 1982.

4. Rhinebarger, R.R., Rovang, J.W., and Popov, A.I., "NMR and Potentiometric Studies of Litium Salts in 1-Butylpyridinium Chloride-Aluminum (III) Chloride Molten Systems," Inorg. Chem., 25, 1986.

5. Floreani, D.A., Stetch, D.J., Wilkes, J.S., Williams, J.L., Persm, B.J., King, L.A., and Vaughn, R.L., "A New Class of Room Temperature Molten Salts for Battery Applications, "Proc. 30th Power Sources Symp., The Electrochemical Society, Princeton, N.J., p. 84, June 1982.

1988 USAF-UES SUMMER FACULTY RESEARCH PROGRAM/

GRADUATE STUDENT RESEARCH PROGRAM

Sponsored by the

AIR FORCE OFFICE OF SCIENTIFIC RESEARCH

Conducted by the

Universal Energy Systems, Inc.

FINAL REPORT

UNSTEADY MULTIPLE BODY STUDIES FOR TWO-DIMENSIONAL AND THREE-DIMENSIONAL EXPERIMENTS

Prepared by:	Salvatore P. Miceli
Academic Rank:	Master's Candidate
Department and University:	Aerospace Engineering Sciences University of Colorado, Boulder
Research Location:	F.J. Seiler Research Laboratories United States Air Force Academy
Focal Point:	Dr. M. C. Robinson

Date:	September 15, 1988
Contract No:	F49620-88-C-0053

UNSTEADY MUTIPLE BODY STUDIES FOR TWO-DIMENSIONAL AND THREE-DIMENSIONAL EXPERIMENTS

by

Salvatore P. Miceli

ABSTRACT

Two different computational codes are being developed to investigate the unsteady aerodynamic phenomena produced by multiple body interactions. Wake-airfoil impingement and store separation represent a similar class of problems where the temporally and spatially variant boundary conditions can be modeled using the chimera mesh scheme. The current status of the code development modeling preliminary steady state results and proposed experimental tests for code verification are reported.

Acknowledgements

I wish to thank the Air Force Systems Command and the Air Force Office of Scientific Research for sponsorship of this research effort. Universal Energy Systems must also be mentioned for their concern and help to me in all administrative and directional aspects of this program

My experience as a participant in the Graduate Student Research Program was enriching and rewarding due to many different influences. Dr. Mike Robinson provided constant support and encouragement. The help of Dr. Carroll Dougherty was invaluable as a constant source of knowledge and experience and without her help most of this would not have been possible. I would also like to thank the F.J. Seiler Laboratory and the USAF Academy for their joint interest in supporting this program.

I. Introduction

With the onset of faster and more maneuverable aircraft, aerodynamicists must utilize novel computational and experimental methods to resolve inherently complex flow fields in order to maximize design performance. Conventional analysis techniques based upon quasi-steady assumptions and simple model geometries cannot adequately predict the dynamically changing flow fields produced in rapid maneuver environments by complicated three-dimensional bodies. Now computational approaches are available which preserve the transient characteristics of the flow while allowing time-variant motions of the body.

Multiple body wake interactions and store separation are typical of this problem class. Multiple body wake interaction problems are characterized by an upstream body driven with a known motion history which creates a transient wake. The wake interaction with downstream surfaces can yield dramatic effects in loading. Helicopter rotors, canard-wing interactions and multiple-staged turbo machinery all possess this type of wake impingement

Store separation is a subset of the general multiple body problem. Multiple bodies in close proximity will alter adjacent load characteristics due to complex flow interactions. This complexity increases an order of magnitude when a multiple body is separated. Individual components are permitted to move independently, driven by the temporally and spatially changing pressure distribution.

From a computational standpoint, the multiple body wake interaction and store separation problem are quite similar. Both require an interactive computational scheme which captures the physics of the time dependent flow field, and simultaneously, permits the application of temporally and spatially dependent boundary conditions. This report focuses on a novel application of an existing computational approach in order to investigate multiple body and store separation. Also, experi-

ments designed to validate these computational codes are discussed.

II. Objectives

a) To perform a two-dimensional computational comparison of an oscillating airfoil trailed by a stationary airfoil with previously obtained experimental results.

b) To perform a computational/experimental comparison for a three-dimensional store separation problem.

c) To undertake a feasibility study for transonic unsteady experiments to validate results from store separation computational codes.

III. Approach

Multiple Airfoils Unsteady wake interactions can have many effects on trailing lifting surfaces. Recent results by Huyer (ref. 1) indicate an enhanced lift is obtained when a lifting surface passes through the wake of unsteady flow. In nature, the dragonfly is a prime example of a biological organism which may exploit this effect. Luttges (ref. 2) has shown that the forward wings on a dragonfly produce vortex structures that interact with the trailing wings and generate large amounts of lift. Many current experimental aircraft such as the X-29 mimic this type of wing geometry with a leading canard. Understanding the wake interaction is essential in realizing the overall control consequences of such tandem designs.

The present interactive wake study concentrates on the flow interactions between an oscillating airfoil and a stationary trailing airfoil With experimental results previously obtained by Huyer, a computational study was initiated to perform a detailed analysis about the multiple airfoil case and to verify a two-dimensional unsteady implicit viscous code.

The multiple airfoil configuration for the computational case was modeled as

close as possible to the actual experiment. The experiment conducted by Huyer consisted of two NACA 0015 airfoils placed in the 16 in. low speed wind tunnel at the University of Colorado, Boulder. The leading airfoil was pitched about the 1/4 chord with a period of 156 msec, a mean angle of attack of 15 deg, and an oscillation amplitude of ± 10 degrees. The trailing airfoil was placed 1/2 chord downstream of the trailing edge of the oscillating airfoil. Six different mean angles between 0 and 25 degrees were tested at Reynolds numbers of 25,000 and 50,000. To change the angle of attack of the trailing airfoil, the airfoil was rotated about its leading edge leaving the nose always on the center line of the oscillating airfoil at 0 degrees angle of attack.

A two-dimensional unsteady flow solver coupled with a multiple mesh package developed by Dougherty (ref. 3) is being modified to solve the flow fields about the two tandem airfoils. This package utilizes a chimera mesh scheme where minor grids about airfoils are overset on a global grid mapping the overall flowfield. This setup permits the minor grids to be moved independently without disturbing the entire mesh system. The minor mesh boundaries are updated by either the global mesh or another minor mesh. Therefore, when a minor mesh is moved, its boundary conditions are automatically changed to reflect its new position. This allows any of the minor meshes to have free movement and exchange of information as long they are within the outer boundaries of the global mesh.

The major grid was a Cartesian grid generated using an exponential expansion routine. The resulting clustering effect can be observed in fig. 1. The minor grids were generated about two NACA 0015 airfoils (fig. 2) using GRAPE, a two-dimensional Poisson grid generator developed by Sorensen (ref. 4). The initial mesh configuration has the two airfoil grids overset on the Cartesian grid (fig. 3). Clustering increased the grid points around the leading and trailing edges of each

of the airfoils (fig. 4). This grid concentration is essential in resolving the flowfield because of the increased dependence on the viscous terms in these areas.

The existing version of the flow solver uses a central-differenced, implicit, ADI scheme for solving the Euler equations. Preliminary steady state calculations in figures 5 and 6 show Mach and pressure contours for alpha equal to zero degrees angle of attack for both airfoils at Mach 0.15.

This case provided reliable steady state data that will be used to validate the final working version of the code. In addition, the validity of the grid initiation, updating, and input/output routines were shown. The double lines indicated on some of the Mach and pressure contours indicate solutions on both the major and minor grids respectively (fig. 6 and 7). Hence, contour overlays are indicative of matched solution sets between grids.

The Euler equations will not adequately model the experimental results. Oscillating airfoils produce very repeatable vortex structures. The flowfield is characterized by the initiation of leading edge and trailing edge vorticies which are shed into the wake of the oscillating airfoil and impinge upon the trailing airfoil. The boundary layer vorticity which produces these vortex structures can only be modeled using the full Navier-Stokes equations.

When using Navier-Stokes equations to solve for boundary layer activity about airfoils, the grid spacing must be very fine ($ds \approx .5/\sqrt{Re}$) to model the viscous flow. In addition, because the leading airfoil is oscillating between 5 and 25 deg., the clustering in the y-direction needs drastically to be improved. After refining all the grids (figures 7, 8, 9, and 10), the total number of grid points jumped to 40,000.

The viscous terms were integrated into the code from a modified version of ARC2D written by Pulliam (ref. 5). To check the new viscous version, a simple NACA 0012 airfoil generated by GRAPE was rotated to 1.4 degrees angle of attack

and was placed in a flowfield with a Mach number of 0.70. Errors were found in the flow solver and current efforts are centered on resolving these problems.

<u>Store Separation</u> Todays' high speed aircraft are intended to carry a variety of stores either externally or submerged, and are rated as to their ability to deliver these stores to their targets reliably and accurately without loss of aircraft performance. Store-induced aerodynamic drag can significantly downgrade aircraft performance while unpredictable aerodynamic interactions may cause the released stores to scatter, run into each other, or impact the aircraft. It is necessary, then, to develop reliable methods to predict the aerodynamics of store/airframe interactions

A computational code developed by Dougherty (ref. 6) has the capabilities for solving three-dimensional unsteady moving body flow fields. The code, a chimera mesh scheme coupled with an ARC3D flow solver, uses multiple overset grids to map complex configurations. With the ability for moving meshes, modeling a store separation experiment becomes very feasible.

Preliminary computational results for the steady state case of an ellipsoid in close proximity with a flat wall are shown in figures 11 and 12. The Mach contours show distinct shocks at the leading and trailing edges of the ellipsoid. The repercussions of the shocks can be seen on the flat plate as well as along the centerline of the ellipsoid. Figure 12 shows the pressure contours of solutions on the center planes of the configuration. Again the shocks are clearly visible at the leading and trailing edges of the store, and the impingement of the shocks on the flat plate can be seen.

Without real experimental results, however, limitations on the code accuracy and applicability are unknown. Hence, a simple three-dimensional, unsteady experiment is needed for validation. The present study focuses on the design of a simple

unsteady experiment to validate store separation codes utilizing the transonic test facility at USAF Academy.

A multiple body, unsteady, transonic experiment will be used to validate existing computational codes. In order to produce the unsteady affects, one body must move with respect to the other. The store and airframe are modeled using a simple axisymmetric body located next to a flat plate. Multiple pressure ports on the store and flat plate are needed to obtain time-accurate pressure data for comparison with computational results.

Physical limitations on the trisonic test facility at the USAF Academy limited somewhat the complexity of the experimental model. The trisonic wind tunnel's 12 in. cross sectional test area restricts the model size to avoid tunnel choking. Also, boundary layer effects along the tunnel walls must be minimized. A smaller model limits the potential number of pressure ports, and reduces the data density for comparison. Initially 25 pressure ports located from the leading to the trailing edge of the store and three rows of 15 pressure ports on the flat plate were desired. After further analysis on the model design, physical restrictions limited the store to 15 pressure ports, and only one row containing 10 pressure ports were allowed on the flat plate. This data density is still sufficient to verify the most critcal flow regions of the store separation problem.

To produce the unsteady flow vital for code verification, the store must be pitched away from the flat plate to an angle which exceeds static stall. The current sting mount can achieve pitch angles to 30 deg. amplitude with a 6-7 deg/sec pitch rate. Although a sinusoidal oscillation of the store would have been optimal to test harmonic effects, the sting apparatus used is limited to single pitch motions.

The trisonic wind tunnel uses a blowdown technique to reach its transonic and supersonic speeds. Large holding tanks are pressurized with air upstream of the test

section. When the compressed air in the tanks are released, the stored reserve is blown down. The Mach number within the test section can be changed by adjusting the inlet throat area ratio. For a transonic case, approximately 60-90 seconds of test time can be expected for every four hours needed to refill the holding tanks.

To assure proper validation, three different test velocity ranges have been selected: M = 0.9 - 0.95, M = 1.0 - 1.05, and M = 1.15 - 1.25. Each test case will be run five different times, rotating the store 45 deg about its axis and translating the flat plate to the left or right each time. These five runs together will collect pressure data covering the entire store and most of the flat plate surface area. The store will be a simple axisymmetric body with a parabolic nose and the tail mounted into the sting and faired off so no rough edges appear. About 15 pressure ports will be placed in a straight line from the nose to the tail of the store with closer spacing at the nose and tail (fig. 13). Non-uniform spacing is necessary to capture shock and expansion effects. The model will be approximately 6 in. long with a 1.25 in. diameter; the nose cone and trailing apparatus will about 1 in. long each. The flat plate will be 10 in. long and 8 in. wide with the pressure ports in a line down the center. The store will be pitched from 0 deg to 30 deg for each test case at about 7 deg/sec. Each run will take approximately 10 - 15 seconds of wind tunnel time, totaling 50 - 75 seconds of air for each test case. Therefore, three tank refills will be necessary to complete the experiment.

IV. Recommendations

Multiple Airfoils A working version of the multiple body wake interactions code with viscous terms should be completed by the middle of October. Computational results of the oscillating airfoil interactions with the trailing airfoil will be compared with the experimental data collected by Huyer (ref. 1). Upon validation various

multiple airfoil configurations over a large parametric range can be investigated.

Store Separation   Experimental runs for the store separation problem will take place sometime in late October or early November. The final model design may be altered based upon current computational results obtained for the described test parameters.

REFERENCES

1. Huyer, Stephen A., Luttges, M. W., "Unsteady Flow Interactions between the Wake of an Oscillating Airfoil and a Stationary Trailing Airfoil," AIAA Paper No. 88-2581, Applied Aerodynamics Conference, Williamsburg, Virginia, June 6-8, 1988.

2. Luttges, M. W., Somps, C., Kliss, M., Robinson, M. C., "Unsteady Separated Flows: Generation and Use by Insects." Workshops on Unsteady Separated Flows, United States Air Force Academy, Aug. 10-11, 1983, p.127-136.

3. Dougherty, F. C., Benek, J. A., and Steger, J. L., "On Application of Chimera Grid Schemes to Store Separation," NASA TM 88193, October 1985.

4. Sorenson, R. L., "A Computer Program to Generate Two Dimensional Grids About Airfoils and Other Shapes by Use of Poisson's Equations," NASA Technical Memorandum 81198, May 1980.

5. Pullium, T. H., "Euler and Thin Layer Navier-Stokes Codes: ARC2D, ARC3D," Computational Fluid Dynamics Users's Workshop, The University of Tennesee Space Institute, Tullahoma, Tennessee, March 12-16, 1984.

6. Dougherty, F. C., and Kuan, J-H. 'Transonic Store Separation Using a Three Dimensional Chimera Grid Scheme, AIAA Paper No. 89-0637, " To be presented at the Winter Aerospace Sciences Meeting, Reno, January 1989.

CARTESIAN GRID FOR EULER SOLVER

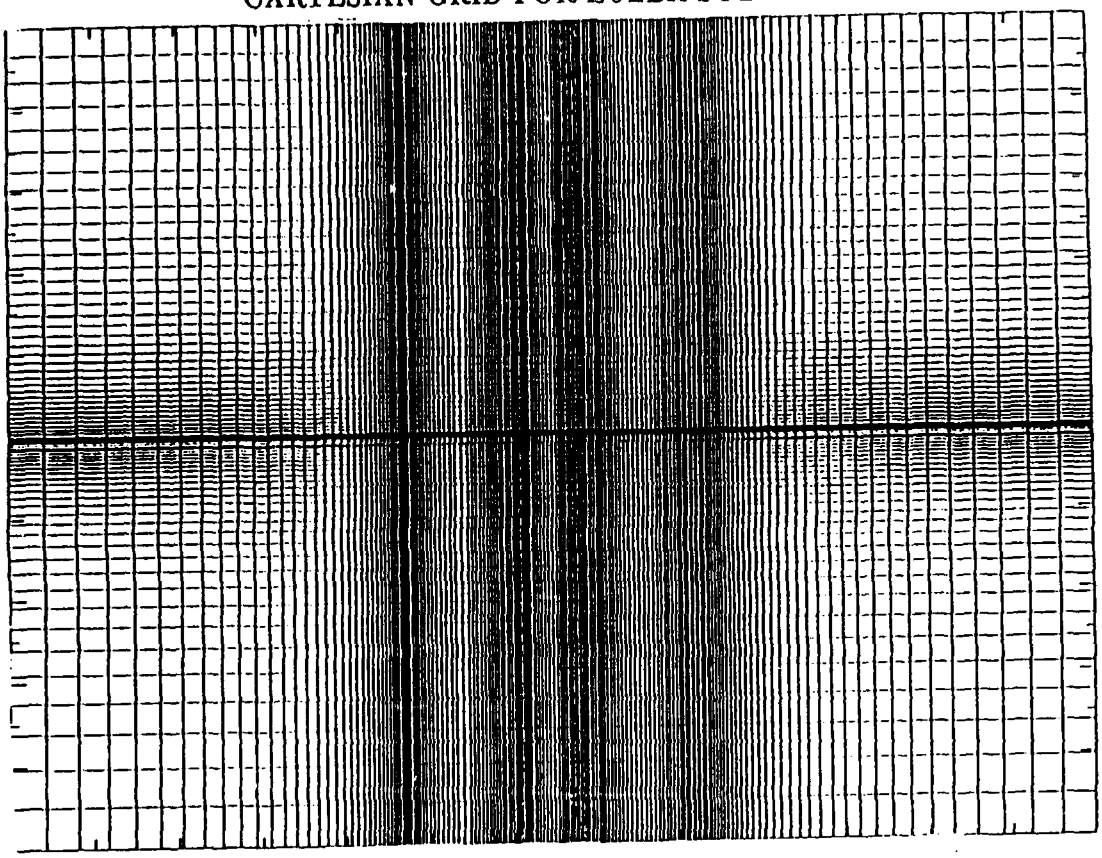

FIGURE 1

NACA 0015 AIRFOIL GRIDS FOR EULER SOLVER

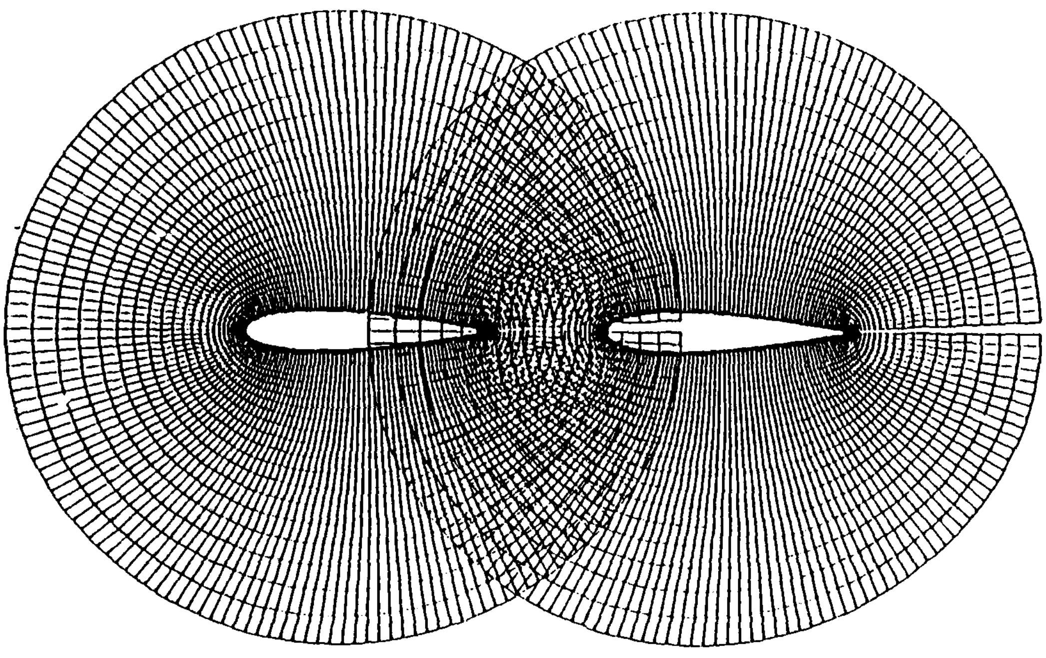

FIGURE 2

MULTIPLE MESH SCHEME FOR EULER SOLVER

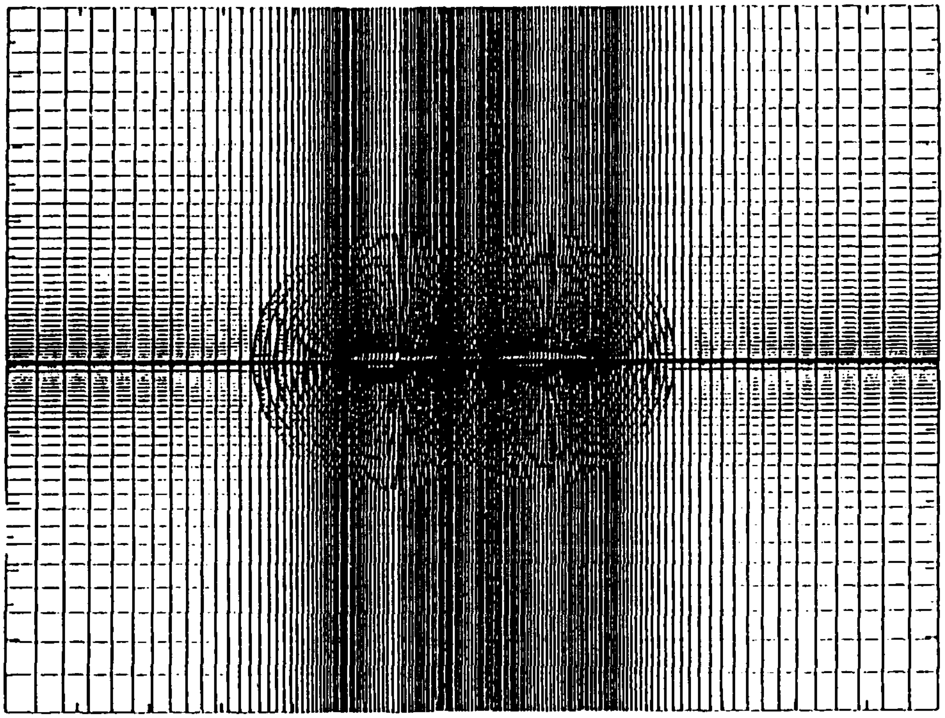

FIGURE 3

MULTIPLE MESH SCHEME CLOSEUP FOR EULER SOLVER

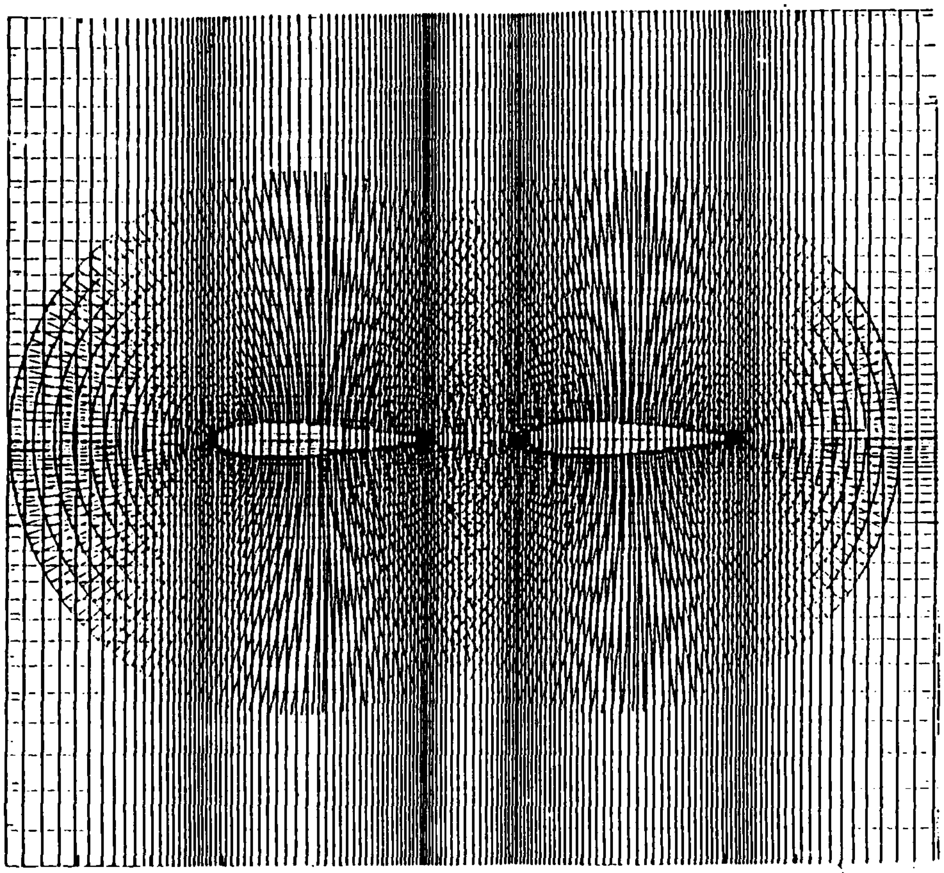

FIGURE 4

MACH CONTOURS FROM EULER SOLVER

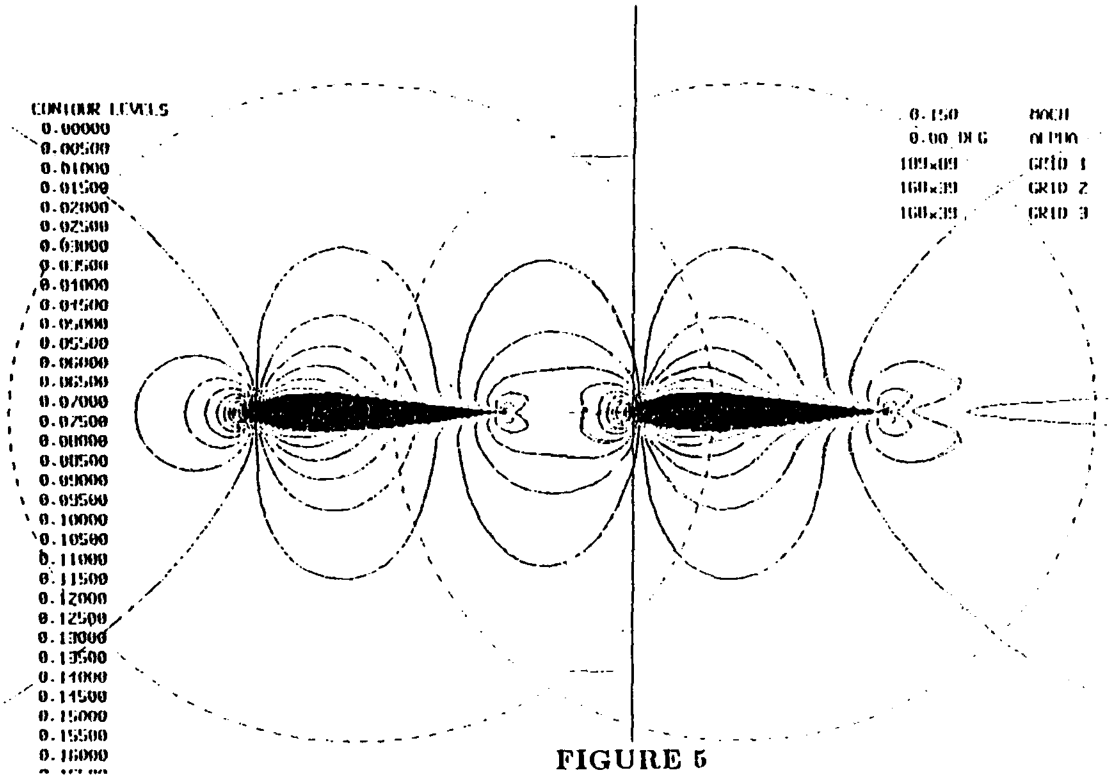

FIGURE 5

PRESSURE CONTOURS FROM EULER SOLVER

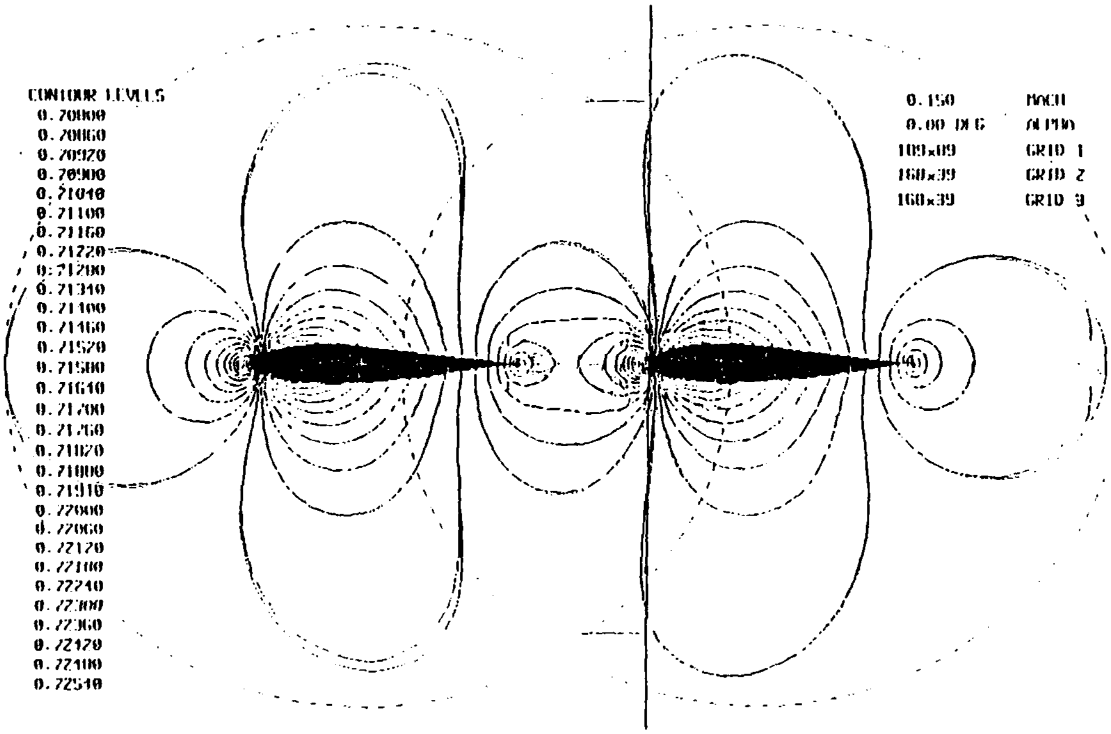

FIGURE 6

CARTESIAN GRID FOR NAVIER-STOKES SOLVER

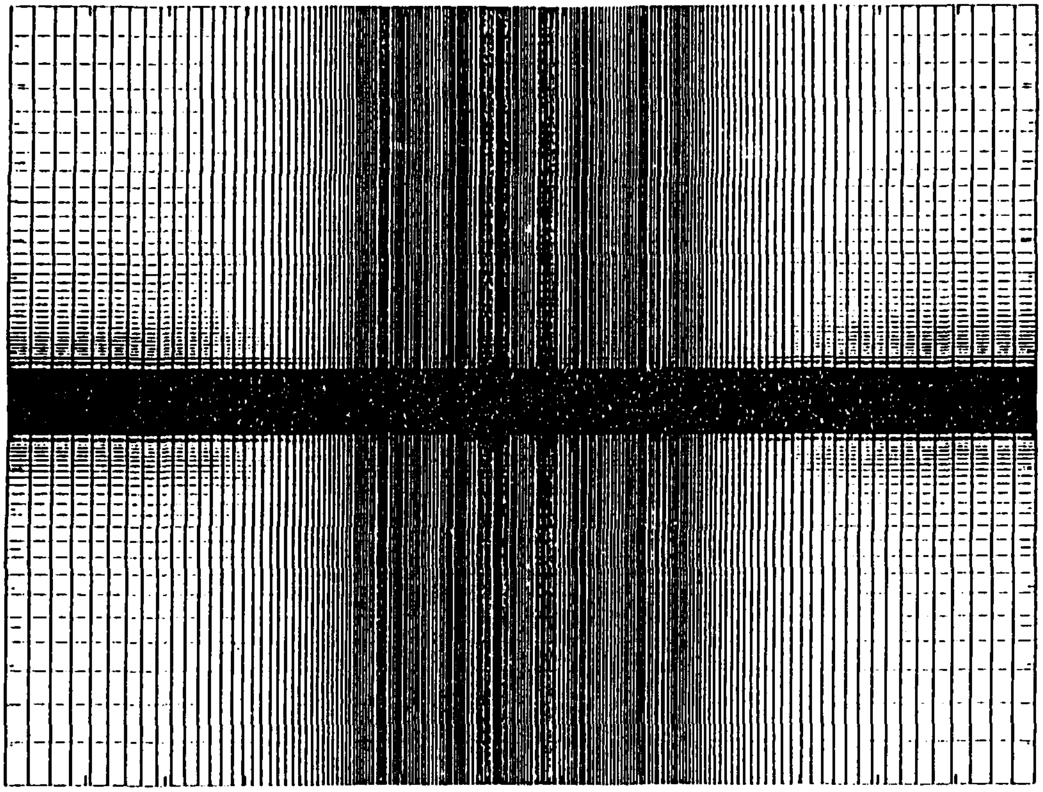

FIGURE 7

NACA0015 AIRFOIL GRIDS FOR NAVIER-STOKES SOLVER

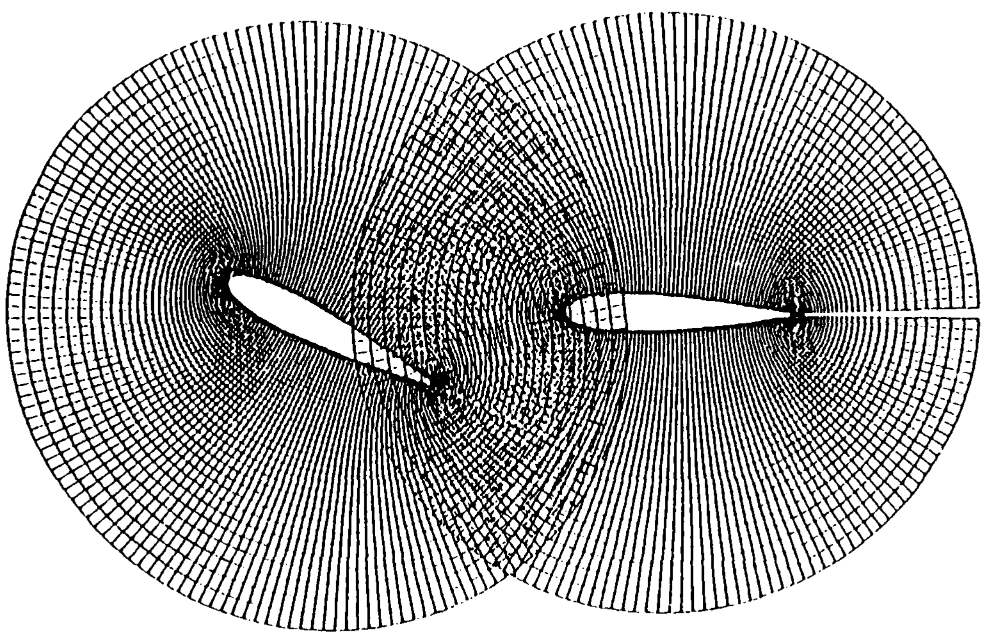

FIGURE 8

MULTIPLE MESH SCHEME FOR NAVIER-STOKES SOLVER

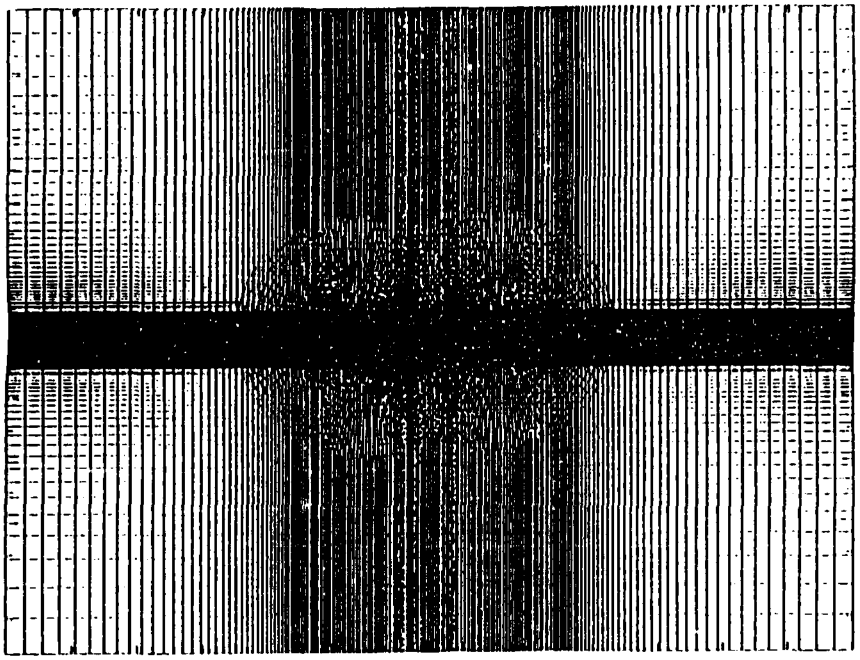

FIGURE 9

MULTIPLE MESH SCHEME CLOSEUP FOR NAVIER-STOKES SOLVER

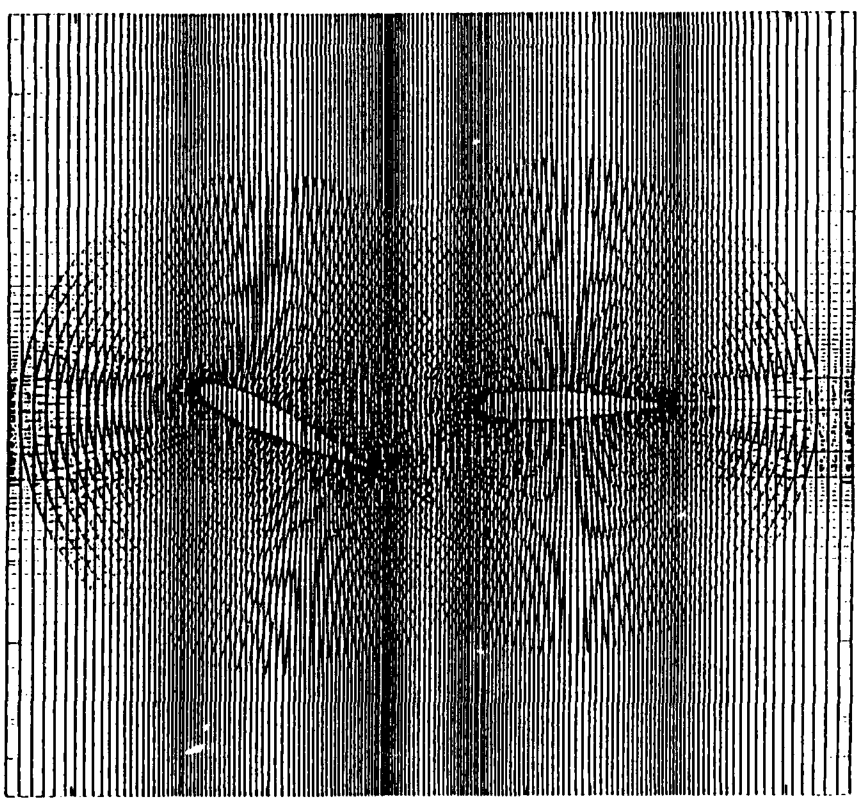

FIGURE 10

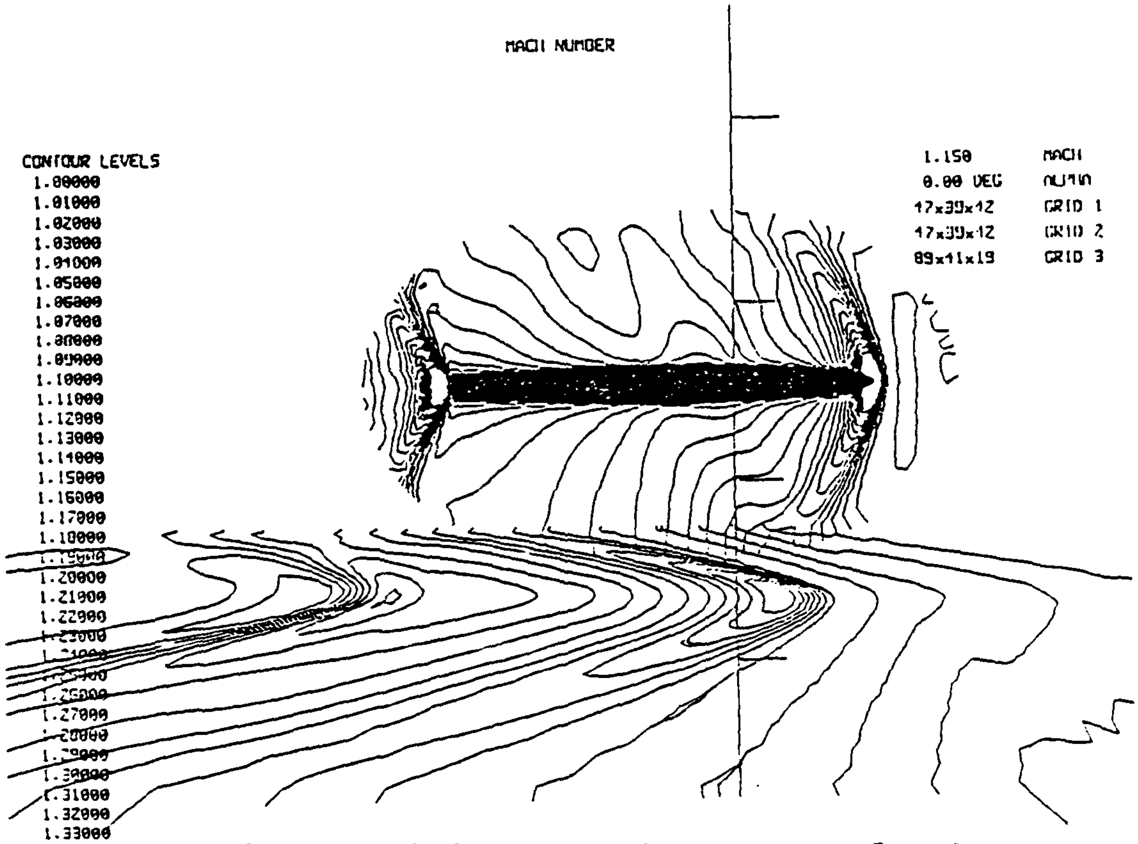

Fig. 11 Mach contours for store near flat plate.

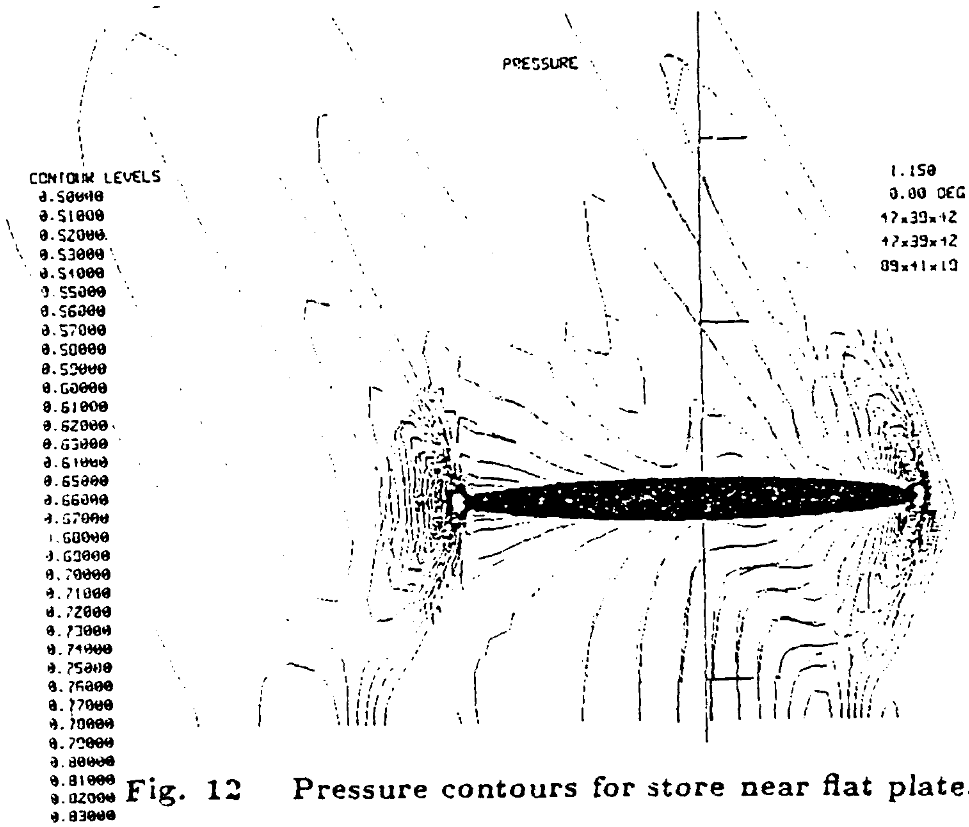

Fig. 12 Pressure contours for store near flat plate.

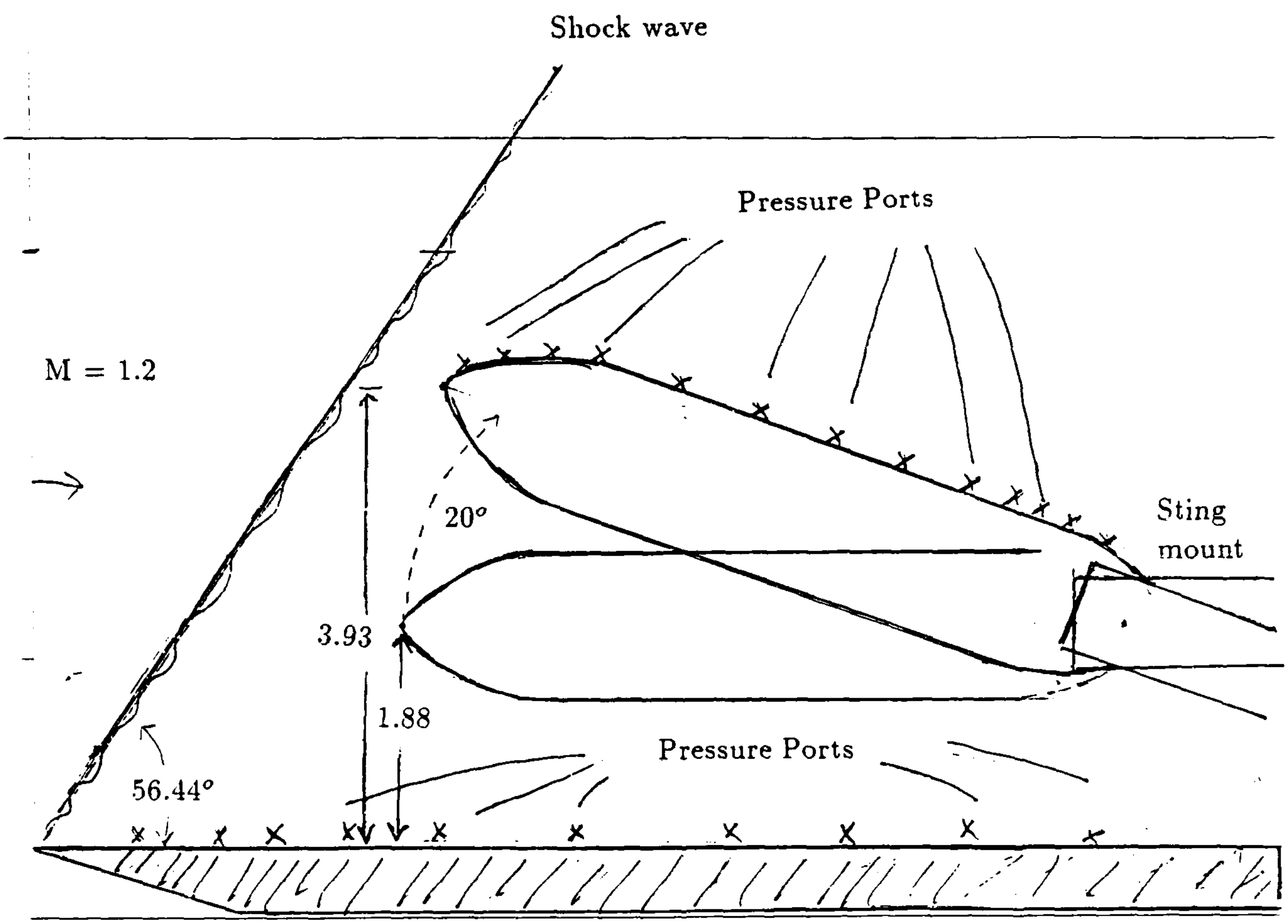

FIGURE 13 STORE SEPARATION CONFIGURATION

MR. THOMAS KIMBLE

FINAL REPORT NUMBER 27

NO REPORT SUBMITTED

1988 USAF-UES SUMMER FACULTY RESEARCH PROGRAM

GRADUATE STUDENT RESEARCH PROGRAM

Sponsored by the

AIR FORCE OFFICE OF SCIENTIFIC RESEARCH

Conducted by the

Universal Energy Systems, Inc.

FINAL REPORT

Prepared by:	Scharine Kirchoff
Academic Rank:	Graduate Student
Department and University:	Geology and Geophysics University of Alaska-Fairbanks
Research Location:	AFGL/LWH Hanscom AFB Hanscom AFB, MA 01731
USAF Researcher:	Dr. John J. Cipar
Date:	August 10, 1988
Contract No:	F49620-85-C-0013

An Investigation of Economic Explosions in Littleton, Massachusetts and Healy, Alaska

by

Scharine Kirchoff

ABSTRACT

In an effort to improve the capability to discriminate between seismic sources, economic explosion signals from the San Vel Quarry in Littleton, MA and the Usibelli Coal Mine in Healy, Alaska were selected for this investigation. Using a theoretical modelling technique, based on generalized ray theory, synthetic seismograms were generated. Synthetic wave patterns revealed obscured phase arrivals and increased complexity of the waveforms as the number of shots and delay interval increase. The complexities in the observed and synthetic seismograms may have arisen from propagation path effects and/or effects at the receiver. Recommendations for further investigation of this research effort are discussed.

I. INTRODUCTION:

During the past decade seismic signals recorded at regional distances have received increased attention due to their potential value in detection, discrimination and yield estimation of underground nuclear explosions. Effective monitoring of any comprehensive or low-level threshold nuclear test ban treaty will require the identification of a large number of small magnitude non-nuclear explosions due to the abundance and widespread nature of mining activity. Economic explosions, such as quarry and mine blasts, constitute a common and convenient seismic energy source for a seismic discrimination investigation.

The Solid Earth Geophysics Branch of the Earth Sciences Division of the Air Force Geophysics Laboratory at Hanscom Air Force Base is particularly interested in the acquisition and interpretation of regional seismic data. For example, the Eastern Massachusetts Quarry Blast Experiment (EMQBE), which took place in July 1987, was designed and implemented to characterize multiple row quarry explosions as a seismic energy source (Figure 1). The EMQBE data was particularly useful for this investigation because the experiment was well-controlled and monitored by field personnel. I was an active participant in this experiment as a 1987 USAF-UES research associate. Vital information on quarry blast size, geometry and

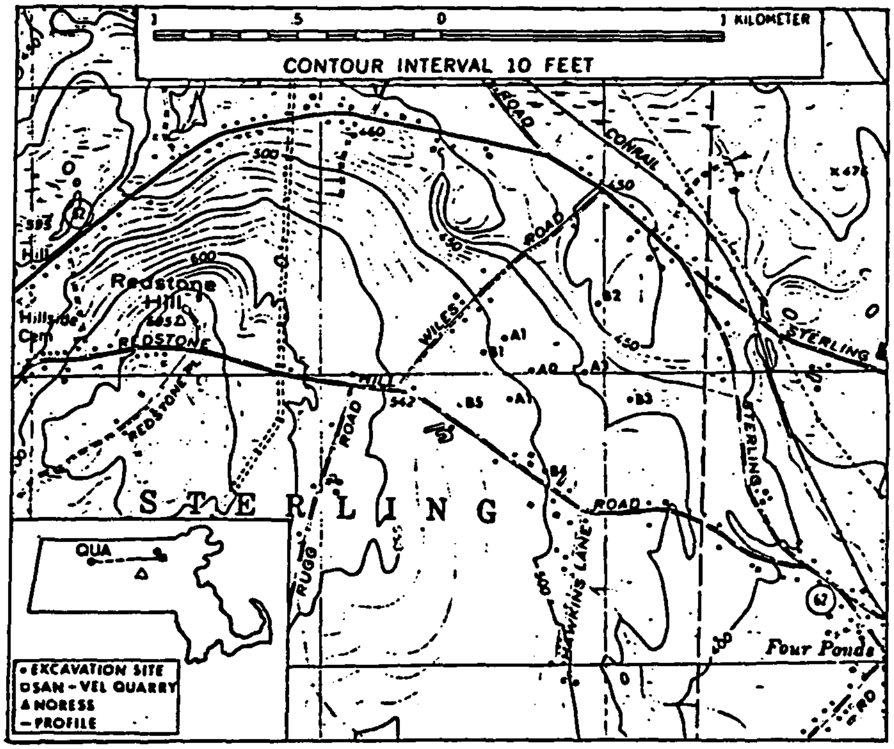

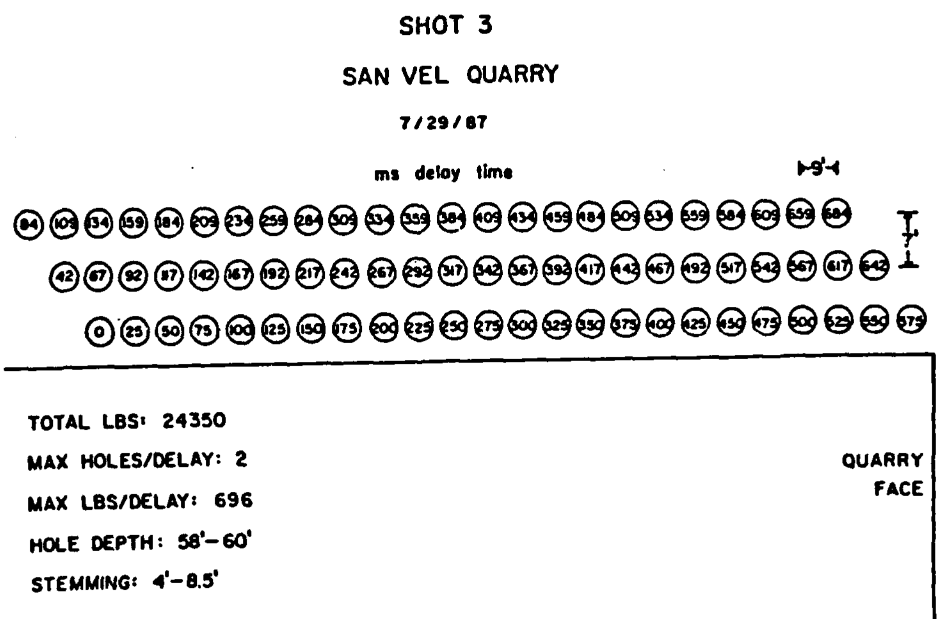

Figure 1. The location of the Eastern Massachusetts Quarry Blast Experiment in Littleton, MA (above). An example of the configuration of a multiple row quarry explosion used at the San Vel Quarry (below).

timing was documented during the experiment, and subsequently, the information, was utilized in the comparison of coal mine blasts from Healy, Alaska. The cooperative interaction and exchange of scientific information, therefore, proved to be invaluable for this investigation.

My research interests and education have been in the field of explosion seismology and geology. My masters thesis encompassed a crustal refraction study of the Southern Rio Grande Rift (Kirchoff, 1986). The 1985 Defense Nuclear Agency Minor Scale surface explosion, a 4.8 kiloton chemical explosion in the White Sands Missile Range, was used as the seismic energy source. More recently, I investigated the differences in seismic signal characteristics of small shallow earthquakes and mine blasts colocated in Healy, Alaska. This investigation was summarized in both a 1987 USAF-UES final report and in Kirchoff and Biswas (1987). My research interests and background are complementary to the Solid Earth Geophysics Branch's interest in the Comprehensive Test Ban Treaty Monitoring program which, therefore, contributed to my assignment to the Earth Sciences Division.

II. OBJECTIVES OF THE RESEARCH EFFORT:

Economic explosions have received limited attention as sources of regional phase signals. Quarry or mine blast signals are frequently regarded as background noise or sometimes, at most, they are utilized for crustal refraction investigations (eg. Hanson, Berg and Gedney,

1968). Short-period recordings from regional seismic networks, such as the seismographic station at the University of Alaska-Fairbanks, have shown that differences in the seismic signal characteristics of small shallow earthquakes and mine blasts, located in the same event area, do, indeed, exist (Figure 2). During the 1987 USAF-UES research effort several observed differences were discerned. For example, recordings of mine blasts revealed strong, relatively low-frequency Rayleigh waves guided by the upper crustal layers while earthquake recordings were dominated by shear and Lg waves (Figure 3). This observation is often explained as a difference of source depth (ie. earthquake sources commonly occur below the sedimentary wave guide). An additional difference between the two source signals was the relatively low frequency content of the mine blast signals relative to the earthquake signals. This observation can be explained as follows: the attenuation of the near surface mine blast energy in the earth's upper crust occurs, thus filtering-out high frequencies by the propagation path; on the other hand, the selected small shallow earthquakes were 2-4 km deep and thus retained their high frequency components as they were less attenuated. Or, the differences in the two source signals could be related to their intrinsic source properties. Although the mine blast sources are approximately the same size as the small shallow earthquakes, they are longer in duration due to the "ripple-firing" technique used at the Usibelli Coal Mine in Healy, Alaska. Ripple-

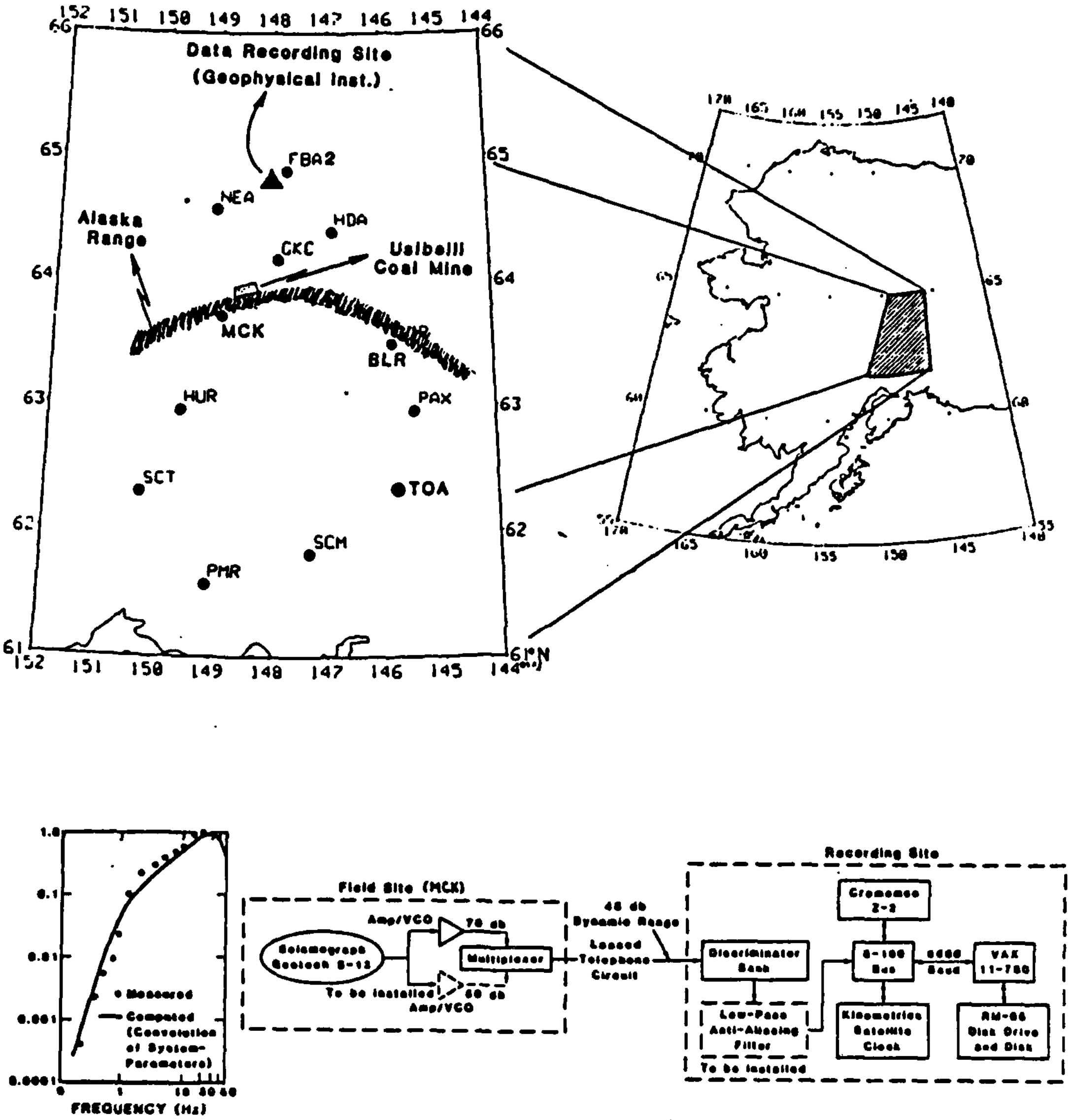

Figure 2. Location of the seismic station MCK, the data recording site at the University of Alaska-Fairbanks, and the location of the Usibelli Coal Mine (above). Configuration of data telemetry and recording of regional seismic data (below).

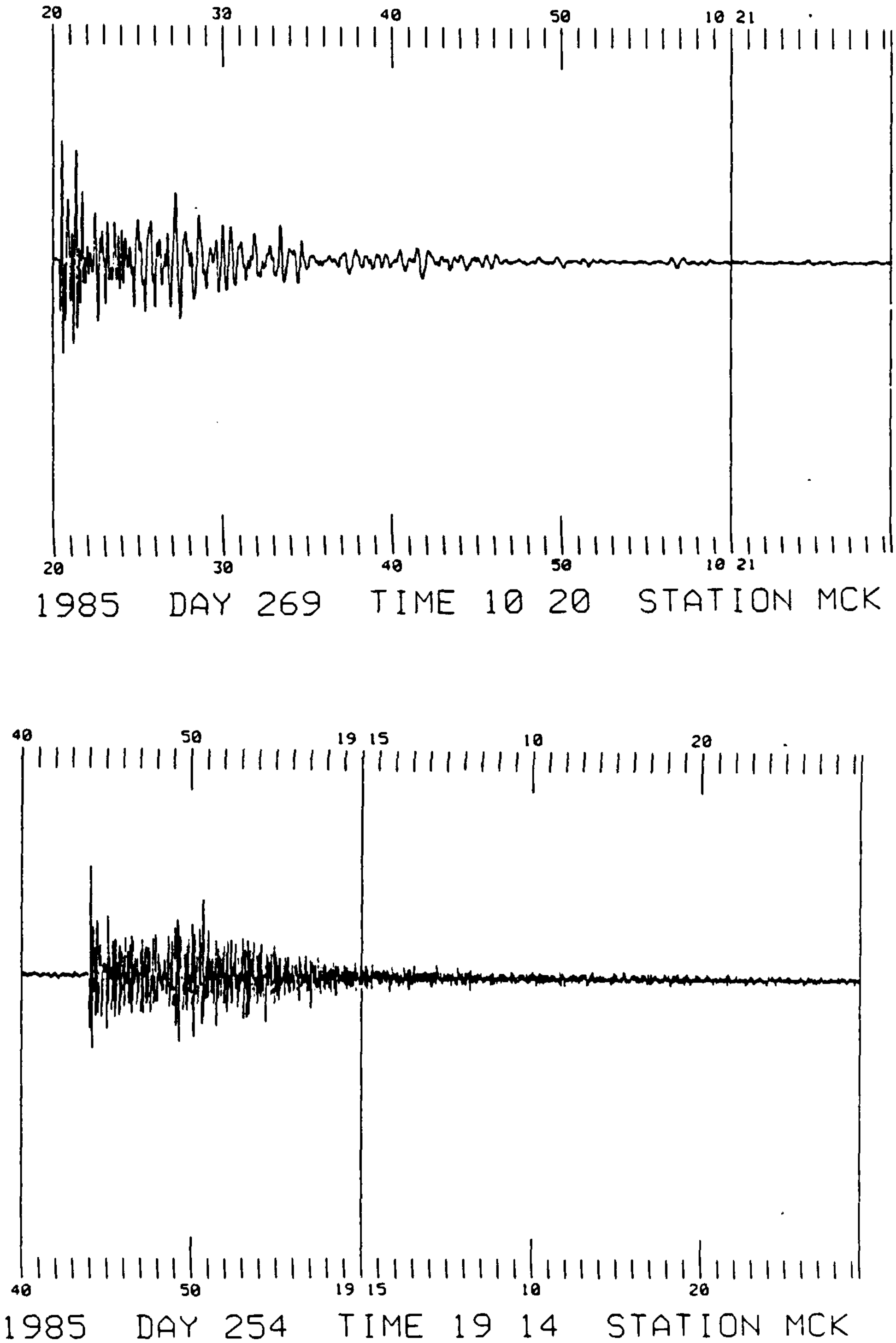

Figure 3. A 10,000 lb. coal mine explosion from the Usibelli Coal Mine in Healy, Alaska (above). A small shallow earthquake $<4\ M_L$ and 2 km hypocentral depth co-located in Healy (below).

firing effects could have been the explanation for the observation of more low-frequency energy in the mine blasts compared to the colocated earthquakes, however differences in near-surface geology could have also produced these differences. Unfortunately, there has not been a published scientific investigation that compares time-domain and spectral measurements for small, shallow earthquakes and economic explosions relevant to the seismic discrimination problem.

My primary goals as a 1987 USAF-UES research associate were to discern the differences between the selected small shallow earthquake and mine blast signals located in the same event area and, in addition, to use a theoretical modelling technique to create synthetic seismograms. Synthetic waveform modelling enables improved understanding of how observed properties of regional seismic signals are affected by source mechanism and propagation path. My research objectives as a 1988 program participant involved the continuation of synthetic waveform modelling and a subsequent quantification of the differences between the mine blast and earthquake signals.

Since previous efforts in synthetic waveform modelling of the Usibelli Coal Mine blasts, in Healy, Alaska, did not generate acceptable synthetic seismograms, several recommendations were made in the 1987 USAF-UES final report. These recommendations involved techniques that, if applied, could improve the fit of the prominant phases of the synthetic

seismograms with those of the observed seismograms. The theoretical modelling program, A-S-R-E-X-P, used last summer was again utilized for this investigation. A discussion of the algorithms can be found in Helmberger (1968) and Helmberger and Harkrider (1977). It was decided that I should apply my previously suggested recommendations to the modelling of the EMQBE data first. The basic philosophy behind this new approach was to identify techniques that worked on the controlled explosion source (the EMQBE data), then apply these techniques to the waveform modelling of the explosion source with the limited controlled source data base (the Healy mine blast data).

III.

a. I began the research effort by expanding the ray files used by the theoretical computer program. The compressional reflected and refracted waves used in generating the synthetic seismograms are specified in the computer program by numerically listing the crustal layers traversed by the seismic rays. Previous attempts at synthetic waveform modelling were made with a limited ray file. The earth's upper crust in Healy, Alaska is an ideal environment for compressional to shear wave (or vice versa) conversion. Sharp velocity interfaces exist between the upper alluvial sediments, schist, and lower granitic rocks (Jones et al., 1982). Therefore, the ray file was expanded to include converted rays and rays that

reverberate between crustal layers. A maximum total of 103 rays were used in the computations.

b. The results of the ray file expansion were successful. Synthetic seismograms generated after the ray file expansion, were more complex and revealed prominant phase arrivals.

IV.

a. The second step in the research effort was the generation of synthetic seismograms representative of the EMQBE data. A simplified model of the New England crust was utilized (Taylor, 1988). Previously, a single explosive source was used, however several researchers have shown that time-delayed blasting procedures, or ripple-firing, produce changes in the seismic signal (Frantti, 1963; Willis, 1963; Pilant and Knopoff, 1964; Greenhalgh, 1980; Baumgardt and Ziegler, 1987). Therefore, synthetic seismograms of the EMQBE data were generated with both a single source and multiple sources with 47, 69 and 72 time delays. For example, shot 3 (Figure 1), 24,350 lbs., had delays of 25 ms between charges in a row and 42 ms between each row. The majority of delays fell between 8-9 ms. The total duration of the explosive array was 659 ms. A more detailed discussion of the EMQBE can be found in Taylor et al., 1988.

b. Note, in figures 4 and 5, that the synthetic seismograms generated lengthen proportionally with increasing duration of the explosive array. In addition, distinct phases from crustal layering are obscured and the complexity of the waveforms increase as the number of shots and the delay interval increase. The observed complexities in the synthetic wave patterns suggest that those complexities, also observed in the EMQBE data, may have arisen partly from propagation path effects (closely arriving refractions and reflections).

V.

a. To improve the fit of the synthetic seismograms generated in section IV, gradational layers were added to the simplified Taylor (1988) model.

b. Note, in figure 6, that the added upper crustal discontinuities have increased the amplitude of the Pg phase (the ray reflected from the uppermost layer of the earth's crust) in the synthetic seismogram. Also note that this procedure has improved the fit of an observed station record with a generated synthetic seismogram.

VI.

a. The Usibelli Coal Mine blasts proved to be much more difficult to model compared to the EMQBE data, however the blasting information obtained from the Usibelli Coal Mine reveal that the coal mine

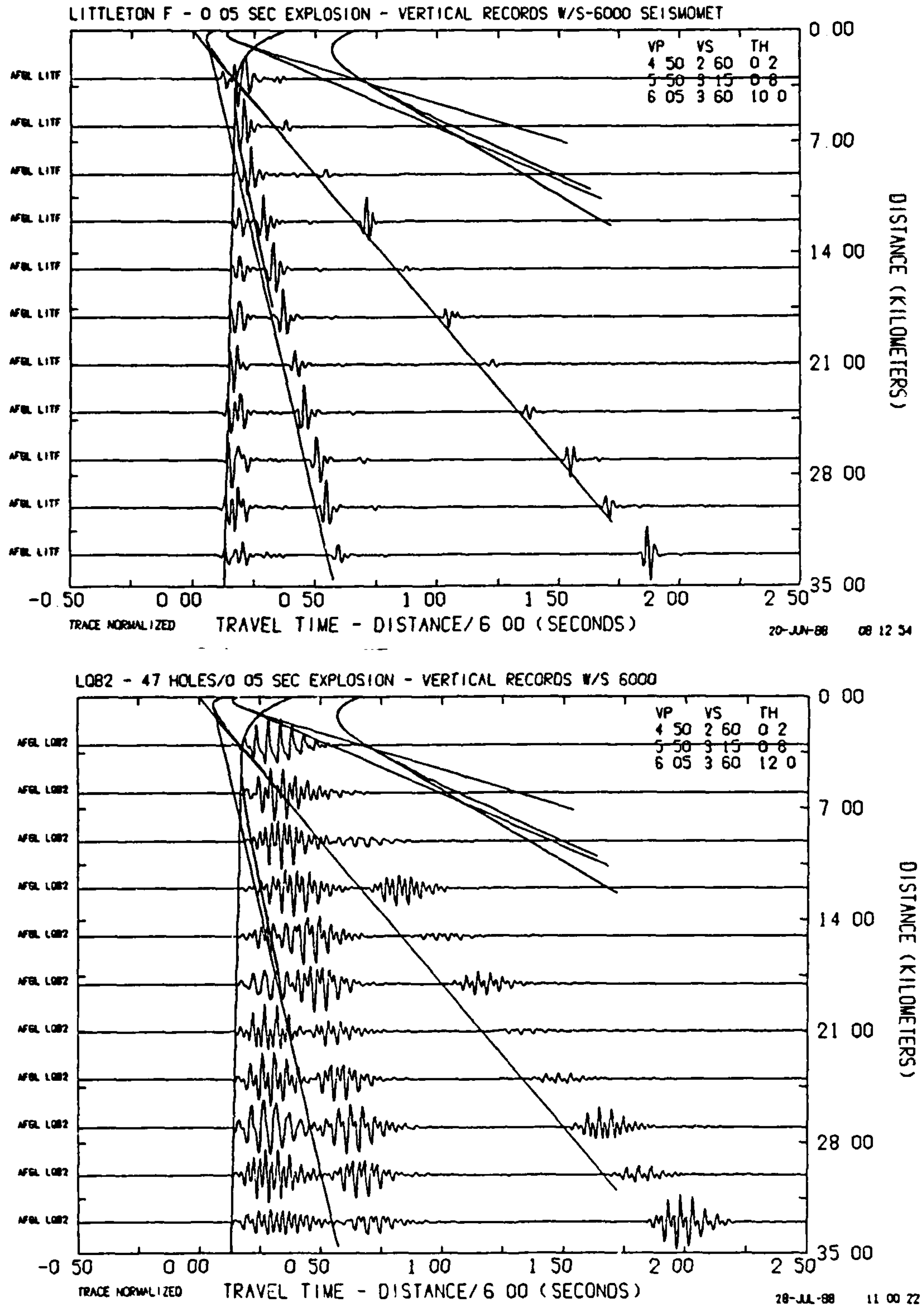

Figure 4. Vertical component synthetic record sections of the Eastern Massachusetts Quarry Blast Experiment. The single source blast (above) compared to the 47 multiple time delay blast (below) is less complex and reveal distinct phases from the crustal layering.

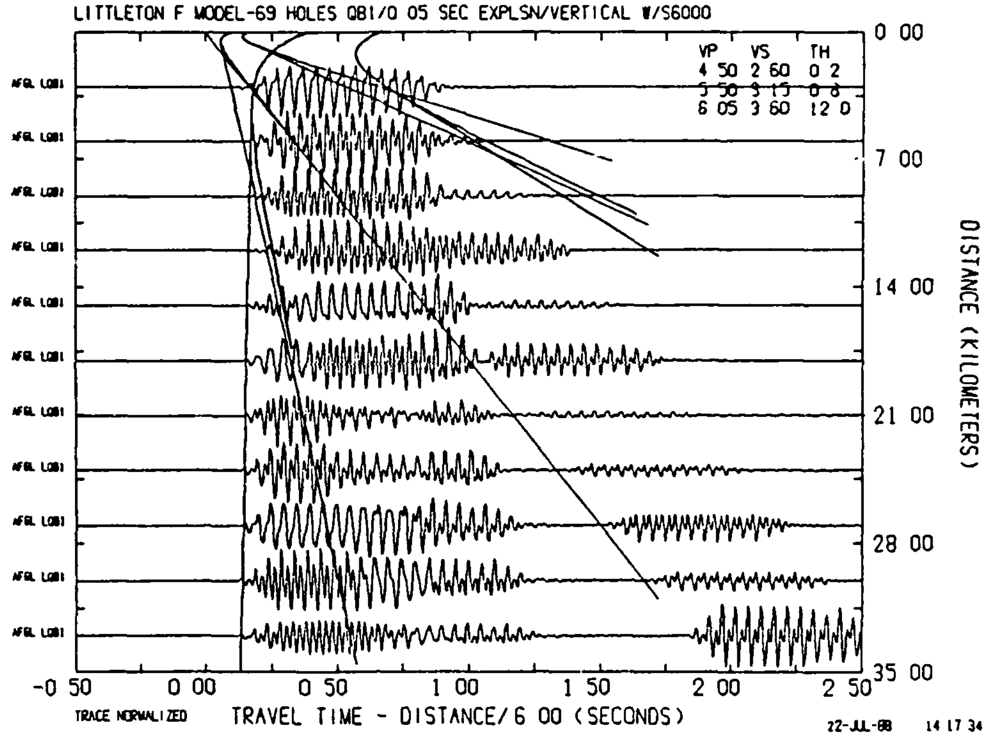

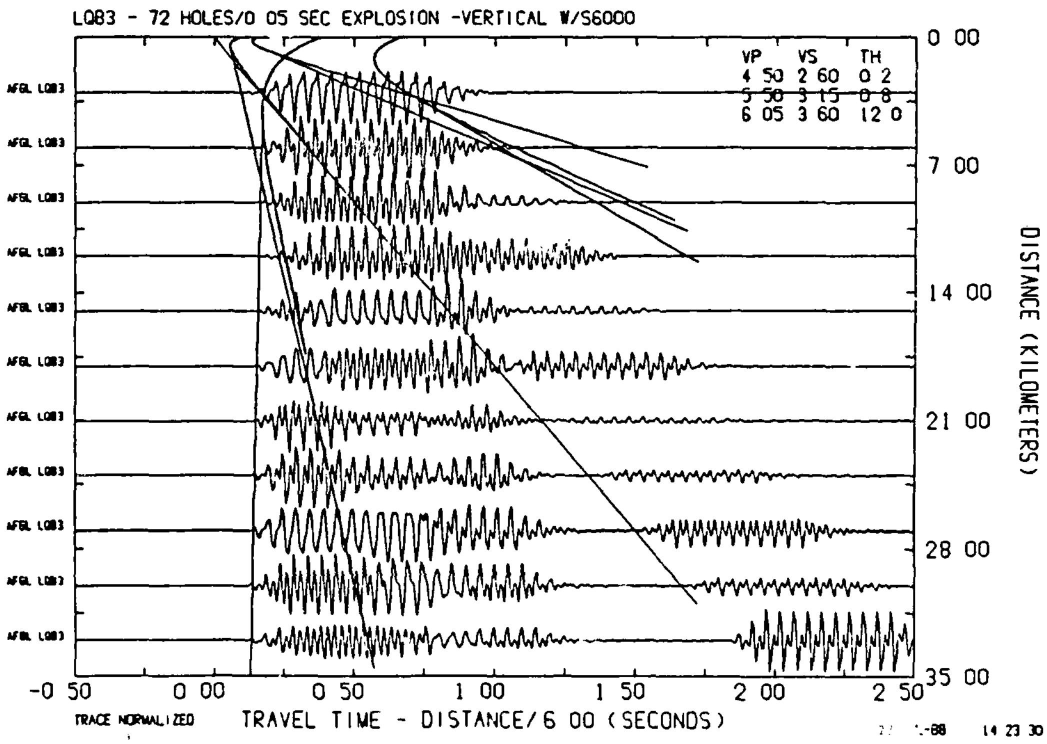

Figure 5. Vertical component synthetic record sections of the Eastern Massachusetts Quarry Blast Experiment. Note that the 69 (above) and 72 (below) multiple time delay blasts are more complex than those in figure 4.

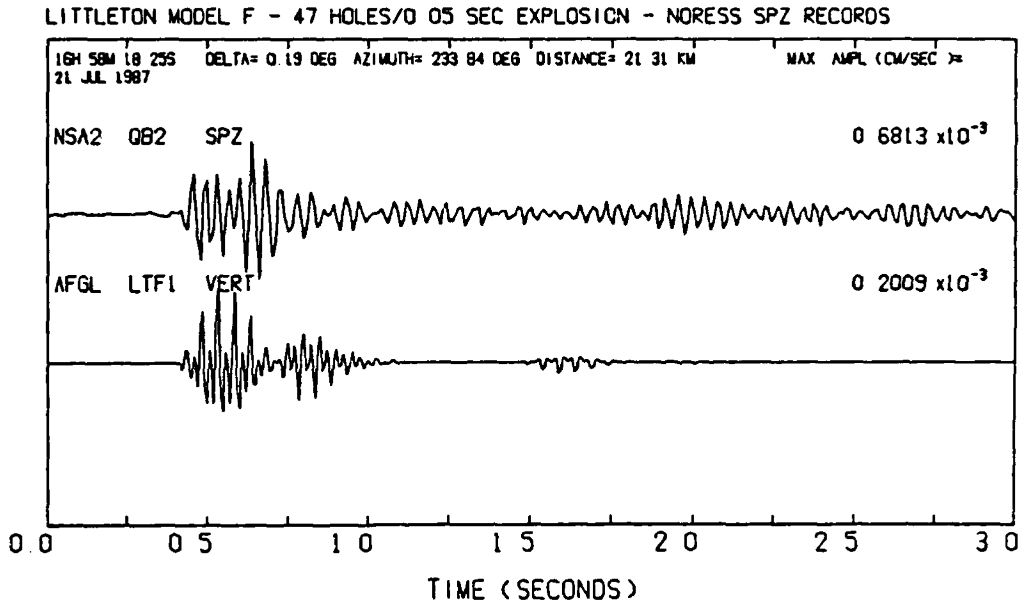

20-JUN-88 14 33 20

Figure 6. A synthetic seismogram (lower seismogram) of an array station used in a 47 multiple time delay blast from the Eastern Massachusetts Quarry Blast Experiment. Note how the synthetic is repre:·ntative of the observed seismogram (above).

blasting procedures vary from those used at the San Vel granodiorite quarry. Mine shot sizes varied from 500-200,000 lbs and the number of delays in a shot array varied from 30 to 200. Each shot had delays of 65 ms ± 10% between charges in a row. The ripple-firing method is intended to minimize ground vibration and to fracture the coal more efficiently. The Usibelli Coal Mine reported that local Healy residents claim that they can differentiate between shots that occur within the coal seams versus those that explode in the alluvial sediment overburden. Apparently, the vibration increases when shooting is located within the coal seam compared to the resultant vibration in the sediments. This suggests that the thick alluvial overburden does act as a sedimentary wave guide, and thus the differences between the colocated earthquakes and mine blast signals are due to near-surface geology. The longer 65 ms delays, compared to those used at the San Vel Quarry shot array, explains the longer period appearance of the Usibelli Coal Mine signals.

b. The results of the theoretical modelling of the Usibelli Coal Mine blasts using the Hanson, Berg and Gedney (1968) crustal model, and following the same procedures used for the EMQBE data, are as follows: First, the expansion of the ray file, procedure III, was successful in producing more complex seismograms with prominent phase arrivals. Second, the synthetic seismograms generated with a single source and increasing multiple source time delays produced the same results as those discussed in procedure IV. The synthetic seismograms lengthened

with increased duration of the explosive array and distinct phases from crustal layering were obscured. In fact, the generated synthetics, representative of the coal mine blast signals, were even more complex than those representative of the EMQBE data. Of course the geology of the Healy area is also more complex than the older, more homogeneous crust of New England. The Usibelli Coal Mine is located in the Alaska Range, a structurally complex melange of accretionary terranes. The observed complexities in the synthetic wave patterns suggest that they may have arisen from both propagation path effects and effects at the MCK station receiver (multiple reverberations). The addition of crustal discontinuities did not increase the complexity of the synthetic wave patterns (Figure 7).

VI. RECOMMENDATIONS:

Any further modelling should include an investigation of the effects of gradational layering in the uppermost crust of the Hanson, Berg and Gedney (1968) model. Since the MCK receiver is only 10 km from the source, the uppermost crust is the most significant. The Usibelli Coal Mine blast signals are less complex than those generated synthetically, therefore further suggesting crustal discontinuities in the uppermost layer(s). Once an appropriate crustal model is found, the modelling of the selected small shallow earthquakes should be easier. Further investigation into the source effects of ripple-firing would additionally prove interesting. A spectral feature that reflects an intrinsic difference between economic explosions and earthquakes would resolve the many questions present in seismic discrimination studies.

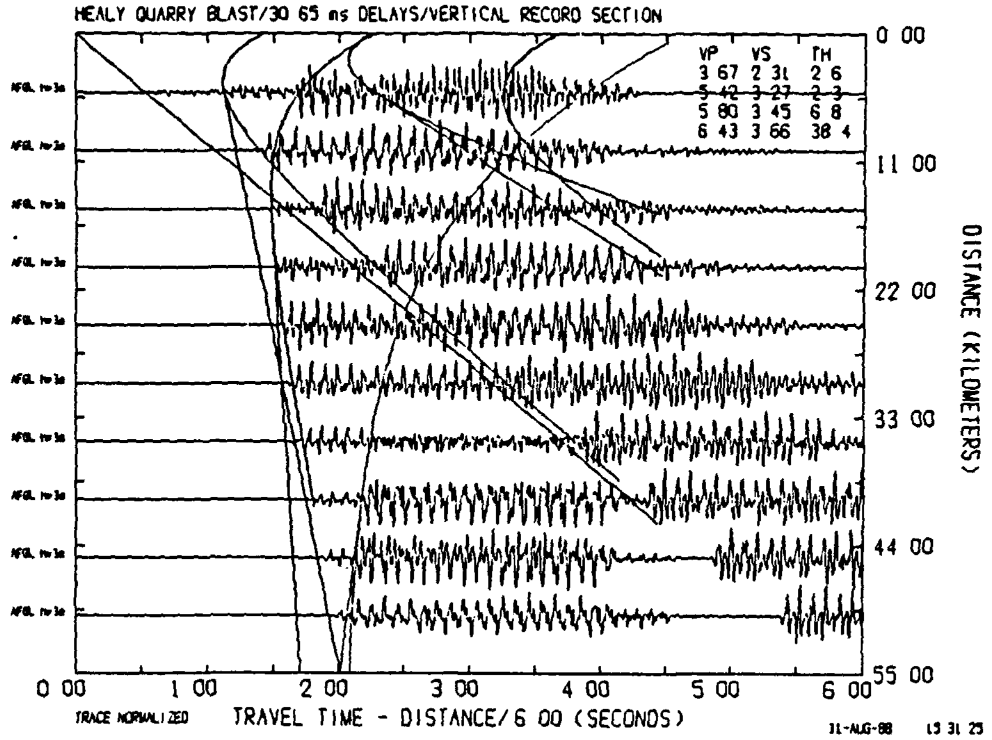

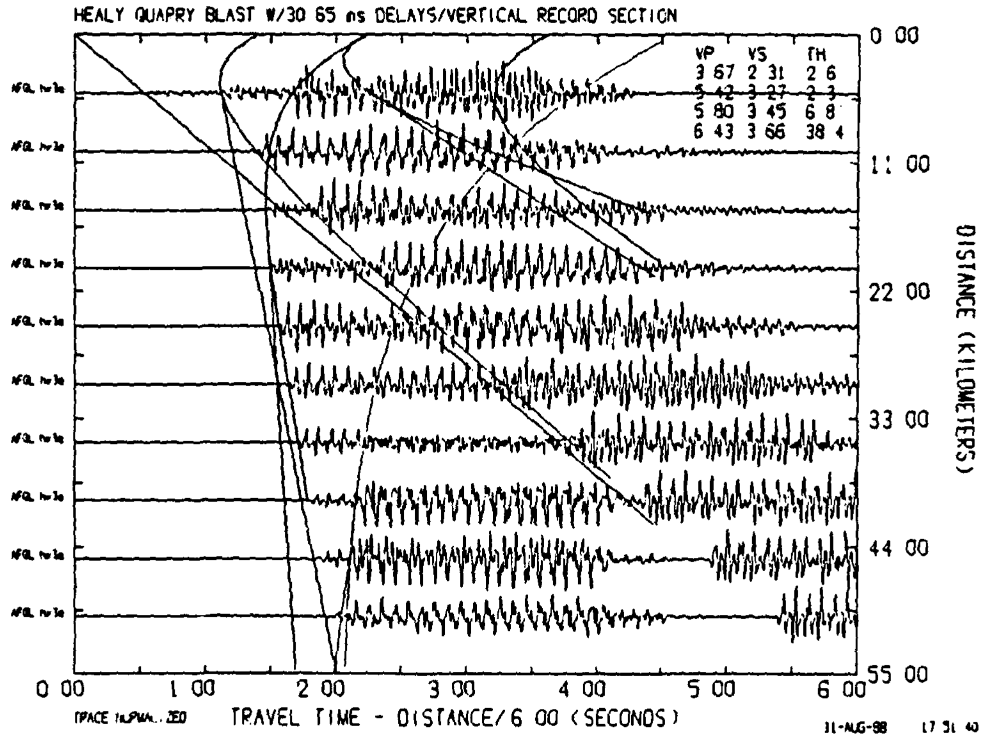

Figure 7. Vertical component synthetic record sections of a Healy Coal Mine blast with 30 multiple time delays. Note the complexity of these seismograms compared to those in figures 4 and 5. Also note that the addition of lower crustal discontinuities in the lower record section do not change the waveforms.

REFERENCES

Baumgardt, D. and K. Ziegler, Spectral Evidence for Source Multiplicity in Explosions, Air Force Geophysics Laboratory Report, AFGL-TR-87-0045, 1987.

Frantti, G., Spectral Energy Density for Quarry Explosions, Bulletin of the Seismological Society of America, 53, 989-996, 1963.

Greenhalgh, S., Effects of Delay Shooting on the Nature of P-Wave Seismograms, Bulletin of the Seismological Society of America, 70, 2037-2050, 1980.

Hanson, K., E. Berg, and L. Gedney, A Seismic Refraction Profile and Crustal Structure in Central Interior Alaska, Bulletin of the Seismological Society of America, 53, 989-996, 1968.

Helmberger, D., Generalized Ray Theory for Shear Dislocations, Bulletin of the Seismological Society of America, 64, 45-64, 1974.

Helmberger, D. and D. Harkrider, Modeling Earthquakes with Generalized Ray Theory, in Modern Problems in Elastic Wave Propagation, edited by J. Miklowitz and J. Achenbach, 499-518, John Wiley and Sons, New York, New York, 1977.

Jones, D., Silberling, N., Gilbert, W., and P. Coney, Character, Distribution, and Tectonic Significance of Accretionary Terranes in the Central Alaska Range, Journal of Geophysical Research, 87, 3709-3717, 1982.

Kirchoff, S., A Study of Small, Shallow Earthquakes and Quarry Blasts in Healy, Alaska, USAF-UES Report of SFRP and GSRP Fellows, 1987.

Kirchoff, S., Differences in Seismic Signal Characteristics between Small, Shallow Earthquakes and Quarry Blasts, EOS, 86, 355, 1987.

Kirchoff, S., Crustal Structure Beneath the Tularosa Basin in the White Sands Missile Range, New Mexico, M. A. Thesis, Boston University, 1986.

Pilant, W. and L. Knopoff, Observations of Multiple Seismic Events, Bulletin of the Seismological Society of America, 54, 19-39, 1964.

Taylor, C., Shallow Crustal Structure of Eastern Massachusetts, EOS, 69, 405, 1988.

Taylor, C., Stump, B., and A. Kafka, Data Report on the Littleton Quarry Blast Experiment (LQBE), Air Force Geophysics Laboratory Report, in press.

Willis, D., A Note on the Effect of Ripple Firing on the Spectra of Quarry Shots, Bulletin of the Seismological Society of America, 53, 79-85, 1963.

Gas Phase Ion-Molecule Reactions of Carbocations

by

Thomas C. Pentecost

ABSTRACT

In an effort to find and characterize association reactions that proceed via radiative stabilization the reactions of CH_3+, CD_3+, CF_3+, and CCl_3+ with NO and SO_2 were studied as functions of temperature and pressure. Pressures ranged from 0.3 to 1.0 torr and temperatures ranged from 190K to 470K. The dependence of α on temperature, pressure, and helium flow was also studied. The results fall into three categories: association reactions, charge transfer reactions, and reactions which do not appear to occur under our experimental conditions. The CH_3+/SO_2 and CD_3+/SO_2 systems were found to give only the association product. The CF_3+/SO_2 system appeared to associate but the data requires further analysis. The CH_3+/NO and CD3+/NO systems were found to charge transfer only. The CF_3+/NO system appeared to charge transfer but the data requires further analysis. In none of the systems studied was charge transfer with SO_2 observed. CCl_3+ did not appear to react with either NO or SO_2. Alpha, α, demonstrated an apparently linear dependence on helium flow. This dependence was found to be much greater than any dependence of α on temperature or pressure.

1988 USAF-UES SUMMER FACULTY RESEARCH PROGRAM/
GRADUATE STUDENT RESEARCH PROGRAM

Sponsored by the

AIR FORCE OFFICE OF SCIENTIFIC RESEARCH

Conducted by the

Universal Energy Systems, Inc.

FINAL REPORT

Gas Phase Ion-Molecule Reactions of Carbocations

Prepared by: Thomas C. Pentecost

Academic Rank: Graduate Student

Department and University: Dept. of Chemistry, Louisiana State University

Research Location: AFGL/LID

USAF Researcher: Dr. John F. Paulson

Date: 05-Sept.-88

Contract No: F49620-88-C-0053

Acknowledgements

This work would not have been possible without several individuals. First of all I wish to thank the Air Force Systems Command and the Air Force Office of Scientific Research for their sponsorship of the summer program that provided me the opportunity to carry out this research. Also I must thank Universal Energy Systems for their administering of this program and their help and advice in the administrative aspects of the summer.

There are many people that contributed to this effort, the foremost being my research advisor Dr. Lucia Babcock. Her vast scientific knowledge, teaching ability, and friendship are all greatly appreciated. I also wish to thank the people at AFGL/LID, in particular John Paulson, Bob Morris, Al Viggiano, Charlie Gallagher, Carol Deakyne, and last but certainly not least Fred Dale for the use of their laboratory. Special thanks go to Fred Dale for his unselfish sharing of his twenty-five years of practical knowledge.

I. INTRODUCTION

The competition between collisional stabilization and radiative stabilization of ion-molecule association products presents an interesting study. The process of radiative stabilization has played an important role in the modeling of interstellar chemistry[1]. This process has been invoked in numerous models, but has only recently begun to receive corroborating experimental evidence[2]. The importance of radiative stabilization in interstellar space is due to the very low number densities of inert third-bodies that can collisionally stabilize the complex.

The mechanism for ion-molecule association reactions which may proceed via both radiative and collisional processes is given, for positive ions, in equations 1-3.

$$A^{+} + B \underset{k_{-1}}{\overset{k_1}{\rightleftharpoons}} (AB^{+})^{*} \qquad (1)$$

$$(AB^{+})^{*} \xrightarrow{k_2(M)} AB^{+} \qquad (2)$$

$$(AB^{+})^{*} \xrightarrow{k_3} AB^{+} + h\nu \qquad (3)$$

In this scheme $(AB^+)^*$ is the excited intermediate complex that may be stabilized by removal of energy, either by a radiative process or by a collisional process, or may dissociate back to reactants. This unimolecular decay coefficient, k_{-1}, in equation 1 is an important parameter in association reactions. It is related to the average lifetime of the excited intermediate with respect to dissociation back to reactants. If any stable association product is to be observed then collisional stabilization and/or radiative stabilization, whose corresponding rate coefficients are k_2 and k_3, must be competitive with respect to unimolecular decay back to reactants.

If one assumes a steady state for the excited intermediate, $(AB^+)^*$, then the overall rate coefficient, k_{OBS}, is given by equation 4:

$$k_{OBS} = \{k_1 [k_2(M) + k_3]\}/\{k_{-1} + k_2(M) + k_3\}. \qquad (4)$$

It can be seen that k_{OBS} depends upon the pressure, since pressure is a direct measure of (M). The general form of the curve generated by this expression is shown in Figure 1 [3]. If radiative stabilization is not important, $k_3 = 0$, the curve in Figure 1 will have the same form but a zero intercept. The presence of a non-zero intercept suggests that radiative stabilization may play an important role in the mechanism, but one must exercise caution in extrapolating outside the experimental pressure range. If one is in the curved region of Figure 1 then extrapolation to zero pressure would give a non-zero intercept with or without an active radiative process.

The temperature dependence of ion-molecule association reactions is not as explicit from the expression of k_{OBS} as is the pressure dependence. The temperature dependence of the overall rate coefficient is determined by the temperature dependence of each of the individual rate coefficients that make up k_{OBS} in equation 4. The term in equation 4 with the strongest temperature dependence is the unimolecular decay back to reactants, whose rate coefficient is given by k_{-1}. The assumption that k_{-1} determines the overall temperature is not unreasonable because collisional stabilization, rate coefficient k_2, has been shown by theory to have a negligible temperature dependence[4]. The process of radiative stabilization, rate coefficient k_3, is not expected to possess any temperature dependence. This leaves only k_1 and k_{-1}. The formation of the initial complex, rate coefficient k_1, will, according to ADO theory[5], demonstrate a slight inverse temperature dependence if the neutral possesses a permanent electric dipole moment. This dependence cannot account for the large magnitude of the observed temperature dependence and does not explain the temperature dependence of reactions where the neutral does not have a permanent electric dipole moment. We can then safely say that the unimolecular decay process dominates the temperature deoendence of k_{OBS}. The unimolecular decay has a positive temperature dependence, and since it is in the denominator of k_{OBS}, we expect k_{OBS}, the overall rate coefficient to show a

negative temperature dependence.

II. OBJECTIVES

The goal of the present study is to find and characterize examples of ion-molecule association reactions which proceed via radiative stabilization. In previous studies[6,7] F- addition to BF_3 was found to proceed via a radiative stabilization process. In this work we have looked for this process in systems isoelectronic or isovalent with BF_3. The reactant ions used were CH_3+, CD_3+, CF_3+, and CCl_3+. Two neutral reactants were used, NO and SO_2. The choice of SO_2 was made because it is isovalent with NO_2- which adds to BF_3, and NO was chosen since energetics of some reactions implied the charge transfer reactions to be near thermoneutral in some cases. It was hoped that, at the lower temperatures, NO might associate and charge transfer, when energetics permit, or just associate when energetics do not allow charge transfer. The temperature and pressure dependence of these reactions were studied and the data are being analyzed in the manner described in the previous study by Herd and Babcock[6]. Upon completion, our work will determine whether radiative stabilization occurs in these association reactions of carbocations, and perhaps will provide additional experimental evidence for the radiative process invoked in interstellar models. If radiative stabilization is observed in these carbocation systems, it will be exciting since carbocations are some of the most abundant ions in interstellar media.

III. EXPERIMENTAL

All the reactions presented in this report were studied on the AFGL-Selected Ion Flow Tube-DRIFT(AFGL/SIFT-DRIFT) at Hanscom AFB, MA. Only the SIFT aspect of this instrument was utilized in this study; therefore, only the SIFT apparatus will be described. The SIFT technique is a modification of the conventional flowing afterglow (FA) experiment. It was developed by Adams and Smith at the University of Birmingham, Birmingham England[8]. The SIFT instrument is shown schematically in Figure 2. It consists of a high pressure ion-source in which ions are generated[9]. The desired reactant ion is then mass selected by a quadrupole mass

filter. It is then injected into the reaction region. This process is complicated by the high pressure of the reaction region, 0.3-1.0 torr, relative to the quadrupole mass filter, 10^{-5} torr. This is overcome by the use of a specially designed injector, the Venturi injector. The ions are then mixed with the buffer gas, helium in this study, and laminar flow is established. At some point downstream the neutral reactant gas is injected into the flow. The ion-molecule reactions occur from this point to a sampling orifice which separates the reaction region from the detection region. The detection chamber is differentially pumped and contains a second quadrupole mass filter which filters product ions. These product ions are then detected by an electron multiplier. The decrease in the reactant ion concentration, in counts per second, is monitored as a function of neutral gas flow rate.

An important parameter in the calculation of the rate coefficient is the ion velocity. This differs from the bulk flow velocity because the ions are sampled at the tip of the parabolic flow profile; recall laminar flow is established. The quantity α is the ratio of the ion velocity to the bulk flow velocity. This α is measured by a time-of-flight experiment; α has a theoretical upper limit of 2[10]. During the course of our study we measured α as a function of temperature, pressure, and helium flow. The time-of-flight experiment involves perturbing the ion swarm at some known distance from the detector and then measuring the amount of time the perturbation takes to reach the detector. Dividing the known distance by this measured time gives us the ion velocity in the flow tube. The time-of-flight is measured using a Davidson multichannel analyzer. As mentioned before, the rate coefficient, k_{OBS}, is measured by observing the decrease in the reactant ion concentration as a function of neutral reactant flow. The rate law for the generalized reaction:

$$A+ \quad + \quad B \longrightarrow C+ \quad + \quad D \tag{6}$$

is given by:

$$d(A+)/dt = -k(B)(A+) \tag{7a}$$

or

$$d(A+)/(A+) = -k(B)dt \quad . \tag{7b}$$

This differential equation gives the loss of (A+) as a function of time. Since in general it is easier to vary (B) than time experimentally, it is most common in FA, SIFT, and SIFT-DRIFT reactors to monitor the loss of (A+) as a function of (B), which is proportional to the flow of (B), at constant time. Using:

$$dt = dz/\bar{v} \quad , \tag{8}$$

where z is the reaction distance and $\bar{v}$ is the bulk flow velocity, upon integration one obtains:

$$\ln(A+) - \ln(A+)_0 = -kz(B)/\bar{v} \quad . \tag{9}$$

This equation may be rearranged to give k as a function of an experimentally measured variable, such as (B). Upon doing this one obtains:

$$k = - \{ [\ln(A+)_2-\ln(A+)_1]/[(B)_2-(B)_1] \}*(\bar{v}\alpha/z) \tag{10}$$

where the term α is included because we need the ion-velocity not the bulk flow velocity; recall α is the ratio of the ion velocity and the bulk flow velocity. Therefore to obtain the value of k_{OBS} one determines the slope of a plot of ln(A+) versus (B) and multiplies it by $(\bar{v}\alpha/z)$ and appropriate conversion factors to get k_{OBS} in units of $cm^3 molecule^{-1} s^{-1}$.

The operating pressure of the upstream, source, quadrupole was typically 10^{-4}-10^{-5} torr, and the downstream, detector, quadrupole was typically 10^{-6}-10^{-7} torr. Pressures in the reaction region ranged from 0.25 torr to 1.00 torr in helium. The helium flow range was 6.50 to 13.80 standard liters per minute (slm). The pressure in the reaction zone was controlled by adjusting the helium flow or by throttling the roots pump with a MKS butterfly valve. The helium buffer gas was passed through molecular sieve at 77K, cooled by liquid nitrogen, to remove any impurities. The reactant ions were generated from commercially available gases and used without purification, except CCl_3+ which was produced from liquid CCl_4 that had undergone a series of freeze-pump-thaw cycles. Freon-13, $CClF_3$, was used to produce CF_3+. Methane (Matheson UHP) and d^4_methane (MSD Isotopes 99.7% d and ICN Biomedicals 99% d) were used as sources of CH_3+ an CD_3+ respectively. The neutral reactant gases were also obtained

AD-A204 243 UNITED STATES AIR FORCE GRADUATE STUDENT RESEARCH 5/8
PROGRAM PROGRAM TECHNIC..(U) UNIVERSAL ENERGY SYSTEMS
INC DAYTON OH R C DARRAH ET AL. DEC 88
UNCLASSIFIED AFOSR-TR-89-0041 F49620-85-C-0013 F/G 5/1 NL

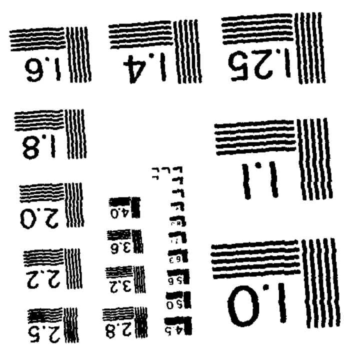
1.0
1.1
1.25
1.4
1.6
1.8
2.0
2.2
2.5
2.8
3.2
3.6
4.0

commercially and used without further purification. The SO_2 used (Scientific Gas Products) was reported to be 99% pure. The NO used (Matheson Gas Products) was 99% pure with impurities of 0.5% N_2, 0.2% CO_2, 0.05% N_2O. and 0.05% NO_2.

Temperature studies were also a large part of this work. The flow tube was heated by five platinum resistance heaters spaced along the flow tube. Cooling was achieved by circulating chilled methanol or liquid nitrogen through a series of copper heat exchanger coils running along the flow tube. The temperature range accessible with this system is roughly 80K to 600K.

IV. RESULTS

The results from the eight systems, each examined at four temperatures, conveniently divide themselves into three categories: association reactions, charge transfer reactions, and reactions which do not appear to occur under our experimental conditions. Also studied was the dependence of α upon temperature, pressure, and helium flow.

A. Association Reactions

1. $CH_3^+ + SO_2 \longrightarrow CH_3SO_2^+$ (11)

The reaction in equation 11 was studied using the AFGL/SIFT. The rate coefficient was measured over a temperature range of 196K to 468K and a pressure range of 0.3 to 0.9 torr in helium. This temperature and pressure range corresponds to a helium concentration range of 9.0 X 10^{15} to 3.9 X 10^{16} molecule^{1}cm^{-3}. The only product ion observed was $CH_3SO_2^+$, at 79 amu. At constant temperature and various pressures the observed rate coefficient, k_{OBS}, shows an apparently linear pressure dependence. In general k_{OBS} shows a negative temperature dependence, whose explicit functional form has yet to be determined from our data; see Figure 3. The largest value of k_{OBS}, at lowest temperature and highest pressure, is forty percent of the ADO rate, recall that the ADO rate is the theoretical upper limit of the rate coefficient. In general k_{OBS} behaves as expected for an association reaction as discussed in the introduction. As shown in Figure 3 there appears to be a non-zero intercept in the plot of k_{OBS} versus helium

concentration. This suggests that radiative stabilization may be playing a role.

2. $CD_3^+ + SO_2 \longrightarrow CD_3SO_2^+$ (12)

This reaction was studied using the AFGL/SIFT. The rate coefficient was measured over a temperature range of 191K to 468K and a pressure range of 0.25 to 0.90 torr in helium. This temperature and pressure range corresponds to a range of helium concentrations of $9.0X10^{15}$ to $3.3X10^{16}$ molecule^{1}cm^{-3}. The only product ion observed was the association product, $CD_3SO_2^+$, at 82 amu. As can been seen from Figure 4 k_{OBS} shows a negative temperature dependence and a positive pressure dependence. The largest value of k_{OBS} is approximately sixty percent of the ADO rate. The CD_3^+ rates are also roughly twice the CH_3^+ values of k_{OBS}. There also appears to be a non-zero intercept in the plot of k_{OBS} versus helium concentration, see Figure 4. This suggests that radiative stabilization may be active in this system.

3. $CF_3^+ + SO_2 \longrightarrow CF_3SO_2^+$ (13)

This reaction was studied using the AFGL/SIFT. The reaction was studied over a temperature range of 213K to 372k and a pressure range of 0.4 to 1.0 torr in helium. The only product ion observed was the association product, CF_3SO_2, at 133 amu. The determination of the rate coefficient was complicated because after an initial decrease in the CF_3^+ concentration the concentration appears to level off as more neutral, SO_2, is added. The overall reaction appears to be very slow and it is not yet clear what is causing the curvature in the plot of $\log(CF_3^+)$ versus flow of SO_2. A more detailed analysis is required to determine what is causing the curvature and to ascertain whether radiative stabilization is playing any role in the formation of $CF_3SO_2^+$.

B. Charge Transfer Reactions

The next group of reactions to be discussed are charge transfer reactions. Initially it was hoped that at low temperatures some association might be seen even where charge transfer is energetically feasible. This was not the case, for even at the lowest temperature of this study, approximately 190K,

only charge transfer products were observed. Table I summarizes the results of the charge transfer experiments. Each reaction will be discussed briefly below.

1. $CH_3+ + NO \longrightarrow NO+ + CH_3$ (14)

The thermochemistry for this reaction indicates that the charge transfer is 0.58 eV exothermic, as calculated from the literature values of the IP(CH_3) and IP(NO)[11]. Our results show the charge transfer rate coefficient not to have any pressure or temperature dependence over our ranges of 193K to 463K and 0.3 to 0.9 torr in helium. This rate coefficient is equal to the ADO rate, within experimental error. The only product ion observed was NO+, at 30 amu. The neutral product in equation 14, CH_3, is inferred since we were not able to detect neutral products under our experimental conditions.

2. $CD_3+ + NO \longrightarrow NO+ + CD_3$ (15)

This reaction is exothermic by 0.57 eV, again calculated from the IP's of CD_3 and NO[11]. This reaction demonstrated no temperature or pressure dependence over our range of 193K to 463K and 0.35 to 0.90 torr in helium. The only product ion observed under our experimental conditions was NO+, at 30 amu. The rate coefficient measured is equal, within experimental error, to the ADO rate.

3. $CF_3+ + NO \longrightarrow NO+ + CF_3$ (16)

This charge transfer is approximately thermoneutral, with $\Delta H = +0.09$ eV calculated from the IP's[11]. Because no strongly exothermic, bimolecular charge transfer exists for this system, there was a possibility that the association reaction might be observed even though no evidence for such a reaction was seen in the CH_3+ or CD_3+ reactions with NO. This was not the case, as even at the low temperature and the highest pressure, conditions which favor association, NO+ at 30 amu was the only product ion detected. The rate coefficient displayed no temperature or pressure dependence over our experimental range of 213K to 372K and 0.4 to 0.9 torr in helium. Unlike the other charge transfer reactions discussed, the rate coefficient for this reaction was found to be only 0.3 percent of the ADO rate. This low k_{OBS}

could be due to the near thermoneutrality of the reaction, to the reaction of a small fraction of excited CF_3^+ ions, or to reaction of CF_3^+ with one of the impurities in NO. This is an area of further work, to determine the thermochemistry of the reactions of CF_3^+ with the NO impurities to give the NO^+ product observed.

TABLE I $CX_3^+ + NO \quad NO^+ + CX_3$

Charge Transfer Rates

CX_3^+	k_{EXP}	k_{ADO}
CH_3^+	$(1.0 + 0.1) \times 10^{-9}$	9.8×10^{-10}
CD_3^+	$(9.9 + 0.7) \times 10^{-10}$	9.2×10^{-10}
CF_3^+	$(1.8 + 0.6) \times 10^{-12}$	6.8×10^{-10}

C. Systems That Do Not Appear To React

Both SO_2 and NO do not appear to react with CCl_3^+ under our experimental conditions, 0.5 torr in helium and temperatures of 215K, 300K, and 500K. This non-reactivity was determined by taking reactant ion mass spectra and then taking mass spectra again upon addition of the neutral reactant. There was no distinguishable decrease in the CCl_3^+ concentration nor did any new ions appear upon addition of SO_2 and NO. This is interesting since the charge transfer reaction

$$CCl_3^+ + NO \longrightarrow NO^+ + CCl_3 \qquad (17)$$

is endothermic by 0.48 eV[10]. It appears that in this case if NO cannot charge transfer it does not associate either. This is similar to the previous results discussed since no association products were seen with CH_3^+, CD_3^+, and CF_3^+. Also none of the reactant ions studied underwent charge transfer with SO_2. These reactions are all very endothermic, 2.5 eV to 3.5 eV[11]. As mentioned earlier CCl_3^+ did not charge transfer or associate with SO_2 under our experimental conditions.

D. Alpha Value Investigation

In the course of our experiments we have determined α values as a function of temperature, pressure, and helium flow rate. The strongest dependence appears to be on upon the helium flow rate. A typical plot of α versus pressure and one of α

versus helium flow at a constant temperature are shown in Figure 5. The points below 0.5 torr on the α versus pressure plot are points in which the helium flow was changed to obtain the desired pressure, so the α's appear to increase as pressure increases. However, for the points above 0.5 torr where the gate valve in the roots pump line was used to increase the pressure, i.e. helium flow is constant, it is clear that α is not dependent upon pressure. Part B of Figure 5 clearly indicates that α increases monotomically as the flow of helium is increased regardless of the pressure.

V. Further Work

There are several aspects of this work to be continued and expanded upon, many of which have already been alluded to in the preceding discussion. These include a detailed calculation from our data of the temperature dependence of the observed rate coefficients. Another aspect is to perform these reactions on our flowing afterglow (FA) at LSU using different third-bodies, an advantage that FA offers over SIFT experiments. Using different third-bodies is useful because it allows one to change the "effective" pressure. This means various regions of the curve in Figure 1 can be sampled. By doing this we can determine if the non-zero intercept we observe is due to of radiative stabilization or due to extrapolation from the curved region of Figure 1. These experiments must be carried out in a FA rather than a SIFT. The SIFT is limited to light third bodies (buffer gases) because of the need to inject ions from the upstream quadrupole at low pressure to the reaction region at high pressure. The FA is not limited to helium and hydrogen as buffer gases and N_2, CH_4, CO_2, as well as other heavier gases can be used. With the FA data to supplement the SIFT data already taken we hope that we can determine whether these systems are undergoing radiative stabilization. Another area of future work involves instrument modifications designed to look spectroscopically for the emitted photon. Therefore it is important to characterize completely any system that might be radiating so as to facilitate the spectroscopic experiments.

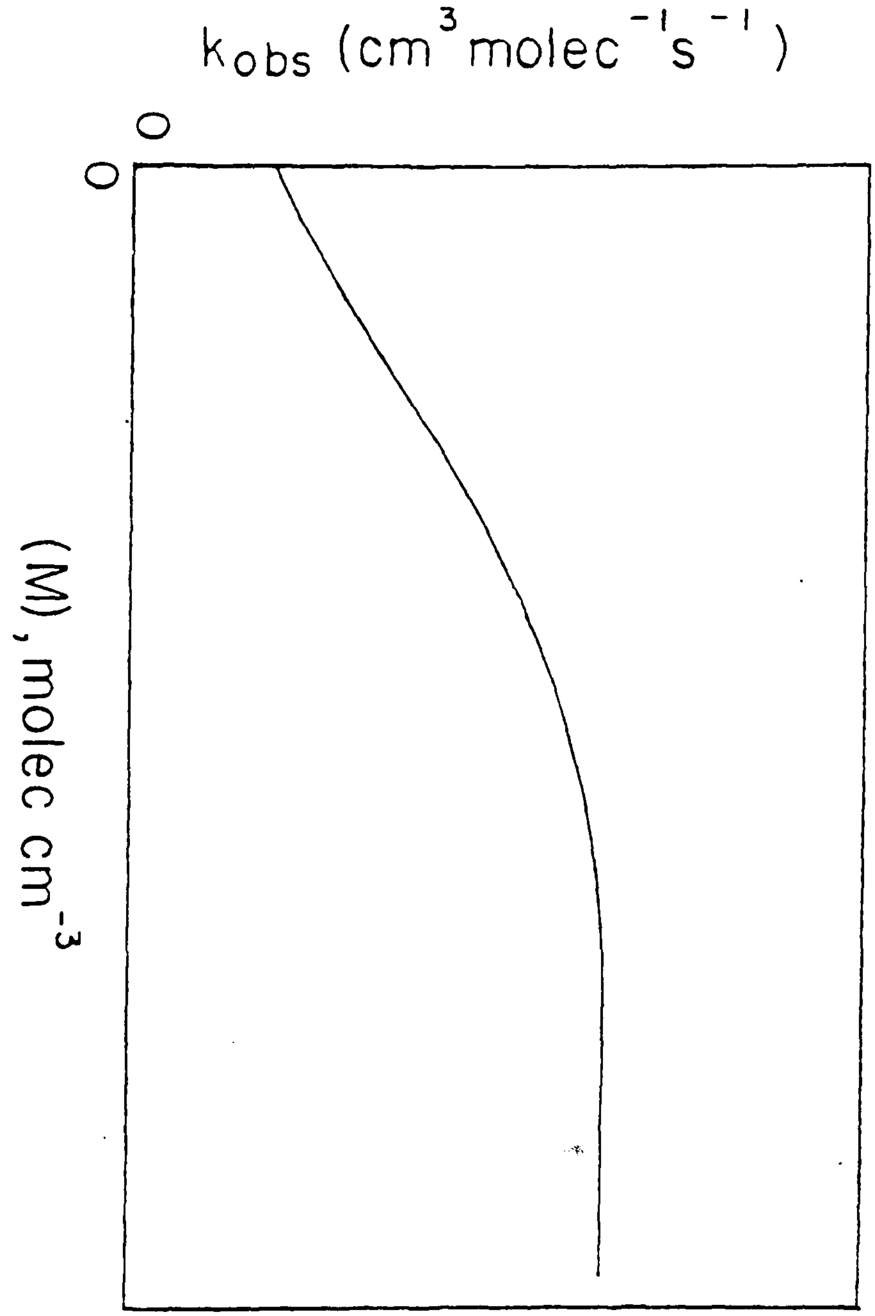

Figure 1 Generalized Pressure dependence of k_{obs}, with radiative stabilization

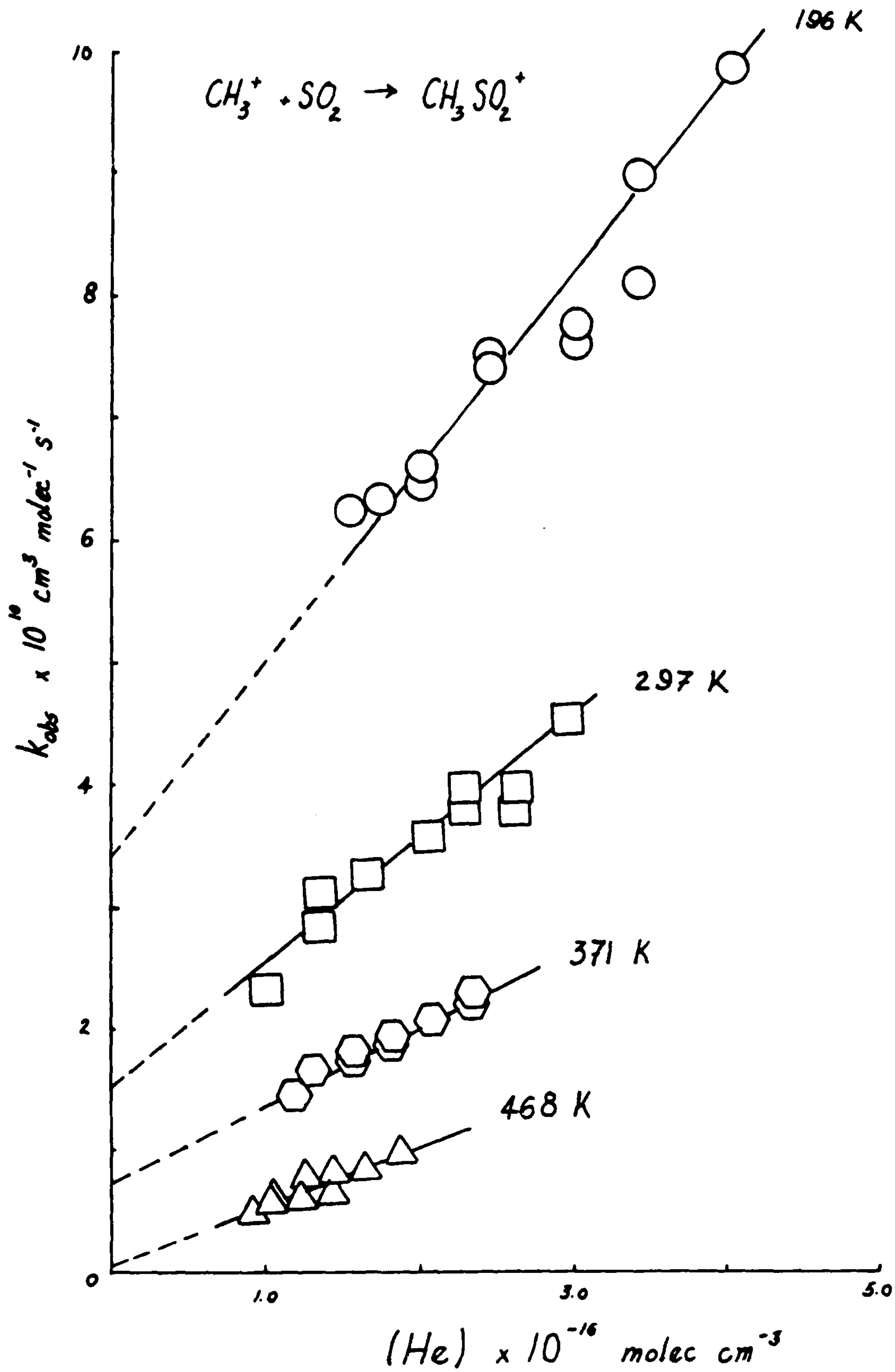

Figure 3: CH_3^+/SO_2 Temperature and (He) Dependences

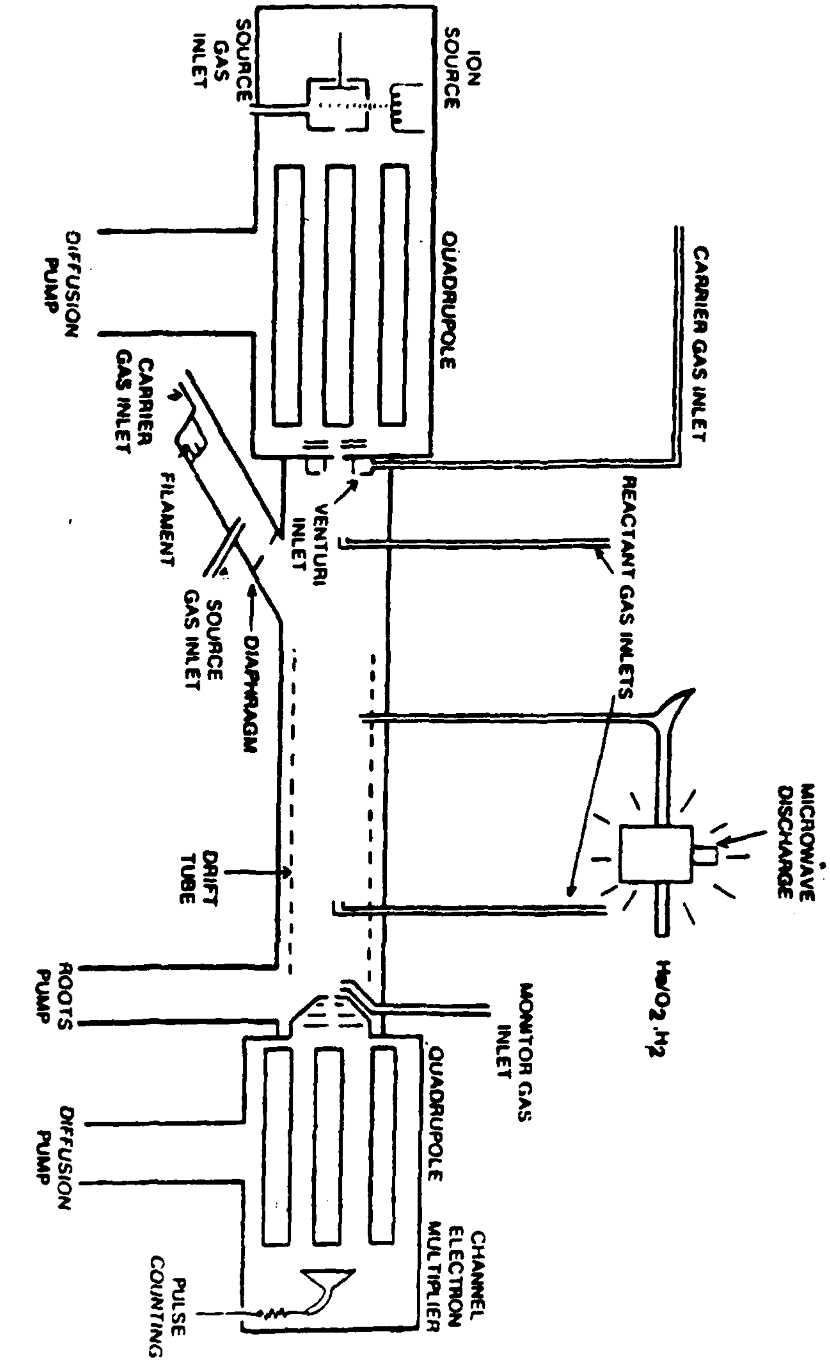

Figure 2: AFGL/SIFT-DRIFT instrument

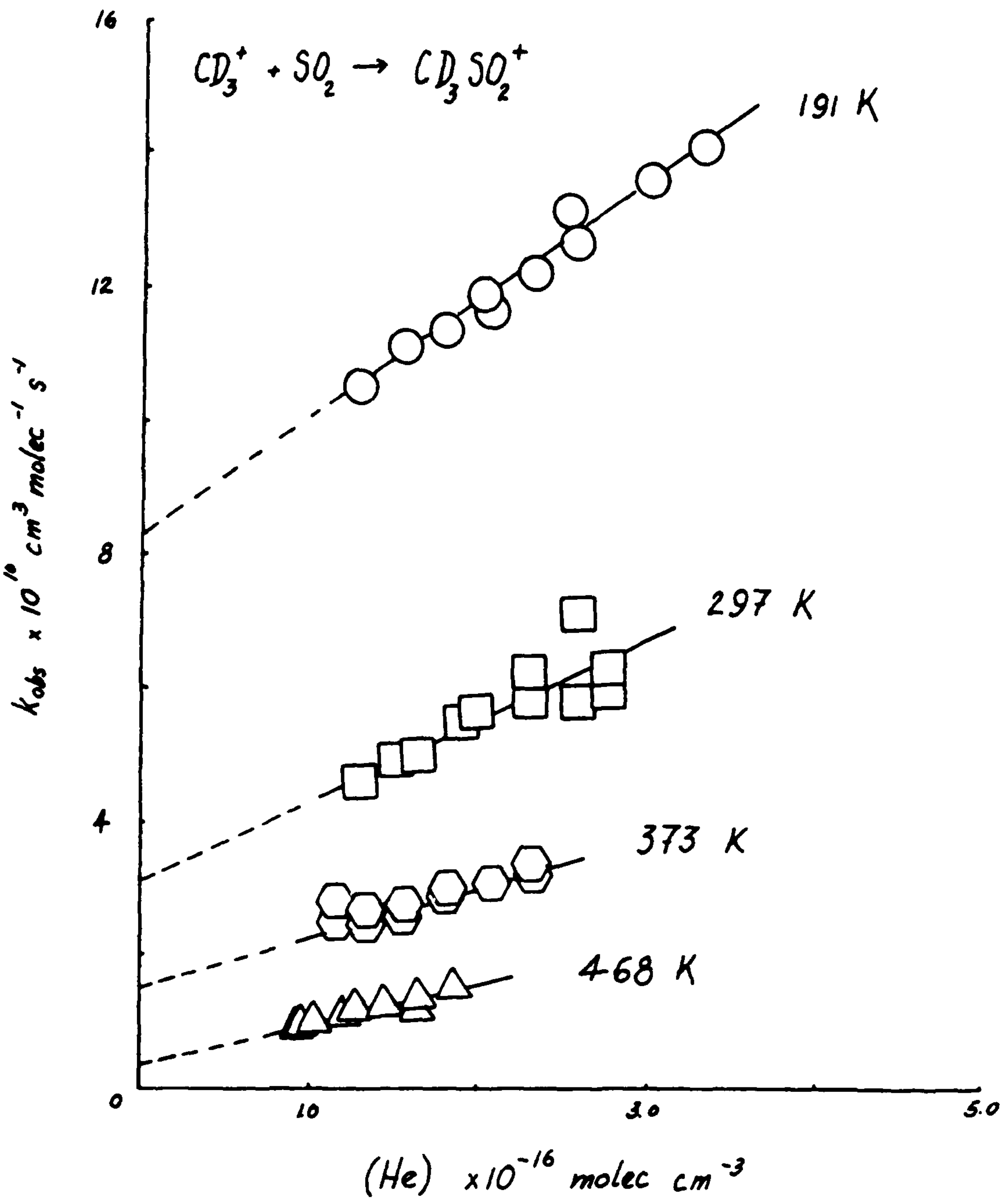

Figure 4: CD_3^+/SO_2 Temperature and (He) dependences

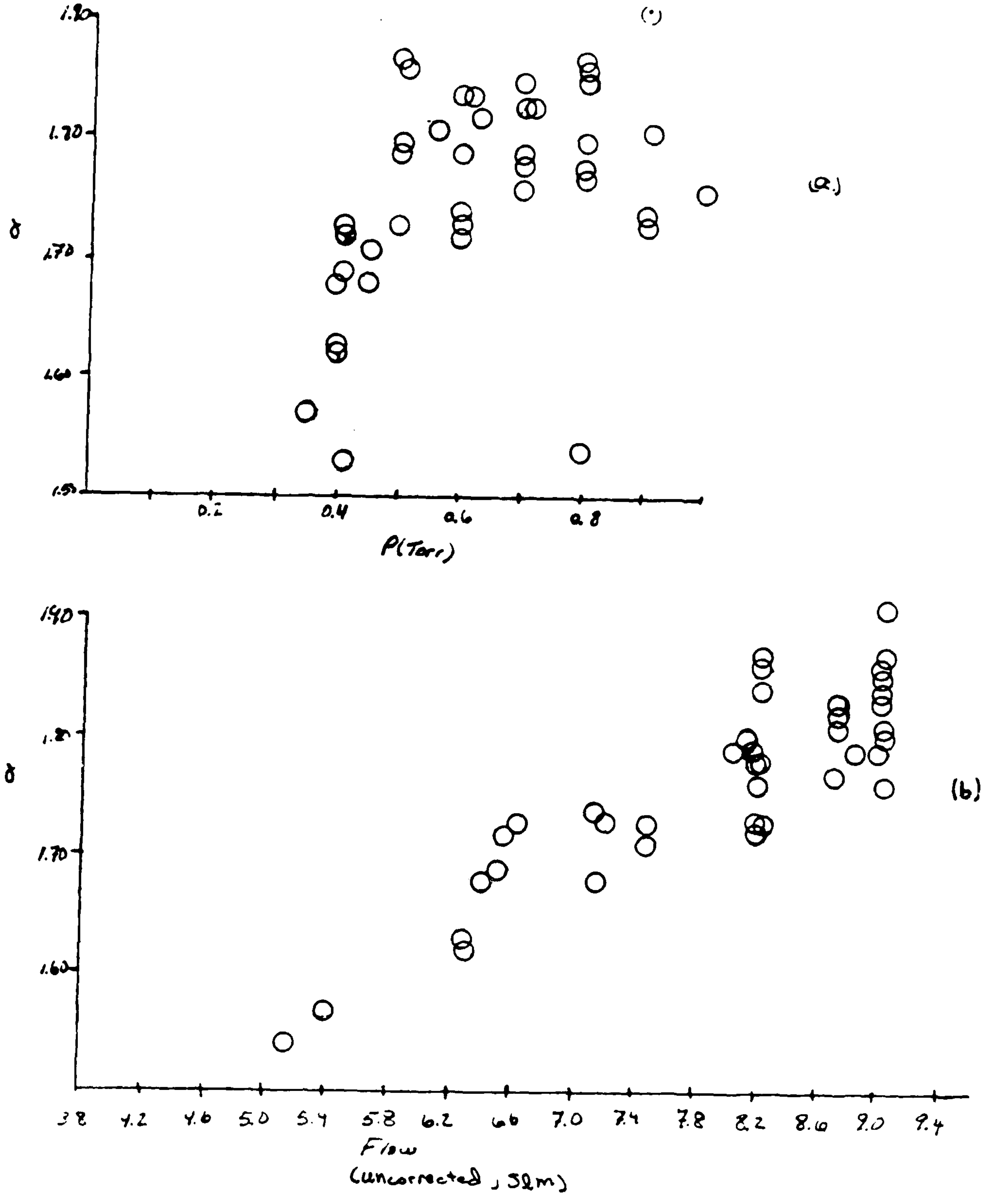

Figure 5: (a) α vs. Pressure at 297K
(b) α vs He flow at 297K

REFERENCES:

[1] Black, J.H.; Dalgarno, A.: " The Formation of CH in Interstellar Clouds "; **Astrophys. Lett.**, 1973, Vol. 15, pp. 79-82.

[2] Barlow, S.E.; Dunn, G.H.; Schauer, M.: " Radiative Association of CH_3+ and H_2 at 13K "; **Phys. Rev. Lett.**, 1984, Vol. 52, pp. 902-905.

[3] Herd, C.H.: **A Study of the Temperature Dependence of Ion-Molecule Association Reactions. Halide Ion Addition to a Selected Group of Lewis Acids**, Ph.D. Dissertation, Louisiana State University, 1987.

[4] Herbst, E.J.: " A Statistical Theory of Three-Body Ion-Molecule Reactions "; **J.Chem. Phys.**, 1979, Vol. 70, pp. 2201-2204.

[5] Su,T.; Bowers, M.T.: " Ion-Polar Molecule Collisions: The Effect of Ion Size on Ion-Polar Molecule Rate Constants; The Parameterization of the Average-Dipole-Orientation Theory "; **Int. J. Mass Spectrom. Ion Phys**, 1973, Vol. 12, pp. 347-356.

[6] Herd, C.H.; Babcock, L.M.: " Radiative Stabilization in the Addition of F- to BF_3 "; **J. Phys. Chem.**,1987, Vol. 91, pp. 2372-2376.

[7] Babcock, L.M.; Streit, G.E.: " Third-Body Effects in Termolecular Reactions "; **J. Phys. Chem.**, 1984, Vol. 88, pp. 5025-5031.

[8] Adams, N.G.; Smith, D.: " The Selected Ion Flow Tube (SIFT); A Technique for Studying Ion-Neutral Reaction " ; **Int. J. Mass Spectrom. Ion Phys.**, 1976, Vol. 21, pp. 349-359.

[9] Paulson, J.F.; Dale, F.: " Reactions of OH^- H_2O With NO_2 "; **J.Chem. Phys.**, 1982, Vol. 77, pp. 4006-4008.

[10] Smith, D.: Private Communication.

[11] Rosenstock, H.M.; Draxal, K.; Steiner, B.W.; Herron, J.T.: " Energetics of Gaseous Ions "; **J. Phys. Chem. Ref. Data**, 1977, Vol. 6, Supplement 1.

1988 USAF-UES SUMMER FACULTY RESEARCH PROGRAM/

GRADUATE STUDENT RESEARCH PROGRAM

Sponsored by the

AIR FORCE OFFICE OF SCIENTIFIC RESEARCH

Conducted by the

Universal Energy Systems, Inc.

FINAL REPORT

EVALUATION OF SOFTWARE STRUCTURED DESIGNS USING METRICS

Prepared by:	Richard E. Courtney
Academic Rank:	PhD aspirant
Department and University:	Computing and Information Sciences Kansas State University
Research Location:	RADC/COEE Griffiss AFB Rome, NY 13441
USAF Researcher:	Roger J. Dziegiel

Date:	14 September 1988
Contract No:	F49620-88-C-0053

EVALUATION OF SOFTWARE STRUCTURED DESIGNS USING METRICS

by

Richard E. Courtney

ABSTRACT

A software design history was analyzed using published software design metrics. The evolution of a student software project provided three versions that were studied recording where changes to the design had occurred from one version to the next, the nature of the change and if any software design measures could indicate that a change was necessary. Additionally a new set of design patterns were generated to be studied using the same design metrics. This design set was developed from the same statement of work, but with different data flow diagrams that lead to different designs. Five designs were created but the project time expired before the metrics were calculated. The intuitive feel is that in both cases the metrics are inconclusive about where change is needed and what makes a better design.

Acknowledgements

I thank the Air Force Systems Command and the Air Force Office of Scientific Research for sponsorship of this research. Universal Energy Systems must be mentioned for their concern and help to me in all administrative and directional aspects of this program.

My experience was rewarding and stimulating because of the environment provided at Rome Air Development Center. Roger J. Dziegiel provided me with guidance at appropriate times. The discussions with Andrew Chruscicki and James Milligan gave valuable insights into the actual use of metrics and automating the entire software life-cycle. The interest shown by Dennis Maynard as well as the problems of software parallelization were stimulating to my curiosity.

I. INTRODUCTION:

Software projects are growing in complexity and have passed the point where one person can completely comprehend the entire project. Thus, owing to communication problems that have always existed, errors are introduced into a software project from the very beginning of the software life-cycle. It has been shown that the earlier in the life-cycle an error is detected, the less it costs to correct the problem (Pr87) (Bo81). Several automated aids exist to check interface consistencies (Bo75) and others to validate requirements (Al85) but there does not exist any automated tool to evaluate the overall design of a software project.

The Software Engineering Section of the Command and Control Division of Rome Air Development Center (RADC) at Griffiss Air Force Base is working with methods to increase software productivity and software quality throughout the software life-cycle. The design phase is a recognized phase in nearly all life-cycle models. If a useful means to evaluate the quality of a software design existed it should result in better designs. Higher quality software at a lower cost for industry is the goal of my research.

I am involved in research to produce an expert system to analyze software hierarchy designs. The expert system will validate the essence of my research which is to discover characteristics that distinguish good design from poor designs and to discover methods to identify errors in designs. My research prior to this summer was examining qualitative features of a hierarchy design. Familiarization

with the effort at RADC identified several quantitative features that could be used.

II. OBJECTIVES OF THE RESEARCH EFFORT:

The major stumbling block preventing automated analysis of software designs is arguments as to what features make one design better than another design. Several qualities of hierarchy designs have been identified as measurable and a number can be generated to give a quantitative evaluation. However, very little work has been done in providing guidelines on how to evaluate the numbers generated. The result has been that the measures are generally done to justify why a project costs so much after the fact and are not used to improve the process as software is being developed. Universities generate several proposals on what to count and how to calculate new metrics, but fail to show what interpretations to give to the numbers except to say one is better than the other.

My assignment as a participant in the 1988 Graduate Student Research Program (GSRP) was to determine if quantitative measures could be used to identify problem areas in a hierarchy design. This includes discovering what the metric is to measure theoretically and practically and if the calculations required to figure the metric could be automated using information stored in a database about the software project. From my work as a teaching assistant in a Software Engineering course at Kansas State University, I had several student projects to study. Measures were computed for a project that was completed on time. Collecting data for the projects that were late or

did not finish was deferred.

Additionally I completed two other reports while at Rome Air Development Center. During the first week, I evaluated and reported on an Automated Software Design Generator package developed by Computer Science Corporation. Towards the end of my stay I was asked to comment on a statement of work for software and system design measures.

III. APPROACHS:

The measures collected were Chapin's Q measure (Ch79), DeMarco's Module Weight (DM82), Myer's Dependency (My75), and Henry-Kafura's Information Flow (He84). These design metrics were collected for three different versions of the project. Version 2.4 is the first complete hierarchy design of the project. Version 2.7 is the last version before coding began and version 3.0 is the revised design documentation after the project was completed. The measures for the designs are in Table 1a and Table 1b.

Chapin's Q measure is based on the premise that the difficulty of composing a software module depends on the work that must be done to fulfill the function of the module. To determine the complexity of a module, before the code is written, one needs to examine the inputs and outputs to the module. The data is scrutinized to determine its "role" in the module; i.e. whether the data is needed for processing the output, or is modified in the module, or controls the processing of the module, or is simply passed through the module. These four

roles have a different influence on the complexity of the module and are assigned different weights. The weights of the inputs and outputs are summed for each call to other modules and then multiplied by an iteration factor. In his paper Chapin then takes the square root of the previous calculation. Taking the square root only influences the magnitude of the numbers but not the direction of change. By not taking the square root, the numbers are more in line with the Henry-Kafura metric which uses squares.

DeMarco's Module Weight is a metric also determined by inspecting the inputs and outputs to a software module. The inputs and outputs are counted in terms of tokens that reduces or multiplies any data structures to the actual components that are to be used by the module. The data structure also determines the decision count of the module. The individual module weight is determined from a lookup table with rows of token counts and columns of decision counts. The module weight for the project is the summation of the module weights.

Myers Dependency metric is used to determine the influence that a change in one module may result in a change in other modules of the software. The dependency metric is calculated by ascertaining the type of module, referred to as the cohesion type, and by determining the type of data exchanged between each pair of modules, called coupling. A good design will have high cohesion and low coupling. The coupling value is placed in a matrix that is then modified by the cohesion types of the two modules involved. This is referred to as the first order dependency matrix and these values are used in Table

1b. Calculation continues by determining other paths to the modules that may result in secondary changes; i.e. a change in one module forces a change in another module which necessitates a change in a third module. The measure for each module is a summation of all the elements in its row in the matrix.

Henry and Kafura's Information Flow metric is based on the data terminating at a procedure or emanating from a procedure. The complexity of a given module is the quantity fan-in times the fan-out squared. This number reflects all the possible combinations of input and output for the module. They also say to multiply the number by the length of the procedure, however others state that that multiplication does not influence the understanding of the metric to a significant degree. Besides, at design you only have an estimated length for the module which is a guess at the difficulty that bias the measure. The length multiplication was not done for the numbers in Table 1b.

IV. RESULTS:

The data in Table 1 shows that as the project evolved that it increased in complexity, but reduced it coupling metric. The increase in complexity can be explained by the project being a student project and a majority of the changes in the design included passing more data items between modules in order that each module had all the information it needed to complete its task. For the metrics that counted inputs and outputs this increase in data passed between modules increased the complexity of the project. On the other hand the reduc-

Name/Version	Chapin's Q 2.4	Chapin's Q 2.7	Chapin's Q 3.0	DeMarco MW 2.4	DeMarco MW 2.7	DeMarco MW 3.0
Trace Program	12.5	20.0	10.0	1.4	9.0	12.2
Create Valid Data File	26.4	9.0	6.0	12.5	5.8	7.8
Get User Choice	2.0	4.0	2.0	2.6	6.3	6.3
Modify Files	10.6	19.4	11.5	3.3	7.9	12.0
Display Legal Output Data Items	6.0	1.1	1.0	7.1	9.5	6.3
Determine Error Messages	3.0	1.0	----	4.9	4.9	----
Generate Trace Reports	11.5	14.5	5.6	7.9	15.3	7.8
Read Filenames	8.0	----	----	7.9	----	----
Validate Filenames	----	13.3	10.0	----	21.2	26.0
Check Srch File Existence	5.0	----	----	4.4	----	----
Check Spec Filetype	5.0	----	----	4.4	----	----
Check Spec Existence	5.0	----	----	4.4	----	----
Check File Existence	----	5.0	6.0	----	4.4	2.6
Determine Valid Data Item	8.3	6.6	20.0	8.5	19.6	26.2
Validate User Choice	5.0	----	----	4.4	----	----
Interpret Choice	6.0	----	----	1.4	----	----
Determine Type of File	5.0	4.0	4.0	6.3	6.3	8.5
Pass Control to vi	1.0	1.0	1.0	4.0	5.8	5.8
Check Data File Existence	4.5	----	----	2.6	----	----
Validate User Data File	7.2	6.6	3.3	6.3	6.3	5.8
Get Report Choice	6.0	6.0	4.0	9.0	6.3	12.0
Produce Reports	----	----	14.4	----	----	10.7
Trace	9.0	7.0	7.2	41.2	7.8	5.8
Create Default Report	5.0	3.0	27.0	25.9	25.9	81.2
Create Default/Act Report	5.0	3.0	27.0	29.6	29.6	81.2
Create Tree Report	5.0	3.0	27.0	25.9	25.9	81.2
Create Tree/Act Report	5.0	3.0	27.0	29.6	29.6	81.2
Read Search File	5.0	3.3	3.3	2.9	6.3	6.3
Read Line of Spec File	4.0	3.0	5.0	2.6	2.4	4.4
Determine if Keyword in Data Line	4.0	----	----	7.1	----	----
Extract Valid Data Item	3.0	----	----	2.9	----	----
Get User Data Item	4.0	3.3	3.3	4.4	4.4	4.4
Get Valid Data Item	3.0	2.2	2.0	2.6	2.6	2.6
Compare Strings	----	----	10.0	----	----	17.8
Compare Data Item	6.0	4.4	11.0	26.0	13.4	22.7
Create Linked Keyword List	----	3.3	5.6	----	19.6	22.3
Create I/O Structure	----	4.4	4.4	----	74.0	18.7
Link T-tree	----	8.0	5.6	----	48.6	33.5
Search	----	----	83.3	----	----	58.2
Zero Input	----	----	16.7	----	----	10.7
n	31	27	30	31	27	30
sum	196.1	162.6	364.2	304.0	418.7	682.2
average	6.3	6.0	12.1	9.8	15.5	22.7
sd	4.5	5.1	15.7	10.4	16.0	25.9

Table 1a

Name/Version	Myers Dependency 2.4	2.7	3.0	Henry-Kafura 2.4	2.7	3.0
Trace Program	5.97	5.80	3.22	16	81	81
Create Valid Data File	5.23	4.76	3.41	144	256	81
Get User Choice	4.97	3.75	0.61	9	9	9
Modify Files	5.12	4.52	4.64	256	144	256
Display Legal Output Data Items	0.00	0.83	0.60	4	9	4
Determine Error Messages	3.45	3.63	----	1	1	----
Generate Trace Reports	5.71	4.21	2.81	576	900	625
Read Filenames	5.31	----	----	64	----	----
Validate Filenames	----	4.52	1.26	----	400	225
Check Srch File Existence	5.11	----	----	4	----	----
Check Spec Filetype	5.01	----	----	4	----	----
Check Spec Existence	4.81	----	----	4	----	----
Check File Existence	----	3.75	1.03	----	4	1
Determine Valid Data Item	1.80	0.83	1.63	25	144	1296
Validate User Choice	4.97	----	----	9	----	----
Interpret Choice	0.52	----	----	1	----	----
Determine Type of File	4.90	3.91	1.21	16	9	16
Pass Control to vi	1.00	0.43	0.40	36	144	144
Check Data File Existence	4.90	----	----	4	----	----
Validate User Data File	4.80	4.56	1.63	36	256	81
Get Report Choice	4.71	5.16	2.66	16	64	64
Produce Reports	----	----	4.26	----	----	400
Trace	1.32	1.60	2.80	64	400	400
Create Default Report	1.32	1.41	3.42	4	16	5929
Create Default/Act Report	1.32	1.41	3.42	4	16	5929
Create Tree Report	1.32	1.41	3.42	4	16	5929
Create Tree/Act Report	1.32	1.41	3.42	4	16	5929
Read Search File	1.00	0.43	0.61	9	9	4
Read Line of Spec File	1.20	0.43	0.82	4	4	16
Determine if Keyword in Data Line	0.80	----	----	4	----	----
Extract Valid Data Item	0.60	----	----	1	----	----
Get User Data Item	1.00	0.40	0.81	4	4	4
Get Valid Data Item	0.40	0.40	0.41	1	1	4
Compare Strings	----	----	0.83	----	----	9
Compare Data Item	5.11	3.35	1.05	16	16	225
Create Linked Keyword List	----	1.80	2.40	----	64	64
Create I/O Structure	----	1.80	2.80	----	16	64
Link T-tree	----	1.80	2.80	----	16	16
Search	----	----	2.42	----	----	1089
Zero Input	----	----	1.80	----	----	1
n	31	27	30	31	27	30
sum	95.0	68.3	62.6	1344	3015	28895
average	3.06	2.53	2.09	43.4	112	963
sd	2.09	1.75	1.25	111.5	196	2005

Table 1b

tion in the dependency metric indicates that the students were doing a better job in partitioning the modules and reducing the amount of extraneous data and control data.

However, the numbers in Table 1 do not indicate where change is likely to occur in the project. Nor do the metrics have any consistency in the changes. The size of change or direction of change does not help predict what the metric will be on the next iteration. One factor that may cause this difficulty is that in each version every module experienced a change in at least two of the metrics. Because the values of the different metrics change in different directions and different relative magnitudes indicates that the metrics are orthogonal and perhaps with additional experience we will be able to provide a better interpretation to the metric values.

V. RECOMMENDATIONS:

The first task should be to automate the collection of metric data. A major difficulty in measuring software is consistency in counting the various items. An automated tool may not count correctly, but in comparing various versions the count would be of the same object. In each of the metrics included in this report the process can be automated without too much additional input needed. Any good database of a software design includes in parsable form the inputs and outputs of each module and the structure of the calls between modules.

My second recommendation is to attempt to use the metrics to manage the development of software. The Software Engineering course

at Kansas State this year is having two teams do each project. For each project, one team will have the metrics calculated and feedback given to the teams. The metrics will not be computed on the other projects until after the project is completed so they cannot be used in influence advice given to the team. The two projects will then be compared to see if having the metrics made a significant difference in the complexity and quality of the project and the effort it took to complete the project.

Because data was obtained from a student project, results owing to the fact that the students were learning techniques may have obscured data that may be valuable to industry. Therefore, another part of my effort at Rome Air Development Center was to develop different designs from the same statement of work.

By keying on certain aspects of a single statement of work, five different data flow diagrams were generated leading to five different designs. Additional variations were made from the basic designs providing over twenty different hierarchy design combinations. I was hoping to have the metrics calculated by this time so I could report of features that make the measure of a design "better." Verification of the metric is to be done by noting the number of errors found in the design during a through study and by recording the number of changes needed to implement several enhancements that could be added to the statement of work.

VI. ADDITIONAL RESEARCH:

During the first two weeks of my GSRP appointment I conducted an evaluation of an automated software design generator that was developed by Computer Sciences Corporation for RADC. The Design Generator is a prototype to demonstrate an object oriented approach is appropriate, the graphical interface is user friendly and the applicability of the algorithms used.

The tool was evaluated for strengths and weaknesses. My report contained recommendations of standard enhancements and expert system techniques that should be added to software to make the tool a marketable product. Since that report I've read Mike Adler's paper and believe that his ideas of data flow decomposition could provide the intelligence necessary to check the data flow which is input to the program. The Design Generator demonstrates that an automated tool can be developed to assist an analyst in the design of software systems. The rules developed for the design too provided me with a basis for a new set of rules to use in an expert system to analyze structured designs.

During the ninth week at RADC I was asked to provide comments on a Statement of Work for Software and System Design Measures. Suggestions were made on two fronts. The first is a detailed list of questions that should be answered by anyone doing the research described. The second was what I feel really needs to be researched in the field of software design measures.

REFERENCES

Adler, Mike. "An Algebra for Data Flow Diagram Process Decomposition." IEEE Transactions on Software Engineering. Vol. SE-14, No. 2; (February 1988) pp 169-183.

Alford, Mack. "SREM at the Age of Eight; The Distributed Computing Design System." Computer. Vol. 18, No 9; (April 1985) pp 36-46.

Boehm, B. W., McClean, R. K. and Urfrig, D. B. "Some Experience with Automated Aids to the Design of Large-Scale Reliable Software." Transactions on Software Engineering. Vol. 1; (1975) pp. 125-133.

Boehm, Barry W. Software Engineering Economics. Englewood Cliffs, NJ.: Prentice-Hall, Inc., 1981.

Chapin, Ned. "A Measure of Software Complexity." Proceedings of the National Computer Conference. 1979, pp. 995-1002.

DeMarco, Tom. Controlling Software Projects. New York, NY: Yourdon Press, 1982.

Henry, Sallie and Kafura, Dennis. "The Evaluation of Software Systems' Structure Using Quantitative Software Metrics." Software--Practice and Experience, Vol. 14, No. 6; (June 1984) pp. 561-573.

Myers, Glenford J. Reliable Software Through Composite Design. New York: Petrocelli/Charter, 1975.

Pressman, Roger S. Software Engineering: A Practitioner's Approach. New York: McGraw-Hill, 1987.

Yourdon, Edward and Constantine, Larry L. Structured Design: Fundamentals of a Discipline of Computer Program and Systems Design. Englewood Cliffs, NJ.: Yourdon Press, 1979.

1988 USAF-UES SUMMER FACULTY RESEARCH PROGRAM/

GRADUATE STUDENT RESEARCH PROGRAM

Sponsored by the

AIR FORCE OFFICE OF SCIENTIFIC RESEARCH

Conducted by the

Universal Energy Systems, Inc.

FINAL REPORT

FREE-SPACE LASER COMMUNICATIONS SIMULATOR PROGRAM

Prepared by:	Gary A. Hellenga
Academic Rank:	Graduate Student (Master's Candidate)
Department and University:	Department of Mathematical Sciences, Montana State University
Research Location:	Rome Air Development Center Intelligence Communications Branch (DCLF) Griffiss AFB, NY 13441-5700
USAF Researcher:	Mr. David Legare
Date:	September 18, 1988
Contract No.:	F49620-88-C-0053

Free-Space Laser Communications

Simulator Program

by

Gary A. Hellenga

ABSTRACT

Previously developed mathematical models of the interaction between light photons and natural or man-made atmospheric obscurants were used to predict the extinction of light caused by these particles. The effects of such obscurants acting on a given communications link were combined to determine the amount of light energy received by the collector. System parameters such as collector diameter, laser output power, and internal and exterior noise were then used to determine the overall quality of the simulated link, expressed as a Signal-to-Noise Ratio (SNR).

ACKNOWLEDGEMENTS

I wish to thank the Air Force Systems Command, the Rome Air Development Center, and the Air Force Office of Scientific Research for sponsorship of this research. Also, thanks are due to Universal Energy Systems for their assistance with the administrative processes involved in the effort.

This project was very educational for me and I owe thanks to many different people for their help. David Legare, my research colleague and Effort Focal Point, provided me with most of the background knowledge and reference materials I needed to get started, helped me in procuring the necessary resources for the project, and guided my efforts toward the project's goals. Lieutenant Dan Eickmeier, Joel Mussman, and Steve George were very helpful, providing technical assistance with the computing equipment and software I was utilizing. I also appreciated the concern and advice of Tony Szalkowski, the Intelligence Communications Branch Chief, who showed interest and support for my effort, and who took the time to enlighten me on the possibilities of continuing my research effort in the future.

I. INTRODUCTION:

The use of optical technology for communications and information processing is increasing rapidly. Optical devices such as fiber-optic telephone circuits and optical recording/retrieval systems demonstrate the improvements in speed and accuracy over similar systems using electrical or magnetic equipment. The use of a laser beam propagating through the atmosphere for military communications offers many possible advantages to convey information between points, such as high portability, ease of installation, and minimal power requirements. The directionality of a laser beam also makes it virtually impossible to intercept, direction-find, or jam. However, natural and man-made obscurants existing in the atmosphere of the modern battlefield, such as smoke, gas clouds, dust, and water vapor, can act to disrupt the propagation of such laser beams. Conducting field tests of proposed laser-based communications systems under the many varying possible combinations of atmospheric conditions and obscurant presence would be time-consuming and costly. The use of a computer program designed to simulate these conditions and their effect on the communications link would allow potential users to study the feasibility of such a laser system in a much faster and economical manner.

My interest in this project stems from the use of mathematical models to describe the interactions between laser light and the various obscuring agents, and the use of numerical techniques in computing the results of these interactions. Additionally, I am a Communications Officer in the United States Army Reserve, and am hence familiar with

the needs of the users of military communications systems. This made the project attractive to me from a professional standpoint, and I am sure it was a factor in my selection for the program.

II. OBJECTIVES OF THE RESEARCH EFFORT:

Lasers have seen significant use recently in fiber-optic communications systems, but free-space lasers systems have largely been ignored. Such systems are generally assumed to be impractical due to potential disruption caused by atmospheric aerosols, contaminants, or turbulence. The many advantages of such a system, however, make the exploration of its feasibility for certain applications desirable, especially if such tests can be done with minimal cost in terms of time and expense. The development of a computer simulator to examine the behavior of such systems, then, would allow such tests to be conducted quickly and inexpensively. If such a simulation were to indicate that a proposed application were feasible, the time and money needed to conduct more exacting field tests using actual hardware components, etc., would be clearly justifiable. The simulator would therefore be a very useful tool for examining many different possible systems and determining which uses might justify the further development of laser-based communications systems.

Prior to my arrival at the Rome Air Development Center, my research colleague had already procured several computer packages designed to calculate the effects of atmospheric aerosols and other environmental factors on photon beams. My function was to examine these various

codes to determine which might be applicable for a communications simulator, then adapt these codes so they could be executed on the local Zenith microcomputers. This would allow greater portability of the codes, and expand the useability of the resulting simulator. Next, an executive program was to be developed to combine the effects of the separate conditions, each of which was calculated in a separate subroutine. This program was to determine the net transmittance from the laser source to the receiver subject to the actions of all the agents and forces acting upon the beam. Additionally, it was to include the contribution of the specific physical system geometry. By also finding the amount of background noise collected by the receiver, the program was to calculate the overall quality of the system, expressed as a Signal-to-Noise Ratio (SNR).

Lastly, the simulator was to be modified to allow the user to select a parameter of interest, then solve for the required value of that parameter, given input values for the other system variables. For example, given the existing atmospheric conditions, the locations of the transmitter and receiver, the power output of the laser, the noise equivalent power of the receiver, and the desired SNR, the program should calculate the minimum diameter the collector must have to achieve the desired SNR.

III. <u>CONDUCT OF THE EFFORT:</u>

The software packages on-hand were the Air Force Geophysics Lab Atmospheric Transmittance/Radiance Computer Code LOWTRAN 6, the 1984

version of the Army Atmospheric Sciences Lab Electro-Optical Systems Atmospheric Effects Library (EOSAEL), and Titan Systems' Scattered Light Communications System code, 1987. The LOWTRAN program was not deemed appropriate for use due to the use of broad-band averaging calculations, which obscured the great differences of behavior possible between laser emissions of only slightly differing wavelengths. The Titan Systems code was never fully examined due to time constraints and the presence of similar modules within the EOSAEL package, which was selected as a base for the simulator. Only the subroutines deemed most pertinent were used, owing to the vast size of the package and the requirement to adapt the simulator for microcomputer usage. The modules utilized were those capable of calculating the effects of the various atmospheric molecules, clouds, natural aerosols such as water vapor, rain, snow, and fog, and fire-caused smoke plumes on the transmitted beam. Other routines were designed to calculate the power received through multiple scattering, the scintillation and jitter effects of atmospheric turbulence, and the amount of optical "noise" that would be received by the collector. Data bases for climatic conditions in certain geographical areas of interest, and for extinction and scattering values as functions of obscurant type and emission wavelength were also included. These allowed the user to either utilize data gathered by the Army Atmospheric Sciences Lab's field tests, or input data from his own experiments or knowledge.

Each routine examined the effect of a certain condition or obscurant on the transmitted beam. Using models describing the interaction with the beam, the total effect due to that agent was usually calculated by

integrating numerically over the total path segment length subject to that condition. Development of these modelling equations is described in the EOSAEL guide booklets listed on the reference page. The models and integration methods were assumed to be acceptably accurate and efficient, and were used without modification.

Before using the codes, which were written to accept input in the form of formatted cards, a user-interactive program (SMART) was developed that would gather the input data from the user and build an input file of 'cards' in the format needed by the EOSAEL codes.

The codes, written for standard Fortran 77 implementation, required slight modification to allow them to compile on the microcomputer using Microsoft Fortran compiler software. The modules were all compiled separately without encountering size difficulties, but could not be linked together with the executive driver (EOEXEC) due to the many large subroutines. Attempts to solve the sizing problem using an overlay linker also failed. Finally, the code was divided into three separate programs, each containing the EOEXEC driver and three to five subroutine modules. In order to calculate the total effect on the laser link due to all the acting obscurants, all three programs had to be run, and a technique for retaining common variable values as one program ended and another began was needed. This was accomplished within each copy of EOEXEC by writing the variable values to a transitional data file, which were then read upon entry to the new program. Each EOEXEC program also restructured the input file, deleting 'cards' already read, so the following program would not

process input already used.

The attempts to convert the modules to microcomputer usage consumed most of the research period. As time became a factor, we decided to return the codes to a larger VAX machine to speed up error-checking and compilations, and allow us to concentrate on the additional coding required to conduct the simulator calculations. This required some modification to the program (the executive driver and all the modules could be linked into a single program on the VAX) to allow the driver to access the necessary variable values from all of the subroutines. Total transmittance was calculated under the assumption that the extinction effects were additive in nature. For example, a beam that intersected both a smoke plume and a low stratus cloud might attain 5% transmittance through the smoke plume, 15% through the cloud, and 80% transmittance through free-space (due to extinction caused by atmospheric gases and water vapor). The transmittance for the total system would then be (.05 X .15 X .80) X 100% = 0.6%. Similarly, all background noise contributions were assumed to be additive in nature.

Overall system performance was evaluated on the basis of the SNR formula:

$$\text{SNR} = \frac{\text{Received direct power + received scattered power}}{\text{total background noise + receiver internal noise}} \quad (1)$$

The user was required to supply the receiver internal noise equivalent power (typically provided by the receiver's manufacturer). The values of the other three variables would be calculated by the simulator, or could default to zero if the user elected not to include certain

modules in the simulation. Rearranging equation (1) would allow the program to solve for a parameter other than the SNR, if desired, provided the user also supplies the value for the SNR.

Scrutiny of the example given on the previous page concerning a beam travelling through a smoke plume and a stratus cloud reveals another assumption made: The receiver is assumed to collect all of the light that manages to penetrate the atmosphere to the receiver's location. However, over long communications distances, beam spread will become so great that the beam spot will be larger than the collector, so the energy contained in the portion of the spot lying outside the collector is wasted (except for the small fraction that may be scattered so as to be received by the collector). Therefore, the direct received power used in equation (1) is found by scaling the total transmittance by the ratio of the collector area to the beam spot area at the receiver (note that this also assumes a uniform distribution of energy across the cross-section of the beam).

IV. RECOMMENDATIONS:

The program as it exists still contains coding errors that prevent it from providing useful simulations. These errors can be remedied with patient debugging actions. To fully complete the development of an accurate simulator, I recommend the following be implemented:

a. The nature of the calculations required by the simulator may render it impossible or impractical to execute on a microcomputer.

Conversion of the program for microcomputer usage should be left as the final development step.

b. Using the EOSAEL modules in their current form makes access to some of the computations difficult, and the results are not always useful for the intent of the simulator. Their principal value lies in the development and use of the underlying models, and the algorithm for applying those models across the length of the beam path segment of concern. A complete revision of the codes, using the models as they are, may prove to be better than trying to use results calculated for a different application.

c. The numerical techniques used in the calculations should be reviewed to determine if they are most appropriate for the given calculation. If the actions suggested in b. above are taken, including routines from additional mathematical software libraries may allow selection of a more efficient integration procedure while still reducing the coding effort.

d. The program as it exists currently includes only one type of the many possible obscurants that may appear on the modern battlefield. To make the simulator more useful, the effects models contained within the COMBIC subroutine of the EOSAEL package should be included. Further improvements could be made by employing the updated models and calculations contained in the newly-produced 1987 version of the EOSAEL library.

e. Several assumptions have been made in the simulator that could lead to large inaccuracies in results, especially for links of considerable distance. One such item is the assumption of plane-parallel geometry, and the neglect of refraction effects. The 1987 version of EOSAEL includes a module to examine these effects.

f. The assumption of additivity of extinction effects is also questionable. The appropriate method of calculating the total transmittance is to examine each segment of the path and integrate along each segment, including the effects of all agents acting on that segment. This is further argument for implementing the recommendation in b. above.

g. The scaling of the total transmittance by the ratio of collector area to beam spot size should be modified to incorporate a Gaussian distribution of intensity across the laser beam cross-section to increase accuracy. In this modification, the axis of the cylindrical beam and the axis of the circular collector would be assumed to be coaxial.

h. The data bases for atmospheric data and phase function values should be capable of expansion to include new data gathered in field experiments. The 1987 version of EOSAEL has already considerably expanded the climatological data base, including several new geographic regions.

For the reasons given in the introduction, I believe further work should be done in this area to develop the most efficient and accurate simulation program possible, either through RADC in-house efforts or through externally contracted means such as the RADC Post-Doctoral contracting system or the UES Mini-Grant program.

REFERENCES

1. Bayse, Robert, Steve Bradley, Robert Lintell, and Julie Martin, Scattered Light Communications System, RADC-TR-87-217, Titan Systems, Inc., November 1987.

2. Duncan, Louis, Richard Shirkey, et. al., Electro-Optical Systems Atmospheric Effects Library Module Guides, Vol. 1-22, U.S. Army Atmospheric Sciences Laboratory, White Sands Missile Range, New Mexico, 1984.

3. Kneizys, F.X., et. al., Atmospheric Transmittance/Radiance: Computer Code LOWTRAN 6, AFGL-TR-83-0187, U.S. Air Force Geophysics Laboratory, Hanscom Air Force Base, Massachusetts, 1983.

1988 USAF-UES SUMMER FACULTY RESEARCH PROGRAM

GRADUATE STUDENT RESEARCH PROGRAM

Sponsored by the

AIR FORCE OFFICE OF SCIENTIFIC RESEARCH

Conducted by the

Universal Energy Systems, Inc.

FINAL REPORT

The Effects of Nonlinearities of High Speed Analog-to-Digital Converters on Digital Beamforming Arrays

Prepared by:	Donald R. Ucci, Ph.D. / Robert G. Petroit
Academic Rank:	Associate Professor / Graduate Research Assistant
Department and	Electrical and Computer Engineering Department
University:	The Illinois Institute of Technology
Research Location:	RADC/EEA Hanscom AFB Bedford, MA 01731
USAF Researcher:	Dr. Hans Steyskal
Date:	12 AUG 88
Contract No:	F49620-87-R-004 / F49620-88-C-0053

SAME REPORT AS
PROF. DONALD UCCI
ROME AIR DEVELOPMENT CENTER # 60

1988 USAF-UES SUMMER FACULTY RESEARCH PROGRAM/

GRADUATE STUDENT RESEARCH PROGRAM

Sponsored by the

AIR FORCE OFFICE OF SCIENTIFIC RESEARCH

Conducted by the

Universal Energy Systems, Inc.

FINAL REPORT

Metal Semiconductor Field Effect Transistor Computer Modelling and Electron Transport Computation

Prepared by:	Matthew S. Rubin
Academic Rank:	Master of Science student
Department and	Department of Electrical and and Computer Engineering
University:	Ohio University, Athens, Ohio
Research Location:	RADC/EEAC Hanscom AFB Bedford, MA 01731-5000
USAF Researcher:	Paul H. Carr, Phd.

Date:	9 Setptember 1988
Contract No.:	F49620-88-C-0053

Metal Semiconductor Field Effect Transistor Computer Modelling

and

Electron Transport Computation

by

Matthew S. Rubin

ABSTRACT

Alterations in geometries and bias conditions of Metal Semiconductor Field Effect Transistors (M.E.S.F.E.T.) layed out on monolithic microwave integrated circuit chips were experimentally evaluated. To interpret laboratory findings, a computer model was needed. An existing M.E.S.F.E.T. simulation program was refined and modified to meet this requirement. An important modification was the addition of an electron propagation time algorithm that helped analyze M.E.S.F.E.T. behavior.

Acknowledgements

I am very grateful to the Air Force Systems Command and the Air Force Office of Scientific Research for their sponsorship of this research. I am also immensely appreciative of Universal Energy Systems for their role in making my appointment possible.

I wish to thank the entire staff at the Rome Air Development Center, Hanscom Air Force Base, for making my experience there an extremely delightful and pleasant one. I am indebted to 1st Lt. Jon S.H. Schoenberg and Dr. Paul H. Carr for their guidance and many helpful suggestions in the course of my research. The on-base consultants from Digital Equipment Corporation, Len D'Alberti and Raina Eckhart, must be mentioned for there help with the software hindrances I encountered. Special thanks to Mrs. Sheila Belliveau for her help with the processing of this manuscript.

I. INTRODUCTION

The Electromagnetic Directorate of the Rome Air Developement Center (R.A.D.C.) located at Hanscom A.F.B. conducts antenna and electromagnetic propagation research. A subdivision of the directorate, the Component Technology Branch does pioneering work on state of the art electronic devices which are implemented for advanced antenna technology. Components are investigated in the Monolithic Microwave Integrated Circuits (M.M.I.C), Photonics, and, superconductivity areas.

As a graduate student of electrical engineering, my area of specialization is M.M.I.C. analysis and design. During my undergraduate years, I received a strong electromagnetics background, including basic antenna theory. These qualifications were responsible for my tour at Hanscom A.F.B..

II. OBJECTIVES OF THE RESEARCH EFFORT

The phased array antenna is used extensively by the military. Its narrow beam, nulling (anti-jamming), beam steering, and multiple beam capability make it a leading device in the Command, Control, Communications, and Intelligence arena. These attributes have fueled its research at R.A.D.C.. One topic of interest concerning the phased array is the reduction in complexity of the electrical system required to drive the antenna. The use of M.M.I.C. technology to do the job is under investigation. The M.M.I.C. effort is emphasizing changes in the geometry and bias conditions of Metal Semiconductor Field Effect

M.E.S.F.E.T. with its primary components labeled is shown in figure 1. Transistors (M.E.S.F.E.T.) layed out on the M.M.I.C. chip. The Several in-house M.E.S.F.E.T. designs were manufactured and tested on the network analyzer. However, a computer simulation of the M.E.S.F.E.T. is needed to explain the experimental observations. An existing computer simulation program was available but was in need of software refinement. It lacked user friendliness and was absent of features such as mean electron path designators and electron propagation time analysis. These features are needed to allow for a complete study of implementing M.M.I.C. component technology to the phased array antenna.

My assignment to Hanscom A.F.B. was to refine the M.E.S.F.E.T. computer model so that it could be run quickly and easily, and to modify it to determine electron propagation time for a variety of M.E.S.F.E.T. geometries and bias conditions. The results of the work will significantly contribute to an understanding of the M.E.S.F.E.T. and help explain the behavior of the devices that were experimentally studied in the R.A.D.C. laboratories.

III. M.E.S.F.E.T. COMPUTER MODEL

The M.E.S.F.E.T. modelling program was procured from work that was performed under contract with Texas Instruments (T.I.). The program was written by T.I. engineer, William Frensley, Phd., who intended the state of condition regarding the program. The program was written in FORTRAN 77 and intended to be run on an I.B.M. 370 mainframe computer. At R.A.D.C., the computer facilities offer a DIGITAL Vax™ 780 main-

frame computer. Fortunately, the I.B.M. and the DIGITAL fortran versions were very close, so there were no recompiliation problems.

In its original form, there were four separate files which constituted the entire modelling program. Through the course of refinement, two more separate files were added. The first four must be run in sequence. The remaining two can be run as needed. These files are called: PRESETUP, SETUP2, INITIAL, FETMODL, (these must run as presented), COMGKS, and TDELAY.

PRESETUP takes the physical dimensions of a planar M.E.S.F.E.T. of interest and converts them into a two dimensional coordinates which are written to external data file DEVCOOR (DEVice COORinates). PRESETUP was not one of the original four files. Previously, one had to take the physical dimensions of the device and determine the two dimensional coordinates of the device by hand. The addition of PRESETUP has significantly increased the data entry process.

SETUP2 reads in the DEVCOOR file. The coordinates of two dimensions are transformed into a one dimensional representaion. These one dimensional coordinates are referred to as "mesh points". They, in a sense, make up an analytical "skeleton" of the device which allows it to be quantitatively studied. Figure 2 depicts a sample M.E.S.F.E.T. with a hypothetical mesh point arrangement. Each mesh point is inspected and designated a number which indicates the mesh point's vicinity on the device. These numbers are placed into an array called KBNDRY.

Three external data files are generated by SETUP2. These are PARAMS

(PARAMeterS), CROSSREF (CROSSREFerenced parameters), and FIELDS (FIELDS data). PARAMS contains basic default electromagnetic constants, terminal voltages, and material constants that are essential for program operation. FIELDS is the storage space for the final product of the program execution. This is mesh point electron densities. The DEVCOOR file is only created at this time and is filled when FETMODL is executed.

SETUP2 has one other vital function. It runs tests on the contents of the DEVCOOR file to ensure that no unphysical entries were written into the file. For example, an error such as the device missing one of its sides or a mesh point representing two material types instead of one.

File INITIAL determines initial values for electron density and electrostatic potential. These preliminary results are placed into the SETUP2 created FIELDS file. However, prior to performing the computation, a feature was added that greatly increased the user efficiency of the program. Upon program execution, the user is prompted if any changes of the default parameters contained in PARAMS are desired. This is accomplished through the display of all the parameters placed on the screen. Each parameter has corresponding number which is depressed to declare the new parameter value. After each change, the updated parameter list is shown. The process is continued until all desired parameters appear. Previously, parameters could only be altered by manually encoding them into the program and then recompiling the updated source code.

File FETMODL, the heart of the modelling software, performs iteration processes required to develop the complete quantitative description of the device under the user specified conditions. This portion of the entire software was left undisturbed since refinement of the supporting software was the focus of the effort. FETMODL determines the electrostatic potential and charge distribution at each mesh point by iterative solution of Poisson's equation and the diffusion equation.

$$\nabla^2 \Phi = - \rho / \epsilon \tag{1}$$

becomes

$$\Phi (x + h,y) + \Phi (x - h,y) + \Phi (x, y + h) + \Phi (x,y - h) - 4 \Phi (x,y) = - \rho h^2 / \varepsilon \tag{2}$$

where h = step size (distance between consecutive mesh points).

The plotting capability offered with the software is performed by file COMGKS. Execution of this file (after the first four described are run in the order presented) displays the M.E.S.F.E.T. and contours of constant electron density and electrostatic potential determined in FETMODL.

COMGKS under went extensive modifications. Originally, the file was called COMPLOT. It performed the device plotting by using CALCOMP software commands. However, the DIGITAL VAX computer facilities at R.A.D.C. did not support CALCOMP software. There were several ways to approach this problem. One possibility could be to rewrite the entire plotting routine with another graphics package. Another alternative could be to down load all of the software onto another available system that had CALCOMP. Another option could be to keep the existing COMPLOT routine

but use another graphics package to simulate CALCOMP commands.

The first option would be by far to great an effort. The second is a good candidate but would require the learning of an unfamiliar operating system and the problem of system incompatibilities in the form of recompilation errors. The final choice presented seemed to be the best option offered since it required the translation from one graphics package to another. Upon applying this strategy, the Graphic Kernel System (G.K.S.) software package was found to best to do the job. A subroutine was written which applied G.K.S. commands which was named SIMCALCOMP (SIMulate CALCOMP). This the routine imitates a specialized option of the CALCOMP PLOT command which draws a line from a specified point to some other specified point. Since this was all that was needed to produce M.E.S.F.E.T. plots, other optional simulations, such as labeling which involved far more complicated simulation, were omitted.

A consequence incurred with the CALCOMP simulation was the difference in the way different graphics packages coordinatize the screen. Adjustments were required to make sure the M.E.S.F.E.T. picture was displayed on the on the screen in its entirety.

The final file in the modelling software is the TDELAY routine. This file, as stated previously, was not part of the original simulation software package. It was written to meet the technical requirements of the M.M.I.C. Component Technology research team.

The electron propagation time was needed for adjustments in M.E.S.-F.E.T. geometries and bias conditions. To determine this, first, an

electron trajectory must be selected over which the time can be measured. This trajectory consists of a set of points where the electron is expected to travel. This expected path is found the following way. For a specified section of the device, a column by column inspection of mesh points is conducted. Each column is tested for the point or group of points that contain the maximum electron density for the column. In those cases where a group of points is selected, the most internal device point becomes the chosen path point. Before progressing to the next column, the elected point is placed into an array. This array, called PATH, upon completion of the section search, will contain the selected trajectory of points that will be used in the time measurement. It was observed, after initial runs, that although the selected trajectory was created under a maximum electron density theoretical basis, the selected path did not appear to conform to the probablistic behavior for electrons. Therefore, implemented into the program, is a smoothing operation which studies the determined electron path (by maximum electron densities) as it is created. If the path appears sporadic, the smoothing function is engaged and corrects the deviance. The degree at which the smoothing function operates can be controlled by the user and this is done by adjusting the value of the DELTA variable (as instructed in the commented statements found in the source code).

Once the electron trajectory has been established, the propagation time can now be determined. To accomplish this, the incremental time at each mesh point is determined by:

$$t = d/v \tag{3}$$

where d is the distance between adjacent mesh points, and v is the mesh

point velocity.

Determing adjacent mesh point distances, the mesh point velocities, and a summation of the incremental propagation times over the selected electron contour will yield the time measurement.

To determine each incremental adjacent mesh point distance, a numerical subtraction is performed of the two mesh points under scrutiny. The value obtained from this subtraction is evaluated in a small routine which can match this value to the spacial orientation of the two adjacent points.

The determination of the velocity of the electrons in the device is a very interesting problem. This is because of the nonlinear behavior exhibited by the M.E.S.F.E.T.. The mesh point velocity is found from the mesh point electric field. There is no single relationship between the two as figure 3 shows. Therefore, an algorithm was taken from FETMODL that reads the mesh point electric field and analytically matches it to the proper ordered equation which yields the velocity. Figure 3 illustrates the idea. For values of electric field below the peak electric field, the following equation is used to determine the mesh point electron velocity:

$$v = \mu E \tag{4}$$

where v is electron velocity at the mesh point, μ is the permeability constant, and E is the mesh point electric field. To determine the mesh point electron velocity for values of electric field greater than the peak electric field, the equation offered below governs the mesh point

electron velocity:

$$v = v_s + ACON / E \qquad (5)$$

where v_s is the carrier saturation velocity, and ACON is a constant used to describe the monotonically decreasing behavior of the curve.

Upon application of incremental electron propagation time formuala, equation (3), the incremental times are placed into an array which then sums the points in the array to complete the integeration process and hence, achieve the time of propagation.

IV. TRIAL RUNS

Although in its preliminary stages, the M.E.S.F.E.T. modelling software was run to compare theoretical data with in house acquired laboratory results.

Two devices were investigated. Both were recessed gate M.E.S.F.E.T.s with 0.3 micron active channal thickness and doping concentrations of $10x10^{17}$ cm^{-3}. The first device had one micron contact lengths and spacings except for four micron spacing between gate and drain. The applied bias conditions were 0.0 source voltage, -2.0 gate voltage, and 2.0 drain voltage. The second device had one micron contact lengths and spacings and a twelve micron spacing between gate and drain.

In the laboratory, the larger device demonstrated a 28% increase in electron propagation time. Two computer simulations were run to compare

these results with the theoretical data. One simulation used a smoothed trajectory, the other, a skew trajectory. In both cases, slightly over a 50% increase in propagation time was observed.

Although the gap between experimental and theoretical results may not appear encouraging, some important conclusions can be drawn. First, the trend in the experimental and computer generated data seem to behave alike. That is, an increase in electron propagation time for the larger device. Second, for the two different electron trajectories, similiar percentage increases in time were observed. Lastly, the data revealed longer propagation time for the sporadic path runs. This verifies the program performance since this makes physical sense (a longer path would require greater time for electron travel).

V. RECOMMENDATIONS

Due to a ten week time constraint, minor refinements to the software and further research into the creation of an electron propagation time calculation program could not be performed. For one to pick up where my research has left off, the following suggestions are offered.

The PRESETUP routine currently writes the DEVCOOR file for planar devices. Since recessed gate devices are investigated, it would be a time saving feature to have the routine have the ability to write the DEVCOOR file for these devices. Since the recessed gate device is a specialized case of the planar device, this effort would require the addition more boundry specifications in the source code.

As indicated earlier, in COMGKS, there appears to be a mismatch of the coordinate systems used for CALCOMP and that used for G.K.S.. This results in portions of the device to be cut off when different geometries are investigated. The G.K.S. WINDOW command was applied to correct for this problem. The arguments of the function were variable to allow adjustment for different geometries studied. Linear equations were used to control the variable arguments and hence change the coordinate system. However, it was found that this approach did not work one hundred percent of the time. Perhaps if nonlinear equations of some kind were utilized, this could alleviate the problem.

There was difficulty in creating prompts for the user when COMGKS was run. The prompts would overwrite the device on screen. There are several "clear screen" commands that could be possibly implemented to resolve this.

Difficulty was experienced in obtaining a paper print out of the device. This requires the creation of a G.K.S. "metafile" and then dumping it to the appropriate G.K.S. compatible device. A version of COMGKS was written where a G.K.S. metafile is created. But the linking process is still to be completed.

The electron propagation time calculation seems to function well at a preliminary level. However, the time calculation yields results that appear to be a few orders greater than theory predicts. This could be due to a dimensional problem in the source code. A complete dimensional analysis of the overall software could resolve this. Especially, an

understanding into how FETMODL manages the dimensions would be a good start.

Another issue concerning the electron propagation time program is the selection of a path that reflects the average mean path. Tests should be conducted with a large varieties of paths to observe differences in calculated electron propagation time. If propagation times are found to be different, then an overall time could be ascertained by taking all time results for the different paths and then making an average. Doing this would take into account all mesh point velocities and not individual ones when a single trajectory is used.

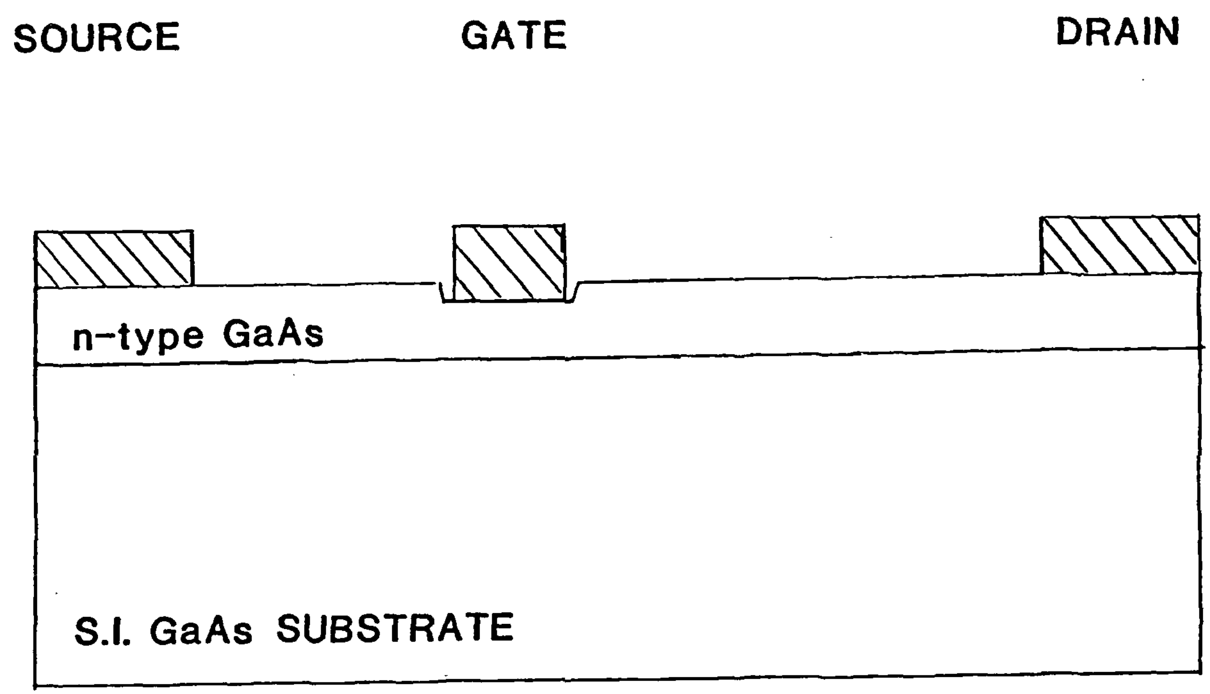

FIG. 1. The M.E.S.F.E.T. with its primary components labeled.

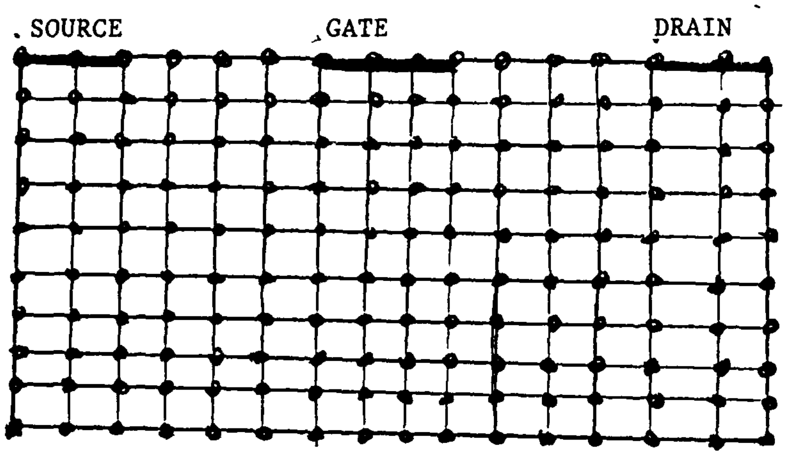

FIG. 2. Sample M.E.S.F.E.T. and hypothetical mesh point scheme.

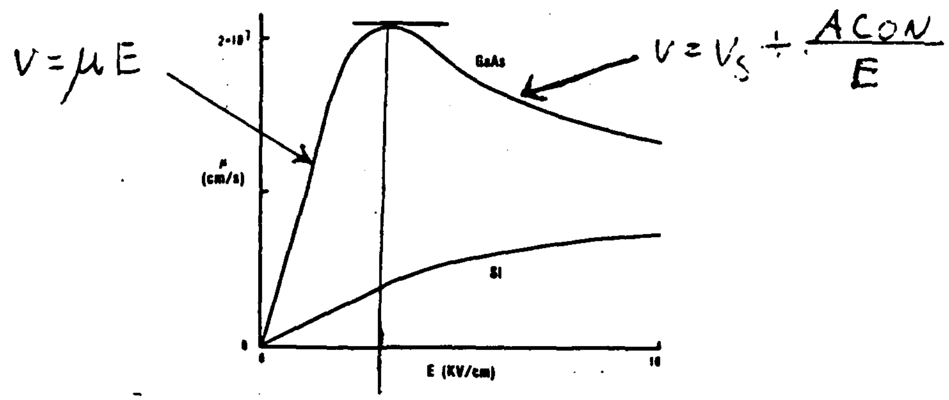

Peak electric field (where it occurs for peak electron velocity).

FIG. 3. Drift velocity of electrons as a function of electric field and the analytic equations used to approximate curve.

REFERENCES

Williams, Ralph E., Gallium Arsenide Processing Technology, Dedham, Massachusetts, Artech House, Incorporated, 1984, page 19.

1988 USAF-UES SUMMER FACULTY RESEARCH PROGRAM

GRADUATE STUDENT RESEARCH PROGRAM

Sponsored by the

AIR FORCE OFFICE OF SCIENTIFIC RESEARCH

Conducted by

UNIVERSAL ENERGY SYSTEMS, INC.

FINAL REPORT

Noise Calculations in a RADAR Receiver

Prepared By:	Beryl L. Barber and Daryl W. Sprehn
Academic Rank:	Assistant Professor and Graduate Student
Department and	Electronic Engineering Technology
University:	Oregon Institute of Technology
Research Location:	AFRADC/OCTP Griffiss AFB, NY 13440-5700
USAF Researcher:	Frank E. Welker

Date:	26 August 1988
Contract No.	F49620-88-C-0053

SAME REPORT AS
PROF. BERYL BARBER
ROME AIR DEVELOPMENT CENTER # 52

1988 USAF-UES SUMMER GRADUATE STUDENT RESEARCH PROGRAM

Sponsored by the

AIR FORCE OFFICE OF SCIENTIFIC RESEARCH

Conducted by the

Universal Energy Systems, Inc.

Chemical Kinetics Information Collected for IF Flow Tube

Report period, 1June to 8Aug 1988

Prepared by: Frank Bynum

Academic Rank: M.S. Candidate,

Dept. and Univ. Physics Dept. Miami University, Oxford Ohio

Research Location: AF Weapons Lab,

Advanced Chemical Lasers Branch, AFWL/ARBI

Albuquerque N.M. 87117-6008

USAF Researcher: Glen Parram, Capt. USAF

Date: Thurs9-29-88

Contract No: F49620-88-C-0053

^Z

Mr. Frank Bynum

ABSTRACT

Information usable for modeling the IF Flow Tube Experiment was compiled. Species are listed which models should track. Diagrams of energy levels of selected species are given. A number of the important reactions are presented. They are categorized by functional region of the flow tube device, for its current configuration, and for future planned additions.

Greatest level of detail was developed on the temperature dependence of rates pertaining to the generator for dissociated F atoms. Density vs. time curves for this part were calculated, and are shown.

CONTENTS

DEDICATION

I would like to express my appreciation of the opportunity to be here and participate in the research activities of the branch. This 10 week session has come to a conclusion all too quickly.

Thinks are extended to:

-- Glen Parram, who was the research contact point with whom I interacted most on technical issues;

--to Bob Crannage, the local contract monitor and my office mate, who shares similar tastes in literature read for enjoyment;

--Gordon Hager, who said that the literature search would be a major need;

--Charley Helms, who will be one of the inheritors of copies of the documents stack found and acquired, and who provided me with an early increment to that stack;

--Richard Kepler, the official AFWL focal point for this AFOSR -UES program;

the AFOSR and UES organizations, that make this program possible.

CATAGORIES of SYMBOLS

The symbols categories used are described here. The principle reason for this is that word processor programs which most of this report were written on don't handle Greek and other math symbols well. Chi-Writer could, and was used to produce a few of the tables and lists. Other cases were spelled out in characters more commonly available on key boards.

>= greater than or equal
=< equal or less than
letter ^ number: molecular state designations, name, multiplicity

superscript.
^ rased to the power of... , or superscript
Greek letters spelled out, (i.e. Sigma), text describing the symbolic character used in the given position. (Pi is another obvious one).
sub... next character is a subscript of preceding character.
symbol1_symbol2 : another way to show subscripts

INTRODUCTION

A current research interest of the Advanced Chemical Lasers Branch of the US Air Force Weapons Lab is the area of visible chemical lasers. One of the projects under study is called the IF Flow Tube. This paper is connected to IF Flow Tube modeling and data interpretation.

It is desirable to obtain laser light at shorter wavelengths--namely the visible region. The process is to have the potential of being scaled eventually to high power levels. The population inversion is to be made by purely chemical (not optical- or electrical-pumping) means.

The over all project theoretically and experimentally studies the problems involved in obtaining laser action from IF (Iodine Monofluoride). It is produced and excited chemically.

In gas dynamic and chemical lasers, reactant streams produce quantities of chosen lasing materials in their excited state. Gas dynamic expansion through nozzle flow paths alters the thermo-physical condition, in ways favorable to getting a population inversion which can lase.

Spectroscopic and quantum mechanical factors yield energy level structures and transitions which may be of use. Chemical kinetics affects which reaction scheme, pressure, temperature, and mixture ratios would work. Gas dynamic considerations govern the mixing by diffusion and laminar or turbulent convection.

HF (or, with the other isotope, DF) and I^* have been used in lasers pumped by purely chemical means. Both undergo stimulated emission in the infra-red. The former involves diatomic molecules in their electronic ground state, but with inverted populations involving vibrational excitation. Iodine is dissociated and rased to the first atomic electronic excited energy level I^* -->I + photon radiative transition involves a spin quantum number change only. Orbital angular momentum and principal quantum number do not change.

For stimulated emission in the visible band, conceder radiative transitions between electronic levels in diatomic molecules. They are to be states which can be generated by being the products of chemical reactions.

An inter-halogen molecule IF, is the focus of current work. Flowing streams of iodine and fluorene yield IF as the intended product. It is a reactive molecule which must be produced as needed, by gas phase chemistry. (It converts to other compounds, such as IF5 in reactions with solid surfaces.)

The long lived metastable electronically excited diatomic oxygen, a state designated O2(a singlet Delta), is a chemically produced energy store. It can undergo electronic energy transfer collisions, by which IF is pumped to the desired higher electronic level. The excited oxygen is evolved from its generator where

heterogeneous reactions occur between gaseous Cl_2, basic hydrogen peroxide. The latter is a mixture of some base such as KOH or NaOH with H_2O_2. The phases are gas plus liquid.

Earlier studies pointed out that some of the key properties data for the aqueous or 2 phase chemistry in the excited oxygen generator were still undetermined. There is contract work underway at other facilities to make those measurements for the first time.

ARRANGEMENT of the IF FLOW TUBE EXPERIMENT

This section relates to figures illustrating the hardware for the IF Supersonic Flow Tube experiment. The apparatus has been assembled within the Chemical Laser Facility of AFWL/ARBI.

Fig 1 shows the IF Flow Tube configuration, with the inlet flow streams of the reactants and non-reacting gases. Note that flow is form left to right. It is this arrangement which shall be tested experimentally first. IF will be produced. The diverging section to the right leads out to the vacuum pump, shown in plan and elevation in Fig2.

Fig3 clarifies the same arrangement by resorting to a schematic diagram for the interior, where the flowing gas mixture will be. Reactants' injection locations, with a point design set of flow rates are apparent. Note that there are 2 throats.

The stage referred to as "R1" is from F_2 and NO injectors to some where near the first throat. Nearer the I_2 injectors is referred to as "R2".

Fig.4 illustrates plans for a later stage in the testing. Here, there has been added a generator for excited molecular oxygen, so that the IF can be rased to an excited state.

The insert is for one early layout for the geometry that would permit the recently generated IF laden stream to interact with the excited oxygen stream. In Aug'88, an alternate layout, where IF producing reaction zones were segregated onto a center body, delaying mixing with O_2^* compared to that shown. The area for mixing with O_2^* is referred to as "R3".

A list was formed for the most important reactions expected in the experiment.[4] They are shown below.

****

Table1

Overview of Reactions for IF Flow Tube

There are 2-3 sequential regions of the IF Flow Tube where the most important reactions are very briefly summarized.

R.1 Combustion. chamber, to generate free F.

R2. Second mixing chamber, I_2 injected at 2nd throat, then nozzle expansion.

R3 output of O_2^* generator output is mixed in. This is not initially present. It may be added later, and so model might or might not include it.

O_2^* is excited molecular oxygen, O_2(singlet Delta)

R1.
NO + F2 --> NOF + F
F + F + M --> F2 + M
F + Wall --> products

R2
F + I2 --> IF (v) + I
IF(v) + M --> IF(v-1) + M   (many v states to track)

R3
IF(v">10) + O2* --> IF(A') + O2(grnd.st.)
IF(A') + O2* --> IF(B,v') + O2(g.s.)
IF(B,v') + M --> IF(B,v'+-n) + M

The IF flow tube experiment initially has regions R1 and R2. The flow is from one to the next in series, presumably without earlier stage products being separated. These are to be modeled first, with the option to add on excited oxygen pumping, as planned for that experiment's future upgrade.

****

Table2 is a summary of I-F Flow Tube Species that are recommended for inclusion in computer numeric models of the relevant chemical kinetics.

Another perspective on these, and other species also to evaluate for inclusion in a later versions of models, may be seen in the following listing. These were gleaned from consultation of a copy of CRC Handbook of Chemistry and Physics.

****

Table3

Species of Conceivable Interest, From Tables (general, no short lived species)

The C.R.C. Chem and Phys. H.B. was consulted for tabulated info in the inorganic compounds category. These were around B98, B118, etc, 64th ed.

The elements in question are N, O, F, I.

Nitrogen: N2; NF3; NI3; NO; N2O; N2O5; NO3; the peroxide di (NO2); N2O3; NO3F; NOF; NO2F.

Fluorene: Mistakenly entered there as monatomic! should be F2 (change formula to this, change Mol.Wt.; F2O; F2O2;

Oxygen: O2; O3; OF2.

Iodine: IN3; IF7; IF5; IO2 or I2O4; I2O5; I4O9; I2.

The particular table listed for each: name; synonyms & formulas; crystal form, properties, refraction index; density or sp. grav.; *solubility (cold water, hot water, other solvent)*; Tmp, Tbp (deg.C).

That is a list of 25 compounds stable enough to be tabulated in this source.

****

An outline was made of desirable activities in literature searches and modeling, which guided this writer's efforts during the summer of research on the IFFT project. It is shown in the table on

'Plan of Attack Outline, IF Flow Tube Study' Some elements in it were completed to the extent that time during the 10 week summer research period permitted. Its other elements are recommended for study by those who remain with or newly join this project.

It was formed, in collaboration with Glen Parrem. The product is to assist Gordon Hager and others associated with the Iodine-Fluoride Flow Tube ongoing research project. That 'product' is, first, this research report to AFOSR and UES, and second, a longer version. That longer version is expected to be for the duel purpose of being a MS thesis, and informing the colleagues at AFWL/ARBI as to more of the information accumulated in this effort.

****

Table4
Plan of Attack Outline, IF Flow Tube Study

OUTLINE:

I. Database Research

* NO + F2 chemistry F atom concentration, temperature, byproducts (NOF)

* F + I2 kinetics; see Davis report, refs. to Trickil. F I2 --> IF(X',v") + I, distribution of IF over vibration levels v". Mechanism: I2 F + I2 --> ? Disproportionation F + IF --> ? IF + IF --> ?

* IF(B) kinetics. ref. to Wolf. IF(B,v') + M --> IF(B,v'+delta v) + M IF(B,v') + Q --> IR(X) ref to Roderik

* IF(X) kinetics, {Estimates}. Check out some I2 rates. ref. to COIL reports

* O2(^1 Delta) + IF kinetics

II. Time profile predictions (spatially lumped without fluid dynamics).

III. Fluid Mechanics.
1-D steady;
2-D Steady.

Time like Relaxation solution for pseudo boundary conditions, or time accurate solution.

Dependant variables to track: velocity, pressure, temp., concentrations, wall heat flux, wall mass flux., over all density.
****

RESULTS from LITERATURE SEARCH RELATED to IF

In this section is given a list of figures for a portion of the *literature gathered, which is relevant to the IFFT experiment.*

(bot. of page) Table5, of energies for Oxygen, Iodine, IF; Einstein A coefficients and transition wavelength

(top of pg) Table2 of species to track in kinetics modeling of IFFT

Fig.5 Potential curves for O2, NO, N2, and 2 states of IF.

Fig.6 IF (B -->X) emission spectra

Fig.7 a typical P-R doublet and table6, rotational assignments of some IF(B <-- X) optical absorption transitions

Fig.8, F + IX --> IF + X, X= I, Br, Cl. Detailed rates for formation of vibrationally excited IF(X,v), v>=0.

Table6 Detailed rate constants k_v , normalized to 1 when v=0, for above figure, X= I, Br, Cl.

Table 7
****

IF FT reactions planned for forming IF

F+I2 -->(k3) IF + I
k3 = (4.3+-1.1)E-10 CM^3 MOLECULE^-1 S^-1 at T= 298K

IF is lost to reactions at the walls

IF-->(IF)_x(s)	k_w	s means at solid surface
(IF)_x(s) --> IF	k_-w	()_x, a polymer
F+ (IF)_x(s) --> IF5	k_p	

[46]

F+ I2 --> IF + I (Delta H_0 ^0 = -118.4 kJ/mole)

Reaction should be considered branched
F + IX -->IF! _ X(^2P_3/2) k_1 !=Vibrational excited
F + IX--> IF + X*(^2P_1/2) k_2 (X=Cl, Br, I)

[47]
F2 + I2 --> I2F + F E threshold=4.2 kcal/mole
F + I2F --> IF + IF. Delta H_0 ^0 = -64 kcal/mole
I2 + F2 --> I2F!+F -->I + IF + F
The minority of IF of this reaction is in the B state [14]
I2 + F2 -->products,
k=sigma* <v(T)> * exp(-E0/(R*T))
k(T=300K) = (1.9+-0.4)E-15 cm^3/(molecule sec)
sigma = 1Ang^2
5/1E4 of collisions at room temperature are energetic enough to make IF2.

4.2 kcal/mole will allow the reaction to go, through F generation, although 37 kcal/mole is required to dissociate F2 or I2 separately.

[48,49]

****

Fig.9 Potential curves for some low lying IF electronic states

Fig.10 Time evolution measured populations for IF (B,v'), v' = 0 to 4, at 2 pressures.

Table7 List of reactions with O_2^*, their kinetics in certain experiments.

Table 8 List of some IF(B) loss paths when I_2 is present

Table.9 rate constants for loss of O^* and O_2^* (* = electronically excited states)

MODELING for F GENERATOR PORTION of the EXPERIMENT

A running example from Numerical Recipes, W. Press et. al. of Runga-Kutta order 4 vector ODE solver has been produced. It is initially configured to solve ydot=y, from x1 to x2, y(x1) = exp(x1).

Next, it is desired to set code, in which it will be included, for solving chem. kinetics problems. The one at hand is initially for the combustor section of the IF Flow Tube Experiment, at AFWL/ARBI.

In that experiment, NO, and F_2, both in streams of a common diluent such as N_2, He, or Ar are to react. This initial program task is to give time-wise profiles of species densities.

Note: rate constants follow general form

k = a * T^N * exp (-E/(R*T))

The reaction set for the IF flow tube F generator (combustor) is:

```
NO + F2 --> (k1) FNO + F    (1)
F + NO + M -->(k2) FNO + M (2)
FNO + M -->(k3) NO + F + M  (3)
F2 + M -->(k4)  M + F + F   (4)
F + O2 + M --> (k5) FO2 + M  (5)
NO2 + F2 -->(k6) NO2F + F    (6)
F + NO2 + M --> (k7) FNO2    (7)
Reaction i has rate Ri
R1=n_NO*n_F2*k1
R2=n_F*n_NO*n_M*k2
R3=n_FNO*n_M*k3
R4=n_F2*n_M*k4
R5=n_F*n_O2*k5
R6=n_NO2*n_F2*k6
R7=n_NO2*n_F*n_M*k7
Time rate of change of species j density
n_NO_dot=-R1-R2+R3
n_F2_dot=-R1-R4
n_FNO_dot=R1-R3
n_F_dot =R1-R2+R3+2*R4-R5+R6-R7
n_O2_dot =-R5
n_NO2_dot=-R6
n_FO2_dot=R5
n_FNO2_dot=R7
```

Table 10
Summary of author(s),date, ref#.

Perrine & Johnston 1953	[43]
Rapp & Johnston 1960	[29]
Shearly,1971	[42]
Hoell 1973	[41]
Zetzsch 1973	[38]
Kolb 1976	[20][30]
Blauer 1979	[31]

Table 11

Rctn #	A cm^3(r-1)particle^-(r-1)s^-1	r	N	E kcal/mole	ref.
1	7.04E-13	2	0	2.3+-0.1	[20]
1	1.8E-12	2	0	3.0	[38]
1	5.5E-14	2	0	1.5	[31]
2	1.1E-31	3	0	0.2+-0.3	[38]
3	5.5E-5	2	-1	0	[31]
4	1.4E-34	3	0	35.1	[31]
5	4.7E-33	3	0	-1.3	[38]
5	5.2E-38	3	-2	0	[38]
6	2.6E-12	2	0	10.47	[43]
	for the combined effect reactions 6&7				[43]
7	8.8E-31	3	0	0.2+-0.3	[38]
7	alone.[38]				

A typical temperature of 600K was assumed, and the values of k_i were thus calculated.

Initial values for densities were set according to the following assumptions. Pressure in the "combustor", upstream of first throat (region referred to as "R1", because I2 would not have been added yet). given as 100 torr. Total density would be that form ideal gas law, assuming that pressure, and the above temperature. Assumed that the "initial densities" were numerically similar to the given reactant molar flow rates. (See the figure on schematic of IF Flow Tube Baseline Flow Conditions.) The mole fractions of the reactants (primary, and also 2 percent contaminate O2 in F2, or NO2 in NO) were found as 0.061 moles/s total, 0.06 being He (or other 'non reactive background gas'), 0.005*0.98 being NO or F2, 0.005*0.02 being NO2 or O2. Initial species densities were set to the mole fractions times the total density for above pressure and temperature.

Due to time constraints, first week in Aug'88, last few days of my research period, these values were tabulated and handed to Bob Crannage, Capt. USAF. The used them to run a program called CHEM which the branch uses routinely in similar 'time profiles' chemical reaction kinetics studies. He was kind enough to run this case and hand to me the graphs, included as figures here, of the results.

CHEM is a program running on a Cray-1 computer. This is a very small reaction system compared to many others it has been used upon. It is reaction kinetics, or rather species balance only, without an energy balance (the latter would be needed to tell of time profiles for temperature, which would feed back on influencing the rates). It has many other features not employed here. Among these are choices of alternate integrator algorithms, or the more expensive (of computer resources) analysis of sensitivity to variations in uncertain rate

constant values and initial densities.

Table.12. shows text for operation of the CHEM code to produce density time profiles from reactions for the 'combustor', or 'R1' suction of the IF Flow Tube experiment. Note initial densities of no, f2, f, fno, etc, in particles /cm^3. Below that is a coding for the reactions, and value of the rate constants at chosen temperature. The symbol m is for a general collision partner.

figures..... Graphs of density vs. time for the 'R1' set of reactions, output from the CHEM code

Fig... at bottom and top of page show the He and NO being of constant, or 'near constant' amounts with time. The NO is consumed by combining with F2 and F, and produced by breakdown of FNO, thus its near constancy, while surprising, is not utterly implausible.

Fig.11. to Fig.19. show consumption of the contaminate NO2, the reactant F2, the contaminate O2. They show that the desired product, Dissociated F, is evolved, approaching 22.5*10^16 particles /cm^3. They show the expected byproduct FNO, and the byproducts due to contaminates, FO2, FNO2, increasing with time. The FNO is predicted to plateau out at concentrations a few orders of magnitude less that the assumed levels of contaminates.

CONCLUSIONS and/or RECOMMENDATIONS

Literature was searched and an early phase of modeling were conducted by the author, as a contribution toward study of IF as a candidate system for chemically pumped visible band laser medium. Activities of this nature, notably those elements appearing under the section "outline and plan of study" merit continuation by those who remain affiliated longer term with this project

There is an ongoing series of tests upon experimental hardware which will, first, produce IF, and later, attempt to excite it in order that gain be measured. The chemical kinetics and fluid mechanics (coupled) modeling will aid in interpretation of the data, and suggesting useful changes in the setup.

An important issue in the scheme for excitation of IF is knowledge of the detailed rates for forming IF(X,v), v=0,1,... high, from the F + IX -->IF + X reaction. (X= I, Br, Cl). Incidentally reports were found that k_v verses v was double humped (one energy path making vibrationally excited IF(X), the other making X*). Other recent measurements of this process should be searched for. The data appearing here in the figures, and that of another author, cited by the Davis et al AFWL report, are several orders of magnitude apart when IX is the molecular species I2.

The implications for the IFFT experiments planning are that not only I2, but also IBr, ICl, should also be considered for tests of making IF(X,v>10).

Ref. notes, and bibl.
****

[1] Chemical Kinetics and Reaction Mechanisms, F. Wilkinson, Van Nostrad Reinhold, c1980 QD502.W54 542'.39 ISBN 0-442-30248-5 pbk

[2] S.J. Davis et al J.Chem.Phys V78(1) 1Jan.1983 pg172

[3] IF(B) v-r states higher than, predissociation level, they get ignored.

[4] Notes of conversations with G.P. and G.H. F3June'88 .
[5,6] of Davis 1980,83 and Wolf 1985-..
[7] The C.R.C. Chem and Phys. H.B. [7] was consulted for tabulated info in the inorganic compounds category. these were around B98, B118, etc, 64th ed.
The elements in question are N, O, F, I.
[8] Numerical Recipes by William H. Press et.al. Cambridge U. Press, Cambridge, c1986 ISBN 0 521 31811 9 QA 297.N866 1986 001.64'2'0151 or 519.4
[9]Incidentally, another program, which most closely represented that listed by Press still exists as well--EXP1MN.FOR It has less features desired for "long" problems though. See features section above.
[10]Step size is still of constant amount as of the M6-27-88 version. Perhaps an adaptive stepsize algorithm will be added, based on [1].
[11]The author may be contacted for code source listings.
[12]Grad. Summer Research Program sponsored by AFOSR, contracted with United Energy Systems Inc. of Dayton OH., at Kirtland AFB AFWL/ARBI, the chemically pumped high power lasers section
[13] Plan of research & brief activities report submitted to UES by
[14] M.J. Coggiola J.J Valentini Y.T Lee LLL Molecular Beam Study of F2 + I2 Int'l. J of Chem Kinetics v 8 605 -608 (1976)
[15] Studies of BrCl by Laser Induced Fluorescence Clyne and McDermid J of the Chem Soc Faraday Trans II v74 (1978) p807 nov77
[16]Quantum-resolved Dynamics of Excited States pt 4 radiative and Predissociative Lifetime of IF B^3 Pi (0^2) Michael A.A.Clyne I. Stuart McDermid Queen Mary Col. London Mr'78 J of the Chem Soc Faraday Trans II V74 (1978) p1644
[17] Wolf et.al. J Chem Phys V82 N5 7Mr85
[18] Physics and Chemistry of Upper Atmospheres Proc. Smps. Summer Adv. Study Inst U. Orleans France 31July-11Aug1972 Ed. by B>M.McCormac D Riedel Pub Co Dordrecht-Holand/ Boston usa C.1073 Qc878.5 n81 V35 Astrophysics and Space Science Library
[19] K. Rapp H.S. Johnson J. Chem Phys V33 N3 sept1960
[20] C.E. Kolb J Chem. Phys V64 N8 15April 1976
[20a] J.A. Blauer et.al. IEEE J. of Q. Elec. V QE 15 N9 July 1979 pg602 Comprehensive Kinetics Model for DF-CO2 Transfer Chemical Lasers.
[21]M.J. Coggiola et.al. Int'l J. of Chem. Kinetics v 8 605-8 (1976)
[22]M.A.A. Clyne I.S. McDermid J of the Chem. Soc. Faraday Trans II V74 (1978) p1644
[22a] see [22] pg1648 for citations
[22b] from ref15 of[2]; J'=J"=0 values
[23]R.A. Durie The Electronic Emission Spectrum and Molecular Constants of Iodine Monofluoride Canadian J. of Physics V41 (1966) Pg337
[24]T. Triclk & J. Wanner high Resolution, Laser-Induced Florescence Spectroscopy of Nascent IF: Determination of X and B- State Molecular Constants. J of Molecular Spectroscopy V104 174-182 (1984)

[25]J.Stregack and G.W Zieders Some Scaling Considerations for Pulsed Chemical Lasers, p711 in Proc. of Int's conf. on Lasers'81 STS Press McLean Ma. 1983
[26]M.S Zediker G.H. Miley Generation of O2(a^1Delta) by Nuclear Pumping Pg.492 Lasers'81 proc. ed. by C.B. Collins Conf sponc. by Soc for Optical & Quantum Electronics

[27]T.G. Slanger Reactions of Electronically Excited Diatomic Molecules, section 5 pg.231 on Reactions of Small Transient Species, Kinetics and Energetics ed. by A. Fontijn and M.A.A. Clyne Academic press c 1983

[28]W.H. Breckenridge Reactions of Electronically Excited Atoms, in Fontijn & Clyne's book (above), section 4 pn157

[29] K. Rapp H.S. Johnson J. Chem Phys V33 N3 sept1960

[30] C.E. Kolb J Chem. Phys V64 N8 15April 1976

[31] J.A. Blauer et.al. IEEE J. Quantum Electronics V QE-15 N.7 July 1979 P602 Comprehensive Kinetics Model for DF-CO2 Transfer Chemical Lasers

[32]Hager, G.D. et.al. Operation Characteristics of a Hi Pressure DF-Co2 CW Chemical Transfer Laser pg595 IEEE J. Quantum Electronics V QE-15 N.7 July 1979

[32b]S.S Bashkin et.al. Sov. J. Quantum Electron. V16 N3 March1985 c'86 Am. Inst. Phys. Feasibility of construction of a chemical laser utilizing the B-->X electronic transition in the IF molecule

[33] R.F, Hiedner III et.al. J. Chem. Phys. V74 N10 15May1981 pg5618 Temperature dependence of O2(^1Delta) + O2(^1Delta) and I(^2P1/2)+ O2(^1Delta) energy pooling

[34]S.J. Davis et.al. Chemical Pump Sources for IF(B) AFWL-TR-87-92 16 Nov. 1987.

****

From mix726.txt, the combined refferences below.

[33] R.F, Hiedner III et.al. J. Chem. Phys. V74 N10 15May1981 pg5618 Temperature dependence of O2(^1Delta) + O2(^1Delta) and I(^2P1/2)+ O2(^1Delta) energy pooling

[34]S.J. Davis et.al. Chemical Pump Sources for IF(B) AFWL-TR-87-92 16 Nov. 1987.

[18]B.M. McCormic Physics & Chem. of Upper Atmosphere, D Ridel Co. Boston C.1973

[38]C. Zetzsch Some Combination Reaction of Fluorine Atoms Pg 35 in Combustion Institute. European Symposium 1973 ed by F.J. Weinberg Academic Press 1973 London

[32] G.D. Hager et.al. IEEE J. Quantum Electronics Vol QE-15 N.7 pg595.

[35] R.H. Obenauf et.al. Production of Electronically Excited Species in Some Exothermic Elementary Reactions pg.41 in Combustion Institute European Symposium 1973 (Sept. U. of Sheffield) ed. by F.J. Weinberg, Academic Press London, New York 1973

[35 ref7 (Indirect reference)] P.N. Clough, P.A. Thrush Trans. Faraday Soc. V63, p915 (1967)

[35 ref9] R.H. Obenauf et.al. J. Chem. Phys V57 p 2674, (1973)

[16]M.A.A. Clyne S. McDermid J Chem Soc. Faraday Trans. II V74 (1978) p1644

[36] CRC Handbook of Chemistry & Physics; Weast; Ed. 64 1983-4 pgF57 Physical Constants of Ozone and Oxygen

[37] Ernest Dorco, private communication W7-13-88

[39] JANAF tables, under IF Iodine Monofluoride

****

Fluorine generator kinetics for simulation

[19] K. Rapp H.S. Johnson J. Chem Phys V33 N3 sept1960

[25]J.Stregack and G.W Zieders Some Scaling Considerations for Pulsed Chemical Lasers, p711 in Proc. of Int's conf. on Lasers'81 STS Press

McLean Ma. 1983
[29]K. Rapp, H.S. Johnston; J. Chem. Phys. v33 n3 sept.1960 pg.695
[20][30] C.E. Kolb J Chem. Phys V64 N8 15April 1976
[31][20a] J.A. Blauer et.al. IEEE J. Quantum Electronics V QE-15 N.7 July 1979 P602 Comprehensive Kinetics Model for DF-CO2 Transfer Chemical Lasers
[32]Hager, G.D. et.al. Operation Characteristics of a Hi Pressure DF-Co2 CW Chemical Transfer Laser pg595 IEEE J. Quantum Electronics V QE-15 N.7 July 1979
[38]C. Zetzsch Some Combination Reaction of Fluorine Atoms Pg 35 in Combustion Institute. European Symposium 1973 ed by F.J. Weinberg Academic Press 1973 London
[41]J.M Hoell et.al. J. Chem Phys V58b N7 1April 1973 pg2896 Measurements of J2, NO, and ONF Raman cross section and depolarization ratios for diagnostics in chemical lasers
[42]J.A.Shirley et.al. Purely Chemical Laser Operation in the HF, DF, HF-CO2, and DF-CO2 Systems. 25-27 Jan1971 AIAA 9th Aerospace Sci. Mtg. New York, New York. AIAA Paper #71-27
[43]R.L. Perrine & H.S Johnston J. Chem. Phys. V21,N12 Dec1953 Pg. 2202. Kinetics of the Fast Reaction between Nitrogen Dioxide and Fluorine
[44]L.J Lawlor et.al. J. Amer. Chem. Soc. V100 N26 20Dec1978 Ab Initio Studies on the Electronic Structure of ONF (Nitrosyl Fluoride) and NOF (Nitrogen Hypofluorite)
[45]L.A. Curtis V.A. Maroni Ab Initio Molecular Orbital Calculation and Semiemperical Analysis of the Vibrational Frequencies and Force Constants of ONF and FON.
****
[46]E.H. Appelmann & M.A.A. Clyne J. Chem Soc. Faraday Trans I 1975 V71 N10 Pg.2072
[47]T.Trickl J. Warner J. Chem. Phys. V78 N10 15 May 1983 pg. 6091
[48]Coggiola et.al. Int'l J. of Chem. Kinetics, V8 p605-8 (1976)
[49]P.D. Whitefield S.J. Davis Chem. Phys. Lett. V83 N1; 1 Oct1981 pg44

[*]References numbering (direct) is based on cumulative scheme for citations, as of 9July88 and afterward, in IF FT related text accumulated by F.A. Bynum.

1988 USAF-UES SUMMER FACULTY RESEARCH PROGRAM/

GRADUATE STUDENT RESEARCH PROGRAM

Sponsored by the

AIR FORCE OFFICE OF SCIENTIFIC RESEARCH

Conducted by the

Universal Energy Systems, Inc.

FINAL REPORT

STOCHASTIC SITE CHARACTERIZATION AND MODELLING

Prepared by:	Alan C. Jewell
Academic Rank:	Master's Candidate
Department and University:	Civil Engineering Department, Colorado State University
Research Location:	AFWL/NTESG, Kirtland AFB, NM 807117-6008
USAF Researcher:	Dr. Robert Reinke

Date:	15 Sep 88
Contract No:	F49620-88-C-0053

Stochastic Site Characterization

and Modelling

by

Alan C. Jewell

ABSTRACT

Cone penetrometer data from a site containing random spatial variations in soil properties was analyzed for stochastic properties. Techniques of analyzing such properties using the autocorrelation function were considered. Basic design parameters for future site characterization surveys were found. The inhomogeneities were modelled stochastically based on three statistical properties (standard deviation of the variations, and horizontal and vertical scale lengths of the inhomogeneities) using three statistical models (Gaussian, exponential, and Von Karman). Non-random vertical trends in the data were incorporated in the model. Preliminary results indicated a good correlation between the model and data.

Acknowledgments

I am very grateful to the Air Force Systems Command and the Air Force Office of Scientific Research for sponsoring my research at Kirtland Air Force Base. Dr. Wayne A. Charlie of Colorado State inspired me to participate in the research program and Universal Energy Systems was helpful and courteous in administering the program.

A great many people at Kirtland Air Force Base made the research experience very beneficial. Dr. Robert Reinke provided technical expertise and encouragement. Kent Anderson collaborated with Dr. Reinke to make the experience enjoyable as well as provide invaluable help with the computer systems. Capt Conrad Felice provided much help and encouragement also. J.J. was particularly helpful with all phases of the project. Maj. Tom Bretz and Al Leverette each helped to make the summer interesting.

I. INTRODUCTION

I am currently studying for a Master's Degree at Colorado State University in Geotechnical Engineering. My undergraduate degree is in Geophysical Engineering from the Colorado School of Mines. I have participated in many types of geophysical exploration projects using seismic reflection and refraction, borehole, gravity and electromagnetic techniques. I spent three years interpreting seismic data using signal processing techniques such as two-dimensional digital filtering and deconvolution. I have worked on data aquisition systems and the design of such systems.

Researchers at the Geologic Response Section of the Civil Engineering Division of the Air Force Weapons Laboratory at Kirtland AFB have analyzed the effect stochastic geologic parameters on blast-induced ground motion. Several tests have been performed which show that scattering of stress waves caused by geologic inhomogeneities tends to significantly reduce the coherency and magnitude of energy from the blast above a threshold frequency. Significant amounts of incoherence were observed above the 70 Hz range for receivers azimuthally spaced .30 m apart at a distance of 20 m from the blast. The threshold frequency has been shown to be related to the scale length of geologic inhomogeneities. Deterministic modeling of a particular site is usually impractical due to the small size of the inhomogeneities, therefore, stochastic modelling is required. A research method utilizing cone penetrometer testing has been designed to determine the stochastic parameters for a particular site. Site

characterization research of this nature is important to the design and location of critical structures.

II. OBJECTIVES OF THE RESEARCH EFFORT

As a participant in the Graduate Student Research Program (GSRP), my goals were to analyze the cone data from the most extensive test of the series (CRAPS III) for the salient stochastic properties, make recommendations on the design of site characterization programs, attempt to model the data stochastically and run a finite difference simulation using the model. Due to the limited time available for research, finite difference simulation of the test bed was not performed. It was deemed necessary to save this work for inclusion with my thesis under possible funding from the AFOSR Mini Grant Program.

III. DETERMINATION OF STOCHASTIC PARAMETERS

a. Aki and Richards (1980) present a method to calculate the amount of scattered energy as a function of frequency known as the Born scattering approximation. If primary waves unchanged by propogation are assumed and only single scattering occurs, the the ratio of scattered energy to total energy is given by:

$$dI/I = 8\langle\mu^2\rangle k^4 a^3 L \quad \text{for} \quad ka < 1, \text{ and} \qquad (1)$$

$$dI/I = 2\langle\mu^2\rangle k^2 a L \quad \text{for} \quad ka > 1$$

where dI/I is the ratio of scattered energy to total energy, u^2 is standard deviation of the velocities of the medium, a is the scale length of inhomogeneities, k is the wavenumber, and L is the length of travel of the wave. Thus, according to the Born approximation the scattering properties of a particular site are dependent on the stochastic properties of scale length and standard deviation of the inhomogeneities.

To obtain the scale length of inhomogeneities present in a given set of data, the autocorrelation function may be used. If a set of equally spaced samples u(r) are present, then the normalized autocorrelation function is given by

$$N(r) = \text{sum}\ (\ u(r)u(r+r')\ )\ /\ \text{sum}\ (\ u(r)u(r)\ ) \qquad (2)$$

Several theoretical autocorrelation functions are considered:

$$N(r) = e^{(-A)},\ A = r^2/a^2 \qquad \text{(Gaussian)} \qquad (3)$$

$$N(r) = e^{(-A)},\ A = r/a \qquad \text{(exponential)} \qquad (4)$$

$$N(a) = K_0(r/a) \qquad \text{(Von Karman)} \qquad (5)$$

Fig 1 shows a typical autocorrelation calculated for a standard cone penetrometer test, along with theoretical exponential and Gaussian functions. Determining which theoretical curve fits the data best is obviously open to interpretation as is the determination of the scale length.

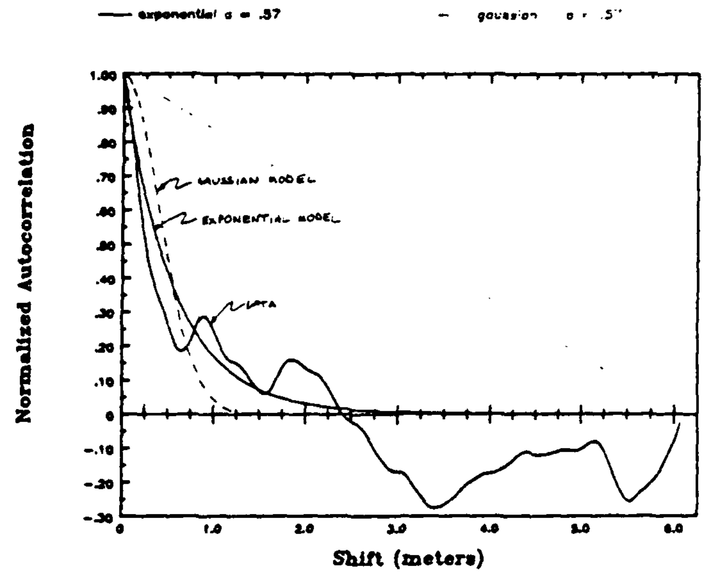

Fig. 1 - Typical vertical normalized autocorrelation for standard cone penetrometer data.

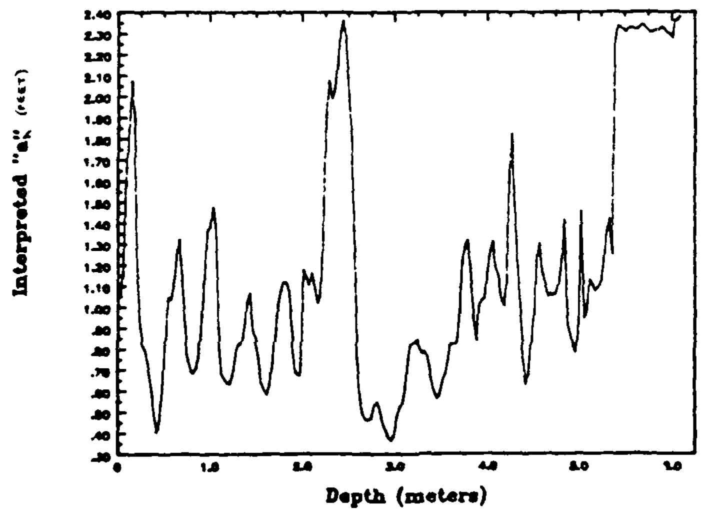

Fig. 2 - Interpreted scale length vs. depth for standard cone penetrometer data.

For exponential data, "a" is equal to the area under the autocorrelation curve or the value of r at $N(r) = .37$. Similarly, it can be shown that for Gaussian data, "a" is equal to 1.128 times the area under the curve or the value of r when $N(r) = .37$. Use of any of these rules to pick "a" on the CRAPS III data did not give good results. By trial and error, it was found that using the area under the curve up to the first zero crossing as the value for "a" gave a good fit to the theoretical curves for all cases examined. This is the technique used to calculate the "a" used for the theoretical curves in Fig 1.

Utilizing this method on some of the CRAPS III arrays, a plot of a_h (horizontal scale length) vs. depth or a_v (vertical scale length) vs. horizontal distance can be generated by an automatic "a" picking program. An a_h vs. depth plot is shown in Fig 2. This plot shows wide (.40 to 2.4 m) variations in the scale length. Most of these plots showed a similar half-order of magnitude variation, however, plots of vertical scale length vs. depth showed about half as much variation as the horizontal case. The values of the scale lengths used in the modelling procedure described later in this paper were simply taken as the median of the variation range. The following values were found: $a_h = .4$ to $.5$ and $a_v = .1$. Data from both standard cone arrays (horizontal spacing = 2m, vertical sample spacing = .1 ft) and mini-cone arrays (horizontal spacing = .2 m, vertical sample spacing = .5 in) were analyzed and found to be in general agreement.

Values for scale length calculated from cone tip, friction sleeve and friction ratio values agreed as well. Since the ratio of vertical to horizontal scale lengths was 4 to 5, it was necessary to distinguish the two for modelling purposes.

The design of a site characterization survey using the cone penetrometer is very important. An equally spaced set of cone soundings will yield both horizontal and vertical scale lengths from the same data. Assuming the geophysical properties of the site are isotropic with respect to the horizontal plane, the orientation of such an array would not matter, however, if dipping layers exist, this condition may not be true. If not enough geological and/or geophysical data exists to insure that the stochastic properties do not vary significantly in the lateral direction several arrays may be necessary.

Particular attention must be paid to the size and sampling distance of the array in both directions. An estimated range of values for the scale lengths must be known beforehand in order to design the array properly. Spatial aliasing of the data can occur when the data is undersampled which will give an incorrect value of scale length. A test was run using a sine wave of varying frequency into the automatic scale length picking program (Fig 3). Synthetic data was generated using these sine waves over an array with a spacing of one unit and length of 10 units. The scale length of a sine wave as picked turns out to be about 1/15 the period. Furthermore the test showed that the data was aliased for scale lengths less than 1/30 the

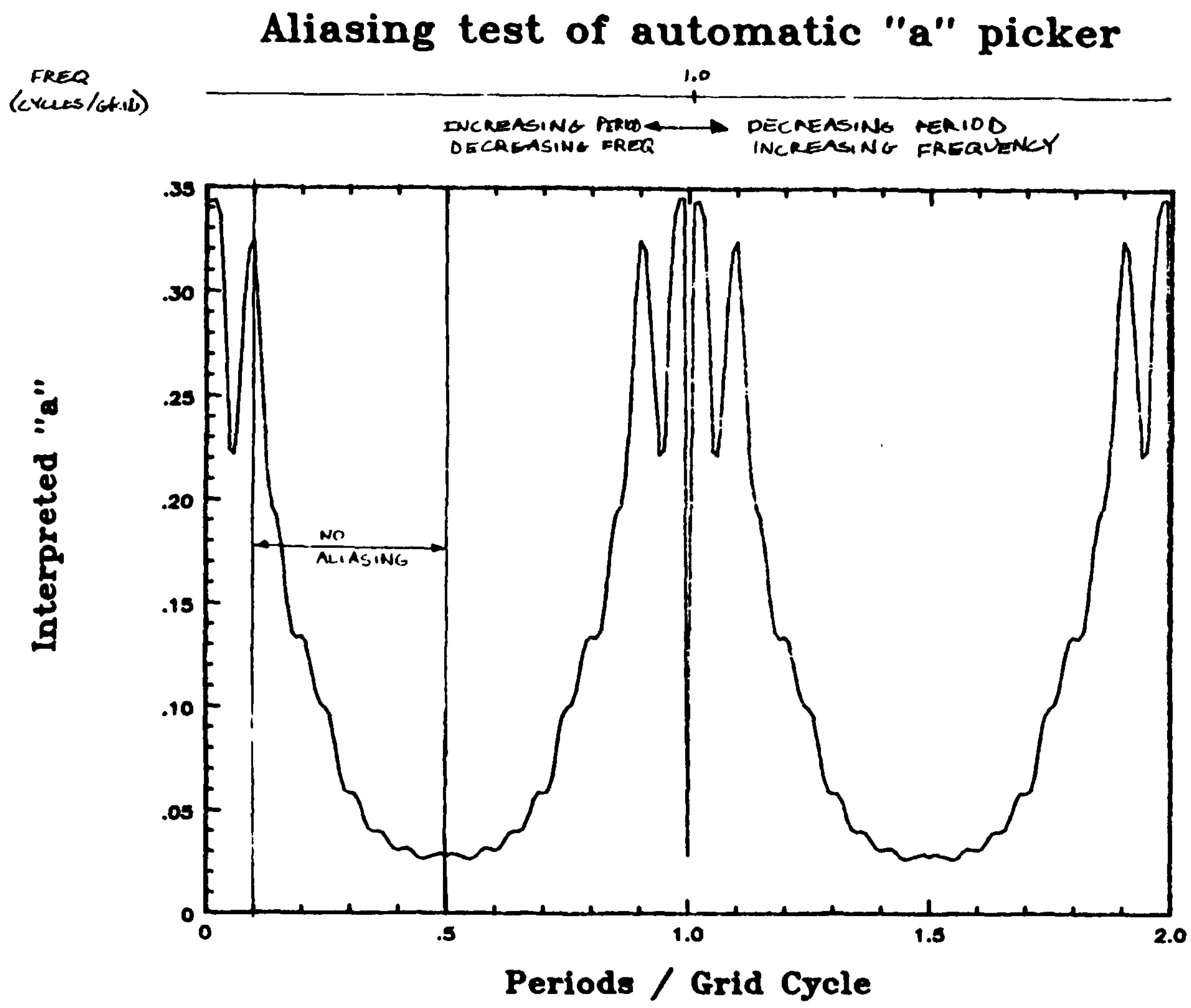

Fig 3 – Test of aliasing for scale length picking method

sample spacing and for scale lengths greater than 1/30 the length of the array. These figures should serve as a rough guide for array design.

IV. STOCHASTIC MODELLING

a. Modelling the CRAPS III test site stochastically was the final goal of the research. A series of equally spaced standard cone penetrometer soundings was chosen to be modelled. The best approach found to model the data combined averaged (smoothed) data from the cone penetrometer tests with synthetic inhomogeneities generated from the stochastic parameters. The geology of the CRAPS III test site implied *horizontal* layering, so variations of soil properties in the horizontal direction were assumed to be completely random. Vertical variations were assumed to be a combination of random variations and non-random layering. The data to be modelled was averaged horizontally, giving the vertical trend representing the non-random layers. This trend was subtracted from the data to yield the random noise. This noise was analyzed using the autocorrelation techniques presented earlier to yield the horizontal and vertical scale lengths as well as the standard deviation of the noise. These parameters were input to the three different probability distribution models (Gaussian, exponential, and Von Karman). The procedure of Frankel and Clayton (1986) was modified to accommodate differing horizontal and vertical scale lengths and used to model the *random* variations. The method works by filtering random noise with the two dimensional Fourier transform of the correlation function (Gaussian, etc.). Each distribution model produced a random two-dimensional noise

field which was constrained to match the standard deviation of the original random variations and then added to the original vertical trend calculated for the data to produce a model of the cone data. The modelling process is summarized in Fig. 4. Using this technique, a two dimensional model of any lateral size can be produced.

b. The data and the three models are shown in Fig 5. Each stochastic model was constrained to match the mean and standard deviation of the data exactly. All other statistical properties of the data and models vary and thus determine the goodness of fit of the model. Figs. 6 and 7 compare some of these properties for the data and three models. The average cone tip resistance, or vertical trend (Fig 6a) match the data relatively well for the Gaussian and Von Karman models, but not as well for the exponential model. The scale lengths measured for the vertical and horizontal autocorrelations match very well with that of the data for all models, however, the shapes of the vertical autocorrelation curve again matches relatively better for the Gaussian and Von Karman models than for the exponential model.

V. RECOMMENDATIONS

a. Stochastic modelling of a site based on a given set of data is only as good as the data itself. Care should be taken that assumptions of horizontal layering are backed by geological data and that the resolution of the data collection tools is in the range of the size of the actual anomalies.

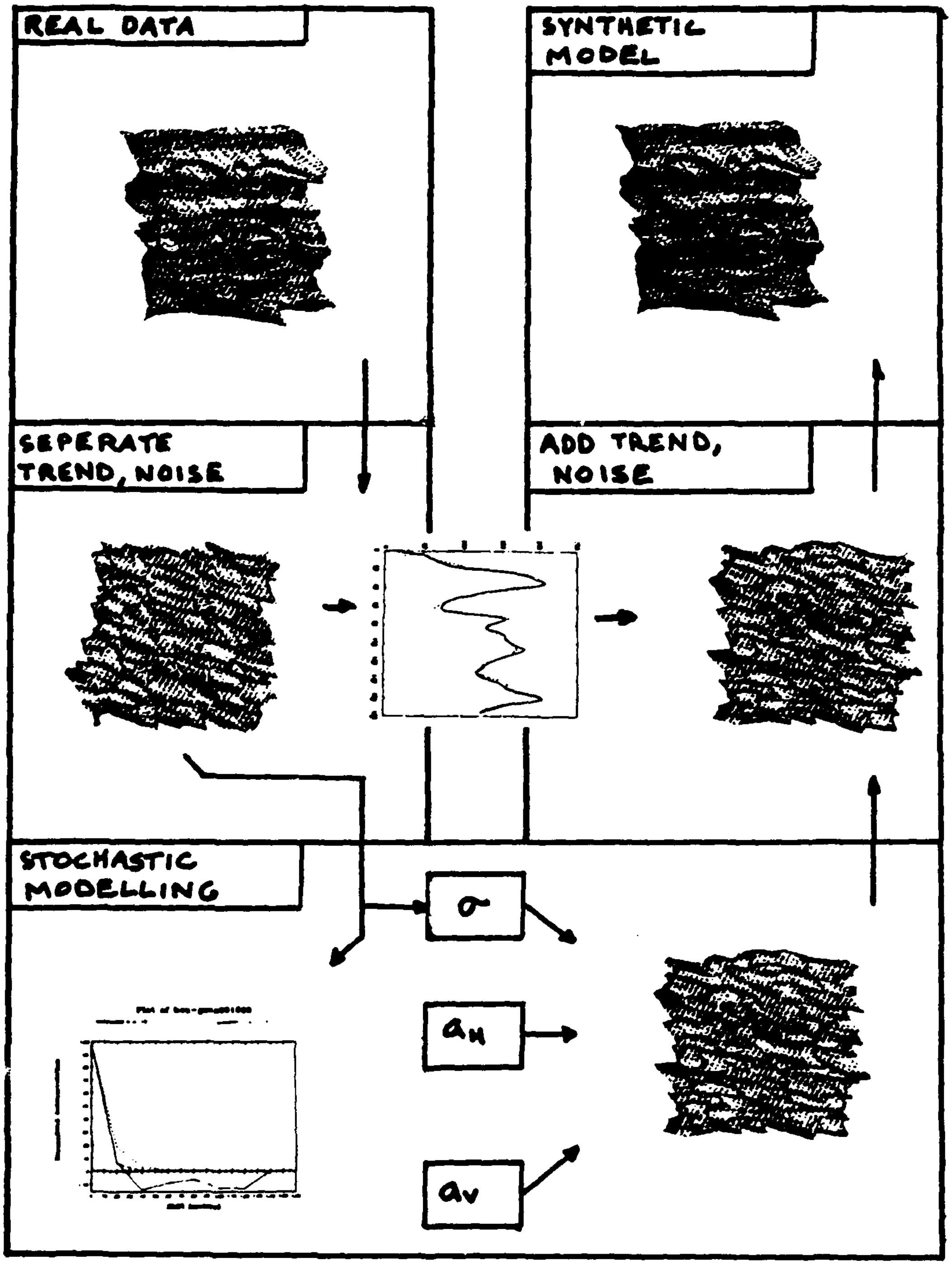

Fig. 4 - Stochastic modelling procedure.

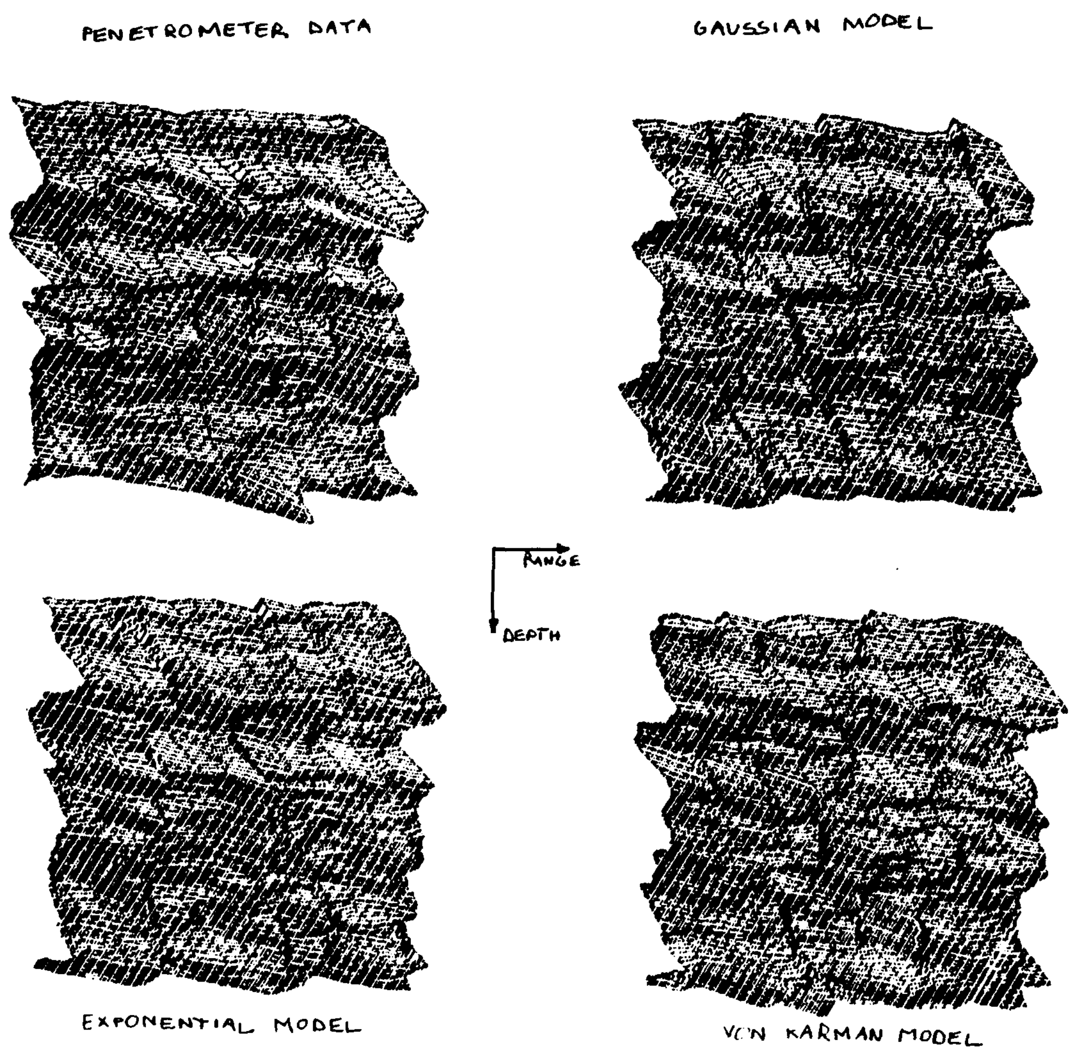

Fig. 5 - CRAPS III penetrometer array data and three stochastic models

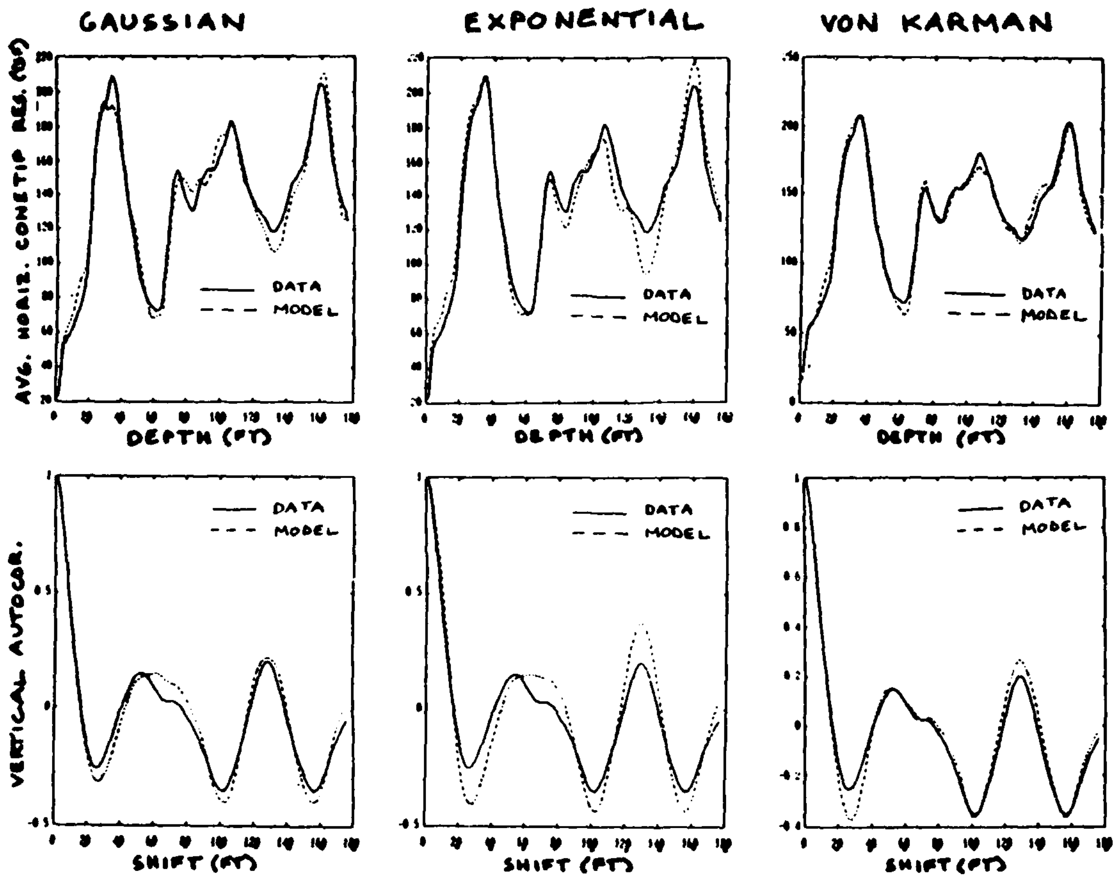

Fig 6 - Comparison of data and models a) vertical trend b) vertical autocorrelation.

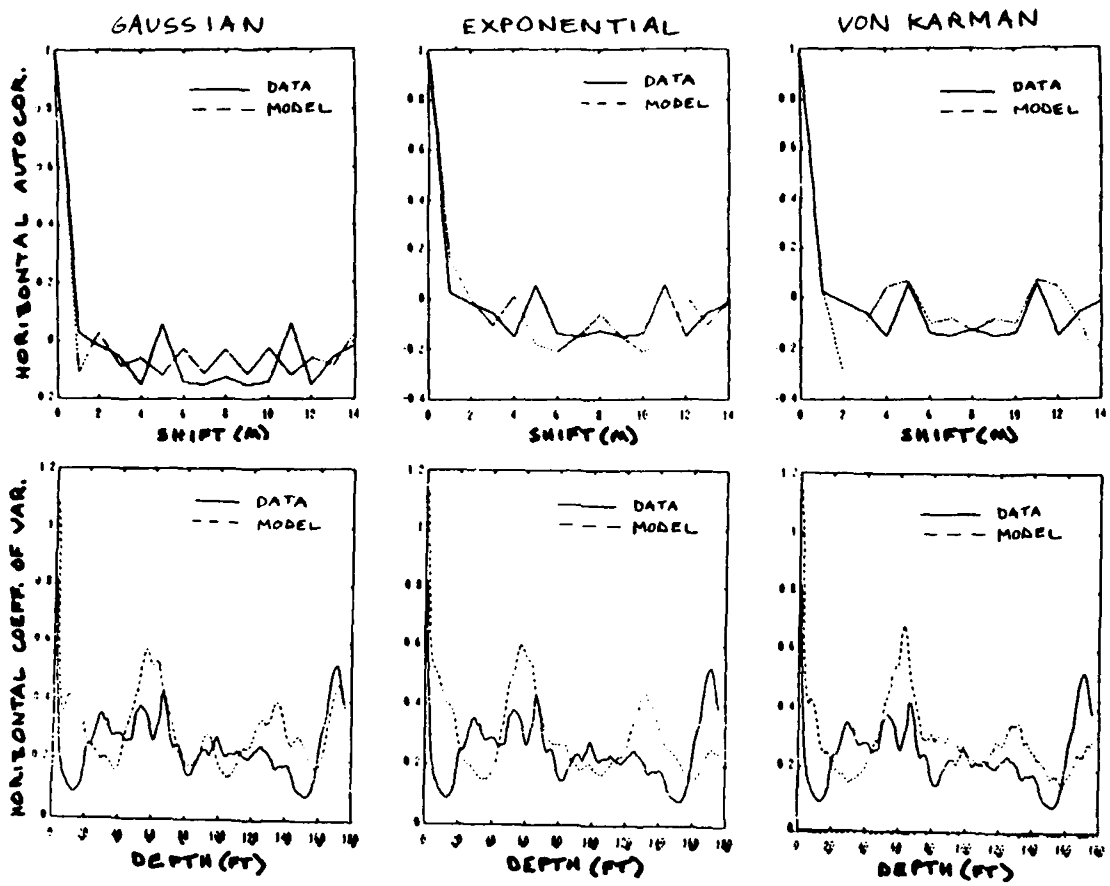

Fig. 7 - Comparison of data and models. a) horizontal autocorrelation b) horizontal coefficient of variation

Bogaards and Stump (1988) describe a direct method of site characterization using the seismic refraction method. This "black-box" approach could be used to verify the finite difference simulation of a generated model.

b. Numerous directions for follow on research exist. First, parameters and methods to calculate the goodness of fit of the model must be identified. The model needs to be tested for validity using a finite difference simulation. This will test the model and answer questions as to the use of the Born approximation. Also, questions pertaining to the modelling of three dimensional sites with a two dimensional model must be answered. More work with the seismic data may result in another way of obtaining the statistical parameters needed to model using the method described earlier. Acoustical and elastic finite difference simulations require either velocities or elastic parameters of the soil, which are not directly related to cone penetrometer readings. Work on the conversion between the field and model parameters needs to be done. Comparison to direct measurements of these parameters using seismic downhole surveys should be done as well.

c. One minor observation results from my work on this project as to the use of the cone penetrometer as a high resolution tool. Foundation theory suggests that the cone penetrometer measures the strength properties of the soil in a zone surrounding it rather than at one specific point. For a minicone with a tip diameter of .75 in, the zone size could be as large as 4

in vertically. For data sampled at .5 in spacing, significant smoothing of the actual soil response occurs. The recorded data can be thought of as the soil response convolved with the tool response. Geophysicists use deconvolution to remove the effects of a known response from measured data. Application of this process to cone penetrometer data could aid in removing the smoothing effect of the tool response from the data. Deconvolution involves relatively minor computer processing of seismic data and is routinely applied to seismic data.

REFERENCES

Aki, K. and P. Richards, Quantitative Seismology, Theory and Methods, San Fransisco, California, W. H. Freeman and Company, 2 volumes, 1980.

Bogaards, M. and B. Stump, "Two Dimensional High Resolution Site Characterization Utilizing Full Wave Seismograms," Department of Geogogic Sciences, Southern Methodist University, Dallas, Texas, 1988.

Frankel, A. and R.W. Clayton, "Finite Difference Simulations of Seismic Scattering: Implications for The Propogation of Short-Period Seismic Waves in the Crust and Models of Crustal Heterogeneity," J. Geop. Res., 1986, Vol. 91, No. B6, pp. 5465-6489.

Reinke, R.E., and B.W. Stump, "Stochastic Geologic Effects On Near-Field Ground Motions in Alluvium," Bull. Seis. Soc. Am., 1988, Vol. 78, No. 3, pp. 1037-1058.

Sudicky, E.A., "A Natural Gradient Experiment on Solute Transport in a Sand Aquifer: Spatial Variability of Hydraulic Conductivity and Its Role in the Dispersion Process," Water Resources Res., 1986, Vol. 22, No. 13, pp. 2069-2082.

1988 USAF-UES SUMMER FACULTY RESEARCH PROGRAM

GRADUATE STUDENT RESEARCH PROGRAM

Sponsored by the

AIR FORCE OFFICE OF SCIENTIFIC RESEARCH

Conducted by the

Universal Energy Systems, Inc.

FINAL REPORT

Prepared by:	John E. McCord
Academic Rank:	Graduate Student
Department and University:	Chemistry Department, Murray State University
Research Location:	ARBI/AFWL Kirtland AFB Albuquerque NM 87111
SFRP Supervisor:	Dr. David A. Dolson

Date:	14 September 1988
Contract No:	F49620-88-C-0053

AD-A204 243 UNITED STATES AIR FORCE GRADUATE STUDENT RESEARCH PROGRAM PROGRAM TECHNIC..(U) UNIVERSAL ENERGY SYSTEMS INC DAYTON OH R C DARRAH ET AL. DEC 88 6/6

UNCLASSIFIED AFOSR-TR-89-0041 F49620-85-C-0013 F/G 5/1 NL

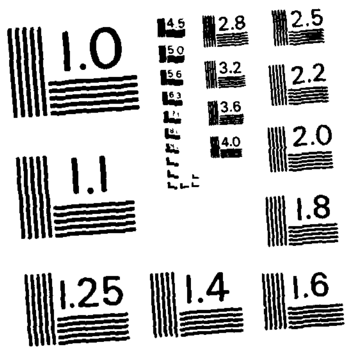
1.0
1.1
1.25
1.4
1.6
1.8
2.0
2.2
2.5
2.8
3.2
3.6
4.0
4.5
5.0
5.6
6.3

Guide for the Diode Laser System to be Used in the Study of SO Radical

by

John E. Mccord

ABSTRACT

An experimental system involving an excimer laser, a high resolution tunable diode laser, and a transient digitizer was set up with the intent of measuring the rates of rotational and vibrational energy transfer in the ground electronic state of the sulfur monoxide(SO) radical. The following is a brief experimental description, along with a guideline for the operation of the laser system.

Acknowledgements

I wish to thank the ARBI branch of the Air Force Weapons Lab for sponsorship of this research. I also wish to thank Universal Energy Systems for giving me the opportunity to participate in this research program.

My research experience was very rewarding, as well as very educational. Dr. David A. Dolson was very supportive of my efforts, and it was a pleasure to work on this project with him. The technical assistance from Sgt. Matt Peterson was invaluable. Thanks to Dr. Mike Mcauliffe for his interest in our work, and a special thanks to Dr. Ernest A. Dorko for his interest and encouragement during this research effort.

I. INTRODUCTION

There is a continuing interest in the development of chemical lasers from compounds in their electronically excited state. Sulfur Monoxide(SO) is one such chemical laser candidate. An assessment of the energy transfer rates in the ground electronic state of SO is recquired to evaluate its potential laser capacity. Rapid energy removal from the lower levels favors population inversion, while slow energy transfer is adverse to the laser oscillation as there is a lower level population build-up.

Essential to this study was the establishment of a system that was capable of monitoring specific rovibrational states of "excited" radicals as they relaxed through energy -exchanging collisions with other molecules. An excimer laser could be used to photolyze sulfur dioxide into excited SO radicals, and a high-resolution tunable diode laser could monitor the radicals in real time. A Cu:Ge detector would then be used to detect the diode laser signal. The detector signal would be recorded with a transient digitizer over several laser pulses, thus improving the signal-to-noise ratio. The set-up of such a system, and a working knowledge of its use would be of great benefit the ARBI branch of the Air Force Weapons Lab.

My personal research efforts have been in the area of kinetics and spectroscopy under the guidance of Dr. David

A. Dolson, formerly of Murray State University, in Murray, Kentucky. My previous experience has been with the major forms of spectroscopy: emission, infrared, atomic absorption, UV, and mass spectroscopy. My current work with Dr. Dolson involved excimer and dye lasers. The fact that I did have some laser experience, and that Dr. Dolson had done prior work involving time-dependent laser spectroscopy, resulted in my assignment to the ARBI chemical lasers branch of AFWL.

II. OBJECTIVES OF THE RESEARCH EFFORT:

At the time of my research effort, no time-dependent rate constants for sulfur monoxide were known for its rotational and vibrational energy removal rates in its lower energy levels involved in laser transition. It was thought that a photolysis beam could dissociate sulfur dioxide into excited SO radical at 193 nm. After photolysis, a tunable diode laser could monitor the relative population of specific rotation-vibration SO energy levels as a function of time. The signals from the diode laser would then be captured by transient digitizer and subsequently analyzed to determine the desired rate constants.

My assignment as a participant in the 1988 Graduate Student Research Program(GSRP) was to set up and test a

diode laser-transient digitizer analysis system. This system would then provide the means to carry out a time-dependent study on the photolysis generated SO radical and determine its rate constants.

Several experimental approaches and set-ups were considered, and these approaches are discussed by my SFRP co-worker, Dr. David A. Dolson, in his final report of effort. My goal in this work is to provide a guide for the laser-digitizer analysis system. Hopefully, this will be of value to the research group headed by Dr. Ernest A. Dorko in their efforts to continue the research.

During my 1988 GSRP, rotational spectra was obtained for sulfur dioxide and ammonia in testing the diode laser system. Attempts at attaining transient absorption signals fo SO radical were made, but problems occurred that were not resolved before the end of the research period.

III. BRIEF EQUIPMENT DESCRIPTION

For the sulfur dioxide dissociation, the 193 nm photolysis beam was supplied by Questek excimer laser operating between 50-65 Joule, and using an Argon-Flouride gas fill. This beam was aligned through a 3 meter sample cell along with the high-resolution tunable diode laser beam. The increased overlap of the two beams in the long

cell was to improve our experimental transient absorptions.

The diode laser system provided a data, sample, and etalon scan for a given wavelength, temperature, and current setting. Each of the three signals were connected to lock-in detectors, and these were connected to a microcomputer. The Spectra Physics program "3-Channel Collect" controlled the diode laser scan and recorded the rotational peaks present in the data, sample, and etalon input signals. The transient absorptions were recorded with a Lecroy transient digitizer, and from these signals the SO radical rate constansts were to be calculated.

IV. OPERATIONAL CONDITIONS

The alignment of the diode laser was done with the system's built in Helium-Neon laser. The diode laser was centered on its internal detector windows, and the laser's passage through the reference and sample cells was also aligned. The diode laser makes two passes through the 3 meter sample cell, and these passes travel along the same axis as the excimer beam, which also makes a pass through the cell. The optics have been adjusted so that the two beams experience a maximum overlap inside the sample cell, which improves the quality of the transient signals.

Filling of the sample cell with the proper total

pressure of gases is also important. Strong absorption peaks can be observed when the total cell pressure is maintained around 2 torr. For sulfur dioxide and argon, this meant an SO flow of 2-3 SCCM and and argon flow of 10-11 SCCM. The respective flow rates were controlled by mass flow meters, and the gas pressure in the cell was measured with a capacitance manometer.

V. EXPERIMENTAL SET-UP

Once alignment is done and the cell is filled, the next step is to bring absorption peaks up on the scope. At this time, the diode laser, the laser control head, the amplifier, the lock-ins, the computer data acquisition system, and the oscillascope should all be on. The input and output interconnections between these modules are as follows(See Figure One):

1. The detector(A) should have 3 seperate inputs into the amplifier(B): a data, reference, and an etalon input.
2. The amplifier has 3 outputs, each going to 2 seperate locations. There should be a data, a reference, and an etalon output going to the scope(C)(with only 2 signals at a time being inputted to the screen), and there should be a data, a reference, and an etalon output

going to the inputs of three seperate lock-in detectors(D).

3. The lock-ins should have 1 output apiece(3 total). There should be data, reference, and etalon outputs going into 3 seperate ADC channels on the computer data acquisition system(E).

4. The computer system will have one DAC output into the reference input of the laser control head. This controls the diode laser scan by controlling the voltage ramp.

5. The laser control head has a sawtooth(low to high) modulation reference output that inputs into the external trigger input of the scope. This scope trigger also inputs into all 3 lock-ins, but with the modulated reference, the lock-ins are not in use.

6. The diode laser chopper has a reference out that can replace the modualated reference at the scope's external trigger input. When this is done, the lock-ins are in use(due to a slower modulation fed in from the computer control system).

VI. MAXIMIZING SCOPE SIGNALS

To bring absorption peaks up on the scope, the data

output and the reference output from the amplifier (the etalon output line can hang freely at this time) should be connected to the channel 1 and channel 2 scope inputs respectively. At this point, the diode laser chopper should be turned on. The scope external trigger input(which is connected to all three lock-ins) should be connected to the reference output on the diode laser control module. The low to high sawtooth modulation should be turned on.

It is now necessary to choose a starting temperature and current at which to begin a scan. One should always keep in mind the threshold parameters of the diode in use. Generally, start with a lower temperature and current. The temperature reading is in volts, and a high voltage reading corresponds to a low temperature(and vice-versa). A voltage-to-temperature conversion chart is supplied for each diode.

On the oscillascope screen at this point will be a sample signal and a reference signal. Each signal may be showing some division into an upper and lower baseline. A manual scan of the monochrometer will show several such modes where this signal splitting occurs. One should pick a mode and try to find the location on the monochrometer that maximizes the top-to-bottom difference of the sample and reference signals.

Correction factors for converting the monochrometer drum reading to a rough estimate of wavelenth are provided. In the maximized mode, absorption peaks may be present. It is important to stay in only one mode when peaking up the intensities in that mode.

Once the mode intensity is maximized with the monochrometer, absorption features can be brought up on the scope by scanning the current with the current coarse control knob on the laser control module. For example, sulfur dioxide absorptions would be seen in the sample channel, and ammonia peaks would be seen in the reference channel.

VII. TEMPERATURE AND CURRENT SCANNING

Another method of scanning absorption peaks and positioning them on the scope is to hold the current steady and to scan the temperature(again keeping in mind the limits of the diode in use). After the temperature has been scanned, further tuning can be done by adjusting the current. This current-to-temperature compensation can be described as follows:

Voltage Adjust	Temperature	Current Compensation
Higher voltage	Lower	Increase Current
Lower Voltage	Higher	Decrease Current

This temperature adjustment and subsequent current compensation is a very useful scan technique in two instances. One instance ivolves the positioning of a mode hop(or change) to the left or right side of a set of desired peaks. Temperature and current fine tuning can move the mode hop feature to the side of the scan range so that a continuous one-mode scan can be made. This method of laser scanning is also useful in scanning peaks located in an area where the laser becomes unstable, denoted by a distinct, visible distortion of the channel signals on the screen. Changing the temperature and current settings to that of a lower current and a higher temperature(lower voltage reading) can bring peaks of interest into a region where the diode laser is more steady.

VIII. FINAL ADJUSTMENTS

Once the desired set of sample absorption peaks is on screen along with the accompanying reference peaks(though not always the case), some final fine tuning can be done. A rescan of the monochrometer drum can insure maximum mode intensity. The reference signal intensity can then be maximized by tuning the micrometers on the parabolic mirror located in front of the diode laser head. The sample signal intensity can be maximized by fine adjustments made to the external mirror optics located

outside of the diode laser by the sample cell.

After these adjustments, a quick check of the etalon peaks is in order. This is done by replacing the reference signal input in channel 2 with the etalon output line from the amplifier(this line previously unused). If the etalon peaks look clear and periodic, proceed with collection set-up. If they do not look clear or very intense, then further temperature-current tradeoff adjustments are recquired.

IX. DATA COLLECTION

To prepare to collect the peaks on screen with the computer, first disconnect the scope external trigger input from the diode laser control reference output and turn off the sawtooth modulation. Reconnect the scope external trigger input to the chopper reference output located on the diode laser. At this point, one should watch for a change in the current reading when the reference output switch is made. This is especially true if the computer data acquisition system is up and running. A readjustment of the current setting may be necessary to return the laser scan to its previous location.

When the external trigger input is connected to the

chopper reference output, the lock-in detectors should begin to work. At this point it is necessary to maximize the needle deflection on all the lock-ins by making the necessary sensitivity adjustments. By scanning the current and watching the data, reference, and etalon lock-ins, one can insure that the absorption signals previously visible on the scope are not off-scale for a given senstivity setting. The lock-ins should all have an input channel into the computer system, and data collection can now begin.

The data, reference, and etalon scans are collected by the program 3 Channel Collect(3CHANN), and data collection begins with the command "COL DA"(Collect Data). Before scanning with the computer, though, there are certain parameters that must routinely be inputted:

PARAMETERS	GENERAL INPUT
POINTS IN SCAN	1024 OR 2048
RANGE OF SCAN	10 - 100 Ma
SCANTIME	103.5 OR 206 s

The program also asks for DATA, REFERENCE, and ETALON sensitivities. These numbers are read directly off of the respective lock-in detectors.

To store the data on disk, a name must be entered under the parameter EXPERIMENT. This name can apply to a series of experimental runs. To increment the run

number, simply enter the function INCREMENT.

There are several other helpful and commonly used commands:

COMMAND	FUNCTION
SAVE DA,RE,PA,OR ET	Saves data, reference, parameter, or etalon files.
VIEW FILE /A	View a scaled data, reference, or etalon file.
PLOT FILE /A	Plot a scaled data, reference, or etalon file.
DIR	Give directory of disk in specified drive(default is B).
EXIT	Returns to system.

LOAD DA,RE,PA,OR ET	Loads data, reference, parameter, or etalon file from previous experiments.

Before using the LOAD command, an experiment name must be entered first. To load different runs within the same experiment, the INCREMENT function is again used. Important:when loading stored files from disk, a parameter file must be loaded first before one can view a data, reference, or etalon file.

X. TRANSIENT SIGNAL COLLECTION

The Lecroy transient digitizer should be used after absorption peaks have already been located with the diode laser system, the scope, and the 3 channel data collection system. This makes it easier to tune to peak locations, fine tune onto the peaks, and then record transient absorptions resultant from laser pulsing. In our case, sulfur dioxide absorption locations were found, SO absorption wavelength locations were then calculated and found, and transient absorption peaks for both molecules were recorded with the Lecroy.

In setting up the digitizer, the input and output interconnections are the same as those used for the 3 signal collection system with the following exceptions(See Figure Two):

1. The external trigger input of the scope(which should still be connected to all 3 lock-ins) should always be left connected to the chopper reference output of the diode laser.
2. An input line should be attached to the Lecroy input channel(A).
3. An input line should be connected to the Lecroy stop pulse input channel(B). This line should be connected to the TTL pulse output channel of the accompanying amplifier module(C). This line provides the pulse that ends data collection by the Lecroy.
4. The amplifier module input should be connected to a photodiode(D) positioned directly behind the excimer beam turning mirror. This line will provide the trigger impulse that begins data collection by the Lecroy.

When fine tuning to a peak, the data signal output from the diode laser system amplifier should be brought into the channel 1 input of the scope. From the scope

connection, the signal should tee-off to the data lock-in amplifier input channel. The external trigger input of the scope should be connected to the chopper reference output of the diode laser, and the chopper should be turned on. At this time, the diode laser should be tuned to a temperature and current associated with a previously scanned absorption peak. This will result in a needle deflection on the lock-in amplifier. To fine tune to the peak location, one should use the fine current control to scan the current associated with the peak. A minimum in the needle deflection on the lock-in signifies that one is sitting on the absorption of interest. In our case, known sulfur dioxide absorptions were tuned to with the lock-in amplifier.

Once the system is sitting on a peak, the chopper should be turned off. The data output line from the amplifier can be disconnected from scope channel 1, and then it can be connected to the input line of the Lecroy. The excimer laser can now be turned on and opened to the sample cell. The WAVELENGTH-CATALYST computer program should be up and running on the Lecroy computer system. With the excimer laser firing providing the trigger impulses, striking B on the keyboard will begin collection of transient absorption peaks.

XI. TRANSIENT SIGNAL LOCATION CALCULATIONS

Scanning from transient absorptions of known current settings to transient absorptions with unknown current settings recquires some calcualation. Peaks that are already assigned to literature wavenumber locations and that have established current settings at a constant temperature can be easily scanned to with the diode laser. Fine tuning to these peaks by checking for minimum needle deflection on the lock-in will yield exact current readings for these peak locations.

If the literature wavelengths and current settings for at least two absorption peaks are known, a shift factor can be derived for calculating the current positions of other desired wavelengths. The slope of a straight line plot of the known data(current vs. wavelength) would be the difference in wavelengths divided by the difference in current settings for the two peaks. A factor with cm-1/Ma units is derived. One can then take any known wavelength and current setting and calculate the current shift needed to scan to a desired wavelength. This involves taking the difference in the two wavelengths, and then multiplying this value by the unit factor. This calculated current value would then added or subtracted to the known current setting based on the wavelength location of the new peak.

EXAMPLE:

At a constant temperature reading of 1.1185 volts, know:

SO	Absorption (cm-1)	Current Location (Ma)
1.	1107.560	440.3
2.	1107.425	427.1
3.	1107.354	420.1

Plot 1 and 3 and Calculate Slope:

Shift Factor = 1107.560-1107.354/440.3-420.1 =

.206/20.2= .010198 cm-1/Ma

Check Factor: Go from 1107.560 cm-1, 440.3 Ma

to 1107.425 cm-1;

1107.560-1107.425= .135 cm-1

.135 cm-1*(1 Ma/.010198 cm-1)

= 13.2 Ma;

440.3-13.2= 427.1 Ma for 1107.425 cm-1

New Absorption: Go to SO transient absorption at

1107.406 cm-1(from literature)

1107.425-1107.406= .019 cm-1

.019 cm-1*(1 Ma/.010198 cm-1)

= 1.9 Ma;

427.1-1.9= 425.2 Ma

New current setting at given temperature to scan SO transient absorption peak.

XII. RECCOMENDATIONS

During attempts at recording transient absorption signals for SO, the expected signal shape was never observed on the transient digitizer to any great extent. The signals that were observed were very noisy and showed an excessively large noise spike resultant from the firing of the excimer laser. Insulation of the electronics from noise was attempted, with only a slight degree of improvement. Further and more complete insulation of the system from external electronic noise interference may improve the transient signal.

Also during the experimental period, it was discovered that infrared emission from the excimer laser was passing through the bandpass filter on our detector. This decreased our ability to distinguish between real and unreal transient absorption features. An additional bandpass filter on the detector may block out the unwanted excimer infrared emission.

The acquirement of a completely function 3 CHANNEL COLLECT program from Spectra Physics would greatly enhance data analysis. It would be most useful in quickly identifying the locations of the rotational peaks from the diode laser's data and sample scans.

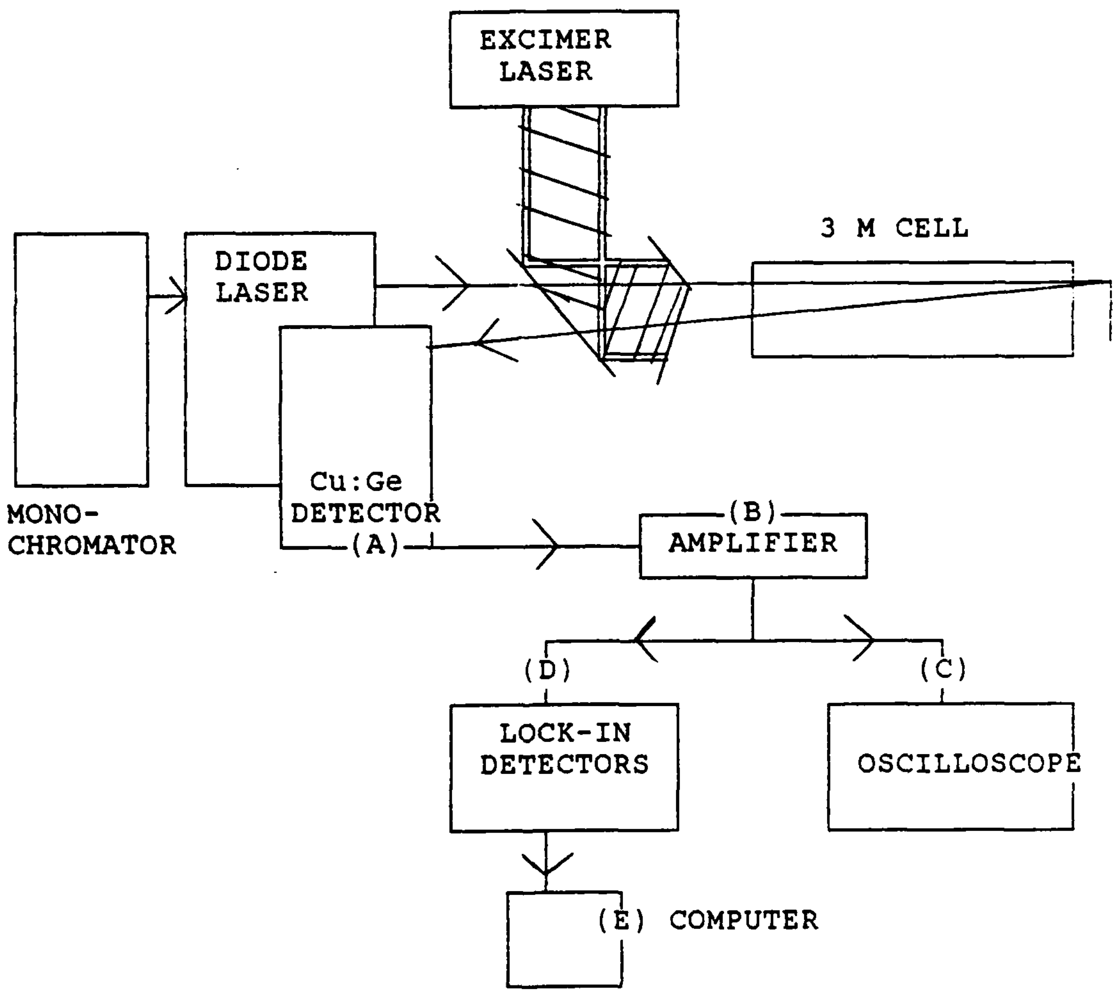

FIGURE 1. Connections for the Collection of Diode Laser Data, Reference, and Etalon Scans.

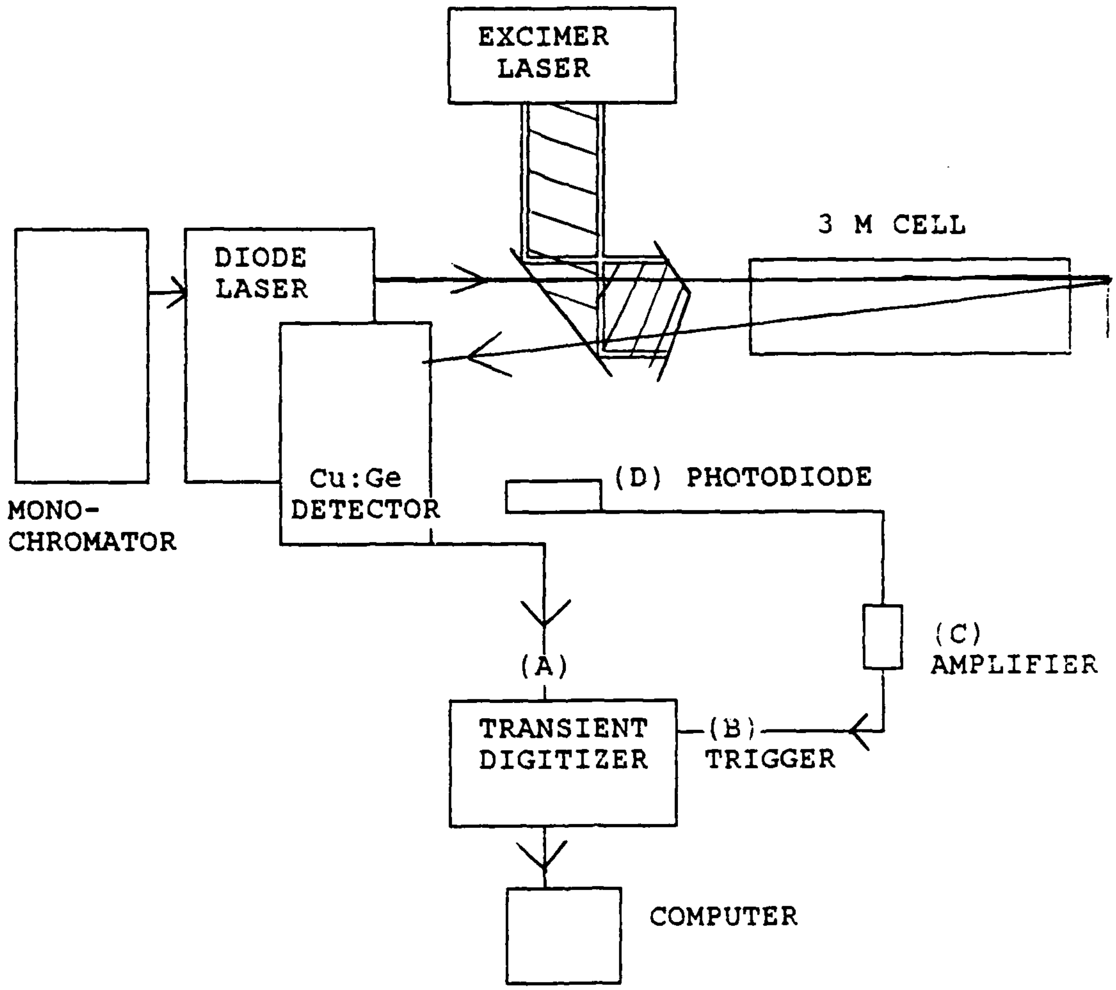

FIGURE 2. Connections for the Collection of Transient Signals

1988 USAF–UES SUMMER FACULTY RESEARCH PROGRAM/

GRADUATE STUDENT SUMMER SUPPORT PROGRAM

Sponsored by the

AIR FORCE OFFICE OF SCIENTIFIC RESEARCH

Conducted by the

Universal Energy Systems, Inc.

FINAL REPORT

The Experimental Validation of Imaging Correlography Through Atmospheric Intensity Scintillations

Prepared by:	Brian Spielbusch
Academic Rank:	Graduate Student
Department and	Electrical and Computer Engineering
University:	University of Missouri – Columbia
Research Location:	AFWL/AROB
	Kirtland AFB, NM 87117
USAF Researcher:	David G. Voelz
Date:	22 September 1988
Contract No:	F49620–88–C–0053

The Experimental Validation of Imaging Correlography Through Atmospheric Intensity Scintillations

by

Brian K. Spielbusch

ABSTRACT

Imaging correlography is a technique for obtaining images of laser illuminated objects. This report describes an experiment which was conducted to determine the effect of atmospheric intensity scintillations on images recovered with the imaging correlography technique. The experimental and processing procedures and the experimental results are presented. Also presented are simulation results illustrating the effect that atmospheric scintillation and the camera modulation transfer function (MTF) have on the correlography data and recovered images. Techniques for correcting scintillation and MTF effects are described and results are presented.

Acknowledgment

I would like to express my appreciation for the summer Support and the research opportunities provided under the sponsor ship of the Air Force System Command, the Air Force Office of Scientific Research, the Air Force Weapons Laboratory and Universal Energy Systems.

I would like to thank Martin Levine for his expertise and notes on atmospheric turbulence and this phase screens. I would also like to thank the personal at the Air Force Weapons Laboratory for their help and support.

Introduction

Imaging correlography[1] refers to a technique for image synthesis that is similar to holography in that it records an interference pattern from a coherently illuminated object. This pattern is the speckle pattern one normally observes when coherent light is reflected from a diffuse object[2]. The speckle represents the coherent interference of many points scatters on the surface of the object. Unlike conventional holography where a reference wave is used to form a hologram, the object to be imaged is in a sense it's own reference. However, because the object and hence the reference wave are both unknown, special processing techniques are used the recover the image.

Image synthesis using imaging correlography is based on the fact that the autocorrelation function of the illuminated object's brightness distribution can be obtained from the average energy spectrum of a laser speckle pattern[3] (The brightness distribution is essentially the object's irradiance distribution had the object been illuminated with an incoherent light source). Since the inverse Fourier transform of the autocorrelation of the object's brightness function[4], an image of the object can obtained if the phase associated with this Fourier transform can be determined. To obtain this phase we use a Fourier modulus estimated from the speckle data together with an iterative transform algorithm of the type previously demonstrated by Fienup[5]. Once the phase associated with the Fourier modulus is determined, the image is recovered by inverse transforming the synthesized Fourier plane data.

One of the primary motivations for using imaging correlography in Air Force applications, as opposed to conventional imaging, is the potentially low cost of imaging hardware with large effective apertures. Imaging correlography also has aberration correcting capability similar to that of conventional holography[6],

such as atmospheric turbulences, which will be investigated in the report.

This work seeks to extend the laboratory demonstration[7] of imaging correlography to include the effect of intensity scintillations produced by clear air turbulence. A specially prepared random phase screen with known statistical properties will be used as a single layer simulation of atmospheric turbulence[8].

I was assigned to this laboratory because of my involvement in developing this new imaging technique in the same laboratory, last year. I'm a Electrical Engineering student at the University of Missouri, where my Master's thesis topic is on Imaging correlography.

Objectives of Research Effort

The preliminary goal, before any work was started was :

1. Using a Gaussian phase screen of known statistics, investigate the effect that intensity fluctuations have on one's ability to recover images from Imaging correlography data.

As work started more goals were added :

2. To measure experimentally the phase screen correlation function.
3. To improve the reconstructed images, by removing the phase screen correlation function in the Imaging correlography lab data.
4. To show the effect, of the MTF (sinc^2) and the measured phase screen correlation function, on reconstructions, using truth data.

Experimental procedure

To investigate the effect that intensity fluctuations have on one's ability to recover images from Imaging correlography data, a laboratory experiment was set up (fig. 1). A coherent plane wave was directed at the target producing a

speckle pattern. A phase screen was set up 2.5 meters from the target illuminated by the speckle pattern, this speckle pattern being modulated by the phase screen was then imaged 1:1, on a camera CCD array. The modulated speckle pattern on the camera was then grabbed and digitized by a computer, windowed by a rectangular window half the array size (512 by 512), FFT, squared, and saved. The target was rotated to produce a new independent speckle pattern, the phase screen was translated to a independent area, and an another pattern was grabbed and processed and averaged with the other processed data. This was done 500 times and 500 patterns were processed and averaged, giving the estimated autocorrelation of the object. To recover object post processing steps (1-9) and post processing steps (11-12) [See Post Processing section]. See results page for various corrections and the reconstructions.

To measure experimentally the phase screen correlation function. The target was removed and replaced with a mirror, and a 300 μm pin hole was placed near the beam expander, approximately 4.5 meters away from the target, or 7 meters away from the phase screen. This pin hole produced a large array diffraction pattern on the phase screen. Covering the same area on the phase screen as before, the pattern was grabbed, processed and averaged, the same as if the phase screen were modulating a speckle pattern, but now the phase screen is modulating a plane wave. After the processing and averaging of 500 patterns, an estimate of the power spectrum of the phase screen alone is obtained. This power spectrum is now processed using post processing steps (1-9). Where this power spectrum will be referred to as an autocorrelation in the post processing section, and the phase screens correlation function will be referred to as a power spectrum in the post processing section.

To improve the reconstructed image, by removing the phase screen cor-

relation function in the Imaging correlography lab data. The power spectrum of the phase screen modulated speckle pattern was used in the equation shown in post processing step 10, along with the measured phase screen correlation function. (See reconstruction results for corrections marked ATM.)

To show the effect, of the MTF (sinc2) and the measured phase screen autocorrelation function, on reconstructions, using truth data. A correct size image of the target was grabbed by the computer (shown in results as truth image), and FFT and squared to give the truth power spectrum. The truth modulus can be found and phase retrieval applied (shown in results as truth data). The truth power spectrum and the phase screen autocorrelation function can be used in the equation shown below to simulate the effect of the phase screen. To simulate the MTF the truth power spectrum was multiplied by a sinc2 function. (See results of simulated effects on truth data, marked ATM EFFECT, SINC^2 EFFECT)

$$\hat{C}_{IT}(\Delta\nu) = \langle I_c \rangle^2 \left[\Gamma^2(\Delta\nu) \frac{\hat{\hat{R}}_{IT}(\Delta\nu)}{\langle I_R \rangle^2} + \left(\frac{\hat{\hat{R}}_{IT}(\Delta\nu)}{\langle I_R \rangle^2} - 1 \right) \right] \quad (1)$$

Where :

$\Gamma^2(\Delta\nu)$ = truth power spectrum

$\hat{C}_{IT}(\Delta\nu)$ = phase screen aberrated truth power spectrum

$\langle I_c \rangle^2$ = average intensity of uncorrected power spectrum estimate

$\hat{\hat{R}}_{IT}(\Delta\nu)$ = phase screen correlation function estimate

$\langle I_R \rangle^2$ = mean intensity of phase screen correlation function estimate

Equipment :

1 Watt single line argon laser.

General Electric CID 512 CCD camera

2 in beam expander, with spatial filter

2 cm, 3 dimenalsion lead target coated with highly reflective non-depolarizing paint, glued to a clear glass plate, mounted on a stepper motor driven driven rotation stage.

Two 500 mm achromatic lens, used in a 1:1 imaging system.

Phase screen, mounted on a stepper motor driven translation stage.

300 μm pin hole, 2" mirror

Post Processing Steps

Step 1

The raw 512 by 512 autocorrelation was processed by removing the camera artifacts. The bright camera artifacts lay out side the center 300 by 300 of the 512 array, and are much brighter than any other camera noise or autocorrelation value. The artifacts can be thresholded and set to one, with the rest of the array set to zero. A bias of -1 can be added to the array, and multiplied by -1, to give an array with zero values at the artifact portions and ones elsewhere.

The raw autocorrelation was multiplied by the array to remove the artifacts.

Step 2

A slice was taken through the fifth the row in the data (arbitrary picked), and the mean value of this row was found. The mean value was then subtracted off of the autocorrelation data. All negatives created by this subtraction were set

to zero.

Step 3

The autocorrelation was then visual inspected. Knowing the approximate size of the true autocorrelation, low value camera noise near the autocorrelation was removed by subtracting off 1 % of the peak value, setting negatives to zero.

Step 4

The dc point was then estimated and an FFT was taken, giving the power spectrum. Any negative values in this power spectrum were set to zero.

Step 5

The center 128 by 128 was cut out of the array. All processing beyond this point was with 128 by 128 arrays.

Step 6

The object is real and positive, it's power spectrum and autocorrelation should be real and positive, therefore a positivity and reality constant algorithm was used. This constant was applied 5 times each to the power spectrum and autocorrelation.

Step 7

After the positivity and reality constant, while in the autocorrelation domain, correction for camera finite pixel width was applied (MTF correction). The MTF was assumed to be a sinc2, those zero's come to the edge of array. The autocorrelation function was multiplied by a filter of the form :

$$\frac{MTF \cdot (auto)^2}{MTF^2 \cdot (auto)^2 + NOISE^2} \tag{2}$$

Where noise was set to 0.001 of peak. This filter function was than multiples by the autocorrelation.

Step 8

The positivity and reality constant was applied 5 times again.

Step 9

The power spectrum was then multiplied by a wiener filter to correct for OTF and noise. Of the form :

$$\frac{OTF \cdot (\hat{C}_{IT}(\Delta v))^2}{OTF^2 \cdot (\hat{C}_{IT}(\Delta v))^2 + noise^2} \quad (3)$$

Where $\hat{C}_{IT}(\Delta v)$ is the estimated power spectrum. The OTF in this case is autocorrelation of the rectangular window function used on the speckle pattern. Where noise was set to 10/255 of peak, meaning a wiener filter of 10. Noise value was determined by visual inspection of square root of power spectrum. (Other noise values were used such as 30)

Step 10 Correction for the phase screen :

To correct for the phase screen the power spectrum was used in this equation :

$$\hat{C}_A(\Delta v) = \frac{\frac{\hat{C}_{IT}(\Delta v)}{\langle I_c \rangle^2} - \left(\frac{\hat{\hat{R}}_{IT}(\Delta v)}{\langle I_R \rangle^2} - 1 \right)}{\frac{\hat{\hat{R}}_{IT}(\Delta v)}{\langle I_R \rangle^2}} \quad (4)$$

Where

$\hat{C}_A(\Delta\nu)$ = phase screen corrected power spectrum estimate

$\hat{C}_{IT}(\Delta\nu)$ = uncorrected power spectrum estimate

$\langle I_c \rangle^2$ = average intensity of uncorrected power spectrum estimate

$\hat{\hat{R}}_{IT}(\Delta\nu)$ = phase screen correlation function estimate

$\langle I_R \rangle^2$ = mean intensity of phase screen correlation function estimate

Any negatives formed by this function were set to zero.

Step 11

Take square root to obtain fourier modulus.

Step 12 Phase retrieval :

A triple intersect method of the autocorrelation was used to obtain an initial guess (shown in results as mask for guess, which will be randomized), phase retrieval was then applied to obtain a close estimate for a mask of the object (shown in results as mask).

Starting with only the center 32 by 32 of the fourier modulus, multiplied by a triangular window, those zero's come to the edges.

10 cycles of 1 input-output (beta=0.7) and 1 error reduction, with the object mask applied after each cycle.

1 cycle of 20 input-output (beta=0.7) and 4 error reduction, with the

triangular window opened 1 pixel after each iteration.

The array size was then increased to 64 by 64.

2 cycles of 100 input-output (beta=0.7) and 5 error reduction.

1 cycle of 20 input-output (beta=0.5) and 4 error reduction, with the triangular window opened 1 pixel after each iteration.

2 cycles of 100 input-output (beta=0.5) and 5 error reduction.

The array size was then increased to 128 by 128, and 1 error reduction iteration was done. (Continued iterations with 128 by 128 arrays not needed because of lack of information beyond 64 by 64 size)

Conclusions and Recommendations

It seems that Imaging correlography inherent ability to resist atmospheric scintillation has been proven. Corrections for the atmosphere, on the Imaging correlography lab data, had little or no effect on the reconstructed images. The simulations of atmosphere on truth data did have a noticeable effect on the reconstructed images, leads me to believe that atmospheric scintillations have a small effect on reconstruction quality, but not as great a degrading effect as the camera noise and MTF. Corrections for theses effects did give a noticeable improvement to the reconstructed images.

It is recommended that computer simulations of atmospheric aberrated speckle along with noise and MTF effects, be ran to determine the degrading effect of each and together. It is also recommended that the experimental work continue with the use of a camera with low noise, and a known MTF for more precise correcting. Only after this work, can any conclusion be made of the importance of atmospheric correction on Imaging correlography data.

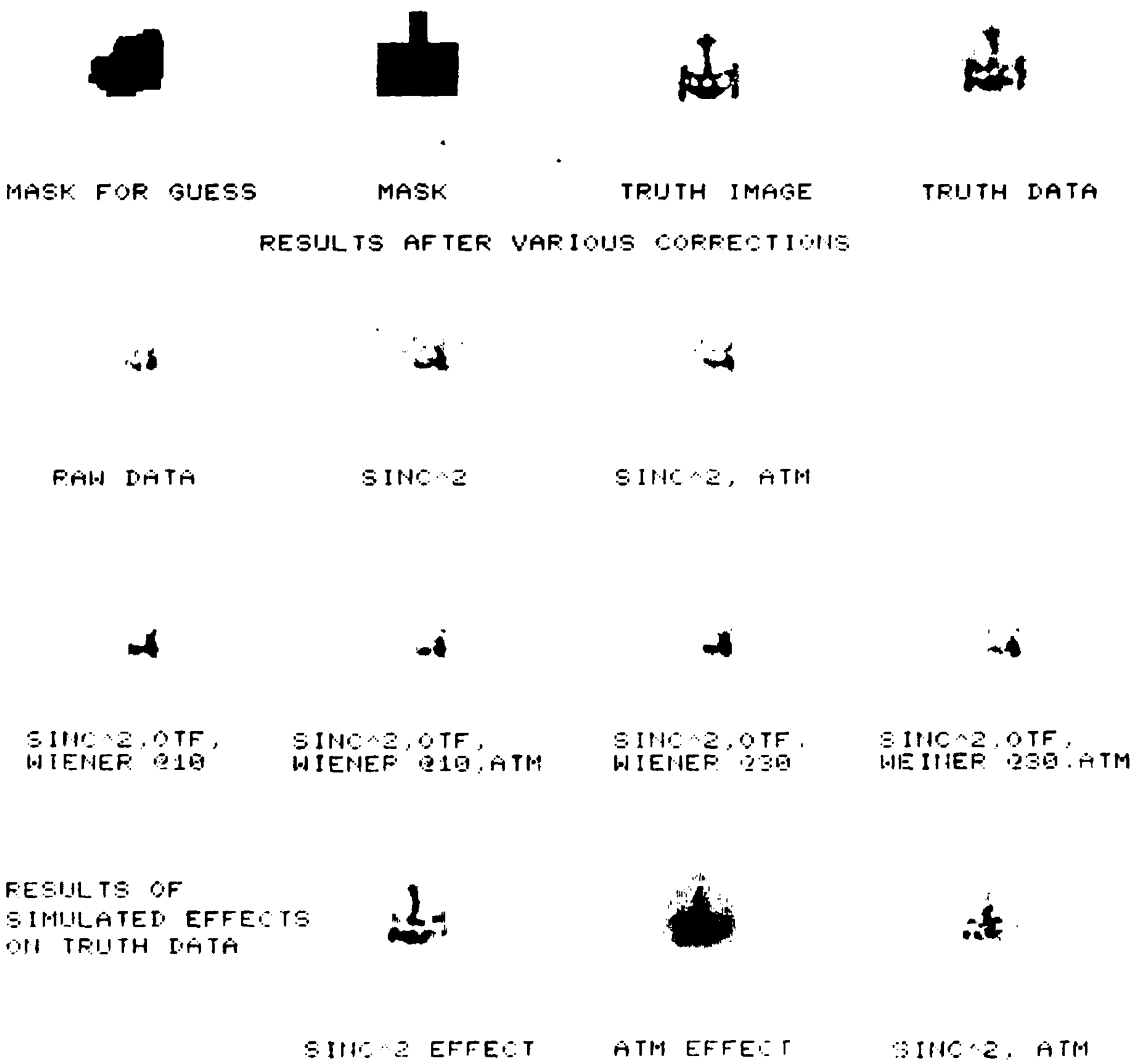
MASK FOR GUESS
MASK
TRUTH IMAGE
TRUTH DATA
RESULTS AFTER VARIOUS CORRECTIONS
RAW DATA
SINC^2
SINC^2, ATM
SINC^2,OTF, WIENER 010
SINC^2,OTF, WIENER 010,ATM
SINC^2,OTF, WIENER 230
SINC^2,OTF, WEINER 230,ATM
RESULTS OF SIMULATED EFFECTS ON TRUTH DATA
SINC^2 EFFECT
ATM EFFECT
SINC^2, ATM

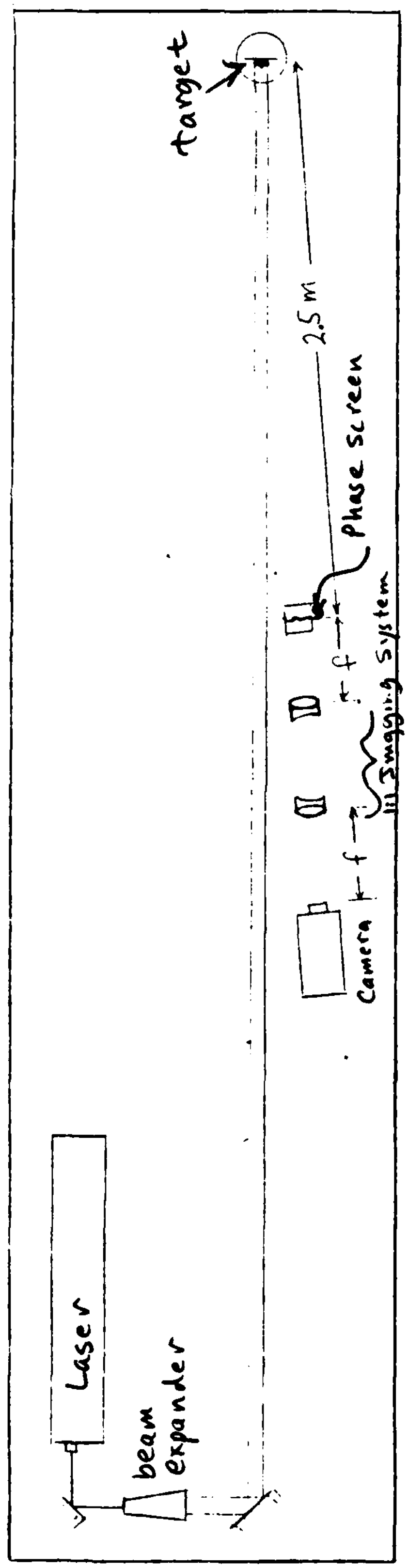

Fig. 1 Laboratory Set Up

References

1. P.S. Idell, J.R. Fienup, and Goodman, (1987), "Image Synthesis from Non-imaged laser speckle patterns", Optics Letters, 12, p858-860.

2. J.C. Dainty (ed.), Laser Speckle and Related Phenomena, 2nd edition, Topics in Applied Physics, Vol. 9, Springer, Berlin, 1982.

3. L.I. Gold Fisher, "Autocorrelation Function and Power Spectral Density of Laser_Produced Speckle Patterns", J. Opt. Soc. Am. , Vol 55, P. 247-253, 1965.

4. Bracewell, R.N., The Fourier Transform and its Applications, McGraw Hill (San Francisco), P. 115, 1978.

5. Fienup J.R., "Reconstruction of an Object From the modulus of its Fourier Transform", Opt. Let., Vol 3, P. 27-29, 1978.

6. Goodman J.W. et al, "Wavefront - Reconstruction Imaging through Random Media, App. Phy. Let., Vol. 8, P. 311, 1966.

7. P.S. Idell, (1988), "MIT/LL paper on Imaging Correlography Experiments".

8. B.M. Levine, and J.C. Dainty, (1983), "Non-gaussian image plane speckle: Measurements from diffusers of known statistics", Optics Communications, 45, p252-257.

END

DATE

FILMED

3-89

DTIC